Universidade do Minho
Escola de Engenharia

Maria Clara Rosa da Silva Correia

Multifunctional and Liquified Capsules for Tissue Regeneration

junho de 2016

Multifunctional and Liquified Capsules for Tissue Regeneration

Maria Clara Rosa da Silva Correia

UMinho | 2016

Universidade do Minho
Escola de Engenharia

Maria Clara Rosa da Silva Correia

Multifunctional and Liquified Capsules for Tissue Regeneration

Tese de Doutoramento em Engenharia de Tecidos, Medicina Regenerativa e Células Estaminais

Trabalho efetuado sob a orientação do
Professor João Filipe Colardelle da Luz Mano

junho de 2016

STATEMENT OF INTEGRITY

I hereby declare having conducted my thesis with integrity. I confirm that I have not used plagiarism or any form of falsification of results in the process of the thesis elaboration.
I further declare that I have fully acknowledged the Code of Ethical Conduct of the University of Minho.

University of Minho, 13th June 2016

Full name: Maria Clara Rosa da Silva Correia

Signature:
Maria Clara Rosa da Silva Correia

Para os meus pais.

Acknowledgements

I acknowledge the vision and leadership of my supervisor, Professor João Mano, for always pushing me further, to do more and better, everyday, fast. It is a great privilege to be part of the team. Thank you.

I acknowledge Professor Rui Reis to create such a competitive and skilled research team, and for the great opportunity to work and learn with the 3B's group. It was a great privilege to do my PhD in this team. I also acknowledge 3B's staff members. Many of them were my Professors while I was a Biomedical Engineering student. It was this team that inspired me to be a researcher.
I also deeply acknowledge all the 3B's technicians. Your valuable work made mine easier and, most importantly, possible. In particular, I am truly thankful to Ana Araújo, Adriano Pedro, Cláudia Costa, Liliana Gomes and Teresa Oliveira. To my other colleagues at 3B's, thank you for all the support and help. I learned so much with many of you. I'm deeply thankful to Diana Costa, my "desk-neighbor", for the numerous times that you helped me with your precious scientific knowledge. You are one of my role models.
In the 3B's I made wonderful friends that made my working days very special. Thank you Alexandre Barros, Ana Rodrigues, Cláudia Costa, Diana Pereira, Ivo Aroso, João Fernandes, Pedro Babo and Tininha (Ana Araújo) for all the great moments. You are the reason why I do like Sundays.

I acknowledge the Portuguese Foundation for Science and Technology (FCT) for my PhD grant (SFRH/BD/69259/2010), co-funded by the Operational Human Potential Program (POPH) developed under the scope of the National Strategic Reference Framework (QREN) from the European Social Fund (FSE).

My deepest and sincerely gratitude is to the most important persons in my life: my parents, brother and boyfriend.
Thank you Hélder, my best friend, my soul-mate.
Thank you João Pedro, mano, my better half.
Thank you pai e mãe, to whom I do not have enough words for all that you do for me. You are my valuable teachers. This thesis is for you.

Abstract

Cell encapsulation systems, in which cells and/or biomaterials and molecules are physically isolated from the surrounding environment, are being increasingly applied as multifunctional strategies in Tissue Engineering and Regenerative Medicine. In the present thesis it is proposed a rather unique combination of functional biomaterials and different cell types for the groundbreaking advance of liquified cell encapsulation systems. The proposed system aims to transfigure the concept of conventional three-dimensional scaffolds, typically associated on the use of porous structures or hydrogels to support cells, by using an alternative and hierarchical methodology. Capsules are composed by different components: (*i*) a permselective multilayered membrane composed by various polyelectrolytes, namely alginate, chitosan, and poly(L-lysine), and also electrostatically bounded magnetic-nanoparticles which confer magnetic-responsive ability to the system; (*ii*) poly(L-lactic acid) microparticles surface functionalized by combining plasma treatment with different coating materials; and (*iii*) different cell types, namely L929, stem and endothelial cells. The membrane wraps the liquefied core of the capsules, ensuring permeability to essential molecules for cell survival, and enhancing direct contact between the encapsulated materials. The microparticles confer cell adhesion sites, and also influence biological processes of the encapsulated cells due to its chemically modified surface. Multilayered and liquified capsules encapsulating microparticles were first validated as successful cell encapsulation systems for tissue regeneration. Different parameters of the production process were optimized, such as the number, type and concentration of multilayers, and the required time de-crosslinker concentration to liquefy the alginate core. Capsules were further successfully proposed as bioencapsulation systems for the regeneration of specific tissues, namely cartilage and bone. Ultimately, the biological outcome of capsules was tested *in vivo*, demonstrating the biotolerability of the developed system. It is expected that the proposed capsules will have a strong impact and open new prospects in cell encapsulation systems for tissue regeneration.

Resumo

Sistemas de encapsulamento celular, nos quais células e/ou biomateriais e moléculas estão fisicamente isolados do exterior, estão a ser cada vez mais propostos como estratégias multifuncionais para Engenharia de Tecidos e Medicina Regenerativa. Na presente tese é proposta a combinação de biomateriais funcionais e vários tipos de células para o progresso de sistemas liquefeitos de encapsulamento celular. O sistema proposto pretende transfigurar o conceito convencional de *scaffolds* tridimensionais, tipicamente associados a estruturas porosas ou hidrogéis para suporte celular, propondo uma metodologia hierárquica. As cápsulas são constituídas por diferentes componentes: (*i*) uma membrana com permeabilidade seletiva composta por vários polieletrólitos, nomeadamente alginato, quitosano e poli(L-lisina), e ainda nanopartículas magnéticas electrostaticamente acopladas à membrana que conferem ao sistema capacidade de resposta magnética; (*ii*) micropartículas de poli(L-ácido láctico) com a superfície funcionalizada por tratamento de plasma combinado com diferentes materiais de revestimento; (*iii*) diferentes tipos de células, nomeadamente L929, estaminais e endoteliais. A membrana envolve o núcleo liquefeito das cápsulas, assegurando a permeabilidade de moléculas essenciais para a viabilidade celular, e ainda maximiza o contacto direto entre os diferentes componentes encapsulados. As micropartículas oferecem locais de adesão celular, e ainda influenciam os processos biológicos das células encapsuladas devido à superfície quimicamente modificada. Cápsulas com multicamadas e liquefeitas com micropartículas encapsuladas foram primeiramente validadas com sucesso como sistemas de encapsulamento celular para regeneração de tecidos. Diferentes parâmetros do processo de produção foram optimizados, tais como o número, tipo e concentração das multicamadas, e o tempo necessário e concentração do des-reticulador para liquefazer o interior de alginato. As cápsulas foram ainda propostas com sucesso como sistemas de bio-encapsulamento para a regeneração de tecidos específicos, nomeadamente cartilagem e osso. Em última análise, a resposta biológica das cápsulas foi testada *in vivo,* demonstrando a biotolerância do sistema desenvolvido. Espera-se que as cápsulas propostas tenham um impacto considerável e que abram novas perspectivas nos sistemas de encapsulamento celular para regeneração de tecidos.

Table of contents

Part 2 – Experimental methodologies and materials

Part 3 – Experimental results

Part 4 – Conclusion

List of abbreviations and acronyms

0-10

2D: two-dimensional

3D: three-dimensional

10T1/2: clonal mouse embryo cell line

A

α-MEM: α-minimum essential medium

ALG: alginate

Alg-Ph: alginate with Ph moieties

ALP: alkaline phosphatase

AMECs: adipose-derived microvascular endothelial cells

ANOVA: analysis of variance

APA: alginate-poly(L-lysine)-alginate

ASC: adipose-derived stem cell

AT: adipose tissue

B

βGP: β–glycerophosphate

BGn: bioactive glass nanoparticles

BHK: baby hamster cells

BMP: bone morphogenic protein

BSA: bovine serum albumin

BSP: bone sialoprotein

C

C2C12: mouse myoblast cell line

CA: contact angle

$CaCl_2$: calcium chloride

$CaCO_3$: calcium carbonate

CD: cluster of differentiation

CEC: Competent Ethics Committee

CHO-K1: chinese hamster ovary cells

CHT: chitosan

cm: centimeter

CO_2: carbon dioxide

CPCs: cardiac progenitor cells

CSCs: cardiac stem cells

CSP: progenitor stem cells from the subchondral bone marrow

D

ΔD: variation of dissipation

ΔF: variation of frequency

DAB: *3,3'*-diaminobenzidine

DAPI: *4',6'*-diamidino-*2*-phenylindole

DD: degree of deacetylation

DEX-MA: methacrylated dextran

Dex: dexamethasone

DMEM: Dulbecco's modified Eagle's medium

DNA: deoxyribonucleic acid

E

EBs: embryoid bodies

EC: endothelial cell

ECM: extracellular matrix

EDS: energy dispersive spectroscopy

EDTA: ethylenediaminetetraacetic acid

EGFP: enhanced green fluorescent protein

ES: embryonic stem cell

F

FBS: fetal bovine serum

FDA: *Food and Drug Administration*

$FeCl_2.4H_2O$: iron (II) chloride tetrahydrate

$FeCl_3.6H_2O$: iron (III) chloride hexahydrate

Fe_3O_4: iron oxide

FITC: fluorescein isothiocyanate

G

G: α-L-guluronate

GAG: glycosaminoglycan

GelMA: methacrylated gelatin

GFP: green fluorescent protein

Gtn–HPA: gelatin–hydroxyphenylpropionic acid

H

h: hour

H_2O: water

H_2O_2: hydrogen peroxide

H&E: Hematoxylin and eosin

HA: hyaluronic acid

HCl: hydrochloric acid

HEK 293: human embryonic kidney 293 cells

HeLa-GFP: human cervical tumor cells stably expressing green fluorescent protein

HNDFs: human neonatal dermal fibroblasts

HepG2: hepatocellular carcinoma cells

HRP: horseradish peroxidase

HUVECs: human umbilical vein endothelial cells

Hz: Hertz

I

ICP: ion coupled plasma

IL-1: interleukin-1

IMR-90: human fetal lung fibroblasts

iPSCs: induced pluripotent stem cells

L

L: liter

L929: mouse fibroblast cell line

LbL: layer-by-layer

LCST: lower critical solution temperature

M

μm: micrometer

μL: microliter

M: *(1,4)*-linked-β-D-mannuronate

MA-TGMs: methacrylated thermogelling macromers

MAEP: mono-acryloxyethyl phosphate

MDCK: Madin-Darby canine kidney cells

ME: microvascular endothelial cells

MES: 2-(N-morpholino)ethanesulfonic acid

MF: magnetic field

Mg: miligram

M-gels: microscale hydrogels

min: minute

mL: milliliter

mm: milimiter

M_w: Molecular weight

MMPs: matrix metalloproteinases

MNPs: magnetic nanoparticles

MSCs: mesenchymal stem cells

MTS: *3*-(*4,5*-dimethylthiazol-*2*-yl)-*5*-(*3*-carboxymethoxyphenyl)-*2*-

(*4*-sulphofenyl)-2H-tetrazolium

N

NaCl: sodium chloride

NaOH: sodium hydroxide

NH_3 ammonia

NHS: normal horse serum

NH_4OH: ammonium hydroxide

NIH 3T3: mouse embryo fibroblast cell line

NiPAAm: N-isopropylacrylamide

nm: nanometer

nt: nucleotide

O

o-NB: *ortho*-nitrobenzyl

OMA: oxidized methacrylated alginate

OTS: octadecyl-trimethoxysilane

P

% v/v: percentage of volume/volume

% w/v: percentage of mass/volume

Pa: Pascal

PAA: poly(acrylic acid)

PAH: poly(allylamine hydrochloride)

PBS: phosphate-buffered saline

PCL: polycaprolactone

PCR: polymerase chain reaction

PCs: placental microvascular pericytes

PDMS: Polydimethylsiloxane

PEG: poly(ethylene glycol)

PEG-DA: poly(ethylene glycol) diacrylate

PEG-DMA: poly(ethylene glycol) dimethacrylate

PEO-PPO-PEO: poly(ethylene oxide)-*b*-poly(propylene oxide)-*b*-poly(ethylene oxide)

PEI: poly(ethyleneimine)

PFDC: perfluorodecalin

PGA: Propylene glycol alginate

PI: photoinitiator

pKa: acid dissociation constant

PLGA: poly(lactic-co-glycolic acid)

PLL: Poly(L-lysine)

PLLA: poly(L-lactic acid)

PMCs: polymeric multilayered capsules

PTCs: proximal tube cells

PVA: poly(vinyl alcohol)

Q

QCM-D: quartz-crystal microbalance with dissipation monitoring

R

RGD: arginine-glycine-aspartic acid

RP: rapid prototyping

rpm: rotations per minute

RT: room temperature

RUNX2: Runt-related transcription factor-2

S

s: second

SD: standard deviation

SEM: scanning electron microscopy

SH: superhydrophobic

SMCs: smooth muscle cells

SU-8: epoxy-based negative photoresist polymer

SYBR: cyanine nucleic acid dye

T

TEMPO: *2,6,6*-tetramethylpiperidine-*1*-oxyl

TERM: Tissue Engineering and Regenerative Medicine

TG-2: transglutaminase-2

TGF: transforming growth factor

TNF-α: tumor necrosis factor-α

TOBC: *2,6,6*-tetramethylpiperidine-*1*-oxyl-mediated oxidized bacterial cellulose

TPB: *1,1,4,4*-tetraphenyl-*1,3*-butadiene

TPP: tripolyphosphate

U

U: units

UCMSCs: Umbilical cord mesenchymal stem cells

UV: ultraviolet

V

VEGF: vascular endothelial growth factor

VIC: aortic valve interstitial cells

vWF: von Willebrand factor

W

WCA: water contact angle

List of figures

Part 1 – General introduction

Chapter I. Design principles and technologies in cell encapsulation systems towards tissue regeneration

Figure I.3 – Different types of fiber-shaped cell encapsulation systems. **(M)** Gelatin–hydroxyphenylpropionic acid (Gtn–HPA) matrix-core fibers encapsulating Madin-Darby canine kidney (MDCK) cells. **(Ma)** Optical micrograph (live-dead assay) and **(Mb)** cryosectional image (DAPI staining) of Gtn-HPA fibers. Scale bar in **(Ma)** is 400 μm and in **(Mb)** 50 μm. Reprinted from ref. [202] with permission from Elsevier. Copyright © 2009 Elsevier Ltd. **(MSa)** Matrix-core/shell fiber encapsulating rat mesenchymal stem cells in the

collagen core and bioactive glass nanoparticles (BGn) releasing silicon and calcium ions encapsulated in the alginate shell. Phalloidin (green) and DAPI (blue) staining after and 21 days of encapsulation in fibers **(MSb)** without or **(MSc)** with BGn. Scale bar is 100 μm. Reprinted from ref. [204] with permission from Elsevier. Copyright © 2015 Acta Materialia Inc. **(LS1)** Liquid-core/shell fibers with 120 μm of diameter encapsulating HEK 293 cells transfected with GFP (293/GFP cells) in the liquid alginate core surrounded by a poly(L-lysine) (PLL) shell. Green fluorescence images were overlaid on bright-field images. Scale bar is 400 μm. Reprinted with permission from ref. [126]. Copyright © 2008 Royal Society of Chemistry. **(LS2a-c)** Optical images of mouse embryonic cells encapsulated in alginate/PLL aqueous microstrands after 5 days of culture. The liquified environment allowed cells to self-assemble into tubular structures while promoting the formation of compact microtissues. Scale bar is 200 μm. Reprinted from ref. [129] with permission from Elsevier. Copyright © 2011 Elsevier Ltd. **(H1)** Schematic representation of alginate hollow fibers encapsulating HIVE-78 cells (red). Hollow fibers were then embedded in agar-gelatin-fibronectin matrix encapsulating HIVS-175 cells (green) to create a 3D vascularized co-culture system. Reprinted from ref. [125] with permission from John Wiley & Sons. Copyright © 2009 WILEY-VCH Verlag GmbH & Co. KGaA, Weinheim. **(H2a)** Hollow-core alginate fibers encapsulating L929 cells stained with red fluorescent dye. L929 cells stained in green were added to the hollow core to evidence the tubular structure of the fibers. **(H2b)** Hollow fibers were cut into pieces and slightly pressed, originating the release of the green cells in the hollow core, while the encapsulated red cells remained within the fiber matrix. Scale bar is 500 μm. Reprinted from ref. [206] with permission from Elsevier. Copyright © 2009 Elsevier B.V.....42

Figure I.4 – Examples of multifaceted and complex systems used for cell encapsulation in TERM applications. **(I)** Liquified capsules encapsulating L929 cells. Hydrogels were assembled by a perfusion-based layer-by-layer technique. Reproduced from ref. [44] with permission from the Royal Society of

Chemistry. **(II)** Production of hydrogels by liquified air-interface-directed self-assembly technique. **(II.a)** The pre-polymer solution (PEG and cells in suspension) is placed on top of an octadecyl-trimethoxysilane (OTS)-treated glass slide between the photomask and spacers. **(II.b)** UV light is selectively filtered through the photomask, leading the pre-polymer solution to polymerize in the desired pattern. **(II.c)** After PBS washing, PEG hydrogels encapsulating cells are obtained. **(II.d)** Microgels are randomly placed on the surface of perfluorodecalin (PFDC) or carbon tetrachloride, which due to the hydrophobicity of the solutions, microgels remain floating. **(II.e)** Due to surface tension, microgels self-assemble to minimize free energy. **(II.f)** Secondary UV polymerization to crosslink the microgels aggregation, originating macroscale engineered constructs. Scale bar is 2 cm. Reproduced from ref. [221] with permission from John Wiley & Sons. **(III)** Self-assembly of hydrogel cubes with uniform giant DNA glue modification. Hydrogel cubes display giant DNA on multiple designated faces, which allows constructing linear chain structures and net-like structures. To make chain structures, two cube species were made: a red cube that displays giant DNA *a* on two opposite faces, and a blue cube that displays giant DNA *a** on two opposite faces. **(III.a)** Schematic representation of giant-DNA-directed hydrogel assembly. Giant DNA containing tandem repeats of complementary 48-nt sequences was uniformly amplified on the surface of red and blue hydrogel cubes. Hybridization between the complementary DNA sequences resulted in assembly of hydrogel cubes. **(III.b)** Hydrogel cubes were assembled in a 0.5 mL tube filled with assembly buffer under mild rotation, transferred to a Petri dish and imaged by microscopy. **(III.c** and **III.d)** Phase contrast and fluorescent microscopy images of the post-assembly system, in which hydrogel cubes were modified with **(III.c)** short 56-nt or **(III.d)** amplified giant DNA strands. Hydrogel cubes carrying complementary DNA *a* or *a** were labeled with red or blue fluorescent microbeads, respectively, and stained with SYBR Gold. **(III.e)** Red and blue hydrogel cubes carrying complementary short (left) or giant (right) DNA strands failed (left) or succeeded (right) to assemble into aggregates, in the presence of competitive yellow hydrogel cubes that were not modified with

DNA. **(III.f)** Aggregates assembled from red and blue hydrogel cubes carrying complementary giant DNA fell apart after 1 h Baseline-ZERO DNase treatment (left: before DNase treatment; right: after DNase treatment). Scale bar is 500 mm in **III.c**, **III.d**, **III.e** and **III.f**. **(III.g–j)** Aggregates were assembled from red and blue hydrogel cubes with various edge lengths: **(III.g)** 30 mm, **(III.h)** 200 mm, **(III.i)** 500 mm and **(III.j)** 1 mm. Giant DNA glue was uniformly amplified on the hydrogel surface. Scale bar is 1 mm in the main panels and 50 mm in the inset of **(III.g)**. Reproduced from ref. [213] with permission from Nature Publishing Group. **(IV)** Magnetic directed assembly of microgels produced by micromolding. Microgels were assembled to fabricate three-layer spheroids through the application of external magnetic fields. First layer gels were stained with rhodamine-B, second layer gels were stained with FITC-dextran, and third layer gels were stained with TPB (*1,1,4,4*-Tetraphenyl-*1,3*-butadiene). Scale bar is 500 μm. Reproduced from ref. [214] with permission from John Wiley & Sons. **(V)** Cell encapsulation in 3D gel objects (modules) in a variety of simple shapes (crosses, squares and cylinders). **(V.a)** Photolithography of SU-8 photoresist on a silicon wafer to generate posts with diameters from 40 to 1000 mm and heights from 100 to 1000 mm. **(V.b)** Spin-casting PDMS around the produced posts generates a membrane that bore an array of holes in a variety of shapes with precise dimensions. **(V.c)** The obtained holes penetrate the PDMS membrane, which allows the modules to be release easily after formation. **(V.d)** Emersion of the fabricated PDMS membrane in a collagen solution containing NIH 3T3 cells in suspension. **(V.e)** Incubation of the membrane containing holes filled with collagen and cells at 37°C for 45 min. **(V.f)** After gelation of collagen, the membrane is immersed in cell culture medium and agitated for 10-15 min until the hydrogel modules are released. **(V.g)** Encapsulated cells proliferate and consequently the hydrogel shrinks without loosing its pre-defined shape. **(V.h-k)** Different shapes of modules. **(V.h)** Cross module fabricated from collagen. **(V.i)** Square cross-section module (40 mm wide) fabricated from collagen containing a single cell (bright spot). **(V.j)** Side view of square cross-section module (200 mm wide) fabricated from 2 % w/v agarose gel without cells. **(V.k)** Cylindrical module (1 mm in diameter)

fabricated from Matrigel. Scale bar is 800 μm in **(V.h, V.j** and **V.k)** and 200 μm in **(V.i)**. Reproduced with permission from ref. [222]. **(VI)** Polarity induction in individual EBs encapsulated in gelMA/PEG hybrid microgels with spatially patterned vasculogenic differentiation. **(VI.a** and **VI.c)** Phase contrast images of individual embryoid bodies (EBs) in hybrid microgel. **(I.4VI.b** and **I.4VI.d)** Microbead (green) laden PEG microgel and streptavidin conjugated rhodamine (red) laden gelMA microgel in hybrid microgel structure and EB morphology stained in blue by DAPI. Scale bar is 600 μm in **(VI.a)** and 300 μm in **(VI.c)**. Reproduced from ref. [217] with permission from John Wiley & Sons. **(VII)** Bioprinting of aortic valve conduit. **(VII.a)** Aortic valve model reconstructed from micro-CT images. The root and leaflet regions were identified with intensity thresholds and rendered separately into 3D geometries into stereolithography format (green color indicates valve root and red color indicates valve leaflets). **(VII.b** and **VII.c)** Schematic illustration of the bioprinting process with dual cell types and dual syringes. **(VII.b)** Root region of first layer generated by hydrogel with human aortic root smooth muscle cells (SMC). **(VII.c)** Leaflet region of first layer generated by hydrogel with porcine aortic valve interstitial cells (VIC). **(VII.d)** Fluorescent image of first printed two layers of aortic valve conduit. Smooth muscle cells (SMC) for valve root were labeled by cell tracker green and aortic valve interstitial cells (VIC) for valve leaflet by cell tracker red. Scale bar is 3 mm. **(VII.e)** As-printed aortic valve conduit. Reproduced from ref. [219] with permission from John Wiley & Sons. **(VIII)** 3D printed rigid filament networks of carbohydrate glass as a cytocompatible sacrificial template in engineered tissues containing living cells to generate cylindrical networks, which could be lined with endothelial cells and perfused with blood under high-pressure pulsatile flow. Cells constitutively expressing EGFP (green) were encapsulated in a variety of ECM materials, then imaged with confocal microscopy to visualize the matrix (red beads), cells (10T1/2, green) and the perfusable vascular lumen (blue beads) shown schematically (bottom right). The materials have varied crosslinking mechanisms (annotated above images) but were all able to be patterned with vascular channels. Scale bars are 200 μm. Reproduced from ref. [218] with

Part 2 – Experimental methodologies and materials

Chapter II. Materials and methods

Part 3 – Experimental results

Chapter III. Liquified chitosan-alginate multilayer capsules incorporating poly(L-lactic acid) microparticles as cell carriers

Chapter VII. *In vivo* osteogenic differentiation of stem cells inside compartmentalized capsules loaded with co-cultured endothelial cells and microparticles

List of tables

Part 1 – General introduction

Chapter I. Design principles and technologies in cell encapsulation systems towards tissue regeneration

List of publications

A – Publications resulting from the work performed during the present PhD thesis

A1 – International *peer-reviewed* journals

1. C.R. Correia, R.L. Reis, J.F. Mano. Design principles and technologies in cell encapsulation systems towards tissue regeneration, 2016 (*submitted*).
2. C.R. Correia, T.C. Santos, R.P. Pirraco, M.T. Cerqueira, A.P. Marques, R.L. Reis, J.F. Mano. *In vivo* osteogenic differentiation of stem cells inside compartmentalized capsules loaded with co-cultured endothelial cells, 2016 (*submitted*).
3. C.R. Correia, S. Gil, R.L. Reis, J.F. Mano, A closed chondromimetic environment within magnetic-responsive liquified capsules encapsulating stem cells and collagen II/TGF-β3 microparticles, **Adv. Healthcare Mater.**, 2016, DOI: 10.1002/adhm.201600034 (*in press)*.
4. C.R. Correia, R.P. Pirraco, M.T. Cerqueira, A.P. Marques, R.L. Reis, J.F. Mano, Semipermeable capsules wrapping a multifunctional and self-regulated co-culture microenvironment for osteogenic differentiation, **Sci. Rep.**, 6 (2016) 1-12.
5. C.R. Correia, R.L. Reis, J.F. Mano, Multilayered hierarchical capsules providing cell adhesion sites, **Biomacromolecules**, 14 (2013) 743–751.
6. C.R. Correia, P. Sher, R.L. Reis, J.F. Mano, Liquified chitosan–alginate multilayer capsules incorporating poly(L-lactic acid) microparticles as cell carriers, **Soft Matter**, 9 (2013) 2125-2130.

A2 – Book Chapters

1. C.R. Correia, R.L. Reis, J.F. Mano, Multiphasic, multistructured and hierarchical strategies for cartilage regeneration, in: L.E. Bertassoni, P.G. Coelho (Eds.), Engineering Mineralized and Load Bearing Tissues - Part II, **Springer International Publishing**, Switzerland, 2015, pp. 143-160.
2. C.R. Correia, R.L. Reis, J.F. Mano, Nanostructured capsules for cartilage tissue engineering, in: P.M. Doran (Ed.), Cartilage Tissue Engineering. Part III – Methods and Protocols, **Springer**, New York, 2015, pp. 181-189.

A3 – Communications in international and national conferences

A3.1 – Oral communications

1. C.R. Correia, S. Gil, R.L. Reis, J.F. Mano, Chondrogenic differentiation within magnetic-multilayered liquified capsules containing collagen II/TGF-β3 microparticles, **4th TERMIS World Congress**, Boston, Massachusetts, USA, September 8-11, 2015.
2. C.R. Correia, R.L. Reis, J.F. Mano, Cell encapsulation within injectable liquified capsules coated with polymeric multilayers, **5th ICVS/3B's Meeting**, Braga, Portugal, 2015.
3. C.R. Correia, R.P. Pirraco, M.T. Cerqueira, A.P. Marques, R.L. Reis, J.F. Mano, Paracrine signaling between adipose tissue stem and microvascular endothelial cells within multilayered capsules trigger osteogenic differentiation, **TERMIS-EU**, Genova, Italy, June 10-13, 2014.
4. C.R. Correia, R.L. Reis, J.F. Mano, Shaping biomaterials into spherical objects, **3rd 3B's Symposium on Biomaterials and Stem Cells in Regenerative Medicine**, Guimarães, Portugal, May 22, 2013.
5. C.R. Correia, R.L. Reis, J.F. Mano, Nanolayered capsules providing cell adhesion sites, **TERM STEM**, Guimarães, Portugal, October 9-13, 2012.

A3.2 – Poster communications

1. C.R. Correia, R.P. Pirraco, M.T. Cerqueira, A.P. Marques, R.L. Reis, J.F. Mano, Osteogenic differentiation of adipose stem cells by endothelial cells co-culture within liquified capsules, **4th TERMIS World Congress**, Boston, Massachusetts, USA, September 8-11, 2015.
2. C.R. Correia, R.L. Reis, J.F. Mano, Injectable multilayered and liquified capsules containing solid microparticles as bioencapsulation systems, **International Symposium on Frontiers In Biomedical Polymers**, Trento, Italy, July 8-11, 2015.
3. C.R. Correia, R.L. Reis, J.F. Mano, Liquified capsules combining immunoprotection and microcarriers, **TERMIS-EU**, Istanbul, Turkey, June 17-20, 2013.
4. C.R. Correia, R.L. Reis, J.F. Mano, Liquified capsules encapsulating microparticles to provide cell adhesion sites enhance cellular functions, **SFB Annual Meeting & Exposition**, Boston, Massachusetts, USA, April 10-13, 2013.

B – Publications in international *peer-reviewed* journal resulting from collaborative work performed during the present PhD thesis

1. R.R. Costa, A.I. Neto, I. Calgeris, C.R. Correia, A.C.M. Pinho, J. Fonseca, E.T. Oner, J.F. Mano, Adhesive nanostructured multilayer films using a bacterial exopolysaccharide for biomedical applications, **J. Mater. Chem. B**, 1 (2013), 2367-2374.
2. A.I. Neto, A.C. Cibrão, C.R. Correia, R.R. Carvalho, G.M. Luz, G.G. Ferrer, G. Botelho, C. Picart, N.M. Alves, J.F. Mano, Nanostructured polymeric coatings based on chitosan and dopamine-modified hyaluronic acid for biomedical applications, **Small**, 10 (2014) 2459–2469.
3. A.I. Neto, C.R. Correia, C.A. Custódio, J.F. Mano, Biomimetic

miniaturized platform able to sustain arrays of liquid droplets for high-throughput combinatorial tests, **Adv. Funct. Mater.**, 24 (2014) 5096–5103.

4. M.B. Oliveira, A.I. Neto, C.R. Correia, M.I. Rial-Hermida, C. Alvarez-Lorenzo, J.F. Mano, Superhydrophobic chips for cell spheroids high-throughput generation and drug screening, **ACS Appl. Mater. Interfaces**, 6 (2014) 9488–9495.
5. A.C. Lima, C.R. Correia, M.B. Oliveira, J.F. Mano, Sequential ionic and thermogelation of chitosan spherical hydrogels prepared using superhydrophobic surfaces to immobilize cells and drugs, **J. Bioact. Compat. Polym.**, 29 (2014) 50–65.
6. S. Gil, C.R. Correia, J.F. Mano, Magnetically labeled cells with surface-modified Fe_3O_4 spherical and rod-shaped magnetic nanoparticles for tissue engineering applications, **Adv. Healthcare Mater.**, 4 (2015) 883-891.
7. N.M. Oliveira, C.R. Correia, R.L. Reis, J.F. Mano, Liquid marbles for high-throughput biological screening of anchorage-dependent cells, **Adv. Healthcare Mater.**, 4 (2015) 264-270.
8. A.I. Neto, C.R. Correia, M.B. Oliveira, M.I. Rial-Hermida, C. Alvarez-Lorenzo, R.L. Reis, J.F. Mano, A novel hanging spherical drop system for the generation of cellular spheroids and high throughput combinatorial drug screening. **Biomat. Sci.**, 3 (2015) 581-585.
9. P. Sher, C.R. Correia, R.R. Costa, J.F. Mano, Compartmentalized bioencapsulated liquefied 3D macro-construct by perfusion-based layer-by-layer technique, **RSC Adv.**, 5 (2015) 2511-2516.

Structure of the thesis

The present thesis is organized in **four parts** that include a total of **eight chapters**. Part 1-3 are based on scientific papers or book chapters published or submitted for publication in international *peer-reviewed* journals. The respective original publication is cited at the beginning of each chapter. Each thesis chapter based on published papers is presented in the original manuscript form: Abstract, Introduction, Materials and methods, Results, Discussion, Conclusion, Acknowledgements, Supplementary Information, and References.

Part 1 is an introductory overview of cell encapsulation strategies applied in tissue regeneration strategies. The alternative path from cell encapsulation strategies to treat endocrine diseases to cell encapsulation strategies for tissue regeneration is discussed. The different designs and methodologies to produce such systems is also detailed discussed, as well as the multifunctionalities of cell encapsulation systems.

Part 2 describes the techniques and materials used to the proposed cell encapsulation system comprising multilayered and liquified capsules encapsulating surface modified solid microparticles and different cell types. *In vitro* and *in vivo* characterization techniques are also presented. The aim of this chapter is to complement and summarize in a single section the Materials and Methods subsection of each chapter from Part 3.

Part 3 comprises five experimental chapters related to the development of a novel cell encapsulation system for tissue regeneration. In Chapter III the different parameters to produce those capsules are optimized and in Chapter IV the applicability of capsules as bioencapsulation systems for tissue regeneration is successfully demonstrated. In Chapters V and VI capsules are

tested in a more specific tissue regeneration field, namely for cartilage and bone regeneration, respectively. Ultimately, in Chapter VII capsules are tested *in vivo* in a preliminary subcutaneous implantation.

Part 4 summarizes the results achieved in this thesis. Additionally, recent progresses on the cell encapsulation towards tissue regeneration and future directions of the field are succinctly discussed.

1

General introduction

Chapter I

Design principles and technologies in cell encapsulation systems towards tissue regeneration

Chapter I

Design principles and technologies in cell encapsulation systems towards tissue regeneration [1]

Abstract

Cell encapsulation systems are being increasingly applied as multifunctional strategies to regenerate damage tissues. Lessons afforded by efforts towards endocrine diseases treatment, the first impetus of primordial cell encapsulation systems, seemed to be highly valuable when the regeneration of tissues is aimed. Innumerous multifunctional systems for cell compartmentalization are being proposed to meet the specific needs required in the Tissue Engineering and Regenerative Medicine field. Here, we review the new methodologies that are being employed to fabricate the next generation of cell encapsulation strategies towards tissue regeneration. We also discuss the variable geometries of those systems, including spherical and fiber-shaped systems, as well as other complex shapes and arrangements that better mimic the highly hierarchical organization of native tissues.

[1] Based on the publication: C.R. Correia, R.L. Reis, J.F. Mano, Design principles and technologies in cell encapsulation systems towards tissue regeneration (2016) (*submitted*).

1. Introduction: From immunoisolation to multifunctional devices

Cell encapsulation is the process in which cells and/or bioactive molecules are encapsulated within a semipermeable barrier, hence being physically isolated from the surrounding environment. The first impetus of cell encapsulation systems was to protect the encapsulated cells from potential hazardous processes of the surrounding host environment, such as the immunological system, while maintaining the normal physiological functions of the encapsulated cells. This immunopriviledge feature of cell encapsulation systems was first demonstrated in 1933 using amniotic membrane tissue as the immunoprotective barrier [1]. Results showed that after implantation in the abdominal cavity of pigs, a prolonged cell survival of encapsulated tumor cells could be observed. However, the therapeutic potential of the technology was not recognized in that time. Later, in 1954, the concept of "diffusion chamber" to graft therapeutic cells was introduced [2], while also emphasizing for the first time the importance of biocompatible polymers on the composition of the cell encapsulation matrix. The release of encapsulated bioactive molecules without encapsulating cells emerges in 1964 [3]. Microcapsules (1-100 μm diameter) encapsulating hemolysate isolated from erythrocytes were produced by the coacervation technique. The successful release of the enzyme, while maintaining its bioactivity, was assessed *in vitro* and *in vivo*. This was the first time that an "artificial cell" was created, by releasing functional bioactive molecules from engineered materials. The creation of an artificial immunopriviledge site with therapeutic potential had then prompted the scientific community into the development of bioartificial organs. In light, in 1975 is developed for the first time an artificial endocrine pancreas [4]. Beta cells were isolated from neonatal rats and then cultured on bundles of artificial capillaries (Amicon XM-50 fibers). Results showed that cells continued to release insulin in similar levels of the flask cultures control, while remained responsive to changes in glucose concentration. The overarching principle of cell encapsulation was then to provide a long-lasting solution for treating secretory cell dysfunction [5-7]. By surrounding the transplanted cells within an immunological barrier opened new prospects in organ transplantation,

specially related with the culmination in the administration of immunosuppressant drugs, an important issue to be considered due to their adverse side effects. This was accomplished with the added benefits of reducing the burden of cell sourcing, since the immunoprotection feature allowed the use of allo- or even xenogeneic cells. Another remarkable study that influenced the pathway in the development of cell encapsulation strategies, is the work of Lim and Sun [8] with the encapsulation of islets in novel poly(L-lysine) (PLL) coated alginate beads. Since then, decades of extensive research have focused on the design and application of immunoisolation devices, which also facilitated the adequate transport of essential molecules for cell survival, namely oxygen and nutrients, as well as therapeutic molecules. Knowing the background of cell encapsulation it is understandable that the majority of works reported in the literature are related with the applicability of the technology in a wide range of endocrine diseases, including anemia [9], dwarfism [10], hemophilia B [11], kidney [12] and liver [13] failure, pituitary gland [14] and central nervous system [15] disorders, and, its major application field, diabetes mellitus [8]. In fact, the research on the encapsulation of pancreatic islets dominates the cell encapsulation field related with the immunoprotection feature. This is driven by the high number of diabetic patients and the recognized benefits of cell encapsulation strategies, which significantly improved their quality of life [16]. In parallel, with the discovery of new polymers and biomaterials, cell encapsulation strategies became more complex, and its use was extrapolated to respond to requirements of complex fields, such as Tissue Engineering and Regenerative Medicine (TERM). In TERM field, the concept of encapsulating cells is different from the immunoprotection required to treat endocrine diseases. In TERM applications, it is often desirable that the encapsulation matrix degrades while the encapsulated cells proliferate and create their own extracellular matrix. Additionally, different pro-healing components, such as growth factors and cytokines can be co-encapsulated with cells, while being released in a sustained fashion through the encapsulation matrix. Moreover, various encapsulation systems allow minimal invasive procedures through injection,

permitting the compartmentalization of cells and other desirable cargo in complex geometries. The large variety of cell encapsulation systems of different geometries proposed for TERM is almost exclusively produced from hydrogels due to a number of appealing features. Hydrogels provide a highly hydrated environment, while allowing the entrance of low-molecular mass nutrients and metabolites, for the encapsulated cells. Moreover, hydrogels can be easily functionalized to present biochemical, cellular, and physical stimuli that guide cellular processes such as migration, proliferation, and differentiation [17-20]. Additionally, the soft and pliable features of the hydrogel reduce the frictional or mechanical irritation to the surrounding tissue at the site of implantation. Some authors also claim that due to its hydrophilic properties, there is virtually no interfacial tension with surrounding tissues and fluids, which minimizes cell adhesion and protein adsorption, resulting in high biocompatibility [21].

In the present review, we intend to highlight the emergence of sophisticated, "smart" and multifunctional-engineered cell encapsulation systems that in common aim to successfully stimulate the regeneration of damaged tissues, while describing their relevant design criteria and the processing methods. In particular, a special focus will be given on the use of hydrogels as such class of materials has become the most effective used for cell encapsulation. We intend to highlight the state-of-the-art of the emerging techniques that are contributing to the development of the new generation of cell encapsulation systems. We critically describe challenges and achievements by giving examples of reported strategies. The new cell encapsulations systems are discussed in terms of its variable three-dimensional (3D) structures, comprising spherical, fiber-shaped and structures with increased 3D complexity, including multiscale devices obtained either from top-down or bottom-up approaches. Additionally, new features added to enhance the new multifunctional cell encapsulation systems are discussed, in which all of them have in common the same impetus: improve viability and functions of the encapsulated cells directing their activity in promoting the formation of new tissue.

2. Cell Encapsulation & Tissue Regeneration

The application of cell encapsulation principles to be used in the regeneration of tissues brought several advantages to the TERM field as compared to conventional strategies. Knowing that the key element in TERM is to combine cells with instructive biomaterials to ultimately regenerate damaged tissues, it is easy to understand that the function of the engineered device is not limited to the protection of cells, as it is its main function when cell encapsulation is applied to treat endogenous diseases. Therefore, the development of cell encapsulation devices that aim to promote tissue regeneration should be carefully pondered before its conception, in order to meet all the complex requirements of the field. Those requirements are here critically discussed. Additionally, the limitations, advantages and practical considerations of cell encapsulation strategies (*"closed scaffolds"*) over the commonly used *"open scaffolds"* in TERM at which cells are in direct contact with the surrounding environment are discussed.

2.1 Critical properties

2.1.1 Mild and sterile conditions

Concerning the multiple methods to produce cell encapsulation devices, which will not be discussed here (we suggest the reading of [17]), all of them have to take in consideration that for TERM applications cells are usually present in the to-be transformed biomaterial, so its transformation into the final structure must ensure the preservation of living components. Therefore, it is logical that all the production methods to produce cell encapsulation devices must ensure mild and sterile conditions. This limits the type of production techniques that can be employed, as well as the list of biomaterials that can be fabricated under those conditions. Allied to a number of appealing features, such as their structural resemblance to many natural biological tissues, viscoelasticity, and high water content, hydrogels have become the most favorable material used for cell encapsulation. Since the first hydrogel application in cell encapsulation when Lim and Sun developed calcium alginate microcapsules for islet

encapsulation [8], both synthetic and naturally derived cell encapsulation matrixes have been developed. Most of previous research has been focused on natural-derived hydrogels, such as alginate, chitosan, agarose, gelatin, collagen, fibrin, hyaluronic acid, among others [22]. The main advantages of natural-derived hydrogels are *(i)* its similar structure with the extracellular matrix (ECM) of many tissues, *(ii)* they are made of polymers similar to the biological macromolecules engineered by nature to perform specific functions in a demanding environment, *(iii)* various natural polymers may be found in large quantities from renewable sources, such as in the marine environment [23], and *(iv)* they can often be processed under mild conditions, thus not compromising the viability of the encapsulated cells [22]. Additionally, some natural polymers have cell-binding domains recognized by cells, thus promoting cell adhesion without requiring functionalization [24]; although this is not applicable for the most widely used natural polymer in cell encapsulation, namely alginate. Batch-to-batch variability and the presence of impurities are considered the main limitations in natural hydrogels. As an alternative, synthetic polymers have been employed, such as poly(ethylene glycol) (PEG), and poly(vinyl alcohol) (PVA), which are commonly used in combination with natural polymers to produce hydrogels. The different natural and synthetic polymers used in cell encapsulation systems and their characteristics are detailed discussed in different reviews [17, 18, 22, 25-27]. The incorporation of bioactive moieties is an increasingly trend being explored in cell encapsulation systems, as further discussed in section *5.2 Incorporation of bioactive molecules*. The most widely used method to produce a viable cell encapsulation matrix is to incorporate cells in a water-based solution of a hydrogel precursor (sol flowing phase) followed by gelation, commonly triggered by thermal, ionic, or photo-crosslinking. Particularly, ionotropic gelation is the most common crosslinking method, since gelation via temperature change or ultraviolet (UV) exposure can influence the cell viability or physiology. In this method, the solutions can be easily sterilized by filtration or autoclaved, and then they can be processed in mild conditions without requiring harsher chemicals to obtain hydrogels with variable structures

encapsulating viable cells. The ionotropic gelation occurs via the interaction of the polymer chains with ions, typically cation-mediated gelation of negatively charged polysaccharides. The most commonly used is the ionotropic gelation of alginate in calcium chloride [28, 29], but also many other ionotropic gelation with different materials have been proposed, such as carrageenan in potassium chloride [30], and pectin in calcium carbonate/D-glucono-δ-lactone [31].

2.1.2 Permeability and mass transfer

Once processed and formed, the cell encapsulation matrix will exhibit different transport properties depending on its structure, chemical composition and, in the particular case of hydrogels, the degree of crosslinking. This aspect will affect the permeability of essential molecules for cell survival, thus dictating the successful of cell encapsulation strategies. In the engineered matrix, either by the presence of a protective enveloping membrane or by the permeability properties of the cell encapsulation matrix itself, an immunobarrier can be created, avoiding the entrance of high molecular cells from the immune system or even deleterious molecules. In fact, even in the absence of a membrane, the hydrogel matrix can act as a mechanical and/or chemical barrier towards in- and out-flowing molecules. The efficiency of the barrier is application dependent, as well as being intrinsically connected with other parameters such as the stability of the cell encapsulation matrix, as further discussed. Nevertheless, in all the encapsulation strategies proposed for tissue regeneration, while the entrance of deleterious cells or molecules can be avoided, they all must ensure exchange of essential molecules for cell survival, such as nutrients, oxygen, metabolites, and waste products, as well as the exchange of important signaling biomolecules in the interaction of cells, either between the encapsulated cells or with the neighboring cells of the host environment. Additionally, in order to promote the integration of the implanted cell encapsulation device with the host tissue, it is desirable that the device should be permeable to the in-growth of blood vessels, except when regenerating avascular tissues such as cartilage. Therefore, either existing or

not the presence of an external membrane, the permeability of essential molecules ensuring cell survival across the entire 3D structure is of great importance in the design of the encapsulation matrix. It is important to highlight that the diffusion of essential molecules for cell survival will have a delay when comparing encapsulated cells localized in the core with the ones in the border of the matrix. This directly influences the size and/or geometry of cell encapsulation matrixes. Consequently, the majority of cell encapsulation systems are spherical and typically limited to a diameter of 400 μm, which is two times the maximum diffusion distance of oxygen and nutrients from blood vessels to cells [32]. With the increasing techniques to fabricate new TERM devices, other geometries have been progressively proposed as discussed in section *4. Engineered cell encapsulation systems with variable geometries*.

Considering the example of hydrogels as the engineered cell encapsulation matrix, its diffusion and permeability feature depends on at least three factors, namely *(i)* the obstruction effect caused by the presence of impenetrate slowly moving polymer chains that increase the path length for diffusion, *(ii)* the hydrodynamic drag at the polymer interface due to polymer-solvent and polymer-solute bonds during the solute diffusion, and *(iii)* the residual charges of the matrix, presence of counter ions, hydrogen bonds, polar and hydrophobic interactions, which will affect the transportation of solutes exhibiting similar interactive groups (especially essential in the transport of biological molecules) [33]. The solute transportation occurs by two main pathways, *(i)* convective, where transport is driven by a pressure gradient, and *(ii)* diffusive, where transport is driven by a concentration gradient [34]. In most cell encapsulation devices, including hydrogels, transport of solutes occurs by diffusion. In terms of solute diffusion depending on their pore size, hydrogels can be divided into three different classes, namely *(i)* macroporous, with pores >0.1 μm, which the transport occurs mainly by convection *(ii)* microporous, with pores ranging from 0.005 to 0.02 μm, which are in most cases smaller than the solute resulting in hindered diffusion, and *(iii)* nonporous hydrogels, the most commonly used in cell encapsulation, in which solute transport occurs only by diffusion through spaces between

macromolecular chains. The different parameters affecting the permeability of cell encapsulation systems using hydrogels have been detailed discussed [34]. Additionally, some cell encapsulation strategies are composed by membranes that surround the encapsulation matrix or directly the encapsulated cells (conformal coating). Although multilayered systems have been commonly used in cell encapsulation for the purpose of cell immunoisolation [35-38], they have been poorly explored in tissue regeneration. This is because in tissue regeneration the presence of a membrane for immunoisolation is not required, although it can confer other advantages to the system. For example, the properties of each membrane can be independently controlled, and the stability and permeability of the system can be easily customized the by varying the number of the multilayers. Multilayered cell encapsulation systems can be obtained by the sequential adsorption of oppositely charged polyelectrolytes using the mild conditions of layer-by-layer (LbL) technology [39, 40], as further discussed in section *3.1 Layer-by-layer methodology*. Of note, the influence on permeability and diffusion properties by the presence of a membrane surrounding the cell encapsulation matrix must be considered, since the different extent of material heterogeneity between the encapsulation matrix and the membrane might create fluctuations of transport properties across the different structures [33].

2.1.3 Stability

The stability of the encapsulation matrix is related with its physical features, namely the mechanical resistance that it can support without disruption of its integrity, or chemical features related with their ability to maintain its structure without being dissolved by physiological chelator agents or degraded. Either physical or chemical instability would lead to the premature release of the encapsulated materials, releasing its content to other regions of the body rather than the implantation site. Increasing the stability of the encapsulation matrix can be performed by different approaches that could, however, influence other important parameters for cell survival. It is thus crucial to find a perfect balance between the semipermeability (i.e. preventing the entrance of

specific cells, while allowing the diffusion of essential molecules for cell survival) of the encapsulated system with an adequate mechanical stability. In fact, developing semipermeable systems with adequate mechanical stability balanced with good mass transport of oxygen and nutrients remains a key challenge in cell encapsulation technology, as they are often inversely related [34]. Since alginate is the most widely applied hydrogel in cell encapsulation systems, efforts have been made to increase its stability. The first approach was to coat alginate beads with the oppositely charged polyelectrolyte PLL [8]. Now, other polymers are being employed to construct improved biocompatible membranes, mainly using the LbL technology [28, 39, 41-44].

Another possibility is to increase the crosslinking density of the cell encapsulation matrix. The simplest example for the case of alginate systems is the use of barium instead of calcium as the gelling divalent agent or to use biopolymers richer in guluronic acid units. However, it may lead to encapsulation matrixes with lower swelling capabilities and decreased mesh sizes, thus influencing the permeability of the construct. Crosslinking control will also result in matrices with distinct stiffness that will play an important role in cell behavior, namely on the ability of stem cells to differentiate into specific lineages [45-50]. For example, different osteogenesis levels could be obtained by controlling the viscoelastic properties [51] and the stress-stiffening effect [52] of hydrogels.

More recently, different groups are increasingly exploring the use of precise chemical routes to produce intrinsically robust hydrogels. A successful strategy was proposed [53] by incorporating 2,6,6-tetramethylpiperidine-1-oxyl (TEMPO)-mediated oxidized bacterial cellulose (TOBC) in alginate hydrogels. TOBC and alginate have similar chemical structures, and they both participate in the crosslinking process by gelling with calcium ions. The carboxyl groups available on the surface of TOBC provided the possibility of participating in the construction of an alginate-based composite and played crucial roles in the structural, mechanical and chemical stability of the formed hydrogel. The encapsulated NIH 3T3 cells in the composite hydrogel with enhanced mechanical properties remained viable and their proliferative ability was

preserved. Others, proposed robust hydrogels with adequate permeability inspired by the role of glycosaminoglycans in providing rigidity to the ECM due to their rigid sugar units and hydrophilic groups [54]. Inspired by that, a polysaccharide containing multivalent methacrylate groups and hydrophilic groups was incorporated into a hydrogel to control its stiffness over a broad range, while controlling the swelling ratio. This was achieved by the chemical crosslinking between methacrylic alginate and PEG-dimethacrylate (PEG-DMA). The increase of gel stiffness resulting from the incorporation of methacrylic alginate into a PEG-DMA hydrogel was related to the high chain rigidity of alginate as well as the multivalent methacrylate groups. In parallel, multiple hydroxyl groups of methacrylic alginate thermodynamically counterbalanced kinetic limits of osmotic water entry. Results showed that the chemical crosslinking of PEG-DMA allowed controlling the hydrogel stiffness without compromising its permeability, as demonstrated by the suitable viability of encapsulated neural cells (PC12 cells). In another study, alginate and PEG were also incorporated into interpenetrating network structures, improving significantly the toughness and elasticity of the final hybrid construct, without compromising the viability of encapsulated mesenchymal stem cells (MSCs) [55]. The resultant toughness relied on two mechanisms, namely the reversible calcium ions crosslinking of alginate that dissipated mechanical energy, while the covalent crosslinking of PEG maintained elasticity under large deformations. Besides alginate, other polymers have also been employed to produce ultra tough hydrogels allowing cell encapsulation by the use of precise chemical routes, as reviewed elsewhere [56]. For example, two chitosan derivatives, namely low molecular weight methacrylamide and medium molecular weight, were mixed with a photoinitiator (I2959) and the weak base β-glycerophosphate (β-GP) [57]. To produce double-network ultra tough hydrogels a sequential dual-crosslinking was performed, first by using UV-light exposure for the methacrylamide chitosan, and then by immersion in a solution containing negatively-charged tripolyphosphate (TPP) for the ionic crosslinking of medium molecular weight chitosan through their positively charged amine groups. This strategy allowed to create tough hydrogels that

were able to withstand an impressive compressive stress in the same order of magnitude as the ones found in native load-bearing soft tissues, with fast recover ability of their mechanical properties upon unloading, while allowing cell encapsulation.

2.1.4 Degradation

There are a number of factors influencing the degradation of cell encapsulation matrixes, which can occur by hydrolysis and enzymatic reactions or simply by dissolution/disruption of the matrix. In the case of the commonly used hydrogels, degradation can be mediated by *(i)* the chemistry of its matrix and the density of degradable groups, *(ii)* the presence and biological activity of cells, including the deposition of ECM and metabolite products, and *(iii)* environmental triggers in the *in vivo* physiological environment of the host. Considering the first referred circumstance, hydrogels produced by ionic or physical crosslinks may break down by processes that reverse the gelation mechanism, originating the dissolution of the encapsulation matrix. Using the example of ionotropic gelation of alginate in calcium chloride, the presence of electrolytes in the *in vivo* environment and/or the deposition of a newly formed ECM can lead to the exchange of divalent calcium ions for monovalent cations from the alginate matrix, leading to the dissolution of polymer chains or disruption of hydrogen bonds associated with physical crosslinks. In many cases, hydrogels are engineered to degrade by hydrolysis and/or enzymatically by adding specific degradable sequences within its chemical structure. This allows control both degradation rate and profile. Different to commonly used "*open*" scaffolds (see section *2.2 "Closed" and "open" scaffolds: Limitations, advantages and practical considerations*) composed by pores in which cells can deposited ECM prior to the scaffold degradation, in the encapsulation matrix degradation has to occur to provide space for ECM deposition. Therefore, the formation of new tissue and hydrogel degradation are intrinsically linked in cell encapsulation strategies. If degradation of the hydrogel occurs too quickly, i.e. prior to an appropriate deposition of ECM, the encapsulate cells will be deprived from the physical support required for different cell anchorage

processes; if degradation occurs too slow the deposition of ECM will occur in the pericellular regions, since those are the regions at which the diffusion of essential molecules for cell survival is higher, leading to an heterogeneous distribution of ECM in the hydrogel as well as cell necrosis at the core of its structure, a very common drawback in 3D systems and particularly in encapsulation matrixes. It is thus highly desirable that degradation of the encapsulation matrix must match the formation of new tissue by ECM deposition by the encapsulated cells, in order to achieve a proper tissue regeneration and integration. One direction is the chemical degradation of hydrogen bonds, usually through hydrolysis, which degradation can be controlled through the chemistry of the degradable linker. For example, slowly degrading linkers such as ε-polycaprolactone are often mixed with rapidly degrading linkers like poly(L-lactic acid) (PLLA) to achieve a proper degradation rate for a PEG hydrogel [58], or esters associated with lactic acid degrade significantly faster than ester linkages of caprolactone [59]. While these methods are frequently used in research today, alternative attractive possibilities involve the use of cell-mediated degradation of the matrix by enzymes activity [60, 61]. Through enzymatic cleavage or degradation, the cells can direct the time line of degradation and adjust their surrounding environment as needed for cellular growth, matrix deposition, and matrix re-organization. Techniques to achieve cellular-mediated matrix degradation can be performed either by using hydrogels from natural biopolymers, such as hyaluronic acid which degrades by hyaluronidases activity [62, 63], or to program short amino acid sequences into the hydrogel network, which are susceptible to enzymatic cleavage [60]. Short peptide sequences have the advantage of being relatively stable for modification, tunable for cell binding, and easy to be synthetized on a large scale [64]. Examples of enzymatically degradable segments used in cell encapsulation strategies are polysaccharide-based systems composed by ECM proteins, such as collagen, fibrin, fibronectin and laminin proteins, and peptide-based linkages that have specific cleavage sites for degradation by enzymes, such as elastase, plasmin or matrix metalloproteinases (MMPs) [64, 65]. Longer enzyme-cleavable chains can also

be used as connecting points for hydrogel formation, such as fibrinogen [66, 67].

Although enzymatically degradable single-phase hydrogel materials offer elegant control over cellular invasion, cell confinement within these systems remains strongly coupled to matrix elasticity, and enzyme-mediated changes to local mechanical properties may be difficult to control in a pre-determined manner. Taking advantage of controlling hydrogel degradation, an interesting work was proposed using void-hydrogels [68]. Void-forming hydrogels were obtained by encapsulating sacrificial gel porogens composed by oxidized hydrolytically labile alginate within a bulk hydrogel composed by high molecular weight alginate, which has thus a slowly degradation rate. The rate of pore formation was controlled by the rate of porogen degradation and cell migration and proliferation within pores. Remarkably, this strategy allowed decoupling the pore formation from elasticity of hydrogels, while controlling MSCs osteogenesis *in vitro.* While maintaining the adequate porosity of the cell encapsulation matrix to the encapsulated stem cells, a wide range of elastic modulus of hydrogels could be tested, with optimal bone formation at 60 kPa.

2.1.5 Biocompatibility/Biotolerability

While some groups claim that biocompatible polymers for cell encapsulation are available [69, 70], others doubt whether such materials can ever be designed [71-73]. This paradox is explained by the "appropriate host response" of the original definition of biocompatibility. During the emerging of artificial organs field, the definition of biocompatibility emerged as "the ability of a biomaterial to perform with an appropriate host response in a specific application" [74]. The referred appropriate host response was characterized by, after implantation of these artificial organs, the formation of a dense layer of fibrotic tissue with further integration with the host tissue. However, for cell encapsulation systems, defining an appropriate host response is more complex because any inflammatory response against the implanted system is potentially harmful to the encapsulated cells, which can lead to the failure of the cell encapsulation system. This failure is mainly related to the overgrowth

of immune cells surrounding the encapsulation system, which compromise the diffusion of essential molecules for cells survival and the exchange of therapeutic molecules, consequently originating death of the encapsulated cells; we recommend the reading of [75] for a deep understand of the interaction between the physicochemical properties and the biological responses in cell encapsulation systems. Encapsulation systems developed for tissue regeneration applications, although its inherent immunoprotective feature, they are not meant to prevent immune responses, which will inevitably occur due to leakage of antigens, breakage of encapsulation matrixes, protrusion due to high proliferation rates of the commonly used anchorage-dependent cells, and to responses associated with the surgery. Therefore, the current leading opinion is that cell encapsulation systems for tissue regeneration should preferably elicit a minimal immune response to avoid cellular overgrowth surrounding the capsules. With that, emerges the term biotolerability as *"the ability of a material to reside in the body for long periods of time with only low degrees of inflammatory reactions"* [76]. The current leading opinion is that, rather than "appropriate host response" of the term biocompatibility, the biotolerability concept of "low degrees of inflammatory reactions" is more appropriate in the cell encapsulation field (for further discussion details about this issue read [75]). Within the abroad spectrum of biomaterials available that induce different appropriate foreign body responses, other factors such as chemical modifications [77] and the dimension of the encapsulation matrix [78] also influence immune-mediated reactions. Combinatorial methods were proposed to study the immunological *in vivo* outcome of different biomaterials [79], or with a large library of the same biomaterial, namely alginate hydrogels, but with variable dimensions and chemical modifications [77]. Alginate has been the material of choice for encapsulation, but batches of this natural polymer need to be standardized to minimize endotoxin and protein content, both of which can affect biocompatibility of the encapsulated cells. In this regard, ultrapure alginate and other polymers are being commercialized.

Independently of the type of strategy used, all TERM strategies aim to regenerate living, healthy, and functional tissues, either partially by tissue grafts or even a total replacement of a severely damaged organ. In the perspective of using scaffolds for TERM, there are two main strategies: *(i)* scaffolds at which seeded cells adhere to a surface and are able to contact with the external milieu, here termed as "*open*" scaffolds, or *(ii)* scaffolds at which core cells are encapsulated, here termed as "*closed*" scaffolds that comprise cell encapsulation strategies (**Figure I.1**). The designation of "*open*" or "*closed*" scaffolds is thus respectively related to the direct contact or isolation between cells and the surrounding environment. In "*open*" scaffolds the production methods can comprise a wide range of precursors and harsh solvents and/or reactants as long as the final scaffold is cytocompatible, including its degradation products. On the other hand, in "*closed*" scaffolds mild production methods must be employed due to the presence of cells, which is also a significant limitation in terms of available technologies and suitable biomaterials that can be processed at those conditions.

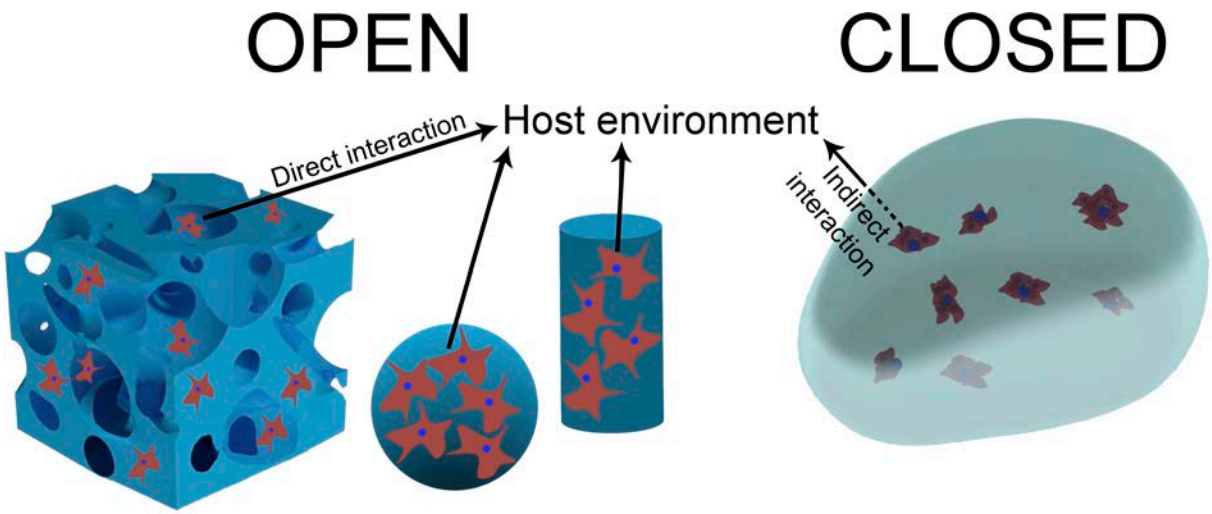

Figure I.1 – Schematic representation of the concept "open and closed" scaffolds for Tissue Engineering and Regenerative Medicine applications. In "open" strategies, cells are in direct contact with the host environment, while in "closed" systems the interaction is indirect due to the presence of the encapsulation matrix.

Despite the current challenges, "*closed*" scaffolds can offer several advantages over "*open*" scaffolds in TERM. Overall, *(i)* allows to create an optimized

microenvironment for cells and protect them from an undesirable severe immunological response by avoiding the entrance of immune cells; *(ii)* it is compatible with *in situ* injectable strategies, in which cells are suspended in a liquid precursor solution and delivered *in vivo* to the site of interest. By curing the hydrogel directly at the lesion site, the precursor solution can diffuse into the entire volume of the defect, leading to an enhanced integration of the scaffolds without requiring glue or sutures [80], as the formed hydrogel can easily adapt o the defect geometry; *(iii)* multiple compartments or elements with distinct functions can be easily grouped in one single structure, conferring multifunctionality to the engineered system as well as facilitating *in vitro* handling and *in vivo* implantation procedures over dealing with various ungrouped materials; and *(iv)* if desirable, the implant can be easily removed after treatment. Ultimately, for a cell encapsulation strategy to be applied successfully in TERM, a number of practical factors must be considered in addition to the critical properties discussed above. The process must be easily scaled up for manufacturing, marketable, and accepted by surgeons, patients, and healthcare providers, and ultimately receive approval form the competent authorities, such as the US *Food and Drug Administration (FDA)* and equivalents. Additionally, the encapsulation process must also be fast, on the order of seconds to minutes, to be clinically accepted [81]. Incorporating these considerations into the early stages of the design will significantly enhance the translation of a cell encapsulation strategy from the bench to the clinic.

3. New technologies for the next generation of cell encapsulation strategies

To face the demanding requirement of cell encapsulation systems for TERM, different methodologies are being recently proposed. In the present section we discussed those methodologies, in our opinion with higher potential to contribute to the new generation of cell encapsulation devices.

3.1 Protective coatings using the layer-by-layer technology

Since the introduction of the LbL methodology [82], it has become one of the most prominent surface engineering strategies in biomaterials science,

capable of providing a reliable, easy, versatile, environment friendly, and cost-effective way of tuning interfaces [39]. The principle of the technique is based on the sequential adsorption of a wide range of polyelectrolytes, which are selected and combined in function of their multipoint interactions [39, 40]. LbL methodology has been widely applied to produce polymeric multilayered capsules (PMCs), in which capsules are fabricated through LbL sequential deposition of polymers onto a sacrificial core template followed by the decomposition of this core yielding hollow capsules [83, 84]. The obtained nanometer thin membrane is permselective allowing diffusion of water and ions but excluding larger molecules. Additionally, the sequential fabrication procedure, combined with post-processing modifications (e.g. crosslinking or protein adsorption), allows a precise fine-tuning of the capsule's physicochemical properties [85]. PMCs have been used in a wide range of applications, such as in medical imaging [86], drug delivery systems [87-89], biosensors [90, 91], synthetic vaccines [92], nanoreactors [93], catalysts [94], and many others. More recently, these properties have put PMCs under attention in the field of cell encapsulation.

The most appealing features that the LbL technique could offer to cell encapsulation field are *(i)* the possibility to be performed at room temperature and in mild conditions, thus the viability of the encapsulated cells is not jeopardized, *(ii)* it is a aqueous-based procedure compatible with a broad range of natural and synthetic polyelectrolytes, thus requiring no exposure to organic and harmful solvents, which is highly desirable when aiming to incorporate biological active molecules due to its limited solubility in non-aqueous solutions and susceptibility to denaturation, *(iii)* it is well suited to the deposition of membranes on 3D structures, including those with complex shapes and irregular topographies, *(iv)* it offers precision control over the composition and thickness of composite membranes through control over the number and nature of layers deposited, allowing to tune the semipermeability of the membrane, and *(v)* it allows increasing the complexity of the encapsulation system by adding new functionalities and capabilities, since the multilayered membrane can act as drug reservoirs or include biological

functional components, such as proteins, enzymes, and peptides that elicit specific biological responses [95-97]. Therefore, LbL can be performed in cell encapsulation strategies by using the jellified hydrogel matrixes as templates to build an engineered membrane over its surface, which in tissue regeneration its presence is not compromised to the immunobarrier role. While being a very promising technique, with the possibility of open new prospects to the function of semipermeable membranes, LbL has been poorly explored in 3D cell encapsulation systems for tissue regeneration. The main exploited field of the LbL technique in cell encapsulation is within the single-cell encapsulation, which although being a promising instrument for engineering cells with enhanced properties is not on the scope of the present review (we recommend the reading of [98, 99]). We believe that this is mainly related to its inherent time-consuming aspect of LbL. Therefore, to the effort required to obtain an engineered cell encapsulation matrix, then adding the time-consuming task of the construction of a multilayered membrane has to be carefully pondered. This aspect is correlated to the viability of the encapsulated cells, limiting the number of layers composing the membrane. Clearly more efforts should be made to decrease the processing time by, for example, reduce the adsorption time of the layers (avoiding the adsorption until equilibrium or increasing the polyelectrolyte concentrations) or by using other assembly mechanisms between the layers, such as fast chemical reaction towards robust covalent bonds formation.

In a recent study, LbL technology was combined with the ionotropic gelation of alginate to produce a liquified cell encapsulation strategy [42]. Alginate hydrogel spheres were used as cell encapsulation templates for the construction of the LbL membrane. Once the LbL membrane was built, the alginate core was liquified by chelation of the calcium ions through ethylenediaminetetraacetic acid (EDTA) treatment. The multilayered membrane was built due to the electrostatic bonds between chitosan and alginate polyelectrolytes. Results showed that the different number of layers influenced the mechanical strength of the capsules as well as the viability of the encapsulated cells. More recently, a liquified cell encapsulation strategy

was developed combining the ionotropic gelation of alginate, LbL assembly, and the co-encapsulation of cells with surface modified PLLA microparticles [28, 43]. In this concept, by providing to the encapsulated cells surface functionalized microparticles as solid cell adhesion sites, the viability of the encapsulated cells could be enhanced. Additionally, the number of layers was increased to 12 layers without compromising cell viability, and the mechanical strength of the capsules was improved by using a three-component polyelectrolytes assembly, namely PLL, chitosan, and alginate. Importantly, the LbL technique allowed creating an encapsulation strategy in which cells are encapsulated in a liquid environment. This allowed to confer freedom for the encapsulated cells to freely self-construct their three-dimensional organization, while providing an appropriate diffusion of essential molecules for cell survival, a major concern in cell encapsulation strategies. However, maximizing the core dissolution to achieve an excellent diffusion required the introduction of solid cell adhesion spots, provided by the PLLA microparticles. Consequently, this innovative cell encapsulation strategy allowed capsules to have a much higher diameter (~2 mm) rather than the established 200 μm for cell encapsulation matrixes. The proposed capsules were proposed as an "inverse" methodology to the commonly used "open" scaffolds, since here cells are also adhered at the surface of a subtract but then the system is wrapped by a membrane, being physically isolated from the environment but without being embedded in an elastic matrix as usually observed in "*closed*" scaffolds. The successful of this strategy boosted its application to the encapsulation of stem cells for bone [100] and cartilage [101] TERM applications. Recently, we successfully propose the liquified capsules as co-culture systems of stem and endothelial cells towards osteogenic differentiation [100]. Additionally, multilayers surrounding liquified capsules encapsulating cells also served as an assembly methodology to construct 3D macrostructures from a bottom-up approach [41, 44].

Alternatively to the diffusion-driven kinetics of classical LbL assembly, which consists of dipping the subtract in the polymer solution, recent advances in LbL assembly technologies have explored other driving forces, namely

dewetting, roll-to-roll, centrifugation, creaming, calculated-saturation, immobilization, spinning, high gravity, spraying, atomization, electrodeposition, magnetic assembly, electrocoupling, filtration, microfluidics, and fluidized beds [98]. Among many other advantages, some of those different assembly technologies are also able to shorten the process. Additionally, there is now a growing realization that the assembly method not only determines the process properties (such as the time, scalability, and manual intervention) but also directly affects the physicochemical properties of the membrane (such as the thickness, homogeneity, and inter- and intra-layer organization). Process and physicochemical properties are both linked to application-specific performance [98]. However, the applicability of such LbL assemblies has not been tested yet in cell encapsulation devices. Nonetheless, we anticipate that its extrapolation and application will have a tremendous impact on the field. Besides the mechanical protection and mass transfer control, multilayers could also elicit specific functions that could have a direct impact on the performance of the device. For example, they could integrate inorganic elements to enhance bioactivity [102], magnetic- [101] and light-responsiveness [103] or gold nanoparticles for light-activated disruption [104]; moreover, they could include or expose biochemical elements to exhibit specific bioinstructive characteristics [105], such as growth factors to stimulate stem cell differentiation [96, 106, 107].

Besides using the LbL methodology to surround cell encapsulation matrixes, conformal coating, in which cells are directly coated with ultrathin (2-100 nm) protective soft shells, are also an application example of LbL in cell encapsulation [108, 109]. The great advantage that conformal coating brought to the cell encapsulation field was the possibility to improve cell functionality and viability using a very simple technique rather than adding soluble factors to the culture medium, as commonly used in *in vitro* culture, or other complex techniques such as genetic manipulation. For example, the multilayers can improve their mechanical stability, to protect them against phagocytosis by masking the cells surface from immunological agents, provide chemical resistance to aggressive environments, and to supply cells with additional

instrumentation for their functionality, as similarly above discussed for cell encapsulation matrixes. The production of ultrathin protective shells directly surrounding cells by LbL technology can be performed through *(i)* synthetic polyelectrolyte shells, in which due to the cell surface negatively charge at physiological pH, the shell assembly begins with the deposition of a polycation, then a polyanion is deposited, and so on, until the planned shell architecture is realized, *(ii)* synthetic hydrogen-bonded shells, in which the assembly occurs via non-covalent hydrogen-bonding interactions and their micromechanical properties can be controlled by changing pH, ionic strength, light conditions, slat concentration, or temperature; additionally, the degradability of the shells can be tuned by adjusting conditions that result in a controllably disassembled, and *(iii)* natural proteins, including hemoglobin, bovine serum albumin, and human serum albumin (the different LbL protective shells have been detailed reviewed elsewhere [109]). The presence of protective shells has been poorly explored in the field of cell encapsulation towards tissue regeneration, since usually the living organisms coated are mainly bacterial and yeast cells. However, the application of conformal coatings on such living organisms has allowed improving one of the main drawbacks of the LbL technique in cell encapsulation, which is related with its extensive time-consuming. In an innovative study, it was eliminated the adsorption step required between polyelectrolytes [110], thus significantly decreasing the required time to produce a thin membrane. For that, during the polycation adsorption, the surface potential of each layer was permanent monitoring. When the surface recharging process to positive is completed, the polycation solution is immediately replaced by the polyanion solution until negative surface charge saturation is reached, and so on.

3.2 Microfluidic systems

Microtechnologies in cell encapsulation allow a high degree of control over the morphological and dimensional (size and shape) properties of the encapsulation matrixes. It is also possible to encapsulate cells in different geometries, such as spherical hydrogels and in fibers, in a short time. The

microspheres and spheres can also be used to construct complex geometries through assembly into larger architectures mimicking the structure of tissues and organs, as discussed in section *4.3 Multifaceted and complex structures*. In the case of microspheres, microfluidics is performed by two major approaches: flow-focusing and T-junction. In the first, microspheres are formed by intercepting the core solution with a sheath stream flowing, while in T-junction microspheres are formed by permitting the core fluid to be swept away by one sheath stream in one direction [111]. Typically, an aqueous alginate solution is emulsified in an oil phase and crosslinked ionically with divalent ions, immediately upon contact of the two solutions [112]. The fast reaction typically results in uncontrolled gelation within the microfluidic device that can cause clogging and nonuniform drop formation [113, 114]. To overcome these problems, different studies had propose the use of calcium carbonate ($CaCO_3$) nanoparticles [115, 116], which allow to deliver calcium ions to the alginate solution without inducing unintended gelation prior to drop formation. The premature gelation of the alginate matrix is avoided by dispersing in the solution water-insoluble $CaCO_3$ nanoparticles, which can dissolve under acidic conditions after drop formation. The main drawback is the heterogeneous distribution of calcium ions inside the microspheres, compromising the homogeneity of the resulting microspheres. Other similar techniques use calcium chloride or acetate particles dispersed in the oil phase to initiate the crosslinking process, which are subsequently dissolved in the emulsion droplet [117, 118]. However, the same drawbacks of inhomogeneous calcium distribution and clogging are observed. Therefore, the new generation of microfluidics system to develop microspheres as cell encapsulation systems are focused in controlling the crosslinking process to produce homogenous microspheres with reliable and precisely tunable properties, which is of great importance in TERM, stem cell research, and disease treatments [119-121]. Alternatively, the generation of alginate microspheres via coalescence of separate droplets containing alginate and calcium chloride has been tried [122]. However, mixing inside the coalesced droplets still results in heterogeneous microspheres since crosslinking occurs before a homogeneous

distribution of calcium ions can be achieved. Recently, the fabrication of monodisperse alginate microspheres with structural homogeneity via droplet-based flow-focusing microfluidics was successfully developed [123]. The solution to overcome the above-mentioned drawbacks observed was to deliver calcium ions by a solution containing water-soluble calcium mixed with the chelator EDTA. By chelating the calcium ions with the EDTA, the ions remained in solution while being inaccessible to the alginate chains. After drop formation, acetic acid is added to the continuous phase to dissociate the calcium-EDTA complex, which results in the release of calcium ions. The free calcium ions react with the alginate chains in a highly controlled fashion, reticulating the alginate microspheres. Results demonstrated that the proposed gelation process was suitable for the encapsulation of living mesenchymal stem cells.

Besides microspheres, microfluidics technique has been also recognized to be an efficient method to fabricate long hydrogel microfibers in a short time. These metre-long microfibers are generally prepared using microfluidic devices by embedding dispersed cells directly within a hydrogel precursor, such as alginate [29, 124-128], chemically modified gelatin [129, 130] and supramolecular hydrogels [131]. Fiber-based systems are an ideal platform for mimicking biological materials and tissue constructs, and current research has begun to exploit fiber matrices for these biomedical applications [29, 111, 132]. It is important to highlight that the fiber fabrication process must be compatible with the next generation of biological soft materials, including proteins and other biomacromolecules that will not withstand the processing conditions of conventional spinning techniques to obtain fibers. As already mentioned, the processing of such biological materials in cell encapsulation systems requires aqueous conditions with precisely tuned temperature and pH in order to do not jeopardize the viability of the encapsulated cells and bioactive molecules. These processing limitations have exacerbated the sort-comings of traditional fiber spinning processes and led to the advent of a new fiber spinning methodology by microfluidics technique. In this context, microfluidic-spinning methodology has been employed to produce fibers in a

microchannel using the coaxial flow of a pre-polymer and the crosslinking agent [111]. It is similar to the wet spinning [133] but here the crosslinking agent is supplied directly by the coaxial flow instead the bath. Microfluidics spinning is thus the most suitable fiber formation technique for cell encapsulation because it does not require high voltage or temperatures, fibers can be fabricated continuously, and allows a precise control over the diameter of the fibers only by regulating the flow rate, which can be tuned from a few microns to a few hundred microns, and a wide diversity of cells can be encapsulated without incurrent significant damage to cells.

3.3 Superhydrophobic surfaces

Superhydrophobic (SH) surfaces arises from a unique surface chemistry and nano/microstructure organization, and can be universally found in nature, such as in lotus leaf and cicada wing, the anisotropic dewetting behavior on a rice leaf, striking superhydrophobic force by legs of water striders among many other examples [134, 135]. Those unique surfaces have inspired biomimetic designs for controlling surface wettability for interesting applications in microfluidics, self-assembly, self-cleaning, anti-fouling, water/oil separation, and cell spheroids formation as discussed in different studies [136-141]. Inspired by the rolling of water drops on the lotus leaf, SH surfaces with water contact angles (WCA) higher than 150° have triggered increasing interest in the scientific community for their application in the biomedical field [134, 136, 142], such as to produce cell spheroids in an innovative hanging drop methodology [143, 144]. Of particular interest to the present review, SH surfaces have been also used as an alternative methodology to produce spherical objects for cell encapsulation. The commonly used cell encapsulation methods imply the combination of two liquid environments, namely the solution containing the encapsulation materials and the precipitation/crosslinking bath. Cell encapsulation process using SH surfaces eliminates the crosslinking bath to harden the polymeric solution into a hydrogel. As first reported [145], the process involves the dispensing of a polymeric solution loaded with cells on its surface, which leads to spherically

shaped droplets due to the repellency properties of the surface, and, subsequently, the liquid droplets are crosslinked under mild conditions, originating cell encapsulated hydrogel spheres. SH polystyrene surfaces were further explored to produce alginate spheres encapsulating MSCs and fibronectin [146]. The developed cell encapsulation system was successfully tested *in vivo* by promoting bone healing in a calvarial bone defect. The alginate drops formed on the top of the SH polystyrene surfaces were crosslinked by adding a small amount of calcium chloride at the top of each spherical shaped droplet. Mild chitosan-based cell encapsulation system with two sequential gelation steps was also developed using similar SH polystyrene surfaces [147]. The acidic chitosan solution was first neutralized with βGP at room temperature to pH 6.2, an appropriate pH that did not jeopardized the viability of the encapsulated L929 cells. At the top of each droplet formed using SH surfaces, the ionic crosslinker sodium tripolyphosphate was added to induce the gelation process through electrostatic interactions. After incubation at 37ºC, a second gelation step occurred due to the thermoresponsive ability conferred by adding βGP to chitosan, while the pH-responsive behavior of chitosan was maintained. Using the same type of SH surfaces, the authors also proposed a multicompartmentalized "onion-like" hydrogel [148]. Methacrylated dextran (DEX-MA) solution containing a photoinitiator and calcium chloride was dispensed on SH surfaces and then crosslinked under UV light. Then, a solution of sodium alginate containing L929 cells was dispensed on the top of the spherical DEX-MA hydrogels. Subsequently, the alginate outer layer was crosslinked by the release of calcium ions previously immobilized in the core of the DEX-MA hydrogels. This is an example of using the core of the particle as a source of the crosslinking agent, avoiding the need of any external action for activating the gelling process.

Other types of SH surfaces were also explored to produce cell encapsulation systems. For example, glass SH surfaces produced by chemical vapor deposition were used to develop a hierarchical cell/drug encapsulation system [149]. For that, microdroplets of DEX-MA in phosphate-buffered saline containing the cytocompatible photoinitiator I2959 and L929 cells were

dispensed through a 350 μm diameter nozzle on the top of the glass SH surfaces. The formed droplets were crosslinked under UV-light exposure. Then, the obtained microspheres were added to an alginate solution and dispensed on the top of the SH surfaces, originating macrospheres encapsulating microspheres.

Using patterned SH surfaces with wettable spots allows to obtain microgels with other geometries besides spheres, by controlling the geometry of such regions where the hydrogel precursors are dispensed. A rapid methodology using superhydrophilic-superhydrophobic patterned microarrays to dispense spatially separated pico- to microliter-sized droplets with defined geometry and volume was developed [150]. Based on discontinuous dewetting, which relies on the extreme wettability contrast between superhydrophilic and superhydrophobic patterns, arrays of droplets of the solution containing the encapsulation material are instantly formed as the liquid moves along the superhydrophilic-superhydrophobic patterned surface. Then, maleimide-polyvinyl alcohol hydrogels encapsulating HeLa cells stably expressing green fluorescent protein (GFP) are created on the top of superhydrophilic spots, with no cells detected outside the hydrogel on the superhydrophobic regions.

The major advantage of using SH surfaces in cell encapsulation is the high encapsulation efficiency of cells and bioactive molecules, which is of almost 100% by eliminating the need of a crosslinking bath to form the hydrogels.

3.4 Hydrogels 3D bioprinting

One of the main disadvantages of processing hydrogels for cell encapsulation systems is the difficulty to shape them in predesigned geometries to mimic the complex microenvironments of natural tissues. To solve this specific drawback, different rapid prototyping (RP) techniques have emerged to produce cell encapsulation systems with complex 3D structures [151]. 3D computer models shape the external design that will dictate the final structure, and such models can either be designed by CAD software or by modeling imaging data (e.g., computer tomography (CT) and magnetic resonance imaging (MRI)). This directly indicates one of the greatest advantages of RP: direct fabrication of

scaffolds with a complex, patient specific external geometry in combination with a precise control over the internal architecture (limited by the resolution of the system) [152, 153]. In the context of TERM, RP techniques can be divided in two main strategies, namely *(i)* scaffold-based TERM systems, in which is assumed that cells require a 3D structure acting as a cell guide and supporting template that mimics the natural environment of the tissue to regenerate [154, 155] or *(ii)* scaffold-free TERM systems, in which cell-cell interactions and self-organization are the main key points of the system to regenerate the damaged tissue [156]. While scaffold-based TERM strategies emphasize the role of biomaterials as a supporting structure to guide cell function, minimizing the self-assembly and self-organization capability of the encapsulated cells, scaffold-free TERM reverses the importance of both contributions. A primary classification of the scaffold-based RP techniques supporting biomedical applications can be made hinged on the working principle, namely laser-based (photopolimerized hydrogels), nozzle-based (pre-polymers by dint of extrusion/deposition), and printer-based (powder beds and deposition of a binder that fuses the particles or directly depositing material using inkjet technology) systems [151]. Although the wide diversity of scaffold-based TERM systems produced by RP technologies for biomedical applications, only some of them are compatible for the processing of hydrogels. Additionally, among of them, the number of cell compatible RP technologies is still reduced when the hydrogels are formed in conditions that cannot allow cell encapsulation, due to the above-discussed mild conditions requirement (see section *2.2.1 Mild and sterile production techniques*). Different studies using the referred scaffold-based RP techniques have been proposed, as very well reviewed elsewhere [151], including a detailed discussion of the advantages and limitations of each technique. On the other hand, scaffold-free RP techniques are based in the principle that cells and tissues do not require an engineered biomaterial, due to their ability of self-assembly (the autonomous organization of components without externally intervention) and self-organization. Based on the implementation of RP technology, a fascinated perspective on scaffold-free TERM systems emerged, commonly termed as

"bioprinting" (or "organ printing") [157, 158]. Bioprinting principle is based on the controlled deposition of "bioink", composed by cells with or without hydrogels, on "biopaper", which is composed by a hydrogel matrix. With this technology 3D biomimetic tissues can be developed in a spatially controlled manner with high precision over the shape, size, and cell location across the hydrogel 3D structure, based on either laser [159, 160], inkjet [158, 161] or extrusion/deposition [162, 163] technology. Bioprinting thus enables the development of functional organs comprising multiple cell types by providing similar cellular microenvironments to those found *in vivo*. Using inkjet or extrusion-based technologies, the bioink objects, typically with spherical or cylindrical shape and composed by single or multiple cell types, are deposited in well-defined topological patterns into biopaper sheets. Then, the obtained construct is transferred to a bioreactor and the assembled bio-ink objects are fused. After that, the biopaper can be removed, if required. Bioprinters can be classified in *(i)* nozzle-based, which can be further divided into intermittent drop-wise printers, such as inkjet printers (both thermal and piezoelectric), and continuous robotic dispensing printers, and *(ii)* dropwise nozzle-free, which is based on laser-induced forward transfer printing techniques [164]. In the case of inkjet technology, individual or small cell clusters are printed. Despite the advantageous speed, versatility and cost, high cell densities are difficult to obtain and considerable cell damage is induced [165, 166]. On the other hand, extrusion-based bio-printers are more expensive but offer a more gentle approach towards cells [151]. Common hydrogels proposed for 3D bioprinting obtained from natural polymers, such as collagen [167], hyaluronic acid (HA) [168], chitosan [169], gelatin [170], and alginate [171]. To be suitable for 3D bioprinting, a hydrogel must be viscous enough to keep its shape during printing and must have crosslinking abilities allowing the maintenance of the 3D structure after printing. Crosslinking can occur by temperature change [167], UV photopolymerization [172-174] and ionic crosslinking [171]. A common challenge when 3D bioprinting hydrogels is that the printed shapes tend to collapse due to low viscosity. The viscosity of alginate, the most widely used polymer in cell encapsulation, can be increased

by varying the concentration and molecular weight [175]; however, it has not been sufficient for achieving shape fidelity while printing [171]. To increase the structural accuracy hydrogels are often printed in combination with other materials. In such cases the printability of alginate has been improved by the addition of gelatin [176], or by printing with a supporting sacrificial polymer [177]. Recently, to improve the mechanical resistance of alginate, it was combined with nanofibrillated cellulose and tested as a bioink to produce anatomically shaped cartilage structures [171]. Human ears and sheep meniscus were successfully bioprinted, encapsulating human chondrocytes. The complex cell encapsulation devices retained its shape during the 7 days of *in vitro* culture, while assuring the viability of the encapsulated cells.

4. Engineering cell encapsulation systems with variable geometries

One of the main drawbacks of using hydrogels in cell encapsulation strategies is the inherent difficulty to shape them in predesigned geometries. Therefore, due to the ease of process, the most widely used hydrogel geometry in cell encapsulation are spherical systems. Over the years, with the development of new technologies to process hydrogels, new conformities are increasingly being developed, including fibers-shaped systems. Additionally, more complex hydrogel structures, mainly resulting from the assembly of variable shaped building blocks are being developed. In the present section, different examples of cell encapsulation systems with spherical and fiber-shaped geometries will be discussed, processed at different sizes, from macro- (engineered structures with dimensions usually between 0.5-1.5 mm diameter and 1-10 mm in length [18]) down to the micro-scale level (usually smaller than 750 μm).

4.1 Spherical systems

Cell encapsulation strategies with spherical shape are the most widely use geometry. Spherical systems are considered advantageous from a mass-transport perspective since they are able to provide an optimal surface-to-volume ratio for the diffusion of essential molecules for cell survival [178]. In particular, microencapsulation strategies facilitate the implantation at different

sites through small diameter catheters, thus allowing minimal invasive procedures. Spherical cell encapsulation strategies comprise *(i)* beads, which is by far the most studied and simple spherical system, and consist of spherical hydrogels and *(ii)* capsules, when a membrane is surrounding the core environment. The terminology of capsules is variable in TERM, since systems that encapsulate other materials are also often called capsules. In the present review, the capsules terminology refers to systems surrounded by a membrane. In order to increase the complexity of beads in cell encapsulation, those systems have been combined with the incorporation of other materials, such as smaller beads [149] or solid microparticles [179], as discussed in section *4.3 Multifaceted and complex structures*. Most of the capsules are derived from beads, which are used as templates to produce the membrane. Capsules can be further divided into subcategories depending on the core state, namely *(i)* matrix-core/shell, *(ii)* liquid-core/shell, and *(iii)* cells-core/shell (or conformal coating).

Matrix-core/shell capsules encapsulate cells within a jellified hydrogel matrix surrounded by a membrane. The most well-known system is the alginate capsules manufactured by gelling alginate droplets containing cells in a solution containing divalent ions, such as calcium or barium, followed by a surface treatment after immersion of the obtained beads in PLL, as first proposed by Lim and Sun [8]. On the other hand, liquid-core/shell capsules encapsulate cells within a liquified matrix surrounded by a membrane. Using again the alginate capsules as an example, the system can be obtained by inverting the solutions used in matrix-core/shell capsules, i.e. by dropping a cell suspension containing divalent ions into an alginate solution [180, 181]. Immediately a hydrogel membrane of alginate is formed surrounding the liquified core containing cells. An alternative methodology to obtain extremely thin membranes in the order of nanometers is to combine cell encapsulation techniques with the LbL methodology as discussed in section *3.1 Protective coatings using the layer-by-layer technology*. Many refinements of the techniques to produce spherical cell encapsulation systems have been attempted over the years, giving raise to the emerging of new production methods and new coating

techniques, mainly produced using principles of microfluidics technology, SH surfaces, and rapid prototyping of hydrogels (see section *3. New technologies for the next generation of cell encapsulation strategies*). The cells-core/shell (or conformal coating) is a more recently technique compared with the referred two types of subcategories of capsules, and comprises the direct coating of a cell mass using LbL technique, as briefly discussed in section *3.1 Protective coatings using the layer-by-layer technology*.

Examples of beads and capsules as spherical systems used for cell encapsulation in TERM applications are illustrated in **Figure I.2**.

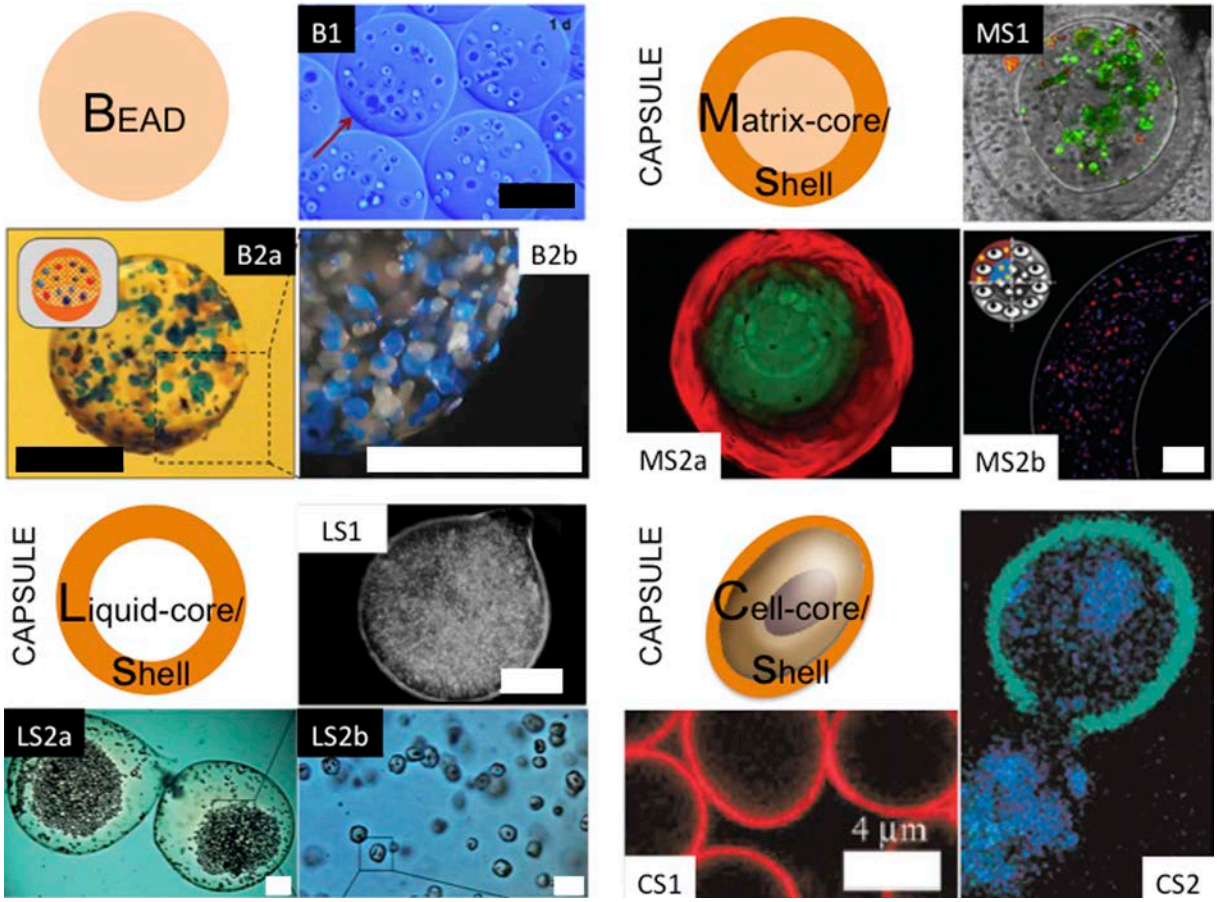

Figure I.2. Different types of beads and capsules as spherical cell encapsulation systems. **(B1)** Alginate microbeads encapsulating human umbilical cord mesenchymal stem cells. Scale bar is 200 µm. Reprinted from ref. [182] with permission from Elsevier. Copyright © 2016 Elsevier Ltd. **(B2a)** DEX-MA microbeads stained with safranin-O (red), alcian blue (light blue) and toluidine (dark blue) encapsulated within alginate beads. Scale bar is 1 mm. **(B2b)** Higher magnification of B2a to evidence the encapsulated microbeads. Scale bar is 200 µm. Reprinted from ref. [149] with permission from John Wiley & Sons. Copyright © 2015 WILEY-VHC Verlag GmbH & Co. KGaA, Weinheim. **(MS1)** Matrix-

core/shell capsule encapsulating baby hamster kidney (BHK) cells. The encapsulated BHK that remained in the core of the capsule are viable as showed by green fluorescence, while BHK cells that migrated to the outer layer were effectively killed (red fluorescence). Reprinted from ref. [183] with permission from Nature Publishing Group. Copyright © 2016 Macmillan Publishers Limited. **(MS2a)** Bi-layered DEX-MA matrix-core/shell capsule with the inner and outer layers stained with green and red fluorescent dyes, respectively. Scale bar is 500 μm. **(MS2b)** Localization of the encapsulated L929 cells in the outer layer of the DEM-MA matrix-core/shell capsule. Cell nuclei were stained in blue (DAPI) and F-actin filaments in red (phalloidin). Scale bar is 200 μm. Reproduced from ref. [148] with permission from John Wiley & Sons. Copyright © 2013 WILEY-VCH Verlag GmbH & Co. KGaA, Weinheim. **(LS1)** Liquid-core/shell capsule composed by a liquified alginate core encapsulating L929 cells and a layer-by-layer chitosan-alginate membrane. Scale bar is 500 μm. Reprinted from ref. [42] with permission from John Wiley & Sons. Copyright © 2011 WILEY-VCH Verlag GmbH & Co. KGaA, Weinheim. **(LS2a)** Liquid-core/shell capsule composed by a liquified alginate core encapsulating L929 cells and solid poly(L-lactic acid) microparticles as cell adhesion sites. The liquified core is surrounded by a multilayered membrane composed by poly(L-lysine), alginate and chitosan. Scale bar is 500 μm. **(LS2b)** Higher magnification of the liquified core of the capsules, showing the encapsulated microparticles. Scale bar is 100 μm. Reprinted with permission from [28]. Copyright © 2013, American Chemical Society. **(CS1)** Yeast cells coated with poly(N-vinyl pyrrolidone)/tannic acid multilayers, using a cationic poly(ethylene imine) as the first layer to facilitate the membrane adhesion. Scale bar is 4 μm. Reprinted with permission from ref. [184]. Copyright © 2010 Royal Society of Chemistry. **(CS2)** Cell-core/shell capsule composed by 6 layers of poly(allylamine hydrochloride) and poly(styrene sulfonate) stained in green surrounding a yeast cell. The resultant daughter cell was able to disrupt the membrane, resulting in a coating-free cell. Reprinted with permission from ref. [185]. Copyright © 2002 American Chemical Society.

Additionally, **Table I.1** summarizes the biomaterial, production technique, type of encapsulated cells, and the TERM application of examples of cell encapsulation systems with spherical structure.

Table I.1 – Examples of spherical cell encapsulation systems for Tissue Engineering and Regenerative Medicine (TERM). The examples cover the type of biomaterial used to produce the different cell encapsulation systems, the production technique, the type of encapsulated cells, and the TERM application.

Abbreviations: hCSCs: Human Cardiac stem cells; rMSCs: Rat mesenchymal stem cells; hMSCs: Human mesenchymal stem cells; IMR-90: Human fetal lung fibroblasts; hCSP: Human progenitor stem cells from the subchondral bone marrow; hPCs: Human placental microvascular pericytes; EDTA: Ethylenediaminetetraacetic acid; HUVECs: Human umbilical vein endothelial cells; hUCMSCs: Human umbilical cord mesenchymal stem cells; RGD: arginine-glycine-aspartic acid peptide sequence; TOBC: *2,6,6*-tetramethylpiperidine-*1*-oxyl radical oxidized bacterial cellulose; PLL: Poly(L-lysine); ES: Murine embryonic stem cells; hASCs: Human adipose-derived stem cells; hAMECs: Human adipose-derived microvascular endothelial cells; MNPs: Magnetic nanoparticles; CHO-K1: Chinese hamster ovary cells.

Spherical Systems		Biomaterial	Production Technique	Encapsulated Cells	TERM App.	Ref.
BEADS		Agarose with fibronectin or fibrinogen	Thermal gelation	hCSCs	Cardiovascular	[186]
		Agarose, collagen I, fibrin and dextran-sulfate	Water/oil emulsion	rMSCs or hMSCs and IMR-90	Cardiovascular	[187]
		Alginate	Calcium gelation	hCSP	Cartilage	[188]
		Alginate	Calcium gelation	hPCs	Vascular	[189]
		Alginate	Calcium gelation with disodium EDTA	D1 MSCs	General	[123]
		Alginate (macrobeads) Dextran-methacrylate (microbeads)	Calcium gelation (macrobeads) Photocrosslinking (microbeads)	L929	General	[149]
		Alginate and fibronectin	Calcium gelation	rMSCs	Bone	[146]
		Alginate and keratine	Calcium gelation	HUVECs	Vascular	[190]
		Chitosan	Sodium tripolyphosphate gelation	L929	General	[147]
		Collagen I	Thermal gelation	hMSCs	Bone	[191]
		Collagen I	Thermal gelation	hMSCs	Cartilage	[192]
		Oxidized alginate and fibrin	Calcium gelation	hUCMSCs	Bone	[182]
		RGD-alginate	Calcium gelation	hMSCs	Bone	[193]
		TOBC-alginate	Calcium gelation with nitrogen	NIH/3T3	General	[53]
CAPSULES	Matrix-core/shell	Alginate (core) PLL (shell)	Calcium gelation (core) Polyelectrolyte complexation (shell)	ES	Neural	[194]
		Alginate and collagen I (core) Collagen I (shell)	Calcium gelation (core) Polyelectrolyte complexation (shell)	hASCs	Adipose	[195]
		Dextran-methacrylate (core) Alginate (shell)	Photocrosslinking (core) Calcium gelation (shell)	L929	General	[148]
	Liquid-core/shell	Alginate (core) Chitosan and alginate (shell)	Calcium gelation followed by EDTA decrosslinking (core) Layer-by-layer (shell)	Saos-2	General	[42]
		Alginate (core) Chitosan and alginate (shell)	Calcium gelation followed by EDTA decrosslinking (core) Layer-by-layer (shell)	L929	General	[43]
		Alginate (core) Chitosan, alginate and PLL (shell)	Calcium gelation followed by EDTA decrosslinking (core) Layer-by-layer (shell)	L929	General	[28]
		Alginate (core) Chitosan, alginate and PLL (shell)	Calcium gelation followed by EDTA decrosslinking (core) Layer-by-layer (shell)	hASCs and hAMECs	Bone	[100]
		Alginate (core) Chitosan, alginate, PLL and MNPs (shell)	Calcium gelation followed by EDTA decrosslinking (core) Layer-by-layer (shell)	hASCs	Cartilage	[101]
		Dextran (core) Tetronic (T1107) derivatives (shell)	Pluronic F127	CHO-K1	General	[196]

4.2 Fiber-shaped systems

Fibers are long, thin and flexible structures that facilitate high-order assemblies such as nanoscale materials [197, 198] and textiles [199] by folding, bundling, reeling and weaving of fibers. In contrast with spherical cell encapsulation systems, fiber-shaped systems were not popularly employed until more recently. This is because the conventional mass-produced fibers widely use industrialized spinning techniques, namely wet, dry, melt, gel, and electrospinning, that after require process parameters (e.g. high shear, melt temperatures, harsh chemical solvents, or high voltages, rapid evaporation/solidification) [132] incompatible with the required mild conditions for cell encapsulation. Nonetheless, fiber-based systems are an ideal platform for mimicking biological materials and tissue structures, and current research has begun to exploit fiber matrices for biomedical applications [111, 132, 151]. Fiber-shaped systems can easily create 3D complex and hierarchical constructs *in vitro* mimicking the interconnected networks of native tissues, such as the immense tubular network of the cardiovascular systems, neural pathways, and even the direct fibrous constructs of the musculoskeletal system [200, 201]. The processing of such biological materials requires aqueous conditions with precisely controlled temperature and pH. The processing limitations coupled with the TERM biomimetic solutions mimicking the complexity and hierarchical organization of native tissues led to the advent of microfluidic fiber fabrication. In comparison to standard fiber-manufacturing technologies, microfluidics offers a combination of improved properties for biomaterials fabrication, including speed, reproducibility, yield, purity, and conservation of the biological component's functionality and viability in part due to the benign reaction conditions [132]. Various fiber-shaped cell encapsulations systems have been proposed to encapsulate different cell types by microfluidic spinning technique [29, 111, 124-131]. Microfibers are continuously formed in a microchannel using a coaxial flow of a fiber precursor solution sheathed by a second fluid that contains the crosslinking agent. The inner phase undergoes either a physical or chemical transformation, inside the microchannel or after ejection,

to produce the solid fiber. This method is similar to the wet spinning [133], although here the crosslinking agent is supplied directly by the coaxial flow instead of by the bath. This technique does not require high voltages or temperatures, thus ensuring mild conditions and, consequently, the viability of the encapsulated cells. Additionally, the diameter of the fibers can be easily tuned from a few to a few hundred microns only by regulating the flow rate [111]. Similarly to spheres, the most common biomaterial used to produce microfluidic-spun fibers is alginate [18, 124-128], but other polymers have been also employed, such as chemically modified gelatin [130, 202], chitosan [203], collagen [204] and supramolecular hydrogels [131]. Among the different polymers employed, also different types of cells have been encapsulated alone or in co-cultures. For example, matrix-core fibers were proposed to encapsulate hepatocytes or fibroblasts using spinning microfluidics [127]. Additionally, those fibers were also tested to encapsulate hepatocytes and fibroblasts by spatiotemporal control of the localization of cells in fibers with multiple parallel layers. Overall, the production methods to produce fibers by microfluidics remain similar between the different strategies with only slight modifications of the technique, such as by exploring different laminar flows. For example, a fiber-shaped cell encapsulation system was proposed using a double-coaxial laminar flow microfluidic device. The advantage of the system is the ability to include within the fibers structural ECM proteins, namely collagen I (both pepsin- and acid-solubilized collagen) and fibrin, which require longer gelation time compared to the polymers used in microfluidic (less than 1s). The double-coaxial laminar flow allowed creating a microfiber-shaped inner core of ECM proteins covered by a thin and tubular outer layer of mechanically stable and rapidly gelating alginate hydrogel [29]. The alginate shell prevented the ECM proteins in the liquified core from diffusing out the core, until finally the structure is solidified into a hydrogel. Different cell types were encapsulated, namely fibroblasts, myocytes, endothelial, nerve or epithelial cells. In a final step, the alginate shell is removed, resulting in a fiber-shaped cell encapsulation system only composed by cells and ECM proteins.

Besides matrix-core fibers, the simplest and commonly used system, fiber-shaped cell encapsulation systems can present other geometries. Therefore, depending on the core state and the presence of a membrane, fibers can be divided into *(i)* matrix-core fibers *(ii)* hollow-core fibers, *(iii)* matrix-core/shell fibers, and *(iv)* liquid-core/shell fibers. In particular, hollow-core and liquid-core/shell fibers have been poorly described in the literature. In the case of hollow-core fibers, the majority of reports are related with the encapsulation of therapeutic cells within the lumen of hollow fibers, which are then sealed with adhesive at both ends [205]. This strategy is mainly employed to produce immunoisolation membranes, thus is not within the scope of the present review. In tissue regeneration, since the immunoisolation feature is not compulsory, hollow-core fibers are widely used as tubular structures usually to mimic the vascular network [199]. Consequently, few studies have employed hollow-core fibers encapsulating cells within its matrix for TERM, although its production have been recently increase with the emerging of new techniques to produce cell encapsulation systems [125, 202, 206, 207]. Hollow fibers encapsulating cells within its matrix were first reported only 7 years ago with alginate fibers encapsulating endothelial cells (HIVE-78) using a three-layer coaxial flow [125]. Calcium chloride solution was used as the core and out-layer fluids to crosslink the middle layer alginate solution. The fabricated hollow fibers were then embedded into agar-gelatin-fibronectin hydrogels encapsulating smooth muscle cells (HIVS-125). However, this method lacked control over the lumen diameter of the microfiber. In fact, the lack of reports might be resultant from the difficulty in controlling the hollow core (lumen) during the fibers processing as well as after by preventing lumen collapse or, especially in the case of hydrogels, obstruction due to its inherent swelling. To control the lumen diameter of hollow microfibers, a coaxial triple cylinder was then suggested [206]. For that, aqueous solutions of dextran (core cylinder), alginate (intermediate cylinder) and calcium chloride (outer cylinder) were simultaneously extruded. The lumen diameter could be controlled only by the ratio of flow volume of dextran solution to total flow volume of dextran and alginate solutions (core volume ratio). Additionally, the outer diameter of the

fiber could also be controlled. Currently, since hollow-fibers are challenge to obtain, cell encapsulation tubular structures for TERM applications are mainly obtained by wrapping a tubular structure with matrix-core fibers using complex microfluidic technologies, such as combined with weaving machines [29] or multilayered structures [208]. On the other hand, liquid-core/shell fibers were barely reported in the literature [126, 129, 209]. Alginate fibers were proposed to encapsulate human embryonic kidney (HEK) 293 cells transfected with GFP and coated with PLL [126]. The alginate core was then liquified by using sodium citrate. Cells remained viable within the liquified core and cells formed a cylindrical multicellular aggregate after two weeks of culture. Others, used alginate fibers to encapsulate L929 cells, which were then coated with multilayers of alginate and chitosan using a LbL perfusion technique [209]. The core was then liquified by using the divalent ions chelator EDTA. The multilayered shell also allowed assembling the liquid-fibers into a spiral structure.

The recent methods to produce fiber-shaped systems allow a fine control of the diameter, composition and radial organization. However, usually the surface of the produced fibers is smooth and thus do not replicate the micro- and nano-features of natural tissues, which guide and regulate cell behavior. In an attempt to re-create such conditions, fibers with microstructured surfaces have successfully proposed encapsulating murine C2C12 myoblast cells and human osteoblasts encapsulation [210].

Examples of different fiber-shaped systems used for cell encapsulation in TERM applications are illustrated in **Figure I.3**.

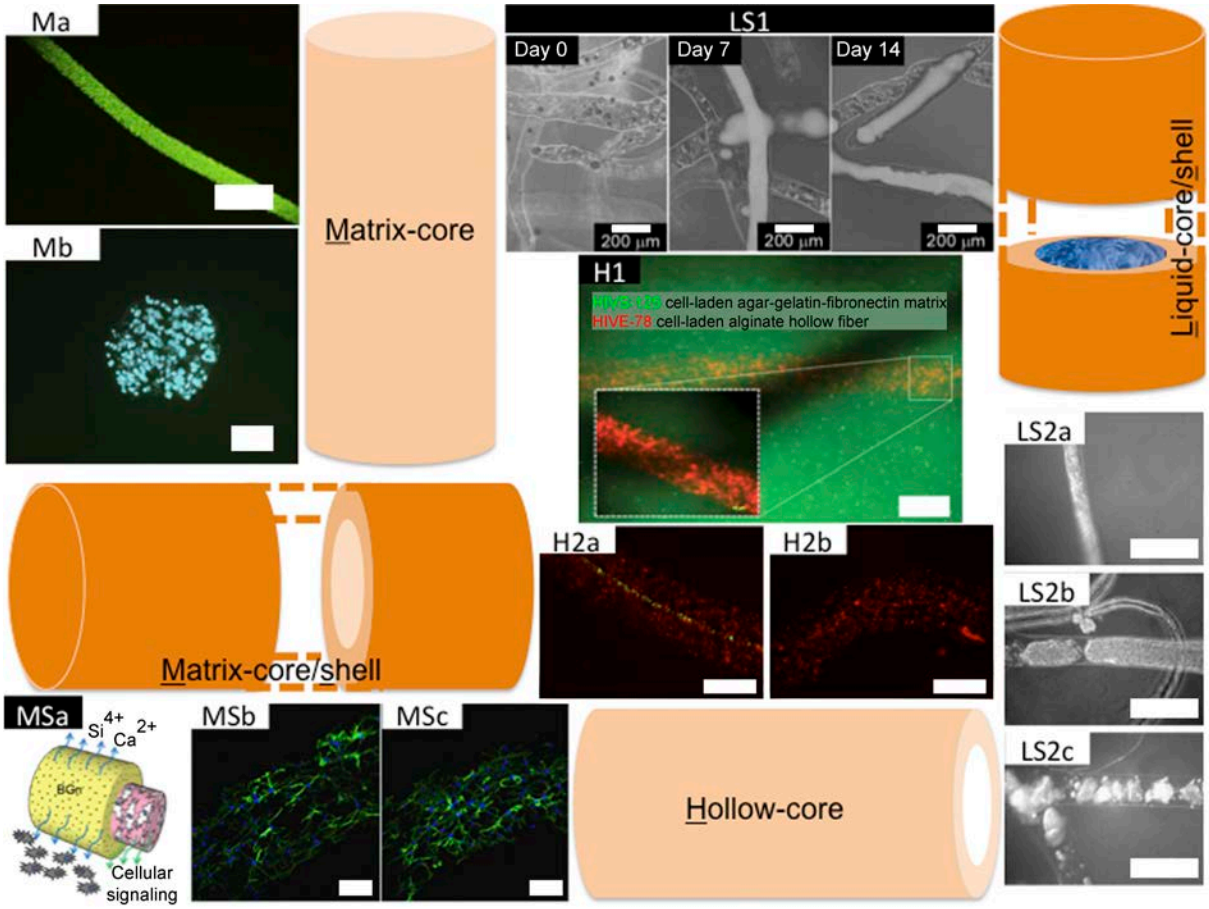

Figure I.3 – Different types of fiber-shaped cell encapsulation systems. **(M)** Gelatin–hydroxyphenylpropionic acid (Gtn–HPA) matrix-core fibers encapsulating Madin-Darby canine kidney (MDCK) cells. **(Ma)** Optical micrograph (live-dead assay) and **(Mb)** cryosectional image (DAPI staining) of Gtn-HPA fibers. Scale bar in **(Ma)** is 400 µm and in **(Mb)** 50 µm. Reprinted from ref. [202] with permission from Elsevier. Copyright © 2009 Elsevier Ltd. **(MSa)** Matrix-core/shell fiber encapsulating rat mesenchymal stem cells in the collagen core and bioactive glass nanoparticles (BGn) releasing silicon and calcium ions encapsulated in the alginate shell. Phalloidin (green) and DAPI (blue) staining after and 21 days of encapsulation in fibers **(MSb)** without or **(MSc)** with BGn. Scale bar is 100 µm. Reprinted from ref. [204] with permission from Elsevier. Copyright © 2015 Acta Materialia Inc. **(LS1)** Liquid-core/shell fibers with 120 µm of diameter encapsulating HEK 293 cells transfected with GFP (293/GFP cells) in the liquid alginate core surrounded by a poly(L-lysine) (PLL) shell. Green fluorescence images were overlaid on bright-field images. Scale bar is 400 µm. Reprinted with permission from ref. [126]. Copyright © 2008 Royal Society of Chemistry. **(LS2a-c)** Optical images of mouse embryonic cells encapsulated in alginate/PLL aqueous microstrands after 5 days of culture. The liquified environment allowed cells to self-assemble into tubular structures while promoting the formation of compact microtissues. Scale bar is 200 µm. Reprinted from ref. [129] with permission from Elsevier. Copyright © 2011 Elsevier Ltd. **(H1)** Schematic representation of alginate hollow fibers encapsulating HIVE-78 cells (red). Hollow fibers were then embedded in agar-gelatin-fibronectin matrix encapsulating HIVS-175 cells (green) to create a 3D vascularized co-culture system. Reprinted from ref. [125] with permission from John Wiley & Sons. Copyright © 2009 WILEY-VCH Verlag GmbH & Co. KGaA, Weinheim. **(H2a)** Hollow-core alginate fibers

encapsulating L929 cells stained with red fluorescent dye. L929 cells stained in green were added to the hollow core to evidence the tubular structure of the fibers. **(H2b)** Hollow fibers were cut into pieces and slightly pressed, originating the release of the green cells in the hollow core, while the encapsulated red cells remained within the fiber matrix. Scale bar is 500 μm. Reprinted from ref. [206] with permission from Elsevier.

Additionally, **Table I.2** summarizes the biomaterial, production technique, type of encapsulated cells, and the TERM application of examples of cell encapsulation systems with fiber-shaped structure.

Table I.2 - Examples of fiber-shaped cell encapsulation systems for Tissue Engineering and Regenerative Medicine (TERM). The examples cover the type of biomaterial used to produce the different cell encapsulation systems, the production technique, the type of encapsulated cells, and the TERM application.

Abbreviations: HepG2: Human hepatocellular carcinoma cells; Gtn-HPA: Gelatin-hydroxyphenylpropionic acid; HRP: Horseradish peroxidase enzyme; H_2O_2: Hydrogen peroxide; MDCK: Madin-Darby canine kidney cells; PEG-DA: Poly(ethylene glycol) diacrylate; hMSCs: Human mesenchymal stem cells; Alg-Ph: Alginate with Ph moieties; hPTCs: Human proximal tube cells; PGA: Propylene glycol alginate; PLL: Poly(L-lysine); BGn: Bioactive glass nanoparticles; rMSCs: Rat mesenchymal stem cells; hME: Human microvascular endothelial cells; EDTA: Ethylenediaminetetraacetic acid; ES: Embryonic stem cells.

Fiber-shaped Systems	Biomaterial	Production Technique	Encapsulated Cells	TERM App.	Ref.
Matrix-core	Alginate	Calcium gelation	L929	General	[124]
	Alginate and chitosan	Polyelectrolyte complexation	Primary rat hepatocytes and L929	General	[127]
	Alginate and chitosan	Calcium gelation	HepG2	General	[203]
	Gtn-HPA	HRP and H_2O_2 crosslinking	MDCK	General	[202]
	PEG-DA	Photocrosslinking	NIH/3T3	Vascular	[208]
	Peptide amphiphile solution	Ionic (calcium) self-assembly	hMSCs or HL-1	Cardiovascular, neural and nerve	[131]
Hollow-core	Alginate	Calcium gelation	HIVE-78	Vascular	[125]
	Alginate	Calcium gelation	L929	General	[206]
	Alg-Ph	HRP and H_2O_2 crosslinking	HeLa	General	[207]
	Gtn-HPA	HRP crosslinking	MDCK	General	[202]
	Gtn-HPA (inner layer) Polysulfone (outer layer)	HRP and H_2O_2 crosslinking	hPTCs	General	[130]
Matrix-core/shell	Alginate and PGA (core) Alginate and PLL (shell)	Calcium gelation (core) Polyelectrolyte complexation (shell)	NIH/3T3, HeLa or PC12	Hepatic, vascular, and musculoskeletal	[128]
	Collagen I (core) Alginate and BGn (shell)	Calcium gelation	rMSCs	Bone	[204]
	Collagen I (pepsin- or acid-solubilized) or fibrinogen (core) Alginate (shell)	Thermal gelation (collagen I-core fibers) or ionic crosslinking with thrombin and calcium chloride (fibrinogen-core fibers)	Fibroblasts (NIH/3T3), myocytes (C2C12 or rat primary), endothelial (HUVECs or MS1), nerve (rat primary cortical cells or mouse primary neural stem cells) or epithelial (HepG2, MIN6m9 or HeLa) cells	Vascular, musculoskeletal or neural	[29]
	Gtn-HPA (core and shell)	HRP and H_2O_2 crosslinking	MDCK	General	[130]
	Gtn-HPA (core and shell)	HRP and H_2O_2 crosslinking	MDCK and hME	General	[202]
Liquid-core/shell	Alginate (core) Alginate and PLL (shell)	Calcium gelation followed by sodium citrate decrosslinking (core) Layer-by-layer (shell)	Human kidney 293 cells	Vascular	[126]
	Alginate (core) Alginate and chitosan (shell)	Calcium gelation followed by EDTA decrosslinking (core) Layer-by-layer (shell)	L929	General	[209]
	Alginate (core) PLL (shell)	Calcium gelation followed by sodium citrate decrosslinking (core) Polyelectrolyte complexation (shell)	Mouse ES	General	[129]

4.3 Multifaceted and complex structures

Native tissues are hierarchical assemblies of heterogeneous types of cells and ECM across multiple length scales. Inspired by that, different cell encapsulation strategies with complex structures have been increasingly proposed. A commonly used strategy is the assembly of hydrogels as building blocks by bottom-up approach (**Figure I.4I-IV**). Bottom-up approaches have the potential to construct tissues with defined properties including spatial and temporal control at cellular level [211]. An example of spherical building blocks composed by alginate beads encapsulating a cell line (L929) assembled by perfusion-based LbL technology was proposed [44]. Due to the spherical shape of the beads, molds with variable shapes could be easily filled, and thus cell encapsulation systems with distinct final 3D macrophages were obtained. After the construction of the membrane, the core was liquified. The system maintained its structural integrity, showing the feasibility of using LbL technology to assemble cell-laden building blocks. Other interesting bottom-up approaches to construct 3D structures of hydrogels are being explored using different assembly techniques. For example, self-assembly of hydrogel modules with different geometries with micro-scale range (i.e., cubes of ca. 1000 μm^3) was demonstrated by placing cubes of methacrylated gelatin (gelMA) into the surface of a higher density hydrophobic liquid (carbon tetrachloride or perfluorodecalin) [212]. Due to surface tension complex aggregates of the hydrogels was observed. A second crosslinking step by UV light radiation was employed to consolidate the complex 3D structure. The hydrogel blocks were proposed to encapsulate different cell types, which could then be combined in one single structure to design multi-cellular structures. Precise control over the assembly process can be achieved by functionalization of the surface of the hydrogel blocks encapsulating cells. For that, cube-shaped hydrogel blocks functionalized with single-stranded DNA segments were proposed as a molecular recognition-assisted self-assembly strategy [213]. Results showed that cubes loaded with long complementary DNA strains could preferentially bind to each other and create complex microarchitectures. Others, produced multifaceted hydrogels co-encapsulating NIH 3T3 mouse embryo fibroblast cell

line and magnetic nanoparticles, which conferred magnetic-response ability to the hydrogels [214]. By spatially controlling the magnetic field, different geometries of the 3D constructs could be obtained, including dome, sphere, tube, and hexagon. These geometries were chosen as examples to mimic structures observed *in vivo*, e.g. dome for diaphragm (dome-shaped muscle) beneath the lungs, tube for vascular structure, spheres for islets, and hexagon for the lobules in pancreas. The different assembly methods of hydrogels encapsulating cells in order to fabricate complex structures by bottom-up approaches were recently reviewed in detail [215].

A different approach is to use micromolding to fabricate complex templated hydrogels on a massive scale (**Figure I.4V and I.4VI**). Generally, the molds can be made from different materials, such as metal and plastics, through soft photolithography and rapid prototyping [111]. Polydimethylsiloxane (PDMS) elastomers are also widely used to fabricate the molding replica due to their tunable mechanical strength, optical transparency, and biocompatibility [216]. The process involves the filling of molds with a pre-polymer solution that, usually by photocrosslinking, is crosslinked and ultimately originates hydrogels with multifaceted shapes. Micromolding was combined with photopatterning techniques to spatially organize 3D hybrid hydrogel arrays based on gelMA and PEG derivatives. Mouse embryoid bodies (EBs) were encapsulated within the engineered constructs to study their interactions with different hydrogel compositions [217]. For that, cells were first seeded into the microwells on a PDMS substrate, followed by the sequential loadings of the two pre-polymer solutions and UV crosslinking through a photomask. The photomask was specifically designed so that the EBs were embedded at the interfaces of the two different hydrogels and therefore were exposed to an asymmetric microenvironment. The EBs were found to preferentially sprout into the gelMA hydrogel part and thus led to induced polarity in the embryonic development, suggesting possible approaches to regulate the behaviors of the stem cell niche for TERM applications.

A more automated strategy to construct cell encapsulation strategies with complex shapes, are those fabricated using hydrogel rapid prototyping (**Figure**

I.4VII-X), as already discussed in section *3.4 Hydrogels 3D bioprinting*. The main advantages are its speed and versatility, although with some strategies cell damage might occur, thus limiting the technique in terms of fabrication processes and also the range of biomaterials than can be employed. Of relevance, the methodology allows to construct anatomically complex cell encapsulation systems, such as vascular networks [173, 218]. The 3D printing of vascular networks is a highly scalable platform that allows fabricating engineered tissue constructs in which vasculature and multiple cell types are precisely placed within a hydrogel matrix. This methodology allows increasing the diffusion of essential molecules by creating an extending network within the 3D structure of the engineered hydrogel, and thus avoids cell necrosis, one of the main issues in cell encapsulation systems. Other example of an anatomically complex cell encapsulation system using hydrogel rapid prototyping was the production aortic valves using hydrogels composed by natural polymers such as alginate/gelatin hydrogels [219] or combined with synthetic polymers such as alginate with PEG diacrylate (PEG-DA) [220]. One of the main disadvantages of having complex 3D structures by hydrogels rapid prototyping is the lack of mechanical resistance. In order to solve this problem, an interpenetrating network of ionically crosslinked alginate and covalently crosslinked PEG was proposed to fabricate a hydrogel possessing high fracture toughness, while allowing the encapsulation of human mesenchymal stem cells [55]. The unique tough and robust properties o the proposed hydrogel relied on the combination of two mechanisms, namely the reversible calcium crosslinking of alginate that dissipates mechanical energy under deformation, while the covalent crosslinked long-chain PEG maintains high elasticity of the hydrogel. The capability of printing PEG-alginate hydrogels into various complicated 3D structures, including hollow cube, hemisphere, pyramid, twisted bundle, and physiologically relevant shapes such as human nose and ear models, was tested. For that, it was include within the hydrogel matrix a biocompatible nanoclay in order to increase the viscosity of the prepolymer solution, required to produce complex shapes. HEK cells were encapsulated into a collagen I solution, which then gelled throughout the interconnected

pores of the printed PEG-alginate-nanoclay mesh to form a composite hydrogel. The encapsulated HEK cells maintained high viability of ca. 95% over the course of 7 days of in vitro culture. The printed hydrogel structures are also highly deformable and tough, demonstrating that the added nanoclay does not significantly affect the superior mechanical qualities of the hydrogel.

Examples of multifaceted and complex systems used for cell encapsulation in TERM applications are illustrated in **Figure I.4**.

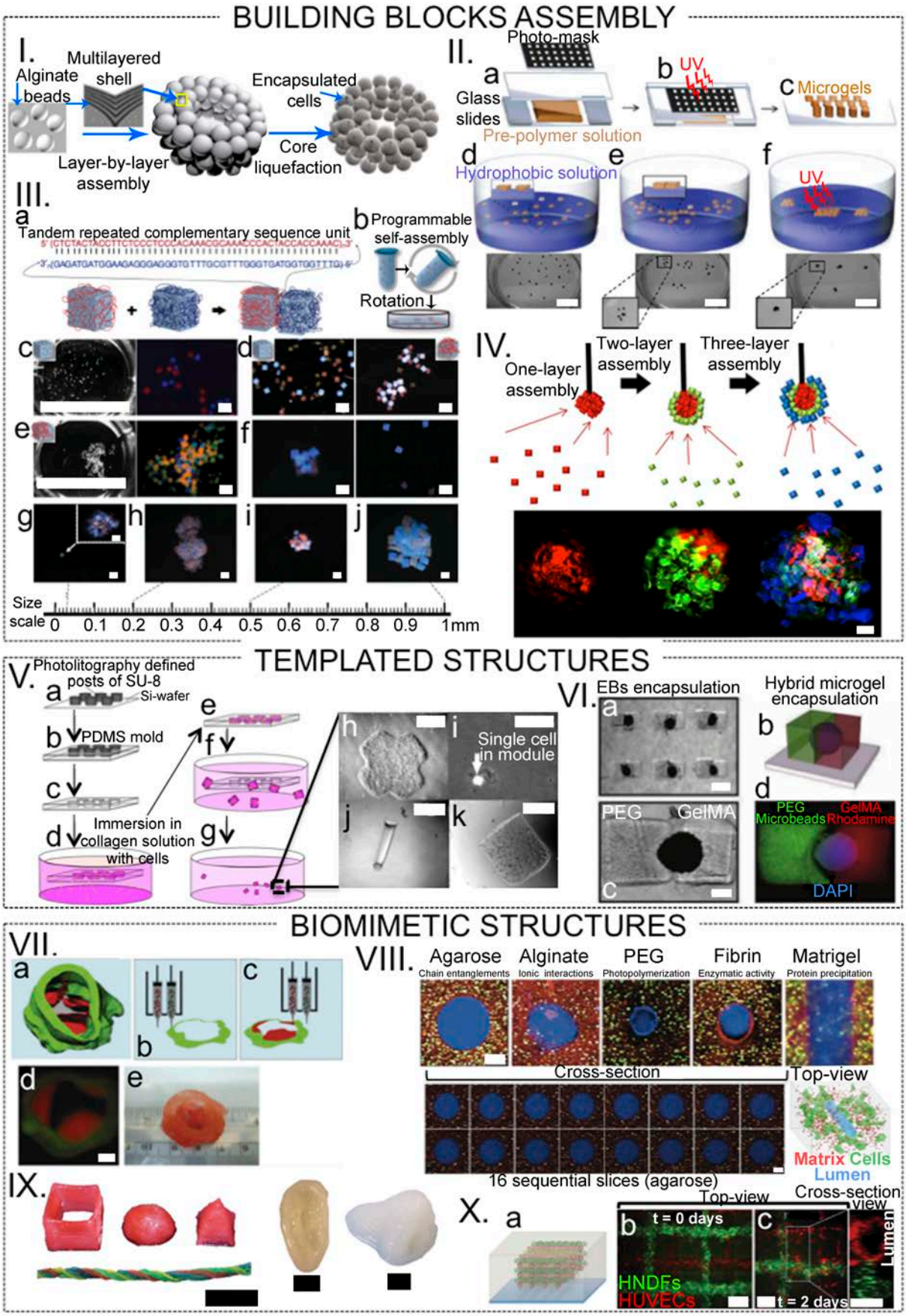

Figure I.4 – Examples of multifaceted and complex systems used for cell encapsulation in TERM applications. **(I)** Liquified capsules encapsulating L929 cells. Hydrogels were assembled by a perfusion-

based layer-by-layer technique. Reproduced from ref. [44] with permission from the Royal Society of Chemistry. **(II)** Production of hydrogels by liquified air-interface-directed self-assembly technique. **(II.a)** The pre-polymer solution (PEG and cells in suspension) is placed on top of an octadecyl-trimethoxysilane (OTS)-treated glass slide between the photomask and spacers. **(II.b)** UV light is selectively filtered through the photomask, leading the pre-polymer solution to polymerize in the desired pattern. **(II.c)** After PBS washing, PEG hydrogels encapsulating cells are obtained. **(II.d)** Microgels are randomly placed on the surface of perfluorodecalin (PFDC) or carbon tetrachloride, which due to the hydrophobicity of the solutions, microgels remain floating. **(II.e)** Due to surface tension, microgels self-assemble to minimize free energy. **(II.f)** Secondary UV polymerization to crosslink the microgels aggregation, originating macroscale engineered constructs. Scale bar is 2 cm. Reproduced from ref. [221] with permission from John Wiley & Sons. **(III)** Self-assembly of hydrogel cubes with uniform giant DNA glue modification. Hydrogel cubes display giant DNA on multiple designated faces, which allows constructing linear chain structures and net-like structures. To make chain structures, two cube species were made: a red cube that displays giant DNA *a* on two opposite faces, and a blue cube that displays giant DNA *a** on two opposite faces. **(III.a)** Schematic representation of giant-DNA-directed hydrogel assembly. Giant DNA containing tandem repeats of complementary 48-nt sequences was uniformly amplified on the surface of red and blue hydrogel cubes. Hybridization between the complementary DNA sequences resulted in assembly of hydrogel cubes. **(III.b)** Hydrogel cubes were assembled in a 0.5 mL tube filled with assembly buffer under mild rotation, transferred to a Petri dish and imaged by microscopy. **(III.c** and **III.d)** Phase contrast and fluorescent microscopy images of the post-assembly system, in which hydrogel cubes were modified with **(III.c)** short 56-nt or **(III.d)** amplified giant DNA strands. Hydrogel cubes carrying complementary DNA *a* or *a** were labeled with red or blue fluorescent microbeads, respectively, and stained with SYBR Gold. **(III.e)** Red and blue hydrogel cubes carrying complementary short (left) or giant (right) DNA strands failed (left) or succeeded (right) to assemble into aggregates, in the presence of competitive yellow hydrogel cubes that were not modified with DNA. **(III.f)** Aggregates assembled from red and blue hydrogel cubes carrying complementary giant DNA fell apart after 1 h Baseline-ZERO DNase treatment (left: before DNase treatment; right: after DNase treatment). Scale bar is 500 mm in **III.c**, **III.d**, **III.e** and **III.f**. **(III.g–j)** Aggregates were assembled from red and blue hydrogel cubes with various edge lengths: **(III.g)** 30 mm, **(III.h)** 200 mm, **(III.i)** 500 mm and **(III.j)** 1 mm. Giant DNA glue was uniformly amplified on the hydrogel surface. Scale bar is 1 mm in the main panels and 50 mm in the inset of **(III.g)**. Reproduced from ref. [213] with permission from Nature Publishing Group. **(IV)** Magnetic directed assembly of microgels produced by micromolding. Microgels were assembled to fabricate three-layer spheroids through the application of external magnetic fields. First layer gels were stained with rhodamine-B, second layer gels were stained with FITC-dextran, and third layer gels were stained with TPB (*1,1,4,4*-Tetraphenyl-*1,3*-butadiene). Scale bar is 500 μm. Reproduced from ref. [214] with permission from John Wiley & Sons. **(V)** Cell encapsulation in 3D gel objects (modules) in a variety of simple shapes (crosses, squares and cylinders). **(V.a)** Photolithography of SU-8 photoresist on a silicon wafer to generate posts with diameters from 40 to 1000 mm and heights from 100 to 1000 mm. **(V.b)** Spin-casting PDMS around the produced posts generates a membrane that bore an array of holes in a variety of shapes with precise dimensions. **(V.c)** The obtained holes penetrate the PDMS membrane, which allows the modules to be release easily after formation. **(V.d)** Emersion of the fabricated PDMS membrane in a collagen solution containing NIH 3T3 cells in suspension. **(V.e)** Incubation of the membrane containing holes filled with collagen and cells at 37ºC for 45 min. **(V.f)** After gelation of

collagen, the membrane is immersed in cell culture medium and agitated for 10-15 min until the hydrogel modules are released. **(V.g)** Encapsulated cells proliferate and consequently the hydrogel shrinks without loosing its pre-defined shape. **(V.h-k)** Different shapes of modules. **(V.h)** Cross module fabricated from collagen. **(V.i)** Square cross-section module (40 mm wide) fabricated from collagen containing a single cell (bright spot). **(V.j)** Side view of square cross-section module (200 mm wide) fabricated from 2% w/v agarose gel without cells. **(V.k)** Cylindrical module (1 mm in diameter) fabricated from Matrigel. Scale bar is 800 μm in **(V.h, V.j** and **V.k)** and 200 μm in **(V.i)**. Reproduced with permission from ref. [222]. **(VI)** Polarity induction in individual EBs encapsulated in gelMA/PEG hybrid microgels with spatially patterned vasculogenic differentiation. **(VI.a** and **VI.c)** Phase contrast images of individual embryoid bodies (EBs) in hybrid microgel. **(I.4VI.b** and **I.4VI.d)** Microbead (green) laden PEG microgel and streptavidin conjugated rhodamine (red) laden gelMA microgel in hybrid microgel structure and EB morphology stained in blue by DAPI. Scale bar is 600 μm in **(VI.a)** and 300 μm in **(VI.c)**. Reproduced from ref. [217] with permission from John Wiley & Sons. **(VII)** Bioprinting of aortic valve conduit. **(VII.a)** Aortic valve model reconstructed from micro-CT images. The root and leaflet regions were identified with intensity thresholds and rendered separately into 3D geometries into stereolithography format (green color indicates valve root and red color indicates valve leaflets). **(VII.b** and **VII.c)** Schematic illustration of the bioprinting process with dual cell types and dual syringes. **(VII.b)** Root region of first layer generated by hydrogel with human aortic root smooth muscle cells (SMC). **(VII.c)** Leaflet region of first layer generated by hydrogel with porcine aortic valve interstitial cells (VIC). **(VII.d)** Fluorescent image of first printed two layers of aortic valve conduit. Smooth muscle cells (SMC) for valve root were labeled by cell tracker green and aortic valve interstitial cells (VIC) for valve leaflet by cell tracker red. Scale bar is 3 mm. **(VII.e)** As-printed aortic valve conduit. Reproduced from ref. [219] with permission from John Wiley & Sons. **(VIII)** 3D printed rigid filament networks of carbohydrate glass as a cytocompatible sacrificial template in engineered tissues containing living cells to generate cylindrical networks, which could be lined with endothelial cells and perfused with blood under high-pressure pulsatile flow. Cells constitutively expressing EGFP (green) were encapsulated in a variety of ECM materials, then imaged with confocal microscopy to visualize the matrix (red beads), cells (10T1/2, green) and the perfusable vascular lumen (blue beads) shown schematically (bottom right). The materials have varied crosslinking mechanisms (annotated above images) but were all able to be patterned with vascular channels. Scale bars are 200 μm. Reproduced from ref. [218] with permission from Nature Publishing Group. **(IX)** 3D printing of tough and biocompatible PEG–alginate–nanoclay hydrogels with various shapes: (from left to right) hollow cube, hemisphere, pyramid, twisted bundle, the shape of an ear, and a nose. Nontoxic red food dye was added postprint on some samples for enhanced visibility). Scale bars are 2 cm. Reproduced from ref. [55] with permission from John Wiley & Sons. **(X)** 3D bioprinting for fabricating engineered tissue constructs replete with vasculature, multiple types of cells, and ECM. **(X.a)** Schematic view and **(X.b** and **X.c)** fluorescence images of an engineered tissue construct cultured for 0 and 2 days, respectively, in which red and green filaments correspond to channels lined with red fluorescent protein-expressing HUVECs and green fluorescent protein-expressing human neonatal dermal fibroblast (HNDFs) cells-laden gelMA ink, respectively. The cross-sectional view shows that endothelial cells line the lumens within the embedded 3D microvascular network. Scale bar is 300 μm. Reproduced from ref. [173] with permission from John Wiley & Sons.

5. Bringing multifunctionality to cell encapsulation systems

5.1 Stimuli-responsive strategies

To sustain life and maintain biological function, nature requires selectively tailored and adaptive molecular assemblies and interfaces that provide a specific chemical function and structure [223]. Based on that, different stimuli-responsive and "adaptative" systems that are capable of conformational and chemical changes on receiving an external signal are being developed. These changes are accompanied by variations in the physical properties of the polymers employed within the hydrogel matrix or within components added to its matrix, such as embedded materials, or by functionalizing coatings that surround the hydrogel matrix. The signal is derived from changes in the matrix environment, such as a change in temperature, pH, chemical composition (e.g. redox stimulus) or applied mechanical force, or that can be triggered exogenously by irradiation with light (UV, laser, visible) or exposure to an electrical and magnetic field. All the referred stimuli are widely used in drug delivery systems, in which pH and redox stimuli are the most common since they exist naturally in certain pathological sites as well as in all cancer cells [224, 225]. However, being the focus of the present review cell encapsulation strategies for tissue regeneration, only temperature-, light-, and magnetic-responsive stimuli will be discussed in the following section, since those are the most common.

5.1.1 Temperature-responsive cell encapsulation systems

The most widely used temperature-responsive systems are related with the crosslinking process to fabricate *in situ* forming hydrogels. Those hydrogels are composed by thermoresponsive polymers that exhibit a lower critical solution temperature (LCST) and form a gel upon temperature increase [226]. The process is reversible, and the polymers return into solution when the temperature is lowered below the LCST. Thermally responsive hydrogel systems based on natural polymers (such as alginate, chitosan, cellulose derivatives, gelatin, hyaluronic acid) and synthetic polymers (e.g., N-

isopropylacrylamide (NiPAAm), poly(ethylene oxide)–*b*-poly(propylene oxide)–*b*-poly(ethylene oxide) (PEO–PPO–PEO) triblock copolymers, PEG-biodegradable polyester copolymers, poly(organophosphazenes) and *2*-(dimethylamino) ethyl methacrylate) have been proposed for biomedical applications [227, 228]. The theories and mechanisms behind thermogelation have already been very well summarized in previous articles [227]. Thermally responsive systems are particularly appealing in biomedical applications, mainly because their gelation can be triggered by temperature change from ambient to physiological conditions. Therefore, it allows the implantation of hydrogels by minimally invasive procedures, since before implantation the hydrogel is in a liquid state. Additionally, after injection of the pre-hydrogels, the solution can easily achieve different complex and matched conformations to the lesion site. Some of the challenges with this type of hydrogels involved precise control over the LCST and gelation kinetics, stability and mechanical properties as well as degradation profiles. A major problem observed in some thermally responsive systems is syneresis, especially in NiPAAm hydrogels. Syneresis is characterized by high amounts of water expel from the hydrogel matrix after gelation. This fact may prove problematic for various biomedical applications, for example in the case of an injectable hydrogel not conforming to the shape of a defect after shrinkage, or reduced water contents impairing diffusion of essential molecules to encapsulated cells compromising its viability [229]. To stabilize hydrogel matrixes and mitigate syneresis biodegradable methacrylated thermogelling macromers (MA-TGMs) have been proposed [230]. These macromers are made from a statistical copolymer of NiPAAm, acrylamide, and mono-acryloxyethyl phosphate (MAEP) that are esterified with glycidyl methacrylate after polymerization to yield dual-gelling macromers. These macromers are particularly promising for cell encapsulation applications, as they facilitate biointegration of the hydrogels and degradation via hydrolysis of phosphate ester bonds of MAEP. Hydrolysis of phosphate ester bonds of MAEP is accelerated in the presence of the naturally occurring enzyme alkaline phosphatase, which is upregulated in areas of regenerating bone tissue. Hydrogels that readily undergo enzymatic degradation have

demonstrated improved bone growth and infiltration into hydrogels [60]. Two formulations (high and low MAEP content) of these dual gelling macromers were selected for *in vitro* and *in vivo* characterization to evaluate their potential to encapsulate MSCs and regenerate bone tissue [231]. Results showed that functionalized hydrogels from macromer solutions and encapsulating MSCs were able to induce bone growth into and across a critical-size rat cranial defect, as well as accelerated mineralization and helped facilitating bony integration. Furthermore, phosphate groups incorporated in MAEP improved bony integration and bone regeneration, while the degradation of phosphate ester bonds helped facilitating infiltration of bone tissue.

In another approach towards tissue regeneration, induced pluripotent stem cells (iPSCs) were encapsulated within thermogelling hydrogels that were implanted by injection based on amphiphatic carboxymethylhexanoyl chitosan [232] and adipose-derived stem cells (ASCs) within aminated hyaluronic acid-*g*-poly(N-isopropylacrylamide) hydrogels [233]. In both temperature-responsive cell encapsulation strategies, encapsulated cells remained viable and expressed stem cell markers within the hydrogels. The former hydrogel promoted corneal wound repair and reconstruction in an animal model with severe cornea damage, while the later was proposed for adipose TERM. The potential of the proposed strategies as *in situ* forming biomaterials has rendered these hydrogels very attractive for TERM applications as they can be implanted by injection, thus allowing minimal invasive procedures.

In a different approach, the thermal behavior of polymers employed in cell encapsulation systems can be also applied as porogens to induce porosity in the hydrogel matrix. The principle of the process is the opposite on *in situ* gelation of hydrogels, i.e. the polymers employed are in gel state at low temperatures and become liquid when the temperature increases to a certain value, depending on the nature of the polymer used. Gelatin is a frequently employed polymer to fabricate those types of cell encapsulation systems. At 4°C gelatin forms a hydrogel matrix and at physiological temperature it becomes a liquid. Based on that, alginate hydrogels incorporating gelatin microbeads as porogens were proposed. The creation of pores inside the

alginate hydrogel matrix was mediated by the dissolution of gelatin microparticles after incubation at 37°C. This thermo-responsive hydrogel architecture resulted in increased cell proliferation compared to alginate hydrogels without the gelatin microbeads [234]. In a similar approach, gelatin microbeads were used both as chondrocytes carriers and porogens in alginate hydrogels [235]. The gelatin microbeads were completely dissolved after two days of incubation at 37°C. Subsequently, the encapsulated chondrocytes occupied the created empty spaces within the alginate matrix and formed viable aggregates. Other shapes of such sacrificial elements could be explored, including fibers or branched structures to allow culture medium or blood perfusion in the hydrogel.

Temperature-responsive polymers can also be used to functionalize the hydrogel matrix and improve specific features important for the success of cell encapsulation strategies. For example, the triblock copolymer PEO-PPO-PEO, a class of synthetic materials with thermally responsive properties, was conjugated with transforming growth factor (TGF)-β1 to induce the chondrogenic differentiation of encapsulated ASCs [236] or with the arginine-glycine-aspartic acid (RGD) peptide sequence, a ubiquitous cell-binding domain found in many ECM molecules, well-known to mediate and enhance cell attachment to the hydrogel matrix [237]. The incorporation of biomolecules within the matrix of hydrogels to modulate the behavior of the encapsulated cells, not necessarily composed by temperature-responsive polymers, will be detailed addressed in section *5.2 Incorporation of bioactive molecules*. Another example of the contribution of a temperature-responsive polymer to enhance specific properties of the hydrogel matrix uses thermosensitive microparticles composed by poly(lactic-*co*-glycolic acid) (PLGA) and PEG within PEO-PPO-PEO hydrogels [238]. When the temperature increased to physiological levels, the microparticles became cohesive and adhered to each other. Then, the hydrophilic environment provided by the temperature-responsive PEO–PPO–PEO hydrogel caused leaching of PEG microparticles. Consequently, with the release of PEG to the hydrogel matrix, its mechanical properties were significantly enhanced. No assay with

encapsulated cells was performed, but the authors suggest its applicability for growth factors incorporation and/or cell encapsulation due to the mild conditions of the process. Due to the observed high mechanical strength, future studies with this hydrogel should focus on its osteogenic potential for bone TERM.

5.1.2 Light-activated cell encapsulation systems

Similar to temperature-responsive strategies for *in situ* crosslinking, light-responsive hydrogels are also of particular interest in biomedical applications requiring *in situ* non-toxic gelation, such as cell encapsulation strategies. The principle in light-responsive hydrogel crosslinking is based on the presence of free radicals that lead to the fast formation of covalent bonds between macromolecular precursor molecules, resulting in the formation of a polymer network with uniform and replicable physical properties [25, 239]. Long-wave UV light-activated polymerization is on of the most common methods of forming cell encapsulation strategies because of the advantages of temporal and spatial control of the reaction, low energy requirements, and clinically acceptable curing times [240]. Photopolymerization can thus be easily performed at physiological temperature and pH, while enabling the implantation of photopolymerized hydrogels encapsulating cells by minimally invasive procedures. The critical aspects to consider in photopolymerized hydrogel in cell encapsulation are the required non-toxicity of the photoinitiator (PI) and the irradiation with an appropriate wavelength and time. As the PI incorporated within the hydrogel matrix is irradiated with light, free radicals dissociate from the PI and attack with high efficiency vinyl groups on precursor macromolecules, creating covalent bonds that rapidly promote the crosslink within seconds to minutes of UV light exposure. However, photoinitiator solutions associated with free-radical generation can lead to cell toxicity [241]. Therefore, some critical shortcomings related with the use of PIs in cell encapsulation strategies, including its limited water solubility, sub-optimal crosslinking efficiency when applied with safe light spectra (i.e. ≥ 350 nm), and the toxic reaction conditions of the free radicals must be considered before

designing cell encapsulation strategies [242]. Consequently, among the many initiator systems available for photopolymerization, only a few have been identified as suitable for cell encapsulation systems. Studies providing a better understanding of the interplay between the radical crosslinking efficiency, hydrogel network formation, and cytotoxicity using photopolymerized hydrogels for cell encapsulating are thus of extreme importance. Hydrogels were photopolymerized from PEG-DA or PEG-fibrinogen precursors using different Irgacure PIs (I2959, I184 and I651), together with the chemical initiator/accelerator ammonium persulfate/tetramethylethylenediamine [239]. The study evaluated the influence of PI type, concentration and UV light intensity, and how these affected the mechanical properties of the hydrogel, the crosslinking reaction time and the viability of encapsulated cells. For this purpose, a biosynthetic hybrid hydrogel synthesized from functionalized PEG conjugated to fibrinogen and encapsulating bovine aortic smooth muscle cells (SMCs) was used. The photoinitiators I2959 and I184 were identified as suitable for achieving both cell viability and efficient crosslinking, contrary to the results obtained with I651. Optimization of PI concentration or irradiation intensity was particularly important for achieving maximum mechanical properties; a sub-optimal choice of PI concentration or irradiation intensity resulted in a substantial reduction in the elastic modulus. The viability of the encapsulated SMCs may be compromised by unnecessarily prolonging exposure to cytotoxic free radicals or inadvertently enhancing the instantaneous dose of radicals in solution, both of which are dependent on the PI type/concentration and irradiation intensity. In the absence of a radical initiator, the short exposures to long-wave UV light irradiation did not prove to be cytotoxic.

I2959 photoinitiator was used to yield the crosslinking of DEX-MA hydrogels [149]. L929 cells were suspended in the DEX-MA solution and dispensed on the surface of the SH surfaces. Due to surface repellency, spherical drops were obtained, which were then crosslinked using UV-light. Subsequently, the microbeads were encapsulated in alginate hydrogels using again the SH surfaces. This type of photo-responsive strategy allowed creating a

multicompartmentalized cell encapsulation strategy. These types of cell encapsulation systems will be discussed in detail in section *5.3 Multicompartmentalization*.

In a different perspective, photo-responsive cell encapsulation systems can be used to control specific properties of the hydrogel matrix, such as its degradation. This strategy emerges as an alternative to hydrolysis and enzymolysis, the two most commonly used mechanisms to control hydrogel degradation. Although both mechanisms are effective, the rate of degradation cannot be adjusted or arrested after the hydrogel is fabricated. Additionally, the degradation of hydrogels occurring by hydrolysis and enzymolysis cannot be spatially controlled. In contrast, photodegradation allows external real-time spatial and temporal control over hydrogel properties. This represents a great advantage for cell encapsulation strategies aiming tissue regeneration, because the properties of the encapsulation matrix can be tailored to match the time required for the natural regeneration process of the damaged tissue. For example, different macromers were synthesized incorporating photodegradable *ortho*-nitrobenzyl (*o*-NB) groups in the macromer backbone [243]. To show the applicability of the synthetized hydrogels to encapsulated cells, human mesenchymal stem cells were used. Results showed high viability rates. By exploiting the differences in reactivity of different *o*-NB linkers, the degradation rate of the hydrogels could be precisely controlled.

Others have proposed controlling the material properties of hydrogels both dynamically and in a user defined fashion using cleavable chemistries whose degradation can be triggered exogenously. Toward this end, different groups have presented a class of photodegradable hydrogels whose physical and chemical properties can be modified by light post-fabrication with full spatial and temporal control [244-246]. Within the TERM field, those hydrogels are particularly interesting since they allow controlling the extracellular microenvironment in the presence of cells in 3D, while providing insights of the microenvironment in real time [247-250].

5.1.3 Magnetic-responsive cell encapsulation systems

While the majority of temperature- and light-responsive cell encapsulation systems emerged as *in situ* crosslinking strategies, magnetic-responsive cell encapsulation systems have emerged as a new strategy to manipulate and/or stimulate cell encapsulation systems. This strategy exploits interactions between encapsulation devices and magnetic fields that can be either static [251] or alternating fields established by a magnet [252] or electromagnet [253]. Magnetic assembly of cell encapsulating systems into 3D structures has been recently reported for TERM [214, 215, 253-255]. Specifically, magnetic nanoparticles (MNPs) have been loaded in cell-encapsulating microscale hydrogels (M-gels) to create composite smart materials responsive to magnetic fields. As an example, gelMA hydrogels were produced co-encapsulating 3T3 cells and MNPs [214]. By spatially controlling the magnetic field, these composite hydrogel building blocks could be manipulated to construct 3D structures with variable geometries, as well as to control the composition of the hydrogel matrix by creating multilayers. MNPs have also been used to stimulate encapsulated stem cells into a specific differentiation lineage. This can be achieved by manipulation or mechanical activation of cellular pathways, such as the mechano-gated potassium channel TREK-1, and integrin signaling such as the RGD transmembrane protein, which have been showed to enhance the osteogenic and chondrogenic potential of magnetic labeled bone marrow MSCs encapsulated in alginate/chitosan spherical hydrogels [256]. Others, have showed to enhance the chondrogenic potential of ASCs encapsulated in κ-carrageenan hydrogels containing within its matrix MNPs [257].

In order to physically isolate the co-encapsulated cells and MNPs, different multicompartmentalized strategies were proposed [86, 258], which will be further discussed in detail (section *5.3 Multicompartmentalization*). A major concern of incorporating MNPs in the cell encapsulation matrix is their release as the hydrogel degrades, although it was demonstrated that the released MNPs from gelMA hydrogels had no adverse effect on the viability of NIH 3T3 cells [259]. However, because of the risk of heavy metal poisoning from iron oxide, the use of such MNPs in clinical applications has to be proven.

Additionally, the distribution of MNPs in M-gels may differ due to aggregation of the MNPs in the pre-polymeric solutions, which may reduce the affinity of M-gels to the magnetic field (MF) [260, 261]. Another potential drawback with this method is that a certain amount of heat generated by MNPs exposure to an alternating current-based MF (magnetic hyperthermia) may compromise the viability of the encapsulated cells [254].

Alternatives without integrating hydrogels with other magnetic components, such as MNPs, were successfully proposed using their paramagnetic free radicals when placed in a magnetic field [214, 262, 263]. Radicals can be utilized to change the magnetic susceptibility of liquids on each the levitation of structures is performed (suspension liquids) or they can be directly incorporated in the encapsulation matrix for guided levitational self-assembly [263]. Magnetization of the TE systems via free radicals is a versatile and robust strategy, and cell encapsulation can be performed before radical exposure for magnetization.

The magnetic manipulation of fibers was also reported to control and align fibers into specific patterns [264, 265]. This hierarchical organization allows the hydrogel matrix to take a variety of forms in different tissues and at different stages of development in the same tissue. Moreover, the biological assemblies, disassembly and re-assembly are dynamic during the transition to accomplish local and global conformational changes. Additionally, with this strategy it is possible to guide the cell growth at specific directions by regulating the magnetic fibers.

5.2 Incorporation of bioactive molecules

Interactions of cells and ECM initiate signaling cascades involved in critical cell functions, such as regeneration [266-268]. An important goal of cell encapsulation systems aiming tissue regeneration is to mimic critical aspects of the extracellular environment in order to ensure the viability of the encapsulated cells while controlling different cellular functions through cell-material interactions. This prompted the encapsulation of cells with biomolecules, which encompass nowadays a major area of investigation in

TERM and regenerative medicine field. Challenges of this strategy include all the critical properties above discussed to fabricate cell encapsulation systems (section *2.1 Critical properties*) with the addition of critical properties to develop systems incorporating biomolecules, such as the bioactivity preservation and a sustained release. Additionally, when designing these types of combined systems, the incorporation of biomolecules at the right concentration in the right context and, when aimed, release with the right profile must be carefully pondered. The incorporation of different biomolecules can be directly within the biomaterials employed or indirectly by first encapsulating the biomolecule in micro- or nano-sized spheres (particles or beads) or fibers, which are then embedded in the system.

Encapsulation of biomolecules directly in the core of the cell encapsulation system is easily achieved during gelation and provides a simple way to entrap molecules of interest. For example, TGF-β1 was co-encapsulated with Sca-1^{+}/$CD45^{-}$ cardiac progenitor cells (CPCs) in high molecular weight heparin-containing hyaluronic acid-based hydrogels [269]. Results showed that TGF-β1 was able to induce the differentiation of CPCs into endothelial cells, which formed vascular-like networks within the hydrogel. Due to the electrostatic association between heparin and TGF-β1, which was enhanced due to the high molecular weight of heparin, a portion of the initially encapsulated growth factor remains immobile. Therefore, TGF-β1 could be provided to the encapsulated cells since it did not diffuse out from the hydrogel. In fact, the rapid loss of the entrapped biomolecule from the system is a major concern when direct encapsulation methodology is employed. Consequently, this method is more appropriate for molecules in a limited molecular weight range (i.e., similar to the network mesh size), and those that are relatively stable and have a long half-life. Therefore, indirect entrapment of biomolecules is more often used in TERM strategies. For example, TGF-β3 was encapsulated in gelatin beads, which were subsequently incorporated in a collagen-low molecular weight hyaluronic acid semi-interpenetrating network encapsulating MSCs. This injectable system supported *in vitro* and *in vivo* the growth of nasal chondrocytes and chondrogenic differentiation and MSCs, and was proposed

for nucleus pulposus regeneration [270]. In a similar strategy, but using fibers as drug carriers, electrospun polycaprolactone (PCL) nanofibers were used as drug carriers of bovine serum albumin [271]. The nanofibers were then embedded in PEG hydrogel encapsulating fibroblasts. In the case of indirect methods, a complex coacervation methodology was recently proposed in order to eliminate the step of encapsulating the biomolecule within drug carriers previous to its addition to the cell encapsulating system [272]. Complex coacervation is defined as liquid-liquid phase separation in an aqueous solution by spontaneous aggregation associated with electrostatic matching between two oppositely charged polyelectrolytes [273]. Based on that, coacervate-laden photo-crosslinked hydrogels were produced from the simple mixing of oxidized methacrylated alginate (OMA) and gelMA in aqueous solution. Bone morphogenic protein (BMP)-2 was incorporated in the gelMA solution, which mainly comprised the resulting coacervate microdroplets, and MSCs in OMA. Within the resultant compartments, MSCs differentiated into the osteogenic lineage due to the internal sustained release of BMP-2. Combined direct and indirect encapsulation of biomolecules was achieved by embedding PLGA microparticles within the matrix of alginate hydrogels through a coaxial electro-dropping method [179]. Two different osteogenic biomolecules, namely BMP-2 and dexamethasone (Dex), were co-encapsulated with bone marrow MSCs. Consequently, two different co-encapsulation systems were produced by switching the position of BMP-2 and Dex, either in the PLGA microparticles or in the alginate matrix. Based on the localization of BMP-2 and Dex, their release profiles were very unique on a temporal basis. An initial burst of biomolecules was highly suppressed when either biomolecule was loaded in the PLGA core. Therefore, the release profiles of each biomolecule could be easily manipulated alternately positioning biomolecules in the embedded microparticles or in the hydrogel matrix domain. Alternatively to large biomolecules and growth factors encapsulation, biochemical signals can also be integrated by incorporating smaller molecules, such as peptides, in cell encapsulation systems, targeting a desired cellular response. MSCs were induced to differentiate towards osteogenic or adipogenic pathways by

introducing in PEG hydrogels tethered small-molecule chemical functional groups, namely *2*-aminoethyl methacrylate, *t*-butyl methacrylate, ethylene glycol methacrylate phosphate, *2,2,3,3*-tetrafluoropropyl methacrylate and methacrylic acid [274]. In response to the small-molecule incorporated, encapsulated MSCs changed its morphology and differentiated in the absence of soluble signals, thus highlighting the crucial role that cell-material interactions have in cell fate.

Another study developed an agarose hydrogel with a concentration gradient of immobilized vascular endothelial growth factor (VEGF)-165 [275]. By mimicking the cues that guide endothelial cells (ECs) during vascular development, ECs were shown to follow the concentration gradient of VEGF-165 in the 3D hydrogel, with the identification of tip and stalk cells and the formation of tubular-like structures. Furthermore, the stem cell differentiation could be controlled in the developed 3D hydrogels by taking advantage of orthogonal physical binding pairs, such as barnase, an extracellular RNase of Bacillus amyloliquefaciens, with its intracellular inhibitor barstar, and streptavidin-biotin [276]. This allowed the simultaneous immobilization of multiple growth factors.

In a different perspective, the encapsulated cells can also release different biotherapeutics itself, which in fact constitute the first impetus when cell encapsulation systems were proposed. However, in the present review, the biotherapeutics release ability of encapsulated cells will not be addressed (for that subject we advise the reading of [277]), as here we intend to review the multifunctionality of cell encapsulation systems on a material engineering basis.

5.3 Multicompartmentalization

Inspired by the natural multicompartmentalized complex system of cells, in which a wide range of isolated components with specific functions are grouped together in a single compartment, different miniaturized compartmental engineered systems have been proposed in fields such as catalysis, sensors, drug delivery, microreators, and theoretical models of cellular events and

diseases [158, 168, 278-280]. The idea is *"to borrow Nature's design strategies to achieve novel functional materials, with highly useful properties exceeding by far those available by current methods"* [281], but *"not to copy Biology: learning in modesty from her principles and to transfer it to materials space and conditions previously not accessible to biology"* [282]. Inspired by that, and particularly for cell encapsulation systems, the idea is not to mimic intracellular reactions, but rather construct a customizable system by assembling subcompartments to ultimately giving raise to a complex system with improved cell viability and functionality. Different groups have recently begun to explore the field and its application in TERM. For example, Janus particles, i.e. anisotropic particles that contain distinct compositions in each hemisphere, were proposed to physically isolate encapsulated cells from MNPs [258]. Alginate Janus particles, produced in a microfluidic chip, were composed by one magnetic hemisphere with MNPs, and one hemisphere with HeLa cells. The strategy was proposed as an alternative to magnetic labeling of cells via uptake of surface functionalized magnetic beads, which can lead to undesirable effects on cells [283]. Also aiming to physically isolate cells from MNPs, a capsule-in-capsule system was proposed for the treatment of diabetes [86]. The idea was to confer to the cell encapsulation system the ability to be detectable by clinically applicable non-invasive imaging modalities, such as magnetic resonance, computed tomography, and ultrasound imaging, in order to monitor over time and assess the efficacy of islets transplantation and engraftment. However, a high concentration of iron and gold nanoparticles is required to achieve a sufficient amount of contrast signal to be detectable by the referred methods, which could be harmful to the encapsulated cells. Therefore, nanoparticles were encapsulated in a primary inner capsule of alginate, and then added to a secondary outer capsule containing the therapeutic isles cells. Also using MNPs, three-layer spheroids composed by magnetic gelMA M-gels encapsulating NIH 3T3 cells were fabricated onto the tip of a magnetic rod [214]. Three fluorochromes, namely rhodamine-B (red) in the first layer, FITC-dextran (green) in the second layer, and *1,1,4,4*-tetraphenyl-*1,3*-butadiene (blue) in the third layer, were used as a proof-of-concept to show that three

different compartments could be easily created (in seconds) by magnetic manipulation. Each layer was stabilized via a second crosslinking procedure using filling layers of PEG. A filling layer between multiple M-gels permitted to increase cell-cell distances and thus isolate the different layer compartments. A similar multicompartmentalized cell encapsulation strategy resembling "onion-like" structure using alginate and L929 cells was achieved without magnetic manipulation but using the unique repellency properties of SH surfaces [148]. A remarkable advantage of this technique, especially when combining cell encapsulation with drug loading, is that high encapsulation efficiencies (of ca. 100%) of non-volatile molecules can be achieved under mild conditions. This is possible because each compartmentalized layer solidifies in air rather than in contact with a liquid solvent. Hence, one avoids the possibility of molecules migration, and thus any loss during the preparation of the particles. Others explored different spatial organization of compartmentalized layers inside a single cell encapsulation system by microfluidic electrostatic spraying technique [284]. For that, cell encapsulation systems were produced using double layer, side-by-side or triple-layer conformities. In each compartment, different cells were encapsulated, each one fluorescently stained with different dyes. The system was tested for different potential applications, such as size-controlled tumor micro tissues and its implications in cancer diagnostics, and a scalable platform for 3D co-culture. Similarly to multilayered spherical systems, also multilayered fiber-shaped systems have been reported for cell encapsulation [127, 204]. Recently, core-shell hydrogel fibers were successfully generated using the dual concentric nozzle by the simultaneous injection of collagen and alginate solutions in the core and shell, respectively [204]. By encapsulating MCs, osteoblasts, and bioactive glass nanoparticles (BGn) were also incorporated within the multilayered fibers. By varying the position and presence of the encapsulated cells and BGn within the fibers compartments, different formulations could be obtained. In a higher scale level, such fibers could be organized into more complex 3D shapes using established rapid prototyping methods.

In a different perspective, compartmentalization was used to avoid protrusion of the encapsulated cells [183]. In the proposed system, alginate with different mechanical stabilities was used to facilitate growth of the cells in the core of the capsules, but to kill cells that might escape from the capsule and invade the host. For that, 3.4% intermediate-G alginate was employed to fabricate the core encapsulating cells, while 2% high-G alginate was employed in the outer layer, since it was showed to jeopardize cell survival.

It is expected that advances in bottom-up and top-down technologies will originate the development of new hierarchical and complex structures with sophisticated geometries [285], as well as production on a massive scale and a wider clinical application of those systems.

6. Conclusion

Since the early pioneering period, the technology of mammalian cell encapsulation has developed significantly in such a way that nowadays cell encapsulation is an evolving branch of TERM. The application of cell encapsulation principles in the TERM field brought new possibilities for the development of highly complex cell culture systems. The use of such systems for tissue regeneration holds tremendous promise, also because this technology attempts to keep pace with recent molecular biology breakthroughs. This allows increasing the complexity of the systems by recreating adequate environmental signals found in native tissue (in particular during the regenerative process) to control the cellular outcome, and conferring multifunctional properties, namely the incorporation of bioactive molecules and the ability to create smart and adaptive systems in response to different stimuli. In parallel, advances in the production methods and characterization techniques have contributed for the improved performance of these systems. Yet many difficulties remain, some of which will certainly challenge our scientific creativity. The stepwise analysis of the essential obstacles, coupled with increased international collaboration, should move the technology forward in a careful and controlled way, and bring it much closer to clinical reality [114]. This ambitious goal requires the interdisciplinary and

integrated effort of scientists with different areas of expertise such as genetics, materials science, physicochemistry and chemical engineering, pharmaceutical technology, cell biology and medicine [178]. Issues on long term viability, risk of immune response, together with the development of high biocompatible materials, with sufficient durability and appropriate permeability, should be addressed to further explore their possible clinical applications.

Acknowledgements

The authors are grateful to the Portuguese Foundation for Science and Technology (PhD grant SFRH/BD/61126/2009) and the European Research Council (grant agreement ERC-2014-ADG-669858-ATLAS) for funding. The authors are also thankful to Dr. Luca Gasperini for his help in Figure I.1.

References

[1] V.V. Bisceglie, Uber die antineoplastische Immunitat, Z. Krebsforsch, 40 (1933) 141-158.

[2] G.H. Algire, J.M. Weaver, R.T. Prehn, Growth of cells in vivo in diffusion chambers - I Survival of homografts in mice, J. Natl. Cancer Inst., 15 (1954) 493–507.

[3] T.M.S. Chang, Semipermeable microcapsules, Science, 146 (1964) 524-525.

[4] W.L. Chick, A.A. Like, V. Lauris, Beta cell culture on synthetic capillaries: An Artificial endocrine pancreas, Science, 187 (1975) 847-849

[5] D. Ferreira, E. Westman, H. Eyjolfsdottir, P. Almqvist, G. Lind, B. Linderoth, A. Seiger, K. Blennow, A. Karami, T. Darreh-Shori, M. Wiberg, A. Simmons, O. Wahlund, L. Wahlberg, M. Eriksdotter, Brain changes in Alzheimer's disease patients with implanted encapsulated cells releasing nerve growth factor, J. Alzheimers Dis., 43 (2015) 1059–1072.

[6] O. Lindvall, L. Wahlberg, Encapsulated cell biodelivery of GDNF: A novel clinical strategy for neuroprotection and neuroregeneration in Parkinson's disease?, Exp. Neurol. , 209 (2008) 82–88.

[7] R. Krishnan, M. Alexander, L. Robles, C.E.F. 3rd, J.R.T. Lakey, Islet and stem cell encapsulation for clinical transplantation, Rev. Diabet. Stud., 11 (2014) 84–101.

[8] F. Lim, A.M. Sun, Microencapsulated islets as bioartificial endocrine pancreas, Science, 210 (1980) 908-910.

[9] J. Koo, T. Chang, Secretion of erythropoietin from microencapsulated rat kidney cells, Int. J. Artif. Organs, 16 (1993) 557–560.

[10] P. Chang, N. Shen, A. Westcott, Delivery of recombinant gene products with microencapsulated cells in vivo, Hum. Gene Ther., 4 (1993) 433-440.

[11] H. Liu, F. Ofosu, P. Chang, Expression of human factor IX by microencapsulated recombinant fibroblasts, Hum. Gene Ther., 4 (1993) 291–301.

[12] D. Cieslinski, H. Humes, Tissue engineering of a bioartificial kidney, Biotechnol. Bioeng., 43 (1994) 678–681.

[13] H. Wong, T. Chang, Bioartificial liver: Implanted artificial cells microencapsulated living hepatocytes increases survival of liver failure rats, Int. J. Artif. Organs, 9 (1986) 335-336.

[14] P. Aebischer, P. Russell, L. Christenson, G. Panol, J. Monchik, P. Galletti, A bioartificial parathyroid, ASAIO Trans., 32 (1986) 134-137.

[15] P. Aebischer, M. Goddard, A. Signore, R. Timpson, Functional recovery in hemiparkinsonian primates transplanted with polymer-encapsulated PC12 cells, Exp. Neurol., 126 (1994) 151-158.

[16] F.B. Barton, M.R. Rickels, R. Alejandro, B.J. Hering, S. Wease, B. Naziruddin, J. Oberholzer, J.S. Odorico, M.R. Garfinkel, M. Levy, F. Pattou, T. Berney, A. Secchi, S. Messinger, P.A. Senior, P. Maffi, A. Posselt, P.G. Stock, D.B. Kaufman, X. Luo, F. Kandeel, E. Cagliero, N.A. Turgeon, P. Witkowski, A. Naji, P.J. O'Connell, C. Greenbaum, Y.C. Kudva, K.L. Brayman, M.J. Aull, C. Larsen, T.W. Kay, L.A. Fernandez, M.C. Vantyghem, M. Bellin, A.M. Shapiro, Improvement in outcomes of clinical islet transplantation: 1999–2010, Diabetes Care, 35 (2012) 1436–1445.

[17] A.K. Brun-Graeppi, C. Richard, M. Bessodes, D. Scherman, O.W. Merten, Cell microcarriers and microcapsules of stimuli-responsive polymers, J. Controlled Release, 149 (2011) 209-224.

[18] S. Mazzitelli, L. Capretto, F. Quinci, R. Piva, C. Nastruzzi, Preparation of cell-encapsulation devices in confined microenvironment, Adv. Drug Delivery Rev., 65 (2013) 1533-1555.

[19] H. Tian, Z. Tang, X. Zhuang, X. Chen, X. Jing, Biodegradable synthetic polymers: Preparation, functionalization and biomedical application, Prog. Polym. Sci., 37 (2012) 237-280.

[20] J. Wilson, T. McDevitt, Stem cell microencapsulation for phenotypic control, bioprocessing, and transplantation, Biotechnol. Bioeng., 110 (2013) 667-682.

[21] A.S. Hoffman, Hydrogels for biomedical applications, Adv. Drug Delivery Rev., 64 (2012) 18-23.

[22] L. Gasperini, J.F. Mano, R.L. Reis, Natural polymers for the microencapsulation of cells, J. R. Soc. Interface, 11 (2014) 20140817.

[23] T.H. Silva, A. Alves, B.M. Ferreira, J.M. Oliveira, L.L. Reys, R.J.F. Ferreira, R.A. Sousa, S.S. Silva, J.F. Mano, R.L. Reis, Materials of marine origin: A review on polymers and ceramics of biomedical interest, Int. Mater. Rev., 57 (2012) 276-306.

[24] J.J. Schmidt, J. Rowley, H.J. Kong, Hydrogels used for cell-based drug delivery, J. Biomed. Mater. Res. Part A, 87 (2008) 1113–1122.

[25] P. de Vos, H.A. Lazarjani, D. Poncelet, M.M. Faas, Polymers in cell encapsulation from an enveloped cell perspective, Adv. Drug Delivery Rev., 67-68 (2014) 15-34.

[26] R. Silva, B. Fabry, A.R. Boccaccini, Fibrous protein-based hydrogels for cell encapsulation, Biomaterials, 35 (2014) 6727-6738.

[27] J.F. Mano, G.A. Silva, H.S. Azevedo, P.B. Malafaya, R.A. Sousa, S.S. Silva, L.F. Boesel, J.M. Oliveira, T.C. Santos, A.P. Marques, N.M. Neves, R.L. Reis, Natural origin biodegradable systems in tissue engineering and regenerative medicine: Present status and some moving trends, J. R. Soc. Interface, 4 (2007) 999-1030.

[28] C.R. Correia, R.L. Reis, J.F. Mano, Multilayered hierarchical capsules providing cell adhesion sites, Biomacromolecules, 14 (2013) 743-751.
[29] H. Onoe, T. Okitsu, A. Itou, M. Kato-Negishi, R. Gojo, D. Kiriya, K. Sato, S. Miura, S. Iwanaga, K. Kuribayashi-Shigetomi, Y.T. Matsunaga, Y. Shimoyama, S. Takeuchi, Metre-long cell-laden microfibres exhibit tissue morphologies and functions, Nat. Mater., 12 (2013) 584-590.
[30] E.G. Popa, S.G. Caridade, J.F. Mano, R.L. Reis, M.E. Gomes, Chondrogenic potential of injectable kappa-carrageenan hydrogel with encapsulated adipose stem cells for cartilage tissue-engineering applications, J. Tissue Eng. Regener. Med., 9 (2015) 550-563.
[31] S.C. Neves, D.B. Gomes, A. Sousa, S.J. Bidarra, P. Petrini, L. Moroni, C.C. Barrias, P.L. Granja, Biofunctionalized pectin hydrogels as 3D cellular microenvironments, J. Mater. Chem. B, (2015).
[32] P. de Vos, M. Faas, B. Strand, R. Calafiore, Alginate-based microcapsules for immunoisolation of pancreatic islets, Biomaterials, 27 (2006) 5603–5617.
[33] P. de Vos, M. Bucko, P. Gemeiner, M. Navratil, J. Svitel, M. Faas, B.L. Strand, G. Skjak-Braek, Y.A. Morch, A. Vikartovska, I. Lacik, G. Kollarikova, G. Orive, D. Poncelet, J.L. Pedraz, M.B. Ansorge-Schumacher, Multiscale requirements for bioencapsulation in medicine and biotechnology, Biomaterials, 30 (2009) 2559-2570.
[34] E.H. Nafea, A. Marson, L.A. Poole-Warren, P.J. Martens, Immunoisolating semi-permeable membranes for cell encapsulation: Focus on hydrogels, J. Controlled Release, 154 (2011) 110-122.
[35] S. Schneider, P.J. Feilen, V. Slotty, D. Kampfner, S. Preuss, S. Berger, J. Beyer, R. Pommersheim, Multilayer capsules: A promising microencapsulation system for transplantation of pancreatic islets, Biomaterials, 22 (2001) 1961–1970.
[36] L.M. Weber, C.Y. Cheung, K.S. Anseth, Multifunctional pancreatic islet encapsulation barriers achieved via multilayer PEG hydrogels, Cell Transplant., 16 (2008) 1049–1057.

[37] Y. Teramura, Y. Kaneda, H. Iwata, Islet-encapsulation in ultra-thin layer-by-layer membranes of poly(vinyl alcohol) anchored to poly(ethylene glycol)-lipids in the cell membrane, Biomaterials, 28 (2007) 4818–4825.
[38] S. Krol, S.d. Guerra, M. Grupillo, A. Diaspro, A. Gliozzi, P. Marchetti, Multilayer nanoencapsulation. New approach for immune protection of human pancreatic islets, Nano Lett., 6 (2006) 1933–1939.
[39] R.R. Costa, J.F. Mano, Polyelectrolyte multilayered assemblies in biomedical technologies, Chem. Soc. Rev., 43 (2014) 3453-3479.
[40] J. Borges, J.F. Mano, Molecular interactions driving the layer-by-layer assembly of multilayers, Chem. Rev., 114 (2014) 8883-8942.
[41] P. Sher, C.A. Custodio, J.F. Mano, Layer-by-layer technique for producing porous nanostructured 3D constructs using moldable freeform assembly of spherical templates, Small, 6 (2010) 2644-2648.
[42] N.L. Costa, P. Sher, J.F. Mano, Liquefied capsules coated with multilayered polyelectrolyte films for cell immobilization, Adv. Eng. Mater., 13 (2011) B218-B224.
[43] C.R. Correia, P. Sher, R.L. Reis, J.F. Mano, Liquified chitosan–alginate multilayer capsules incorporating poly(L-lactic acid) microparticles as cell carriers, Soft Matter, 9 (2013) 2125-2130.
[44] P. Sher, C.R. Correia, R.R. Costa, J.F. Mano, Compartmentalized bioencapsulated liquefied 3D macro-construct by perfusion-based layer-by-layer technique, RSC Adv., 5 (2015) 2511-2516.
[45] Y. Navaro, N. Bleich-Kimelman, L. Hazanov, I. Mironi-Harpaz, Y. Shachaf, S. Garty, Y. Smith, G. Pelled, D. Gazit, D. Seliktar, Z. Gazit, Matrix stiffness determines the fate of nucleus pulposus-derived stem cells, Biomaterials, 49 (2015) 68-76.
[46] T.H. Kim, D.B. An, S.H. Oh, M.K. Kang, H.H. Song, J.H. Lee, Creating stiffness gradient polyvinyl alcohol hydrogel using a simple gradual freezing-thawing method to investigate stem cell differentiation behaviors, Biomaterials, 40 (2015) 51-60.
[47] L.S. Wang, J. Boulaire, P.P. Chan, J.E. Chung, M. Kurisawa, The role of stiffness of gelatin-hydroxyphenylpropionic acid hydrogels formed by enzyme-

mediated crosslinking on the differentiation of human mesenchymal stem cell, Biomaterials, 31 (2010) 8608-8616.
[48] J.R. Tse, A.J. Engler, Stiffness gradients mimicking in vivo tissue variation regulate mesenchymal stem cell fate, PloS One, 6 (2011) e15978.
[49] Y.S. Pek, A.C. Wan, J.Y. Ying, The effect of matrix stiffness on mesenchymal stem cell differentiation in a 3D thixotropic gel, Biomaterials, 31 (2010) 385-391.
[50] S.H. Oh, D.B. An, T.H. Kim, J.H. Lee, Wide-range stiffness gradient PVA/HA hydrogel to investigate stem cell differentiation behavior, Acta Biomater., (2016).
[51] O. Chaudhuri, L. Gu, D. Klumpers, M. Darnell, S.A. Bencherif, J.C. Weaver, N. Huebsch, H.-p. Lee, E. Lippens, G.N. Duda, D.J. Mooney, Hydrogels with tunable stress relaxation regulate stem cell fate and activity, Nat. Mater., 15 (2016) 326–334.
[52] R.K. Das, V. Gocheva, R. Hammink, O.F. Zouani, A.E. Rowan, Stress-stiffening-mediated stem-cell commitment switch in soft responsive hydrogels, Nat. Mater., 15 (2016) 318–325.
[53] M. Park, D. Lee, J. Hyun, Nanocellulose-alginate hydrogel for cell encapsulation, Carbohydr. Polym., 116 (2015) 223-228.
[54] C. Cha, S.Y. Kim, L. Cao, H. Kong, Decoupled control of stiffness and permeability with a cell-encapsulating poly(ethylene glycol) dimethacrylate hydrogel, Biomaterials, 31 (2010) 4864–4871.
[55] S. Hong, D. Sycks, H.F. Chan, S. Lin, G.P. Lopez, F. Guilak, K.W. Leong, X. Zhao, 3D Printing of highly stretchable and tough hydrogels into complex, cellularized structures, Adv. Mater., 27 (2015) 4035-4040.
[56] A.M.S. Costa, J.F. Mano, Extremely strong and tough hydrogels as prospective candidates for tissue repair – A review, Eur. Polym. J., 72 (2015) 344-364.
[57] A.M. Costa, J.F. Mano, Highly robust hydrogels via a fast, simple and cytocompatible dual crosslinking-based process, Chem. Commun., 51 (2015) 15673-15676.

[58] R. MA, S.-A. J, A. KS, Exogenously triggered, enzymatic degradation of photopolymerized hydrogels with polycaprolactone subunits: Experimental observation and modeling of mass loss behavior, Biomacromolecules, 7 (2006) 1968-1975.

[59] A. Sawhney, C. Pathak, J. Hubbell, Bioerodible hydrogels based on photopolymerized poly(ethylene glycol)-co-poly(alpha-hydroxy acid) diacrylate macromers, Macromolecules, 26 (1993) 581–587.

[60] M. Lutolf, J. Lauer-Fields, H. Schmoekel, A. Metters, F. Weber, G. Fields, J. Hubbell, Synthetic matrix metalloproteinase-sensitive hydrogels for the conduction of tissue regeneration: Engineering cell-invasion characteristics, Proc. Nat. Acad. Sci. U. S. A., 100 (2003) 5413–5418.

[61] M.P. Lutolf, G.P. Raeber, A.H. Zisch, N. Tirelli, J.A. Hubbell, Cell-responsive synthetic hydrogels, Adv. Mater., 15 (2003) 888-892.

[62] K. Xu, F. Lee, S. Gao, M.H. Tan, M. Kurisawa, Hyaluronidase-incorporated hyaluronic acid-tyramine hydrogels for the sustained release of trastuzumab, J. Controlled Release, 216 (2015) 47-55.

[63] N. Cui, J. Qian, T. Liu, N. Zhao, H. Wang, Hyaluronic acid hydrogel scaffolds with a triple degradation behavior for bone tissue engineering, Carbohydr. Polym., 126 (2015) 192-198.

[64] Y. Aizawa, S.C. Owen, M.S. Shoichet, Polymers used to influence cell fate in 3D geometry: New trends, Prog. Polym. Sci., 37 (2012) 645-658.

[65] Y. Park., M. Lutolf, J. Hubbell, E. Hunziker, M. Wong, Bovine primary chondrocyte culture in synthetic matrix metalloproteinase-sensitive poly(ethylene glycol)-based hydrogels as a scaffold for cartilage repair, Tissue Eng, 10 (2004) 515-522.

[66] L. Almany, D. Seliktar, Biosynthetic hydrogel scaffolds made from fibrinogen and polyethylene glycol for 3D cell cultures, Biomaterials, 26 (2005) 2467–2477.

[67] M.B. Oliveira, O. Kossover, J.F. Mano, D. Seliktar, Injectable PEGylated fibrinogen cell-laden microparticles made with a continuous solvent- and oil-free preparation method, Acta Biomater., 13 (2015) 78–87.

[68] N. Huebsch, E. Lippens, K. Lee, M. Mehta, S.T. Koshy, M.C. Darnell, R.M. Desai, C.M. Madl, M. Xu, X. Zhao, O. Chaudhuri, C. Verbeke, W.S. Kim, K. Alim, A. Mammoto, D.E. Ingber, G.N. Duda, D.J. Mooney, Matrix elasticity of void-forming hydrogels controls transplanted-stem-cell-mediated bone formation, Nat. Mater., 14 (2015) 1269-1277.

[69] P. de Vos, C.G.V. Hoogmoed, J.v. Zanten, S. Netter, J.H. Strubbe, H.J. Busscher, Long-term biocompatibility, chemistry, and function of microencapsulated pancreatic islets, Biomaterials, 24 (2003) 305–312.

[70] E. Santos, J. Zarate, G. Orive, R.M. Hernandez, J.L. Pedraz, Biomaterials in cell microencapsulation, Adv. Exp. Med. Biol., 670 (2010) 5-21.

[71] A.M. Rokstad, S. Holtan, B. Strand, B. Steinkjer, L. Ryan, B. Kulseng, G. Skjak-Braek, T. Espevik, Microencapsulation of cells producing therapeutic proteins: Optimizing cell growth and secretion, Cell Transplant., 11 (2002) 313–324.

[72] G. Langlois, J. Dusseault, S. Bilodeau, S.K. Tam, D. Magassouba, J.P. Halle, Direct effect of alginate purification on the survival of islets immobilized in alginate-based microcapsules, Acta Biomater., 5 (2009) 3433–3440.

[73] G. Orive, S.K. Tam, J.L. Pedraz, J.P. Halle, Biocompatibility of alginate–poly-L-lysine microcapsules for cell therapy, Biomaterials, 27 (2006) 3691–3700.

[74] D.F. Williams, On the mechanisms of biocompatibility, Biomaterials, 29 (2008) 2941–2953.

[75] A.M. Rokstad, I. Lacik, P. de Vos, B.L. Strand, Advances in biocompatibility and physico-chemical characterization of microspheres for cell encapsulation, Adv. Drug Delivery Rev., 67-68 (2014) 111-130.

[76] B.D. Ratner, The biocompatibility manifesto: Biocompatibility for the twenty-first century, J. Cardiovasc. Transl. Res., 4 (2011) 523–527.

[77] A.J. Vegas, O. Veiseh, J.C. Doloff, M. Ma, H.H. Tam, K. Bratlie, J. Li, A.R. Bader, E. Langan, K. Olejnik, P. Fenton, J.W. Kang, J. Hollister-Locke, M.A. Bochenek, A. Chiu, S. Siebert, K. Tang, S. Jhunjhunwala, S. Aresta-Dasilva, N. Dholakia, R. Thakrar, T. Vietti, M. Chen, J. Cohen, K. Siniakowicz, M. Qi, J. McGarrigle, S. Lyle, D.M. Harlan, D.L. Greiner, J. Oberholzer, G.C. Weir, R.

Langer, D.G. Anderson, Combinatorial hydrogel library enables identification of materials that mitigate the foreign body response in primates, Nat. Biotechnol., 34 (2016) 345-352.

[78] O. Veiseh, J.C. Doloff, M. Ma, A.J. Vegas, H.H. Tam, A.R. Bader, J. Li, E. Langan, J. Wyckoff, W.S. Loo, S. Jhunjhunwala, A. Chiu, S. Siebert, K. Tang, J. Hollister-Lock, S. Aresta-Dasilva, M. Bochenek, J. Mendoza-Elias, Y. Wang, M. Qi, D.M. Lavin, M. Chen, N. Dholakia, R. Thakrar, I. Lacik, G.C. Weir, J. Oberholzer, D.L. Greiner, R. Langer, D.G. Anderson, Size- and shape-dependent foreign body immune response to materials implanted in rodents and non-human primates, Nat. Mater., 14 (2015) 643-651.

[79] M.B. Oliveira, M.P. Ribeiro, S.P. Miguel, A.I. Neto, P. Coutinho, I.J. Correia, J.F. Mano, In vivo high-content evaluation of three-dimensional scaffolds biocompatibility, Tissue Eng. Part C, 20 (2014) 1-14.

[80] G. Peretti, V. Campo-Ruiz, S. Gonzalez, M. Randolph, J. Xu, K. Morse, R. Roses, M. Yaremchuk, Tissue engineered cartilage integration to live and devitalized cartilage: A study by reflectance mode confocal microscopy and standard histology, Connect. Tissue Res., 47 (2006) 190-199.

[81] G.D. Nicodemus, S.J. Bryant, Cell encapsulation in biodegradable hydrogels for tissue engineering applications, Tissue Eng. Part B, 14 (2008) 149-165.

[82] G. Decher, J.D. Hong, J. Schmitt, Buildup of ultrathin multilayer films by a self-assembly process: III. Consecutively alternating adsorption of anionic and cationic polyelectrolytes on charged surfaces, Thin Solid Films, 210–211 (1992) 831-835.

[83] S. De Koker, L.J. De Cock, P. Rivera-Gil, W.J. Parak, R. Auzely Velty, C. Vervaet, J.P. Remon, J. Grooten, B.G. De Geest, Polymeric multilayer capsules delivering biotherapeutics, Adv. Drug Delivery Rev., 63 (2011) 748-761.

[84] K. Ariga, Y.M. Lvov, K. Kawakami, Q. Ji, J.P. Hill, Layer-by-layer self-assembled shells for drug delivery, Adv. Drug Delivery Rev., 63 (2011) 762-771.

[85] R.R. Costa, E. Castro, F.J. Arias, J.C. Rodriguez-Cabello, J.F. Mano, Multifunctional compartmentalized capsules with a hierarchical organization from the nano to the macro scales, Biomacromolecules, 14 (2013) 2403-2410.
[86] J. Kim, D.R. Arifin, N. Muja, T. Kim, A.A. Gilad, H. Kim, A. Arepally, T. Hyeon, J.W. Bulte, Multifunctional capsule-in-capsules for immunoprotection and trimodal imaging, Angew. Chem., 50 (2011) 2317-2321.
[87] R. Cheng, F. Meng, C. Deng, H.A. Klok, Z. Zhong, Dual and multi-stimuli responsive polymeric nanoparticles for programmed site-specific drug delivery, Biomaterials, 34 (2013) 3647-3657.
[88] R.R. Costa, C.A. Custódio, F.J. Arias, J.C. Rodríguez-Cabello, J.F. Mano, Nanostructured and thermoresponsive recombinant biopolymer-based microcapsules for the delivery of active molecules, Nanomedicine, 9 (2013) 895–902.
[89] J.M. Silva, A.R. Duarte, S.G. Caridade, C. Picart, R.L. Reis, J.F. Mano, Tailored freestanding multilayered membranes based on chitosan and alginate, Biomacromolecules, 15 (2014) 3817-3826.
[90] C. Lin, W. Zhu, H. Yang, Q. An, C.A. Tao, W. Li, J. Cui, Z. Li, G. Li, Facile fabrication of stimuli-responsive polymer capsules with gated pores and tunable shell thickness and composite, Angew. Chem., 50 (2011) 4947-4951.
[91] H.-Y. Lee, K.R. Tiwaria, S.R. Raghavan, Biopolymer capsules bearing polydiacetylenic vesicles as colorimetric sensors of pH and temperature, Soft Matter, 7 (2011) 3273-3276.
[92] B.G. de Geest, M.A. Willart, B.N. Lambrecht, C. Pollard, C. Vervaet, J.P. Remon, J. Grooten, S.D. Koker, Surface-engineered polyelectrolyte multilayer capsules: Synthetic vaccines mimicking microbial structure and function, Angew. Chem., 124 (2012) 3928-3932.
[93] M. Sanlés-Sobrido, M. Pérez-Lorenzo, B. Rodríguez-González, V. Salgueiriño, M.A. Correa-Duarte, Highly active nanoreactors: Nanomaterial encapsulation based on confined catalysis, Angew. Chem., 51 (2012) 3877–3882.
[94] Q. Jin, J. Bao, H. Sakiyama, N. Tsubaki, Preparation, structure and performance of TS-1 zeolite-coated Au–Pd/TiO_2–SiO_2 capsule catalyst for

propylene epoxidation with oxygen and hydrogen, Res. Chem. Intermed., 37 (2011) 177-184.

[95] D.M. Lynn, Layers of opportunity: Nanostructured polymer assemblies for the delivery of macromolecular therapeutics, Soft Matter, 2 (2006) 269.

[96] S.M. Oliveira, V.E. Santo, M.E. Gomes, R.L. Reis, J.F. Mano, Layer-by-layer assembled cell instructive nanocoatings containing platelet lysate, Biomaterials, 48 (2015) 56-65.

[97] R.R. Costa, M. Alatorre-Meda, J.F. Mano, Drug nano-reservoirs synthesized using layer-by-layer technologies, Biotechnol. Adv., 33 (2015) 1310-1326.

[98] J.J. Richardson, M. Bjornmalm, F. Caruso, Technology-driven layer-by-layer assembly of nanofilms, Science, 348 (2015) aaa2491.

[99] K. Ariga, Y. Yamauchi, G. Rydzek, Q. Ji, Y. Yonamine, K.C.W. Wu, J.P. Hill, Layer-by-layer nanoarchitectonics: Invention, innovation, and evolution, Chem. Lett., 43 (2014) 36-68.

[100] C.R. Correia, R.P. Pirraco, M.T. Cerqueira, A.P. Marques, R.L. Reis, J.F. Mano, Semipermeable capsules wrapping a multifunctional and self-regulated co-culture microenvironment for osteogenic differentiation, Sci. Rep., 6 (2016) 21883.

[101] C.R. Correia, S. Gil, R.L. Reis, J.F. Mano, A closed chondromimetic environment within magnetic-responsive liquified capsules encapsulating stem cells and collagen II/TGF-β3 microparticles, Adv. Healthcare Mater., (2016) (*in press*).

[102] D.S. Couto, N.M. Alves, J.F. Mano, Nanostructured multilayer coatings combining chitosan with bioactive glass nanoparticles, J. Nanosci. Nanotechnol., 9 (2009) 1741-1748.

[103] L.C. Rodrigues, C.A. Custódio, R.L. Reis, J.F. Mano, Light responsive multilayer surfaces with controlled spatial extinction capability, J. Mater. Chem. B, 4 (2016) 1398-1404.

[104] M.F. Bedard, B.G. De Geest, A.G. Skirtach, H. Mohwald, G.B. Sukhorukov, Polymeric microcapsules with light responsive properties for encapsulation and release, Adv. Colloid Interface Sci., 158 (2010) 2-14.

[105] C.A. Custodio, R.L. Reis, J.F. Mano, Engineering biomolecular microenvironments for cell instructive biomaterials, Adv. Healthcare Mater., 3 (2014) 797-810.
[106] S.G. Caridade, C. Monge, J. Almodovar, R. Guillot, J. Lavaud, V. Josserand, J.L. Coll, J.F. Mano, C. Picart, Myoconductive and osteoinductive free-standing polysaccharide membranes, Acta Biomater., 15 (2015) 139-149.
[107] N.J. Shah, J. Hong, M.N. Hyder, P.T. Hammond, Osteophilic multilayer coatings for accelerated bone tissue growth, Adv. Mater., 24 (2012) 1445-1450.
[108] R.F. Fakhrullin, Y.M. Lvov, "Face-lifting" and "make-up" for microorganisms: Layer-by-layer polyelectrolyte nanocoating, ACS Nano, 6 (2012) 4557–4564.
[109] I. Drachuk, M.K. Gupta, V.V. Tsukruk, Biomimetic coatings to control cellular function through cell surface engineering, Adv. Funct. Mater., 23 (2013) 4437-4453.
[110] G. Bantchev, Z. Lu, Y. Lvov, Layer-by-layer nanoshell assembly on colloids through simplified washless, Process. J. Nanosci. Nanotechnol., 9 (2009) 396–403.
[111] A. Kang, J. Park, J. Ju, G.S. Jeong, S.H. Lee, Cell encapsulation via microtechnologies, Biomaterials, 35 (2014) 2651-2663.
[112] C.J. Martinez, J.W. Kim, C. Ye, I. Ortiz, A.C. Rowat, M. Marquez, D. Weitz, A microfluidic approach to encapsulate living cells in uniform alginate hydrogel microparticles, Macromol. Biosci., 12 (2012) 946-951.
[113] D. Velasco, E. Tumarkin, E. Kumacheva, Microfluidic encapsulation of cells in polymer microgels, Small, 8 (2012) 1633–1642.
[114] G. Orive, R.M. Hernández, A.R. Gascón, R. Calafiore, T.M.S. Chang, P.D. Vos, G. Hortelano, D. Hunkeler, I. Lacík, A.M.J. Shapiro, J.L. Pedraz, Cell encapsulation: Promise and progress, Nat. Med., 9 (2003) 104-107.
[115] W.H. Tan, S. Takeuchi, Monodisperse alginate hydrogel microbeads for cell encapsulation, Adv. Mater., 19 (2007) 2696-2701.

[116] H. Zhang, E. Tumarkin, R.M.A. Sullan, G.C. Walker, E. Kumacheva, Exploring Microfluidic routes to microgels of biological polymers, Macromol. Rapid Commun., 28 (2007) 527-538.
[117] H. Zhang, E. Tumarkin, R. Peerani, Z. Nie, R.M.A. Sullan, G.C. Walker, E. Kumacheva, Microfluidic production of biopolymer microcapsules with controlled morphology, J. Am. Chem. Soc., 128 (2006) 12205-12210.
[118] M. Lian, C.P. Collier, M.J. Doktycz, S.T. Retterer, Monodisperse alginate microgel formation in a three-dimensional microfluidic droplet generator, Biomicrofluidics, 6 (2012) 044108.
[119] R.O. Hynes, The extracellular matrix: Not just pretty fibrils, Science, 326 (2009) 1216-1219.
[120] D.E. Discher, D.J. Mooney, P.W. Zandstra, Growth factors, matrices, and forces combine and control stem cells, Science, 324 (2009) 1673-1677.
[121] B. Geiger, A. Bershadsky, Exploring the neighborhood: Adhesion-coupled cell mechanosensors, Cell, 110 (2002) 139–142.
[122] C.-H. Choi, J.-H. Jung, Y.W. Rhee, D.-P. Kim, S.-E. Shim, C.-S. Lee, Generation of monodisperse alginate microbeads and in situ encapsulation of cell in microfluidic device, Biomed. Microdevices, 9 (2007) 855-862.
[123] S. Utech, R. Prodanovic, A.S. Mao, R. Ostafe, D.J. Mooney, D.A. Weitz, Microfluidic generation of monodisperse, structurally homogeneous alginate microgels for cell encapsulation and 3D cell culture, Adv. Healthcare Mater., 4 (2015) 1628-1633.
[124] S.-J. Shin, J.-Y. Park, J.-Y. Lee, H. Park, Y.-D. Park, K.-B. Lee, C.-M. Whang, S.-H. Lee, “On the fly” continuous generation of alginate fibers using a microfluidic device, Langmuir, 23 (2007) 9104-9108.
[125] Kwang Ho Lee, Su Jung Shin, Yongdoo Park, S.-H. Lee, Synthesis of cell-laden alginate hollow fibers using microfluidic chips and microvascularized tissue-engineering applications, Small, 5 (2009) 1264-1268.
[126] S. Sugiura, T. Oda, Y. Aoyagi, M. Satake, N. Ohkohchic, M. Nakajimab, Tubular gel fabrication and cell encapsulation in laminar flow stream formed by microfabricated nozzle array, Lab Chip, 8 (2008) 1255-1257.

[127] E. Kang, G. Jeong, Y. Choi, K. Lee, A. Khademhosseini, S. Lee, Digitally tunable physicochemical coding of material composition and topography in continuous microfibres, Nat. Mater., 10 (2011) 877-883.
[128] M. Yamada, S. Sugaya, Y. Naganuma, M. Seki, Microfluidic synthesis of chemically and physically anisotropic hydrogel microfibers for guided cell growth and networking, Soft Matter, 8 (2012) 3122-3130.
[129] N. Raof, M. Padgen, A. Gracias, M. Bergkvist, Y. Xie, One-dimensional self-assembly of mouse embryonic stem cells using an array of hydrogel microstrands, Biomaterials, 32 (2011) 4498-4505.
[130] M. Hu, R. Deng, K.M. Schumacher, M. Kurisawa, H. Ye, K. Purnamawati, J.Y. Ying, Hydrodynamic spinning of hydrogel fibers, Biomaterials, 31 (2010) 863-869.
[131] S. Zhang, M.A. Greenfield, A. Mata, L.C. Palmer, R. Bitton, J.R. Mantei, C. Aparicio, M.O. de la Cruz, S.I. Stupp, A self-assembly pathway to aligned monodomain gels, Nat. Mater., 9 (2010) 594-601.
[132] M.A. Daniele, D.A. Boyd, A.A. Adams, F.S. Ligler, Microfluidic strategies for design and assembly of microfibers and nanofibers with tissue engineering and regenerative medicine applications, Adv. Healthcare Mater., 4 (2015) 11-28.
[133] D. Puppi, D. Dinucci, C. Bartoli, C. Mota, C. Migone, F. Dini, G. Barsotti, F. Carlucci, F. Chiellini, Development of 3D wet-spun polymeric scaffolds loaded with antimicrobial agents for bone engineering, J. Bioact. Compat. Polym., 26 (2011) 478-492.
[134] A. Lima, J. Mano, Micro/nano-structured superhydrophobic surfaces in the biomedical field: Part I: Basic concepts and biomimetic approaches, Nanomedicine, 10 (2015) 103–119.
[135] T. Sun, L. Feng, X. Gao, L. Jiang, Bioinspired surfaces with special wettability, Acc. Chem. Res., 38 (2005) 644-652.
[136] E. Ueda, P.A. Levkin, Emerging applications of superhydrophilic-superhydrophobic micropatterns, Adv. Mater., 25 (2013) 1234-1247.

[137] K. Kerstin, W. Barthlott, Superhydrophobic and superhydrophilic plant surfaces: An inspiration for biomimetic materials, Philos. Trans. R. Soc., 367 (2009) 1487-1509.

[138] W. Song, D. Veiga, C. Custódio, J. Mano, Bioinspired degradable substrates with extreme wettability properties, Adv. Mater., 21 (2009) 1830–1834.

[139] X. Yao, Y. Song, L. Jiang, Applications of bio-inspired special wettable surfaces, Adv. Mater., 23 (2011) 719-734.

[140] Y.Y. Yan, N. Gao, W. Barthlott, Mimicking natural superhydrophobic surfaces and grasping the wetting process: A review on recent progress in preparing superhydrophobic surfaces, Adv. Colloid Interface Sci., 169 (2011) 80-105.

[141] M.J. Hancock, K. Sekeroglu, M.C. Demirel, Bioinspired directional surfaces for adhesion, wetting, and transport, Adv. Funct. Mater., 22 (2012) 2223-2234.

[142] A. Lima, J. Mano, Micro/nano-structured superhydrophobic surfaces in the biomedical field: Part II: Applications overview, Nanomedicine, 10 (2015) 271–297.

[143] M.B. Oliveira, A.I. Neto, C.R. Correia, M.I. Rial-Hermida, C. Alvarez-Lorenzo, J.F. Mano, Superhydrophobic chips for cell spheroids high-throughput generation and drug screening, ACS Appl. Mater. Interfaces, 6 (2014) 9488-9495.

[144] A.I. Neto, C.R. Correia, C.A. Custódio, J.F. Mano, Biomimetic miniaturized platform able to sustain arrays of liquid droplets for high-throughput combinatorial tests, Adv. Funct. Mater., 24 (2014) 5096-5103.

[145] W. Song, A.C. Lima, J.F. Mano, Bioinspired methodology to fabricate hydrogel spheres for multi-applications using superhydrophobic substrates, Soft Matter, 6 (2010) 5868.

[146] A.C. Lima, P. Batista, T.A. Valente, A.S. Silva, I.J. Correia, J.F. Mano, Novel methodology based on biomimetic superhydrophobic substrates to immobilize cells and proteins in hydrogel spheres for applications in bone regeneration, Tissue Eng. Part A, 19 (2013) 1175-1187.

[147] A.C. Lima, C.R. Correia, M.B. Oliveira, J.F. Mano, Sequential ionic and thermogelation of chitosan spherical hydrogels prepared using superhydrophobic surfaces to immobilize cells and drugs, J. Bioact. Compat. Polym., 29 (2013) 50-65.
[148] A.C. Lima, C.A. Custodio, C. Alvarez-Lorenzo, J.F. Mano, Biomimetic methodology to produce polymeric multilayered particles for biotechnological and biomedical applications, Small, 9 (2013) 2487-2492, 2486.
[149] A.M. Costa, M. Alatorre-Meda, C. Alvarez-Lorenzo, J.F. Mano, Superhydrophobic surfaces as a tool for the fabrication of hierarchical spherical polymeric carriers, Small, 11 (2015) 3648-3652.
[150] E. Ueda, F.L. Geyer, V. Nedashkivska, P.A. Levkin, Facile formation of arrays of microdroplets and hydrogel micropads for cell screening applications, Lab Chip, 12 (2012) 5218-5224.
[151] T. Billiet, M. Vandenhaute, J. Schelfhout, S. Van Vlierberghe, P. Dubruel, A review of trends and limitations in hydrogel-rapid prototyping for tissue engineering, Biomaterials, 33 (2012) 6020-6041.
[152] S.M. Peltola, F.P.W. Melchels, D.W. Grijpmab, M. Kellomäki, A review of rapid prototyping techniques for tissue engineering purposes, Ann. Med., 40 (2008) 268-280.
[153] E. Sachlos, J. Czernuszka, Making tissue engineering scaffolds work. Review on the application of solid freeform fabrication technology to the production of tissue engineering scaffolds, Eur. Cell Mater., 5 (2003) 29-39.
[154] R. Dutta, A. Dutta, Cell-interactive 3D-scaffold; Advances and applications, Biotechnol. Adv., 27 (2009) 334-339.
[155] D. Hutmacher, S. Cool, Concepts of scaffold-based tissue engineering-the rationale to use solid free-form fabrication techniques, J. Cell Mol. Med., 11 (2007) 654-669.
[156] V. Mironov, T. Boland, T. Trusk, G. Forgacs, R. Markwald, Organ printing: Computer-aided jet-based 3D tissue engineering, Trends Biotechnol., 21 (2003) 157-161.

[157] S.R. Pajoum Shariati, S. Moeinzadeh, E. Jabbari, Hydrogels for cell encapsulation and bioprinting, in: K. Turksen (Ed.), Bioprinting in Regenerative Medicine, Springer International Publishing, Switzerland, 2015, pp. 89-108.
[158] P. Calvert, Printing cells, Science, 318 (2007) 208-209.
[159] F. Guillemot, A. Souquet, S. Catros, B. Guillotin, J. Lopez, M. Faucon, B. Pippenger, R. Bareille, M. Rémy, S. Bellance, P. Chabassier, J. Fricain, J. Amédée, Highthroughput laser printing of cells and biomaterials for tissue engineering, Acta Biomater., 6 (2010) 2494-2500.
[160] B. Guillotin, A. Souquet, S. Catros, M. Duocastella, B. Pippenger, S. Bellance, R. Bareille, M. Rémy, L. Bordenave, J. Amédée, F. Guillemot, Laser assisted bioprinting of engineered tissue with high cell density and microscale organization, Biomaterials, 31 (2010) 7250-7256.
[161] X. Cui, T. Boland, Human microvasculature fabrication using thermal inkjet printing technology, Biomaterials, 30 (2009) 6221-6227.
[162] A. Skardal, J. Zhang, L. McCoard, X. Xu, S. Oottamasathien, G. Prestwich, Photocrosslinkable hyaluronan-gelatin hydrogels for two-step bioprinting, Tissue Eng. Part A, 16 (2010) 2675-2685.
[163] A. Skardal, J. Zhang, G. Prestwich, Bioprinting vessel-like constructs using hyaluronan hydrogels crosslinked with tetrahedral polyethylene glycol tetracrylates, Biomaterials, 31 (2010) 6173-6181.
[164] J. Malda, J. Visser, F. Melchels, T. Jungst, W. Hennink, W. Dhert, J. Groll, D. Hutmacher, Engineering hydrogels for biofabrication, Adv. Mater., 25 (2013) 5011–5028.
[165] K. Jakab, C. Norotte, F. Marga, K. Murphy, G. Vunjak-Novakovic, G. Forgacs, Tissue engineering by self-assembly and bio-printing of living cells, Biofabrication, 2 (2010) 022001.
[166] V. Mironov, G. Prestwich, G. Forgacs, Bioprinting living structures, J. Mater. Chem., 17 (2007) 2054-2060.
[167] L. Vivian, S. Gurtej, T.J. P., B. Chris, X. Xiawei, T.T. Nga, Y. Seung-Schik, D. Guohao, K. Pankaj, Design and fabrication of human skin by three-dimensional bioprinting, Tissue Eng. Part C, 20 (2014) 473-484.

[168] S.-J. Song, J. Choi, Y.-D. Park, J.-J. Lee, S.Y. Hong, K. Sun, A three-dimensional bioprinting system for use with a hydrogel-based biomaterial and printing parameter characterization, Artif. Organs, 34 (2010) 1044-1048.
[169] C. Almeida, T. Serra, M. Oliveira, J. Planell, M. Barbosa, M. Navarro, Impact of 3-D printed PLA- and chitosan-based scaffolds on human monocyte/macrophage responses: Unraveling the effect of 3-D structures on inflammation, Acta Biomater., 10 (2014) 613-622.
[170] M. Du, B. Chen, Q. Meng, S. Liu, X. Zheng, C. Zhang, H. Wang, H. Li, N. Wang, J. Dai, 3D bioprinting of BMSC-laden methacrylamide gelatin scaffolds with CBD-BMP2-collagen microfibers, Biofabrication, 7 (2015) 044104.
[171] K. Markstedt, A. Mantas, I. Tournier, H.M. Ávila, D. Hägg, P. Gatenholm, 3D bioprinting human chondrocytes with nanocellulose-alginate bioink for cartilage tissue engineering applications, Biomacromolecules, 16 (2015) 1489–1496.
[172] L. Pescosolido, W. Schuurman, J. Malda, P. Matricardi, F. Alhaique, T. Coviello, P. van Weeren, W. Dhert, W. Hennink, T. Vermonden, Hyaluronic acid and dextran-based semi-IPN hydrogels as biomaterials for bioprinting, Biomacromolecules, 12 (2011) 1831-1838.
[173] D.B. Kolesky, R.L. Truby, A.S. Gladman, T.A. Busbee, K.A. Homan, J.A. Lewis, 3D bioprinting of vascularized, heterogeneous cell-laden tissue constructs, Adv. Mater., 26 (2014) 3124-3130.
[174] L.E. Bertassoni, J.C. Cardoso, V. Manoharan, A.L. Cristino, N.S. Bhise, W.A. Araujo, P. Zorlutuna, N.E. Vrana, A.M. Ghaemmaghami, M.R. Dokmeci, Direct-write bioprinting of cell-laden methacrylated gelatin hydrogels, Biofabrication, 6 (2014) 024105.
[175] H.-J. Kong, K.Y. Lee, D.J. Mooney, Decoupling the dependence of rheological/mechanical properties of hydrogels from solids concentration, Polymer, 43 (2002) 6239-6246.
[176] J.H.Y. Chung, S. Naficy, Z. Yue, R. Kapsa, A. Quigley, S.E. Moulton, G.G. Wallace, Bio-ink properties and printability for extrusion printing living cells, Biomater. Sci., 1 (2013) 763-773.

[177] J.-S. Lee, J.M. Hong, J.W. Jung, J.-H. Shim, J.-H. Oh, D.-W. Cho, 3D printing of composite tissue with complex shape applied to ear regeneration, Biofabrication, 6 (2014) 024103.

[178] R.M. Hernandez, G. Orive, A. Murua, J.L. Pedraz, Microcapsules and microcarriers for in situ cell delivery, Adv. Drug Delivery Rev., 62 (2010) 711-730.

[179] D.H. Choi, C.H. Park, I.H. Kim, H.J. Chun, K. Park, D.K. Han, Fabrication of core-shell microcapsules using PLGA and alginate for dual growth factor delivery system, J. Controlled Release, 147 (2010) 193-201.

[180] E. Martins, D. Renard, J. Davy, M. Marquis, D. Poncelet, Oil core microcapsules by inverse gelation technique, J. Microencapsul., 32 (2015) 86-95.

[181] S. Abang, E.S. Chan, D. Poncelet, Effects of process variables on the encapsulation of oil in Ca-alginate capsules using an inverse gelation technique, J. Microencapsul., 29 (2012) 417-428.

[182] H. Zhou, H.H. Xu, The fast release of stem cells from alginate-fibrin microbeads in injectable scaffolds for bone tissue engineering, Biomaterials, 32 (2011) 7503-7513.

[183] S.V. Bhujbal, B. de Haan, S.P. Niclou, P. de Vos, A novel multilayer immunoisolating encapsulation system overcoming protrusion of cells, Sci. Rep., 4 (2014) 6856.

[184] V. Kozlovskaya, S. Harbaugh, I. Drachuk, O. Shchepelina, N. Kelley-Loughnane, M. Stone, V.V. Tsukruk, Hydrogen-bonded lbl shells for living cell surface engineering, Soft Matter, 7 (2011) 2364–2372.

[185] A. Diaspro, D. Silvano, S. Krol, O. Cavalleri, A. Gliozzi, Single living cell encapsulation in nano-organized polyelectrolyte shells, Langmuir, 18 (2002) 5047–5050.

[186] A.E. Mayfield, E.L. Tilokee, N. Latham, B. McNeill, B.K. Lam, M. Ruel, E.J. Suuronen, D.W. Courtman, D.J. Stewart, D.R. Davis, The effect of encapsulation of cardiac stem cells within matrix-enriched hydrogel capsules on cell survival, post-ischemic cell retention and cardiac function, Biomaterials, 35 (2014) 133-142.

[187] A. Blocki, S. Beyer, J.Y. Dewavrin, A. Goralczyk, Y. Wang, P. Peh, M. Ng, S.S. Moonshi, S. Vuddagiri, M. Raghunath, E.C. Martinez, K.K. Bhakoo, Microcapsules engineered to support mesenchymal stem cell (MSC) survival and proliferation enable long-term retention of MSCs in infarcted myocardium, Biomaterials, 53 (2015) 12-24.

[188] M. Endres, N. Wenda, H. Woehlecke, K. Neumann, J. Ringe, C. Erggelet, D. Lerche, C. Kaps, Microencapsulation and chondrogenic differentiation of human mesenchymal progenitor cells from subchondral bone marrow in Ca-alginate for cell injection, Acta Biomater., 6 (2010) 436-444.

[189] J.W. Andrejecsk, J. Cui, W.G. Chang, J. Devalliere, J.S. Pober, W.M. Saltzman, Paracrine exchanges of molecular signals between alginate-encapsulated pericytes and freely suspended endothelial cells within a 3D protein gel, Biomaterials, 34 (2013) 8899-8908.

[190] R. Silva, R. Singh, B. Sarker, D.G. Papageorgiou, J.A. Juhasz, J.A. Roether, I. Cicha, J. Kaschta, D.W. Schubert, K. Chrissafis, R. Detsch, A.R. Boccaccini, Hybrid hydrogels based on keratin and alginate for tissue engineering, J. Mater. Chem. B, 2 (2014) 5441-5451.

[191] Barbara Pui Chan, Ting Yan Hui, Mei Yi Wong, Kevin Hak Kong Yip, G.C.F. Chan, Mesenchymal stem cell-encapsulated collagen microsphere for bone tissue engineering, Tissue Eng. Part C, 16 (2010) 225-235.

[192] C.H. Li, T.K. Chik, A.H. Ngan, S.C. Chan, D.K. Shum, B.P. Chan, Correlation between compositional and mechanical properties of human mesenchymal stem cell-collagen microspheres during chondrogenic differentiation, Tissue Eng. Part A, 17 (2011) 777-788.

[193] S.J. Bidarra, C.C. Barrias, M.A. Barbosa, R. Soares, P.L. Granja, Immobilization of human mesenchymal stem cells within RGD-grafted alginate microspheres and assessment of their angiogenic potential, Biomacromolecules, 11 (2010) 1956-1964.

[194] L. Li, A.E. Davidovich, J.M. Schloss, U. Chippada, R.R. Schloss, N.A. Langrana, M.L. Yarmush, Neural lineage differentiation of embryonic stem cells within alginate microbeads, Biomaterials, 32 (2011) 4489-4497.

[195] R. Yao, R. Zhang, F. Lin, J. Luan, Biomimetic injectable HUVEC-adipocytes/collagen/alginate microsphere co-cultures for adipose tissue engineering, Biotechnol. Bioeng., 110 (2013) 1430-1443.
[196] F. Cellesi, W. Weber, M. Fussenegger, J.A. Hubbell, N. Tirelli, Towards a fully synthetic substitute of alginate: Optimization of a thermal gelation/chemical cross-linking scheme ("tandem" gelation) for the production of beads and liquid-core capsules, Biotechnol. Bioeng., 88 (2004) 740-749.
[197] Y. Dzenis, Spinning continuous fibers for nanotechnology, Science, 304 (2004) 1917-1919.
[198] P. Rothemund, Folding DNA to create nanoscale shapes and patterns, Nature, 440 (2006) 297-302.
[199] C.-H. Xue, J. Chen, W. Yin, S.-T. Jia, J.-Z. Ma, Superhydrophobic conductive textiles with antibacterial property by coating fibers with silver nanoparticles, Appl. Surf. Sci., 258 (2012) 2468-2472.
[200] B.J. Vakoc, R.M. Lanning, J.A. Tyrrell, T.P. Padera, L.A. Bartlett, T. Stylianopoulos, L.L. Munn, G.J. Tearney, D. Fukumura, R.K. Jain, B.E. Bouma, Three-dimensional microscopy of the tumor microenvironment in vivo using optical frequency domain imaging, Nat. Med., 15 (2009) 1219-1223.
[201] V.J. Wedeen, D.L. Rosene, R. Wang, G. Dai, F. Mortazavi, P. Hagmann, J.H. Kaas, W.-Y.I. Tseng, The geometric structure of the brain fiber pathways, Science, 335 (2012) 1628-1634.
[202] M. Hu, M. Kurisawa, R. Deng, C.M. Teo, A. Schumacher, Y.X. Thong, L. Wang, K.M. Schumacher, J.Y. Ying, Cell immobilization in gelatin-hydroxyphenylpropionic acid hydrogel fibers, Biomaterials, 30 (2009) 3523-3531.
[203] B. Lee, K. Lee, E. Kang, D.-S. Kim, S.-H. Lee, Microfluidic wet spinning of chitosan-alginate microfibers and encapsulation of HepG2 cells in fibers, Biomicrofluidics, 5 (2011) 022208.
[204] J. Olmos Buitrago, R.A. Perez, A. El-Fiqi, R.K. Singh, J.H. Kim, H.W. Kim, Core-shell fibrous stem cell carriers incorporating osteogenic nanoparticulate cues for bone tissue engineering, Acta Biomater., 28 (2015) 183-192.

[205] F. Schwenter, B.L. Schneider, W.F. Pralong, N. Déglon, P. Aebischer, Survival of encapsulated human primary fibroblasts and erythropoietin expression under xenogeneic conditions, Hum. Gene Ther., 15 (2004) 669-680.
[206] T. Takei, N. Kishihara, S. Sakai, K. Kawakami, Novel technique to control inner and outer diameter of calcium-alginate hydrogel hollow microfibers, and immobilization of mammalian cells, Biochem. Eng. J., 49 (2010) 143-147.
[207] S. Sakai, Y. Liu, E.J. Mah, M. Taya, Horseradish peroxidase/catalase-mediated cell-laden alginate-based hydrogel tube production in two-phase coaxial flow of aqueous solutions for filament-like tissues fabrication, Biofabrication, 5 (2013) 015012.
[208] T. Yue, M. Nakajima, M. Takeuchi, C. Hu, Q. Huang, T. Fukuda, On-chip self-assembly of cell embedded microstructures to vascular-like microtubes, Lab Chip, 14 (2014) 1151-1161.
[209] P. Sher, S.M. Oliveira, J. Borges, J.F. Mano, Assembly of cell-laden hydrogel fiber into non-liquefied and liquefied 3D spiral constructs by perfusion-based layer-by-layer technique, Biofabrication, 7 (2015) 011001.
[210] X. Shi, S. Ostrovidov, Y. Zhao, X. Liang, M. Kasuya, K. Kurihara, K. Nakajima, H. Bae, H. Wu, A. Khademhosseini, Microfluidic spinning of cell-responsive grooved microfibers, Adv. Funct. Mater., 25 (2015) 2250-2259.
[211] A. Leferink, D. Schipper, E. Arts, E. Vrij, N. Rivron, M. Karperien, K. Mittmann, C. van Blitterswijk, L. Moroni, R. Truckenmuller, Engineered micro-objects as scaffolding elements in cellular building blocks for bottom-up tissue engineering approaches, Adv. Mater., 26 (2014) 2592-2599.
[212] S. Ahadian, J. Ramón-Azcón, M. Estili, X. Liang, S. Ostrovidov, H. Shiku, M. Ramalingam, K. Nakajima, Y. Sakka, H. Bae, T. Matsue, A. Khademhosseini, Hybrid hydrogels containing vertically aligned carbon nanotubes with anisotropic electrical conductivity for muscle myofiber fabrication, Sci. Rep., 4 (2014) 1-11.
[213] H. Qi, M. Ghodousi, Y. Du, C. Grun, H. Bae, P. Yin, A. Khademhosseini, DNA-directed selfassembly of shape-controlled hydrogels, Nat. Commun., 4 (2013) 1-10.

[214] F. Xu, C.A. Wu, V. Rengarajan, T.D. Finley, H.O. Keles, Y. Sung, B. Li, U.A. Gurkan, U. Demirci, Three-dimensional magnetic assembly of microscale hydrogels, Adv. Mater., 23 (2011) 4254-4260.
[215] S. Guven, P. Chen, F. Inci, S. Tasoglu, B. Erkmen, U. Demirci, Multiscale assembly for tissue engineering and regenerative medicine, Trends Biotechnol., 33 (2015) 269-279.
[216] K. Yue, G. Trujillo-de Santiago, M.M. Alvarez, A. Tamayol, N. Annabi, A. Khademhosseini, Synthesis, properties, and biomedical applications of gelatin methacryloyl (GelMA) hydrogels, Biomaterials, 73 (2015) 254-271.
[217] H. Qi, Y. Du, L. Wang, H. Kaji, H. Bae, A. Khademhosseini, Patterned differentiation of individual embryoid bodies in spatially organized 3D hybrid microgels, Adv. Mater., 22 (2010) 5276-5281.
[218] J.S. Miller, K.R. Stevens, M.T. Yang, B.M. Baker, D.H. Nguyen, D.M. Cohen, E. Toro, A.A. Chen, P.A. Galie, X. Yu, R. Chaturvedi, S.N. Bhatia, C.S. Chen, Rapid casting of patterned vascular networks for perfusable engineered three-dimensional tissues, Nat. Mater., 11 (2012) 768-774.
[219] B. Duan, L.A. Hockaday, K.H. Kang, J.T. Butcher, 3D Bioprinting of heterogeneous aortic valve conduits with alginate/gelatin hydrogels, J. Biomed. Mater. Res. Part A, 101A (2013) 1255-1264.
[220] L.A. Hockaday, K.H. Kang, N.W. Colangelo, P.Y.C. Cheung, B. Duan, E. Malone, J. Wu, L.N. Girardi, L.J. Bonassar, H. Lipson, Rapid 3D printing of anatomically accurate and mechanically heterogeneous aortic valve hydrogel scaffolds, Biofabrication, 4 (2012) 035005.
[221] B. Zamanian, M. Masaeli, J.W. Nichol, M. Khabiry, M.J. Hancock, H. Bae, A. Khademhosseini, Interface-directed self-assembly of cell-laden microgels, Small, 6 (2010) 937-944.
[222] A.P. McGuigan, D.A. Bruzewicz, A. Glavan, M.J. Butte, G.M. Whitesides, Cell encapsulation in sub-mm sized gel modules using replica molding, PloS One, 3 (2008) e2258.
[223] M.A. Stuart, W.T. Huck, J. Genzer, M. Muller, C. Ober, M. Stamm, G.B. Sukhorukov, I. Szleifer, V.V. Tsukruk, M. Urban, F. Winnik, S. Zauscher, I.

Luzinov, S. Minko, Emerging applications of stimuli-responsive polymer materials, Nat. Mater., 9 (2010) 101-113.
[224] R. N, Physical stimuli-responsive polymeric micelles for anti-cancer drug delivery, Prog. Polym. Sci., 32 (2007) 962-990.
[225] F. Meng, W. Hennink, Z. Zhong, Reduction-sensitive polymers and bioconjugates for biomedical applications, Biomaterials, 30 (2009) 2180-2198.
[226] H.G. Schild, D.A. Tirrell, Microcalorimetric detection of lower critical solution temperatures in aqueous polymer solutions, J. Phys. Chem., 94 (1990) 4352–4356.
[227] L. Klouda, Thermoresponsive hydrogels in biomedical applications: A seven-year update, Eur. J. Pharm. Biopharm., 97 (2015) 338-349.
[228] J.F. Mano, Stimuli-responsive polymeric systems for biomedical applications, Adv. Eng. Mater., 10 (2008) 515-527.
[229] T. Gan, Y. Guan, Y. Zhang, Thermogelable PNIPAM microgel dispersion as 3D cell scaffold: Effect of syneresis, J. Mater. Chem., 20 (2010) 5937-5944.
[230] B.M. Watson, F.K. Kasper, P.S. Engel, A.G. Mikos, Synthesis and characterization of injectable, biodegradable, phosphate-containing, chemically crosslinkable, thermoresponsive macromers for bone tissue engineering, Biomacromolecules, 15 (2014) 1788-1796.
[231] B.M. Watson, T.N. Vo, A.M. Tatara, S.R. Shah, D.W. Scott, P.S. Engel, A.G. Mikos, Biodegradable, phosphate-containing, dual-gelling macromers for cellular delivery in bone tissue engineering, Biomaterials, 67 (2015) 286-296.
[232] Y. Chien, Y.W. Liao, D.M. Liu, H.L. Lin, S.J. Chen, H.L. Chen, C.H. Peng, C.M. Liang, C.Y. Mou, S.H. Chiou, Corneal repair by human corneal keratocyte reprogrammed iPSCs and amphiphatic carboxymethyl-hexanoyl chitosan hydrogel, Biomaterials, 33 (2012) 8003–8016.
[233] H. Tan, C.M. Ramirez, N. Miljkovic, H. Li, J.P. Rubin, K.G. Marra, Thermosensitive injectable hyaluronic acid hydrogel for adipose tissue engineering, Biomaterials, 30 (2009) 6844-6853.

[234] C.M. Hwang, M.M. S. Sant, N.N. Kachouie, B. Zamanian, S.H. Lee, A. Khademhosseini, Fabrication of three-dimensional porous cell-laden hydrogel for tissue engineering, Biofabrication, 2 (2010) 035003.

[235] W. Leong, T.T. Lau, D.A. Wang, A temperature-cured dissolvable gelatin microsphere-based cell carrier for chondrocyte delivery in a hydrogel scaffolding system, Acta Biomater., 9 (2013) 6459–6467.

[236] H.H. Jung, K. Park, D.K. Han, Preparation of TGF-β1-conjugated biodegradable pluronic F127 hydrogel and its application with adipose derived stem cells, J. Controlled Release, 147 (2010) 84–91.

[237] M.H. Cha, J. Choi, B.G. Choi, K. Park, I.H. Kim, B. Jeong, D.K. Han, Synthesis and characterization of novel thermo-responsive F68 block copolymers with cell adhesive RGD peptide, J. Colloid Interface Sci., 360 (2011) 78–85.

[238] C.V. Rahman, G. Kuhn, L.J. White, G.T. Kirby, O.P. Varghese, J.S. McLaren, H.C. Cox, F.R. Rose, R. Muller, J. Hilborn, K.M. Shakesheff, PLGA/PEG-hydrogel composite scaffolds with controllable mechanical properties, J. Biomed. Mater. Res. Part B, 101 (2013) 648-655.

[239] I. Mironi-Harpaz, D.Y. Wang, S. Venkatraman, D. Seliktar, Photopolymerization of cell-encapsulating hydrogels: Crosslinking efficiency versus cytotoxicity, Acta Biomater., 8 (2012) 1838-1848.

[240] B. Baroli, Photopolymerization of biomaterials: Issues and potentialities in drug delivery, tissue engineering, and cell encapsulation applications, J. Chem. Technol. Biotechnol., 81 (2006) 491–499.

[241] K.M. Gattas-Asfura, C.L. Stabler, Chemoselective cross-linking and functionalization of alginate via Staudinger ligation, Biomacromolecules, 10 (2009) 3122–3129.

[242] B. Fairbanks, M. Schwartz, C. Bowman, K. Anseth, Photoinitiated polymerization of PEG-diacrylate with lithium phenyl-2,4,6-trimethylbenzoyl phosphinate: Polymerization rate and cytocompatibility, Biomaterials, 30 (2009) 6702–6707.

[243] D.R. Griffin, A.M. Kasko, Photodegradable macromers and hydrogels for live cell encapsulation and release, J. Am. Chem. Soc, 134 (2012) 13103-13107.
[244] A. Kloxin, A. Kasko, C. Salinas, K. Anseth, Photodegradable hydrogels for dynamic tuning of physical and chemical properties, Science, 324 (2009) 59-63.
[245] A.M. Kloxin, M.W. Tibbitt, K.S. Anseth, Synthesis of photodegradable hydrogels as dynamically tunable cell culture platforms, Nat. Protoc., 5 (2010) 1867-1887.
[246] C.A. DeForest, K.S. Anseth, Cytocompatible click-based hydrogels with dynamically tunable properties through orthogonal photoconjugation and photocleavage reactions, Nat. Chem., 3 (2011) 925-931.
[247] A.M. Kloxina, J.A. Bentona, K.S. Anseth, In situ elasticity modulation with dynamic substrates to direct cell phenotype, Biomaterials, 31 (2010) 1-8.
[248] April M. Kloxin, Mark W. Tibbitt, Andrea M. Kasko, Jonathan A. Fairbairn, K.S. Anseth, Tunable hydrogels for external manipulation of cellular microenvironments through controlled photodegradation, Adv. Mater., 22 (2010) 61-66.
[249] M.W. Tibbitt, A.M. Kloxin, K.U. Dyamenahalli, K.S. Anseth, Controlled two-photon photodegradation of PEG hydrogels to study and manipulate subcellular interactions on soft materials, Soft Matter, 6 (2010) 5100-5108.
[250] C.A. DeForest, K.S. Anseth, Photoreversible patterning of biomolecules within click-based hydrogels, Angew. Chem., 124 (2012) 1852–1855.
[251] A.F. Demirörs, P.P. Pillai, B. Kowalczyk, B.A. Grzybowski, Colloidal assembly directed by virtual magnetic moulds, Nature, 503 (2013) 99-103.
[252] B.A. Grzybowski, H.A. Stone, G.M. Whitesides, Dynamic self-assembly of magnetized, millimetre-sized objects rotating at a liquid–air interface, Nature, 405 (2000) 1033-1036.
[253] A. Snezhko, I. Aranson, Magnetic manipulation of self-assembled colloidal asters, Nat. Mater., 10 (2011) 698–703.

[254] Y. Li, G. Huang, X. Zhang, B. Li, Y. Chen, T. Lu, T.J. Lu, F. Xu, Magnetic hydrogels and their potential biomedical applications, Adv. Funct. Mater., 23 (2013) 660-672.
[255] E. Castro, J.F. Mano, Magnetic force-based tissue engineering and regenerative medicine, J. Biomed. Nanotechnol., 9 (2013) 1129-1136.
[256] J.M. Kanczler, H.S. Sura, J. Magnay, D. Green, R.O. Oreffo, J.P. Dobson, A.J. El Haj, Controlled differentiation of human bone marrow stromal cells using magnetic nanoparticle technology, Tissue Eng. Part A, 16 (2010) 3241-3250.
[257] E. Popa, V. Santo, M. Rodrigues, M. Gomes, Magnetically-responsive hydrogels for modulation of chondrogenic commitment of human adipose-derived stem cells, Polymers, 8 (2016) 28.
[258] L.B. Zhao, L. Pan, K. Zhang, S.S. Guo, W. Liu, Y. Wang, Y. Chen, X.Z. Zhao, H.L. Chan, Generation of Janus alginate hydrogel particles with magnetic anisotropy for cell encapsulation, Lab Chip, 9 (2009) 2981-2986.
[259] F. Xu, F. Inci, O. Mullick, U.A. Gurkan, Y. Sung, D. Kavaz, B. Li, E.B. Denkbas, U. Demirci, Release of magnetic nanoparticles from cell-encapsulating biodegradable nanobiomaterials, ACS Nano, 6 (2012) 6640-6649.
[260] Y. Wang, B. Li, Y. Zhou, D. Jia, Chitosan-induced synthesis of magnetite nanoparticles via iron ions assembly, Polym. Adv. Technol., 19 (2008) 1256-1261.
[261] H.-B. Xia, J. Yi, P.-S. Foo, B. Liu, Facile fabrication of water-soluble magnetic nanoparticles and their spherical aggregates, Chem. Mater., 19 (2007) 4087-4091.
[262] S. Tasoglu, D. Kavaz, U.A. Gurkan, S. Guven, P. Chen, R. Zheng, U. Demirci, Paramagnetic levitational assembly of hydrogels, Adv. Mater., 25 (2013) 1137-1143.
[263] S. Tasoglu, C.H. Yu, H.I. Gungordu, S. Guven, T. Vural, U. Demirci, Guided and magnetic self-assembly of tunable magnetoceptive gels, Nat. Commun., 5 (2014) 4702.

[264] C. Hu, M. Nakajima, H. Wang, T. Yue, Y. Shen, M. Takeuchi, Q. Huang, M. Seki, T. Fukuda, Magnetic manipulation for spatially patterned alginate hydroge microfibers, IEEE-NANO, (2013) 529-534.
[265] T. Sun, Q. Huang, Q. Shi, H. Wang, X. Liu, M. Seki, M. Nakajima, T. Fukuda, Magnetic assembly of microfluidic spun alginate microfibers for fabricating three-dimensional cell-laden hydrogel constructs, Microfluid. Nanofluid., 19 (2015) 1169-1180.
[266] E. Amis, Combinatorial materials science: Reaching beyond discovery, Nat. Mater., 3 (2004) 83–85.
[267] P. Bianco, M. Riminucci, S. Gronthos, P. Robey, Bone marrow stromal stem cells: Nature, biology, and potential applications, Stem Cells, 19 (2001) 180-192.
[268] J.F. Mano, Designing biomaterials for tissue engineering based on the deconstruction of the native cellular environment, Mater. Lett., 141 (2015) 198-202.
[269] A.K. Jha, A. Mathur, F.L. Svedlund, J. Ye, Y. Yeghiazarians, K.E. Healy, Molecular weight and concentration of heparin in hyaluronic acid-based matrices modulates growth factor retention kinetics and stem cell fate, J. Controlled Release, 209 (2015) 308-316.
[270] R. Tsaryk, A. Gloria, T. Russo, L. Anspach, R. De Santis, S. Ghanaati, R.E. Unger, L. Ambrosio, C.J. Kirkpatrick, Collagen-low molecular weight hyaluronic acid semi-interpenetrating network loaded with gelatin microspheres for cell and growth factor delivery for nucleus pulposus regeneration, Acta Biomater., 20 (2015) 10-21.
[271] H.J. Lee, Y.H. Park, W.-G. Koh, Fabrication of nanofiber microarchitectures localized within hydrogel microparticles and their application to protein delivery and cell encapsulation, Adv. Funct. Mater., 23 (2013) 591-597.
[272] O. Jeon, D.W. Wolfson, E. Alsberg, In-situ formation of growth-factor-loaded coacervate microparticle-embedded hydrogels for directing encapsulated stem cell fate, Adv. Mater., 27 (2015) 2216-2223.

[273] J.N. Hunt, K.E. Feldman, N.A. Lynd, J. Deek, L.M. Campos, J.M. Spruell, B.M. Hernandez, E.J. Kramer, C.J. Hawker, Tunable, High modulus hydrogels driven by ionic coacervation, Adv. Mater., 23 (2011) 2327-2331.
[274] D.S. Benoit, M.P. Schwartz, A.R. Durney, K.S. Anseth, Small functional groups for controlled differentiation of hydrogel-encapsulated human mesenchymal stem cells, Nat. Mater., 7 (2008) 816-823.
[275] Y. Aizawa, R. Wylie, M. Shoichet, Endothelial cell guidance in 3D patterned scaffolds, Adv. Mater., 22 (2010) 4831–4835.
[276] R. Wylie, S. Ahsan, Y. Aizawa, K. Maxwell, C. Morshead, M. Shoichet, Spatially controlled simultaneous patterning of multiple growth factors in three-dimensional hydrogels, Nat. Mater., 10 (2011) 799–806.
[277] G. Orive, E. Santos, J.L. Pedraz, R.M. Hernandez, Application of cell encapsulation for controlled delivery of biological therapeutics, Adv. Drug Delivery Rev., 67-68 (2014) 3-14.
[278] B. Guillotin, F. Guillemot, Cell patterning technologies for organotypic tissue fabrication, Trends Biotechnol., 29 (2011) 183–190.
[279] M. Marguet, C. Bonduelle, S. Lecommandoux, Multicompartmentalized polymeric systems: Towards biomimetic cellular structure and function, Chem. Soc. Rev., 42 (2013) 512-529.
[280] K. Sun, M. Liu, H. Liu, P. Zhang, J. Fan, J. Meng, S. Wang, Semi-egg-like heterogeneous compartmentalization of cells controlled by contact angle hysteresis, Adv. Funct. Mater., 25 (2015) 4506-4511.
[281] A.M. Kushner, Z. Guan, Modular design in natural and biomimetic soft materials, Angew. Chem., 50 (2011) 9026-9057.
[282] M. Antonietti, P. Fratzl, Biomimetic Principles in polymer and material science, Macromol. Chem. Phys, 211 (2010) 166-170.
[283] N. Lewinski, V. Colvin, R. Drezek, Cytotoxicity of nanoparticles, Small, 4 (2008) 26-49.
[284] Y.-C. Lu, W. Song, D. An, B.J. Kim, R. Schwartz, M. Wu, M. Ma, Designing compartmentalized hydrogel microparticles for cell encapsulation and scalable 3D cell culture, J. Mater. Chem. B, 3 (2015) 353-360.

[285] S.M. Oliveira, R.L. Reis, J.F. Mano, Towards the design of 3D multiscale instructive tissue engineering constructs: Current approaches and trends, Biotechnol. Adv., 33 (2015) 842-855.

2

Experimental methodologies and materials

Chapter II

Materials and methods

Chapter II

Materials and methods [2]

Abstract

In this chapter are described the different materials and methodologies to produce liquified and multilayered capsules. Capsules are composed by an external multilayered membrane produced by the layer-by-layer adsorption of poly(L-lysine), alginate, and chitosan. Additionally, magnetic-nanoparticles were electrostatically bounded to the multilayered shell, conferring magnetic-responsive ability. Within the liquified core different types of cells were encapsulated, namely *(i)* L929 cells, *(ii)* stem cells, and *(iii)* endothelial cells, as well as different surface modified poly(L-lactic acid) microparticles, namely microparticles coated with *(i)* collagen I and *(ii)* collagen II combined with TGF-β3. The different capsules were tested *in vitro* and *in vivo* as bioencapsulation devices for tissue regeneration.

[2] Partially based on the publication: C.R. Correia, R.L. Reis, J.F. Mano, Nanostructured capsules for cartilage tissue engineering, in: P.M. Doran (Ed.), Cartilage Tissue Engineering – Methods and Protocols, Springer, New York, 2015, pp. 181-189.

1. Introduction

Since the pioneering study of Decher [1], the layer-by-layer technique (LbL) has been used in a wide range of biomedical applications, including the production of polymeric multilayered capsules (PMCs). Particularly, PMCs have found great applicability in bioencapsulation systems for tissue engineering and regenerative medicine purposes [2-8]. The production of PMCs is based on the LbL setwise adsorption of polyelectrolytes with oppositely charged macromolecules. Polyelectrolytes are assembly on the surface of spherical particles used as sacrificial templates, and, ultimately, the core is dissolved or eliminated, originating PMCs [9-13]. Due to the high versatility of the LbL technique, different properties of the capsules can be easily tailored; for example, the permeability of the shell can be controlled by varying the number of layers deposited and the surface of the capsules can be customized by endowing nanoparticles, lipids, viruses, among others [14]. While the liquified core ensures the viability of the encapsulated cells by allowing a rapid diffusion of nutrients, oxygen, waste products, and metabolites, the LbL membrane provides an immune privilege environment by blocking the entrance of high molecular weight immune system compounds, such as immunoglobulins and immune cells [15].

The main drawback of capsules in cell encapsulation approaches is related with the fact that most cells are anchorage dependent and, thus, deprived of a physical support cells are not able to adhere and proliferate [16]. Therefore, the liquefaction of the core to achieve an excellent diffusion of essential molecules will, on the other hand, compromise the biological outcome of the encapsulated cells. To ensure an efficient diffusion provided by the liquified environment of PMCs, and simultaneously provide cell adhesion sites to the encapsulated cells, we propose liquified and multilayered capsules encapsulating microparticles as cell supports.

The aim of this chapter is to present in a more comprehensive manner the details concerning both the materials and techniques to produce multilayered and liquified capsules encapsulating surface modified microparticles and different types of cells. The *in vitro* and *in vivo* procedures used to characterize

the developed system are also described. Moreover, the specific processing techniques, namely (*i*) the layer-by-layer technique to produce the multilayered membrane, (*ii*) the plasma treatment for the surface modification of microparticles, and (*iii*) the isolation of cells from adipose tissue are here described. The detailed specifications of the different materials and equipment suppliers can be found in the experimental subsection of each chapter of **Part 3**.

2. Materials

2.1 Membrane materials

2.1.1 Alginate

Alginate is a naturally occurring anionic polymer typically extracted from brown algae, such as *Laminaria hyperborea* and *Iessonia*, by treatment with aqueous alkali solutions. Briefly, after filtration, sodium or calcium chloride is added and an alginate salt is obtained. This alginate salt can be transformed into alginic acid by treatment with diluted hydrochloric acid. Ultimately, upon purification and conversion, a water-soluble sodium alginate powder is obtained [17]. Structurally, alginate embraces a whole family of linear unbranched copolymers composed by homopolymeric blocks of consecutive or alternating *(1,4)*-linked-β-D-mannuronate (M) and α-L-guluronate (G) residues. D-Mannuronic acid is $^{4}C_{1}$ with diequatorial links, while L-guluronic acid is $^{1}C_{4}$ with diaxial links. The blocks are similar (MMMMM or GGGGGG) or strictly alternating (GMGMGM), and the relative amount is dependent on the origin of the alginate [18]. Due to its biocompatibility, low toxicity, low cost, and mild gelation conditions, alginate has been extensively used to produce hydrogels for biomedical applications. Disadvantages of this material include that it is not naturally broken down enzymatically in mammals and hence has poorly regulated degradation *in vivo*. In addition, cells do not naturally adhere to alginate. Over the past decade there has been significant research to overcome these drawbacks and to broaden the utility of alginate hydrogels.

The most common method to produce alginate hydrogels is to crosslink with divalent cations, usually calcium chloride. The divalent cations bind exclusively to the G blocks of the adjacent alginate chains through interactions with the carboxylic groups, since the structure of the L-guluronate offers a greater flexibility than the D-mannuronate chains. By creating ionic inter-chain bridges, divalent ions replace the hydrogen bonds between the carboxyl group of D-mannuronate (pKa 3.38) and the 2-OH and 3-OH groups of the subsequent L-guluronate (pKa 3.65), originating the gelation of aqueous alginate solutions by the egg-box conformation [19].

2.1.2 Chitosan

Chitosan is a cationic polymer resulting from the deacetylation of chitin under alkaline conditions or by enzymatic hydrolysis in the presence of a chitin deacetylase [20]. Due to the semi-crystalline morphology of chitin, when chitosan is obtained from a solid-state reaction, it has a heterogeneous distribution of acetyl groups along the chains. Depending on the origin of the polymer and on the distribution of acetyl groups, when the degree of deacetylation (DD) of chitin is c.a. 50%, it becomes soluble in aqueous acidic solutions and is called chitosan [21]. The solubilization occurs by protonation of the $–NH_2$ function on the C2 position of the D-glucosamine repeat unit [20]. Therefore, the polysaccharide is converted to a polyelectrolyte in acidic solutions, which favors its solubility due to electrostatic repulsions. Owing to its well-established biocompatibility and a number of other appealing properties, chitosan has been widely used in biomedical applications to produce different biomaterials, such as hydrogels [22], films [23], fibers [24] or, sponges [25].

The solubility of chitosan is influenced by different parameters, namely the DD, ionic concentration, pH, nature of the acid used for protonation, and the distribution of the acetyl groups along the polymer chain [20, 21]. The isolation of chlorohydrate or acetate salt forms in chitosan results in direct water solubility, giving an acidic solution with pKa of c.a. 6.5 [26, 27]. Along the different chitosan derivatives described in literature [20] it is important to

highlight the specific reactions involving the $–NH_2$ group at the C2 position or non-specific reactions of –OH groups at the C3 and C6 positions, especially esterification and etherification [28]. The $–NH_2$ in the C2 positions is the main key difference between chitosan and cellulose, where three –OH groups of nearly equal reactivity are available. The main reactions easily performed involving the C2 position are the quaternization of the amino group or the reductive amination between an aldehydic function with $–NH_2$. Particularly, the reductive amination has the advantage of being performed in aqueous solutions at mild conditions. Therefore, this method has been proposed to produce a wide range of chitosan derivatives by the introduction of different functional groups. In order to obtain more regular and reproducible chitosan derivatives, especially when biological applications are aimed, the modification reactions should be performed in highly deacetylated chitin, assuring quality control of the initial material that originates chitosan. Many companies, such as NovaMatrix with Protasan UP CL 213 used in our experiments, commercialize purified water-soluble chitosan with ultra low levels of endotoxins and proteins and with a DD between 75% to more than 90%. Those purified chitosans has been used in wide range of biomedical applications, including tissue repair, wound healing, local delivery of cells, drugs, proteins, genes and other therapeutics, orthopedics, rheumatology, and reconstructive surgery [21].

2.1.3 Poly(L-lysine)

Poly(L-lysine) (PLL) is the most widely used polycation to coat alginate hydrogels for cell encapsulation. In fact, it has been reported that more then 85% of the articles about cell encapsulation technology published since the original manuscript of Lim and Sun [29] have involved modifications of the alginate-PLL system [30]. Since charged PLL is known to be immunogenic [31], the PLL-alginate hydrogels usually undergo a final incubation with alginate, known as APA capsules. However, several studies have reported that APA capsules are not fully biocompatible since induced the production of cytokines involved in the systemic inflammation, such as tumor necrosis factor

(TNF)-α and interleukin (IL)-1 [32-34], suggesting that the external alginate coating is not effectively masking and/or neutralizing the immunogenic PLL. Consequently, different attempts have been made to improve knowledge about all the variables that might affect the biocompatibility of the encapsulation devices. Efforts should be focused on either properly balancing any net positive charge that is created at the capsule surface due to excessive exposure of NH_3^+ residues, or finding a way to physically mask all the PLL [35]. Therefore, in the present thesis, to produce the multilayered membrane of liquified capsules, PLL was combined with alginate and chitosan by layer-by-layer technique. The objective was to take advantage of the high biocompatibility of the two natural polymers alginate and chitosan, while PLL was expected to enhance the mechanical stability of the system. This assembly of three-component polyelectrolytes via alternate deposition has fuelled much interest due to its demonstrated superior tunability and versatility to the traditional two-component method [36, 37].

2.1.4 Magnetic-nanoparticles

As a *proof-of-concept*, magnetic-nanoparticles (MNPs) of iron oxide (Fe_3O_4) were electrostatically bond to the multilayered membrane to confer magnetic-response ability to the capsules. Fe_3O_4 nanoparticles have received enormous interests and attracted the most attention due to its unique magnetic properties and biocompatibility. Therefore, capsules and MNPs have been combined in several biomedical applications, including targeted drug delivery, tissue engineering, magnetic thermotherapy (hyperthermia), magnetic resonance imaging, among others [38-40]. By employing magnetic manipulation we envisage that magnetic-responsive capsules can aggregate and form moldable and complex macrostructures, in which each liquified capsules could work as compartmentalized building blocks. Capsules can be fixated *in situ*, and their motion can be controlled and guided into a specific spot. These features might be useful for the handling of the capsules during *in vitro* studies but also to guide and fixate the injectable capsules into a lesion site during implantation procedures. Besides movement control, the high

surface area to volume ratio of MNPs provides abundant chemically active sites for functionalization and biomolecule conjugation, which may allow the implementation of other features to increase the complexity of the capsules.

2.2 Encapsulated core materials

2.2.1 Microparticles bulk and coating materials

In order to provide cell adhesion sites to the encapsulated cells within the liquified core of capsules, poly(L-lactic acid) (PLLA) was used as a bulk material to produce microparticles. PLLA is a biodegradable thermoplastic aliphatic polyester derived from the polymerization of L-lactide in lactic acid [41]. Polyesters have been well documented for their excellent biodegradability, biocompatibility, nontoxicity and their biocompatible degradation products. Therefore, PLLA has gained the approval of US Food and Drug Administration (FDA) [42]. However, poor hydrophilicity and the lack of natural recognition sites on polyester surfaces for covalent cell-recognition signal molecules to promote cell attachment have limited the utility of PLLA as tissue engineering biomaterials [43, 44]. Different techniques to modify the surface of those biomaterials have been proposed to enhance cell-material interaction. In the present thesis, the modification of PLLA surface was achieved by combining plasma treatment with different types of collagen, namely *(i)* collagen type I as a control material to allow the adhesion of L929 cells to PLLA microparticles (**Chapters III** and **IV**) as a *proof-of-concept* of the multilayered and liquified capsules as bioencapsulation systems for tissue regeneration, or to apply the developed multilayered and liquified capsules encapsulating adipose-derived stem cells (ASCs) and endothelial cells towards bone regeneration (**Chapters VI** and **VII**); and (ii) collagen type II (**Chapter V**) to apply the developed multilayered and liquified capsules encapsulating ASCs towards cartilage regeneration. Collagen type I is the most abundant type of collagen in bone, providing to the tissue the ductility and ability to absorb energy (toughness) [45]. Collagen II is the major component of the collagen fibrillar network, being also essential for the mechanical stability and the

proper function of the tissue [46]. Additionally, TGF-β3 was also immobilized at the surface of collagen II coated PLLA microparticles (**Chapter V**). TGF-β3 was selected since it has the highest and rapid chondrogenic potential among the different isoforms [47-49]. The immobilization of TGF-β3 was performed by the enzyme transglutaminase-2 (TG2). TG2 is a ubiquitously expressed member of an enzyme family catalyzing Ca^{2+} dependent transamidation of proteins via ε(γ-glutamyl)lysine bonds, being its ability to crosslink proteins, including collagen II, well described in the literature [50-52].

2.2.2 Encapsulated cells

To test the ability of the multilayered and liquified capsules as bioencapsulation systems, different cells were encapsulated within the liquified core, namely *(i)* L929 cells (**Chapters III** and **IV**), *(ii)* human ASCs (**Chapter V**) and *(iii)* ASCs co-cultured with human adipose-derived microvascular endothelial cells (ECs, **Chapters VI** and **VII**).

L929 is an immortalized cell line able to proliferate indefinitely, being thus very useful to study different cell-materials interactions *in vitro.* Such cell source offers the advantage of being more homogeneous and standardized than primary cultures. Therefore, L929 cells were encapsulated within the capsules to prove the concept in **Chapter III** and **IV**.

Directing the application of the capsules towards specific tissue regeneration fields, namely of bone and cartilage, stem and endothelial cells were used as the biological encapsulating material, namely (i) ASCs (**Chapters V**, **VI** and **VII**) and (ii) ECs (**Chapters VI** and **VII**). Due to a number of appealing features such as multipotent character [53], being available in large quantities, and easy accessibility, both cell types were isolated from human adipose-tissue.

3. Specific techniques

3.1 Production of micro and nanoparticles

PLLA microparticles were produced by oil/water emulsion technique. For that, 5% w/v of PLLA was dissolved in methylene chloride (CH_2Cl_2). Under agitation,

this solution was added to 0.5% w/v polyvinyl alcohol. After 2 days at room temperature (RT) to evaporate the organic solvent, the produced microparticles were subsequently collected, washed with distilled water, and lyophilized for 3 days.

Iron oxide (Fe_3O_4) nanoparticles were synthesized by the co-precipitation reaction of ferrous ($FeCl_2.4H_2O$) and ferric ($FeCl_3.6H_2O$) salts in the presence of ammonium hydroxide (NH_4OH) under a nitrogen atmosphere at 60ºC. The obtained MNPs were washed with deionized water and ethanol for several times, and ultimately dried in a vacuum oven.

3.2 Layer-by-layer technique to produce the multilayered membrane

Layer-by-layer (LbL) is one of the most prominent surface engineering strategies in biomaterials science, capable of providing a reliable, easy, versatile, environment friendly, and cost-effective way of tuning interfaces [8]. The principle of the technique is based on the sequential adsorption of a wide range of polyelectrolytes, which are selected and combined in function of their multipoint interactions [8, 54]. LbL methodology has been widely applied to produce PMCs, in which capsules are fabricated through LbL sequential deposition of polymers onto a sacrificial core template followed by the decomposition of this core yielding hollow capsules [55, 56]. The obtained nanometer thin membrane is permselective allowing diffusion of water and ions but excluding larger molecules.

Using the LbL principle, different polyelectrolytes at 0.5 $mg.mL^{-1}$ and previously sterilized by filtration were used to coat the surface of alginate hydrogels. For that, alginate hydrogel particles were first immersed in chitosan (**Chapter III**) or in PLL (**Chapters IV, V, VI, and VII**) solutions, and subsequently in alginate solution. The polyelectrolyte solutions were dissolved in 0.15 M sodium chloride (NaCl) containing 25 mM MES hydrate buffer. Following a 10 min period for each polymer adsorption, the excess of macromolecules was removed by immersion in NaCl for 5 min. This process was repeated until the desired number of layers is achieved. Additionally, to confer magnetic-response properties to capsules, in the last adsorption of chitosan solution 1

mg.mL^{-1} of magnetic-nanoparticles (MNPs) (**Chapter V**) were added. MNPs could be incorporated within the multilayered membrane due to the electrostatic attraction between the negatively charged MNPs and the positively charged chitosan polyelectrolyte solution.

3.3 Plasma treatment combined with collagen coating

Plasma treatment is an effective and widely used method for modifying the surface of biomaterials to improve cell-material interaction. The principle is based on the presence free electrons in the air, which are accelerated by a high voltage discharge and ionize the gas. As a result, chemical and physical modifications occur on the treated surfaces, creating reactive sites such as amine group and carboxyl [41].

In the present thesis, plasma treatment was used to modify the surface of PLLA microparticles. Microparticles were placed in a plasma reactor chamber fitted with a radio frequency generator. Air was used as the working atmosphere. A glow discharge plasma of 0.2 mbar at 30 V was created for 15 min. Subsequently, 500 mg of microparticles were sterilized by 30 min of UV radiation and immediately immersed in 1200 μg of collagen I 4 h at RT (**Chapters III, IV, VI** and **VII**) or 1700 μg collagen II overnight at 37°C (**Chapter V**). Additionally, after washing with phosphate-buffered saline (PBS), collagen II-microparticles were then immersed in a solution containing TGF-β3 (10 ng per 50 mg of microparticles) and TGs (0.01 U per 50 mg of microparticles) overnight at 4°C (**Chapter V**).

3.4 Isolation of stem and endothelial cells from human adipose tissue

Subcutaneous adipose tissue from liposuction procedures was used to isolate both ASCs [39] and ECs [57]. The collected tissues were obtained under a cooperation agreement between the 3B's Research Group and Hospital da Prelada (Porto, Portugal), after approval of the Competent Ethics Committee (CEC). The human tissues received were handled in accordance with the guidelines approved by the CEC. Informed consent was obtained from all subjects. Tissue samples were transported in PBS supplemented with

penicillin-streptomycin (10%, pen-strep) and kept at 4°C. The lipoaspirates were washed with PBS and incubated with collagenase type II A (0.05% w/v) for 45 min at 37°C in a shaking water bath. The digested samples were filtered (200 µm) and centrifuged at 800 g for 10 min at 4 °C. The obtained stromal vascular fraction (SVF) was resuspended in erythrocyte lysis buffer at pH 7.4 containing ammonium chloride (155 mM), potassium bicarbonate (5.7 mM), and ethylenediaminetetraaceticacid (0.1 M, EDTA) in distilled water. After 10 min of incubation at RT, the mixture was centrifuged at 300 g for 5 min.
To isolate the ASCs the red blood cell-free SVF was resuspended in α-MEM medium supplemented with fetal bovine serum (10%, FBS) and pen-strep (1% v/v). To isolate the ECs the red blood cell-free SFV was resuspended in EndoGro™-MV-VEGF complete media kit. The ECs were plated in cell culture flasks, previously coated with gelatin (0.7% w/v, porcine skin type A) for 30 min at 37°C. Culture medium was changed 48 h after initial plating and then every 3-4 days for both cell phenotypes.

3.5 Bioencapsulation set-up

At 90% confluence, cells grown in tissue culture flasks were washed with PBS and subsequently detached using TrypLE™ Express solution at 37°C for 5 min. PBS was added and the cell suspensions were centrifuged for 5 min at 300 g. Low viscosity sodium alginate from brown algae (1.5% w/v) was dissolved in 0.15 M NaCl containing 25 mM MES hydrate at pH 7. The solution was sterilized by 0.22 µm filtration. Different cells were then ancapsulated, namely (*i*) $1x10^6$ L929 cells (**Chapters III and IV**), (*ii*) $5x10^6$ ASCs alone (**Chapters V, VI and VII**) or mixed with $5x10^6$ ECs (**Chapters VI and VII**) were added to the different microparticles (50 $mg.mL^{-1}$ of alginate). The alginate solutions were then used to produce liquified and multilayered capsules.
The alginate solutions containing cells and microparticles were added drop wise using 18 G (**Chapters III and IV**) or 21 G needles (**Chapters V, VI and VII**) to 0.1 M calcium chloride ($CaCl_2$) buffered with 25 mM MES hydrate at pH 7. After 20 min at RT, alginate hydrogels were collected and rinsed in a washing

solution of 0.15 M NaCl. The external membrane was processed by subsequent adsorption of oppositely charged polyelectrolytes by layer-by-layer deposition as referred at *3.1 Layer-by-layer technique to produce the multilayered membrane.* The coated hydrogels were ultimately immersed in 20 mM EDTA at pH 7 for 5 min to liquefy the alginate core. The scheme for the production of liquified and multilayered capsules encapsulating surface modified microparticles and cells is shown in **Figure II.1.**

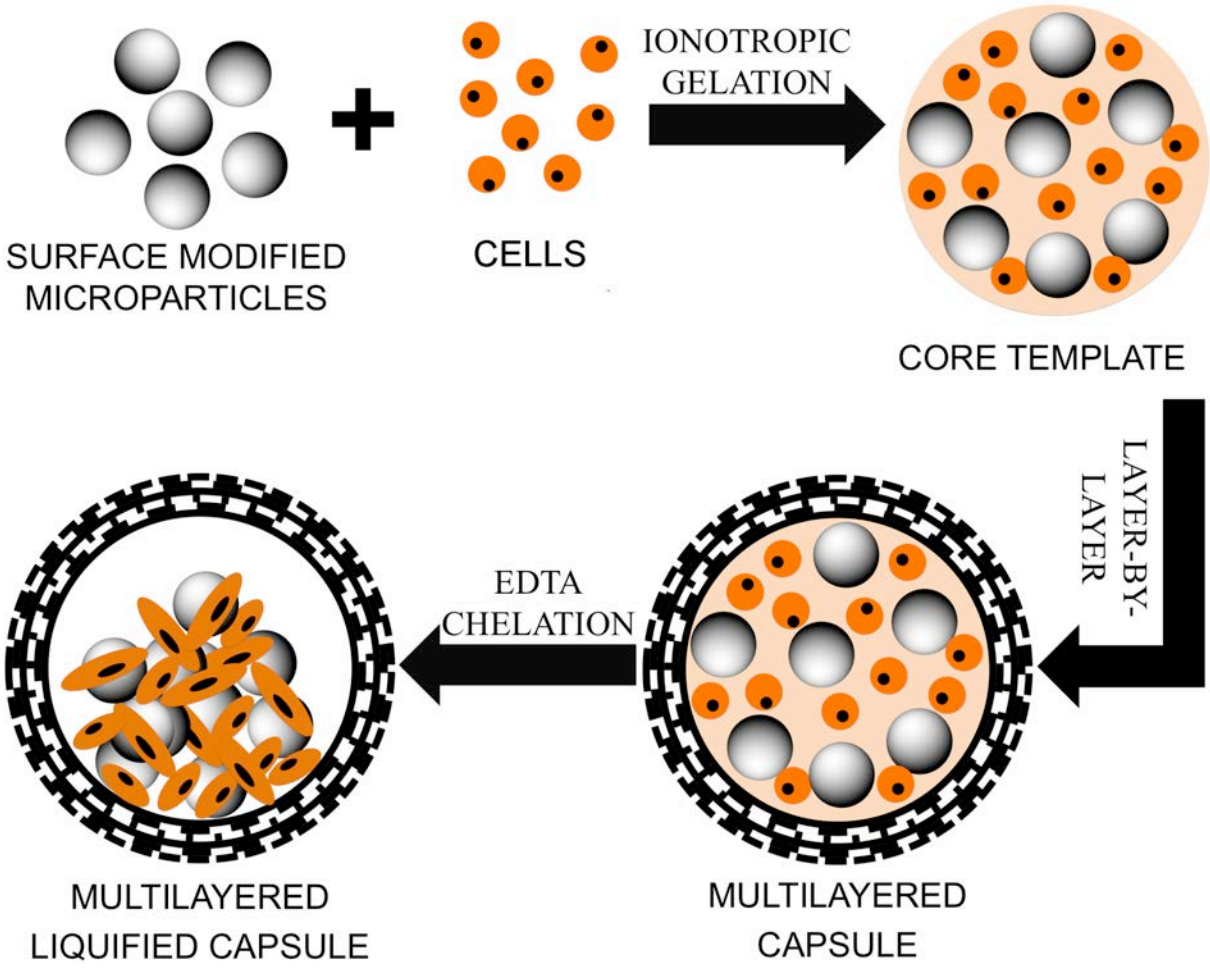

Figure II.1 · Schematic representation of the production steps of liquefied and multilayered capsules encapsulating surface-modified microparticles and cells.

The different capsules were ultimately cultured in different cell culture media according to the type of cells encapsulated and the application propose of the developed bioencapsulation system. Therefore, capsules encapsulating (*i*) L929 cells were cultured in low glucose DMEM supplemented with 3.7 $g \cdot L^{-1}$

sodium bicarbonate, 10% FBS, and 1% pen-strep at pH 7.4 (**Chapters III and IV**); (*ii*) ASCs for cartilage regeneration (**Chapter V)** in DMEM High glucose, FBS (10% v/v) and pen/step (1:100) with or without supplementation with ITS + premix (1:100), MEM sodium pyruvate (1:100), proline ($0.4x10^{-4}$ M), dexamethasone ($100x10^{-9}$ M) and TGF-β3 (10 $ng.mL^{-1}$); (*iii*) ASCs co-cultured with ECs for bone regeneration (**Chapters VI** and **VII**) in EndoGro™-MV-VEGF complete kit media without ascorbic acid. To this endothelial medium, β-glycerophosphate (10 mM) was added. Additionally, capsules were also cultured in endothelia medium supplemented with osteogenic differentiation factors, namely, dexamethasone (10 nM), ascorbic acid (50 $\mu g.mL^{-1}$), and β-glycerophosphate (10 mM).

All the capsules were transferred to non-adhesive plates and incubated at 37°C in a humidified 5% CO_2 air atmosphere. The entire procedure was performed under sterile conditions in appropriate flow chambers. All the solutions used at this step were sterilized by filtration through a 0.22 μm filter.

4. Methods

4.1 Physicochemical characterization

4.1.1 Quartz-crystal microbalance with dissipation monitoring

The build-up process of the multilayered membrane growth was monitored by a quartz-crystal microbalance with dissipation monitoring (QCM-D) in a liquid environment (**Chapters III and IV**). An equivalent circuit model was fitted to the impedance curve, and the obtained parameters were used to calculate the thickness of the multilayers. For that, PLL, alginate and chitosan polyelectrolytes were deposited on gold-coated quartz crystals. Before adsorption, the quartz crystals were cleaned with 0.15 M sodium chloride solution at 25ºC until a baseline was obtained. Polymeric and washing solutions were alternatively introduced into the measuring chamber at a flow rate of 100 $mL.min^{-1}$. Variations in frequency (ΔF) and in dissipation (ΔD) were

monitored in real time up to a deposition of 8 cycles. The frequency of each overtone was normalized to the fundamental resonant frequency of the quartz-crystal ($\Delta F_v/v$, in which v stands for the overtone). Thickness assessment was estimated using the Voigt viscoelastic model.

4.1.2 Ion coupled plasma

Ion coupled plasma (ICP) was performed to quantify the release of calcium during and after the liquefying process (**Chapter III**). Capsules were placed in EDTA solution with different concentrations, namely 0.02 M, 0.05 M or 0.1 M. After each 5 min, 3 mL of EDTA solution were withdrawn and replaced by fresh solution. The concentration of calcium in solution was then automatically measured by ICP. Additionally, capsules were placed in EDTA solutions for 5 min and then transferred to a 0.15 M NaCl. Similarly, after each 5 min, 3 mL of NaCl were withdrawn and replaced by fresh solution. For both experiments, after 30 min, capsules were destroyed ensuring the total release of the remaining calcium in the core. Data analysis was performed as a cumulative release assay.

4.1.3 Scanning electron microscopy and energy dispersive X-ray spectroscopy

The membrane morphology of capsules (*i*) composed by different number of layers (**Chapter III**) or (*ii*) with MNPs adhered at the surface (**Chapter V**) was visualized by scanning electron microscopy (SEM). Additionally, SEM was also used to visualize the surface morphology of microparticles before and after plasma treatment (**Chapter IV**). Due to the magnetite composition of the MNPs, their spatial dispersion could be also assessed by iron detection through energy dispersive X-ray spectroscopy (EDS) analysis (**Chapter V**). Capsules were dehydrated using sequential ethanol series, namely 45%, 50%, 60%, 70%, 80%, 90%, 96% and 100% v/v, 10 min each. Prior to SEM visualization EDS analysis was performed. Then, samples were gold-coated using a sputter coater.

4.1.4 Membrane mechanical stability

The influence of depositing different number of layers on the mechanical stability of capsules was evaluated using a rotational stress test. Different types of membrane were tested, namely (*i*) to assess the influence of the number of layers in the mechanical resistance of the membrane (**Chapter III**) 4-, 6- or 8- bilayered capsules composed by an alginate and chitosan membrane (n = 15 in triplicates) were tested; and (*ii*) to assess the contribution of the PLL presence into the stability of the multilayered membrane 12-layered capsules with PLL and 12-layered capsules without PLL (n = 10 in triplicates) were tested (**Chapter IV**). Capsules were placed in centrifuge tubes containing 5mL of PBS. The tubes were rotated at a speed of 200 rpm for 60 min at RT. After every 15 min of rotation, the number of damage capsules was observed and counted under a light microscope. The intact capsules were placed again inside the centrifuge tubes to continue the rotational test.

4.2 *In vitro* biological performance analysis

4.2.1 MTS

Capsules were tested for cytotoxicity and suitability for living cell encapsulation using a MTS colorimetric assay. This metabolic activity assay is based on the bioreduction ability of mitochondrial dehydrogenase enzymes present in viable cells to convert the *3*-(*4,5*-dimethylthiazol-*2*-yl)-*5*-(*3*-carboxymethoxyphenyl)-*2*-(*4*-sulphofenyl)-2H-tetrazolium (MTS) compound into a cell culture soluble brown formazan product.

The different bioencapsulation systems, namely (*i*) alginate particles and capsules encapsulating L929 cells (**Chapters III and IV**), (ii) capsules encapsulating ASCs (**Chapter V**), and (iii) capsules encapsulating ASCs co-cultured with ECs (**Chapter VI**) were placed in cell culture plate and incubated at 37°C and 5% CO_2. At different pre-determined periods, MTS assay was performed protected from light. Briefly, culture medium was removed and 1 mL of serum-free DMEM containing MTS solution with a dilution ratio of 1:5

was added to each well. Samples were then incubated in the dark at 37°C and 5% CO_2. After 3 h, 100 µL of each well (in triplicate) was transferred to a 96-well plate. The amount of formazan product was measured by absorbance at a wavelength of 490 nm using a multiwall spectrophotometer.

4.2.2 DNA

Capsules ability to support the proliferation of encapsulated cells was tested by DNA quantification assay. The different bioencapsulation systems, namely (*i*) alginate particles and capsules encapsulating L929 cells (**Chapters III and IV**), (ii) capsules encapsulating ASCs (**Chapter V**), and (iii) capsules encapsulating ASCs co-cultured with ECs (**Chapter VI**) were placed in cell culture plate and incubated at 37°C and 5% CO_2. At different pre-determined periods each well was washed with PBS and 1 mL of ultrapure sterile water was added. Upon mixing, contents were transferred to eppendorf tubes, which were then placed in a shaking water bath at 37°C for 1 h. Ultimately, the tubes were immediately stored at -80°C until use. Quantification of total DNA was determined after cell lysis, according to the manufacturer's description. After transferring each solution to a 96-well white opaque plate (in triplicate), the plate was incubated at RT protected from light for 10 min. The standard curve for DNA analysis was generated with provided DNA from the assay kit. Fluorescence was read at excitation of 485/20 nm and emission of 528/20 nm using a multiwall spectrophotometer.

4.2.3 Flow cytometry

The phenotypic profile of ASCs and ECs before and after encapsulation within capsules for bone regeneration (**Chapter VI**) was assessed regarding mesenchymal (CD105-FITC, CD90-APC, and CD73-PE) and endothelial (CD31-APC) markers. Isolated and encapsulated cells were harvested by TrypLE™ Express solution at 37°C for 5 min, and centrifuged. Samples were resuspended in PBS solution containing bovine serum albumin (3% w/v, BSA) and the specified antibodies at the dilutions defined by the manufacture's specifications. After 20 min at RT, samples were subsequently washed with

PBS, centrifuged, fixed in PBS with formaldehyde (1% v/v), and analyzed in a flow cytometer.

4.2.4 Alkaline phosphatase activity and calcium quantification

Alkaline phosphatase (ALP) is an enzyme secreted by active osteoblasts, and is responsible for the cleavage of pyrophosphate ions, which are inhibitors of the formation of hydroxyapatite crystals. The hydrolysis reaction results in the saturation of the extracellular fluid with orthophosphates that induce mineralization [58, 59]. Increased levels of ALP activity are thus correlated with enhanced osteogenic differentiation [60]. Therefore, capsules encapsulating ASCs and ECs for bone regeneration (**Chapters VI** and **VII**) were tested for ALP quantification. The activity of ALP was determined by the amount of p-nitrophenol. A substrate solution at pH 9.8 was prepared by dissolving *4*-nitrophenylphosphate disodium salt hexahydrate (0.2% w/v) in diethanolamine (1 M). Each sample (20 µL, in triplicate) was mixed with the prepared substrate solution (60 µL). After 45 min at 37°C protected from light, the reaction was stopped (80 µL) with sodium hydroxide (NaOH, 2 M) and EDTA (0.2 mM). A standard curve with a range of concentrations was prepared by diluting *4*-nitrophenol solution (10 mM) in the stop solution. Absorbance was read at 405 nm in a microplate reader. Results were normalized with dsDNA quantification data.

The amount of calcium in the extracellular matrix (ECM) of capsules encapsulating ASCs and ECs for bone regeneration (**Chapter VI**) was also quantified. Samples were washed with PBS and resuspended in 100 µL of HCl (6 M). A standard curve was prepared with a $CaCl_2$ solution (5 mM). 10 µL of each sample and standard (in triplicate) were transferred to a 96-well plate. Upon mixing the calcium kit components according to manufacture's specifications, absorbance was read at 570 nm in a microplate reader.

4.2.5 TGF-β3, BMP-2 and VEGF cytokines quantification

The amount of TGF-β3 in the supernatant coating solution after immersion of

surface modified PLLA microparticles (**Chapter V**) was quantified by a commercially available human TGF-β3 ELISA kit. Absorbance was read at 450 nm with correction wavelength set to 570 nm in a microplate reader. The amount of TGF-β3 coating the microparticles was calculated by subtracting the ELISA quantification results to the initial amount of the prepared TGF-β3 solution (10 ng). Then, the PLLA microparticles immobilized with TGF-β3 were immersed in PBS for 7 days. The PBS solution was also quantified by ELISA to assess if TGF-β3 was released from the surface of microparticles.

The profile of BMP-2 and VEGF cytokines release into the supernatants of capsules encapsulating ASCs co-cultured with ECs for bone regeneration (**Chapter VI**) was assessed by ELISA quantification assay. The supernatants (500 µL) were stored at -80ºC with a diluted protease inhibitor cocktail (1:100) until analysis. Commercially available human BMP-2 and VEGF ELISA development kits were used according to manufacture's specifications. Absorbance was read at 405-650 nm in a microplate reader.

4.2.6 Glycosaminoglycans quantification

The quantification of sulfated glycosaminoglycans (GAGs) was performed by the dimethylmethylene blue (DMB) assay [61]. Briefly, a digestion buffer at pH 6.8 composed by phosphate buffer ($200x10^{-9}$ M) and EDTA ($1x10^{-4}$ M) was prepared. To the digestion buffer (50 mL), papain (25 mg) and L-cysteine hydrochloride anhydrous were added. The prepared papain solution was added to each well containing capsules encapsulating ASCs for cartilage regeneration (**Chapter V**) (1 mL, n = 4 capsules, in triplicate). Samples were incubated at 65ºC for 18 h. To perform the DMB assay, a standard curve with chondroitin *4*-sulfate was prepared. Additionally, the DMB dye (16 mg) was dissolved in absolute ethanol (5 mL), and then NaCl (2.37 g) and glycine (3.04 g) dissolved in distilled water (900 mL) were added. The pH was set to 3 and distilled water was added to make up 1 L. Samples or chondroitin sulfate standards (20 µL) were mixed with the prepared DMB dye (250 µL) in a transparent 96-well plate. Absorbance was read at 595 nm using a microplate reader. Total DNA

quantification was used to normalize the DMB content.

4.2.7 RNA extraction, cDNA production and quantitative real-time polymerase chain reaction (qPCR)

The extraction of mRNA was performed using TRIzol reagent. Capsules (n = 5 per well in triplicate) were stored in TRIzol (800 µL) at -80ºC until analysis. Samples were slowly defrosted on ice and chloroform (160 µL) was added. After 15 min at 4ºC, samples were centrifuged at 13000 rpm for 15 min. The aqueous part of each sample was collected and isopropanol (400 µL) was added. Following an overnight incubation at -20ºC, samples were centrifuged at 13000 rpm for 10 min at 4ºC. The supernatant was discarded and the resulting pellets were washed with ethanol (70% v/v) in RNase/DNase free distilled water. The pellets were let to partially dry on air, and dissolved in RNase/DNase free distilled water (10 µL). RNA quantity and purity was determined in nanodrop spectrophotometer. Samples with a 260/280 purity ratio higher than ~1.8 were used for cDNA synthesis. The cDNA synthesis was performed using a qScript cDNA SuperMix kit and a MiniOpticon Real-time PCR Detection System. All samples were normalized (1 µg of RNA in 20 µL of RNase/DNase free distilled water).

The expression of different genes were quantified in the cDNA samples using a real-time PCR reaction. Different genes were analyzed, namely (*i*) chondrogenic gene, specifically collagen I, II, and X, aggrecan and SOX9 (**Chapter V**), (*ii*) osteogenic genes, specifically bone morphogenic protein-2 (BMP-2), transcription factor RUNX2, and bone sialoprotein (BSP) (**Chapter VI**), (*iii*) angiogenic genes, specifically von Willebrand factor (vWF), CD31, and vascular endothelial growth factor A (VEGF-A) (**Chapter VI**). The target genes were normalized with 18S rRNA as the housekeeping. The primers (200 nM) were designed to span exon-exon junctions using the primer-BLAST tool. The primers sequences are showed in **Table II.1**.

Table II.1 – Primer sequences used for real-time polymerase chain reaction, with the respective purpose of selection.

Type	Name	Forward/reverse sequence	Purpose
Housekeeping	18S	5'-GAAACCTTCCGACCCCTCTC-3' 5'-TACGAGGTCGATTTGGCGAG-3'	18S ribosomal RNA is a widely used control for qPCR analyses because of its invariant expression across tissues, cells, and experimental treatments.
Chondrogenic markers	Collagen I	5'-AAGAACCCCAAGGACAAGAG-3' 5'-GTAGGTGATGTTCTGGGAGG-3'	Type I collagen is highly expressed in ASCs. Monitoring this marker transcript reveals the degree to which fibrous tissue may develop.
	Collagen II	5'-CGGTGAGAAGGGAGAAGTTG-3' 5'-GACCGGTCACTCCAGTAGGA-3'	Type II collagen is the primary protein in the extracellular matrix of articular cartilage and provides a critical mechanical function. Thus, high expression of This marker is desirable.
	Collagen X	5'-CAGGCATAAAAGGCCCACTA-3' 5'-AGGACTTCCGTAGCCTGGTT-3'	Type X collagen is the hallmark hypertrophic chondrocyte marker. Type X collagen is found in the transition from articular cartilage to bone. Hence, some expression of this marker is desirable. Excessive expression may indicate tissues tending toward an ossification pathway.
	Aggrecan	5'-TGAGTCCTCAAGCCTCCTGT-3' 5'-TGGTCTGCAGCAGTTGATTC-3'	Aggrecan is a large aggregating proteoglycan found in articular cartilage. High levels of this marker transcription are desirable in chondrogenesis.
	SOX9	5'-TTCATGAAGATGACCGACGC-3' 5'-GTCCAGTCGTAGCCCTTGAG-3'	SOX9 encodes a potent chondrogenic transcription factor and is closely correlated with the transcription of collagen II marker.
Osteogenic markers	BMP-2	5'-TGAATCAGAATGCAAGCAGG-3' 5'-TCTTTTGTGGAGAGGATGCC-3'	BMP2 induces DLX3, a homeodomain protein that activates RUNX2 gene transcription.
	RUNX2	5'-TTCCAGACCAGCAGCACTC-3' 5'-CAGCGTCAACACCATCATTC-3'	RUNX2 is the master switch (earliest transcription) for osteogenic differentiation. It is crucial for the generation of a mineralized tissue.
	BSP	5'- ACTGAGCCTGTGTCTTGAAA-3' 5'-CTTCCAACAGCCAATCACTG-3'	BSP is a significant component of the bone extracellular matrix. High levels of this marker transcription are related to the mineralizing potential of the cells.
Angiogenic markers	vWF	5'-CCCTGGGTACAAGGAAGAAAAT-3' 5'-AGTGTCATGATCTGTCTCCTCTTAG-3'	vWF is a glycoprotein produced uniquely by endothelial cells, and is responsible to regulate angiogenesis.
	CD31	5'-AAGGCCAGATGCACATCC-3' 5'-TTCTACCCAACATTAACTTAGCAGG-3'	CD31 is expressed by endothelial cells. The encoded protein is a member of the immunoglobulin superfamily, and transcription of this marker is correlated to angiogenesis.
	VEGF-A	5'- GATCCGCAGACGTGTAAATG-3' 5'-TACGAGGTCGATTTGGCGAG-3'	VEGF is a very potent angiogenic agent that has a central role in normal physiological angiogenesis.

The real-time PCR reaction was done using the PerfeCTa SYBR Green FastMix Reaction Mixes, according to manufacturer's specifications. The reactions were monitored in a Mastercycler using the software *Realplex* (version 2.2). The relative quantification of the markers expression was performed using the $2^{-\Delta\Delta CT}$ method (Perkin-Elmer). Results in **Chapter V** are expressed relatively to capsules without TGF-β3 supplementation **at day 1,** and in **Chapter VI** relatively to gene expression levels of each formulation of capsules at day 3.

4.2.8 Scanning electron microscopy visualization

The morphology of the different encapsulated cells, namely (*i*) L929 cells (**Chapters III and IV**), (ii) ASCs (**Chapters V, VI and VII**), and (iii) ECs (**Chapter VI**) was visualized by SEM. After pre-determined periods, capsules (n = 4 per well in triplicate) were washed with PBS and fixed at RT in formalin (10% v/v).

After 1 h at RT, samples were dehydrated in an increasing gradient series of ethanol for 10 min each. The membrane of capsules was destroyed to expose the core contents. After gold sputtering, samples were visualized by SEM.

4.3 *In vivo* implantation: animal's surgery, euthanasia, and implants retrieval

The animal experimentation project (**Chapter VII**) was approved by the institutional Animal Welfare Body (SECVS 032/2015) and the *National Authority Direção Geral de Alimentação e Veterinária*. Five week-old male nude mice (average weight of 25 g) were used to subcutaneously implant the different developed capsules. Four mice were used for each formulation and at each timepoint (1, 3, and 6 weeks). Under surgical sterile conditions, animals were anaesthetized with an intraperitoneal injection of a mixture of ketamine (75 $mg.kg^{-1}$) and metedomidine (1 $mg.kg^{-1}$). One medial incision of approximately 0.7 cm was performed in the dorsum of the mice and two craniolateral-oriented pockets were subcutaneously created by blunt dissection. Three capsules were inserted into each pocket. Pockets without capsules were also used as control. Subsequently, the *panniculus carnosus* and the skin were carefully sutured with non-resorbable 4/0 sutures. After the surgical procedure, the animals were induced to recover from anaesthesia with an intraperitoneal injection of Atipazemol (1 $mg.kg^{-1}$). The animals were kept housed together (different conditions in each cage) with standard diet and water *ad libitum* during all the time of the experiment. After 1, 3, and 6 weeks of implantation, the animals were sacrificed by carbon dioxide inhalation. The implanted capsules and the respective surrounding tissue were explanted from each animal. The collected explants were subjected to macroscopic observation and fixed in 10% formalin for 24 h at RT. Samples were then processed for standard histological evaluation.

4.4 Histological procedures and stainings

At predetermined periods, the different capsules cultured *in vitro* (**Chapters V** and **VI**) or the respective tissue explants with the implanted capsules (**Chapter**

VII) were collected and processed in an automatic ethanol-xylene spin tissue processor for histological analysis. Afterward, samples were embedded in paraffin and cut into sections of 5 μm thickness using a microtome. Sections were subsequently deparaffinized, rehydrated, and stained.

4.4.1 Safranin-O and alcian blue

Sections were automatically stained for safranin-O (0.1% w/v) and alcian blue (1% w/v) stainings. Samples were then dehydrated and immersed in xylene, before being mounted. The stained sections were analyzed by microscopy.

4.4.2 Alizarin red

To assess the presence of a mineralized matrix within the capsules, alizarin red staining was performed. This staining was performed on capsules (**Chapters VI** and **VII**) collected after 21 days in order to visualize calcium-rich deposits. Deparaffinized sections were immersed in alizarin red staining solution for 5 min at RT. Samples were then mounted and analyzed by microscopy.

4.4.3 Hematoxylin and eosin

The explants collected after pre-determined periods of subcutaneously implanted capsules (**Chapter VII**) were automatically processed for hematoxylin and eosin (H&E) staining. Briefly, histological sections were subsequently immersed in hematoxylin and after bluing in an ammonia solution (1% v/v) in eosin y. Samples were then mounted and analyzed by microscopy.

4.4.4 CD31

The explants collected after pre-determined periods of subcutaneously implanted capsules (**Chapter VII**) were processed for CD31 staining. Antigen retrieval was performed in heat-mediated (95-100°C) sodium citrate buffer (10 mM) for 20 min. After cool down for 20 min, endogenous peroxidases were inactivated with hydrogen peroxide (3% v/v) and non-specific binding blocked

with normal horse serum incubation (2.5% v/v, NHS) for 30 min at RT. The sections were incubated with the primary antibody rabbit polyclonal anti-human to CD31 (1:50 diluted in PBS with NHS) in a humidified chamber at 4°C overnight. The second antibody (kit) was added for 1 h at RT, and the stained revealed with a DAB solution prepared according to manufacturer's specifications. Sections were counterstained with hematoxylin before microscopic analysis.

4.4.5 Masson's trichrome

The explants collected after pre-determined periods of subcutaneously implanted capsules (**Chapter VII**) were processed for Masson's trichrome staining. Sections were stained for 5 min in a solution containing azure B (0.5 g), ammonium iron (5 g, ammonium iron sulfate (III) dodecahydrate) and distilled water (100 mL). Sections were then subsequently stained with hematoxylin and picric ethanol (1% w/v) for 5 min each. After 10 min washing in running tap water, sections were stained with the solutions from the Trichrome Stain Masson kit according to the manufacturer's specifications.

4.5 Fluorescence stainings

4.5.1 Live-dead assay

To assess the ability of capsules to support living cell encapsulation, calcein-AM and propidium iodide dyes were used to perform live-dead assays (**Chapters III** and **IV**). Calcein-AM is a membrane-permeant dye, which is hydrolyzed by endogenous esterase into the highly negatively charged green fluorescent cell marker calcein retained in the cytoplasm. Propidum iodide is a membrane impermeant and, thus, binds to DNA of dead cells. Briefly, at each time point, culture medium was removed and 1 mL of PBS containing 2 µL of calcein-AM and 1 µL of propidium iodide was added to each well. Samples were then incubated at 37°C for 10 min protected from light. Afterward, samples were washed three times with PBS and immediately visualized in the dark by fluorescence microscopy. With calcein-AM, through a fluorescent filter

(fluorescence excitation of 494 and emission of 517 nm), living cells appeared bright green. With propidium iodide, through a rhodamine filter (fluorescence excitation of 535 nm and emission of 617 nm), dead cells appeared bright red. Double staining was obtained in Z-stack mode with a resolution of 17 μm between slides.

4.5.2 DAPI-phalloidin

DAPI and phalloidin dyes were used to perform DAPI-phalloidin assays. DAPI stains preferentially double-stranded DNA by delineating cells nuclei in blue. Phalloidin is a bicyclic peptide with selectivity to label F-actin, revealing the distribution of actin filaments in fixed cells. Prior to staining, at each time point, culture medium was removed and 10% formalin was added to each well (n = 5 particles or capsules per well, in triplicate). After 1 h at RT, formalin was removed and replaced by 0.1% Triton X for 5 min to permeabilize cells. Upon PBS washing, 1 mL of PBS containing 1 μL of DAPI and 10 μL of phalloidin was added to each well. After 1 h at RT protected from light, samples were washed three times with PBS and immediately visualized in the dark by fluorescence microscopy. Cell nuclei appeared bright blue and F-actin filaments appeared bright red due to DAPI and phalloidin dyes, respectively. Double staining was obtained in Z-stack mode with a resolution of 17 μm between slides.

4.5.3 Osteopontin-DAPI and osteopontin-CD31-DAPI

At pre-determined periods, capsules (**Chapter VI**) were fixed in formalin (10% v/v) for 30 min at RT. After fixation, capsules were destroyed and cells were permeabilized for 5 min at RT with Triton-X (0.1% v/v). Samples were immersed in BSA (3% w/v) for 30 min at RT to block non-specific binding and then incubated overnight at 4°C with the primary antibody rabbit anti-human osteopontin (1:100 in 1% BSA). After PBS washing, samples were incubated for 1h at RT with the secondary antibody anti-rabbit AlexaFluor 488 (1:500 in 1% BSA). Samples were immediately visualized in the dark by confocal

microscopy. Double staining was obtained in Z-stack mode with a resolution of 17 μm between slides. Additionally, the same type of capsules (**Chapter VI**) were used for osteopontin-CD31-DAPI staining, however after histological procedure (**Chapter VI**). Samples were fixed in formalin (10% v/v) for 30 min at RT, and processed in an automatic spin tissue processor for histological analysis. Afterwards, samples were embedded in paraffin and cut into sections of 5 μm thickness using a microtome. After the deparaffinization process, the antigen retrieval was performed in a microwave-heated sodium citrate buffer (10 mM). Samples were immersed in hydrogen peroxide (3% v/v) at RT for 30 min. The primary antibody mouse anti-human CD31 (1:100 in 1% BSA) conjugated with the osteopontin and the secondary antibody anti-mouse AlexaFluor 594 (1:500 in 1% BSA). Ultimately, samples were counterstained with DAPI (1 $mg.mL^{-1}$ diluted 1:1000 in PBS) for 5 min at RT and analyzed by microscopy. Triple staining was obtained in Z-stack mode with a resolution of 10 μm between slides.

Tissue explants containing the implanted capsules (**Chapter VII**) were also used for osteopontin-DAPI staining after histological procedure. Samples were fixed in formalin (10% v/v) for 30 min at RT, and processed in an automatic spin tissue processor for histological analysis. Afterwards, samples were embedded in paraffin and cut into sections of 5 μm thickness using a microtome. After the deparaffinization process, the antigen retrieval was performed in a microwave-heated sodium citrate buffer (10 mM). Non-specific binding was blocked by immersion in BSA (3% w/v) for 30 min at RT. Samples were then incubated overnight at 4°C with the primary antibody rabbit anti-human osteopontin (1:100 in 1% BSA). After a PBS washing, samples were incubated for 1 h at RT with the secondary antibody anti-rabbit AlexaFluor 488 (1:500 in 1% BSA). Samples incubated only with the secondary antibody were used as controls. Ultimately, samples were subsequently counterstained with DAPI (1 $mg.mL^{-1}$ diluted 1:1000 in PBS) for 5 min at RT, immediately mounted, and analyzed by fluorescence microscopy. Double staining was obtained in Z-stack mode with a resolution of 10 μm between slides.

4.5.4 TGF-β3

After surface functionalization of PLLA microparticles with collagen II and TGF-β3 (**Chapter V**) as described in *3.2 Plasma treatment combined with collagen coating to modify the surface of microparticles,* microparticles were immersed in PBS at 37ºC for 7 days. Samples were collected by centrifugation and subsequently immersed in BSA (3% w/v) for 30 min at RT, and then incubated overnight at 4ºC with the primary antibody rabbit anti-human TGF-β3 (5 μg mL^{-1}). After PBS washing, samples were incubated for 1 h at RT with the secondary antibody anti-rabbit AlexaFluor 488 (1:500, BD Biosciences). Samples were visualized by fluorescence microscopy.

4.5.5 Collagen II

The presence of collagen II in the ECM of encapsulated cells within capsules was assessed after histological procedures (**Chapter V**). At pre-determined periods, capsules were collected and processed in an automatic ethanol-xylene spin tissue processor for histological analysis. Afterward, samples were embedded in paraffin and cut into sections of 5 μm thickness using a microtome. Sections were subsequently deparaffinized and rehydrated. The antigen retrieval was performed in a heat-mediated sodium citrate buffer ($10x10^{-4}$ M). Nonspecific binding was blocked by immersion in hydrogen peroxide (3% v/v) followed by BSA (3% w/v), each for 30 min at RT. Samples were then incubated overnight at 4ºC with the primary antibody rabbit anti-human collagen II (1:200 in 1% w/v BSA). After PBS washing, samples were incubated for 1 h at RT with the secondary antibody anti-rabbit AlexaFluor 488 (1:500 in 1% BSA). Ultimately, samples were subsequently counterstained with DAPI (1 $mg.mL^{-1}$ diluted 1:1000 in PBS) for 5 min at RT, immediately mounted, and analyzed in the dark by fluorescence microscopy.

4.5.6 DIL and DIO lipophilic dyes

Prior to encapsulation, ASCs and ECs (**Chapter VI**) were incubated with the lipophilic dyes *3,3'*-dioctadecyloxacarbocyanine perchlorate (DIO) and *1,1'*-

dioctadecyl-*3,3,3',3'*-tetramethylindocarbocyanine perchlorate (DIL), respectively. Cells were incubated with each dye (1 mL, 2 μM per $1x10^6$ cells) at 37ºC for 10 min. Labeled cells encapsulated in liquified and multilayered capsules were visualized by confocal microscopy.

5. Statistical analysis

Statistical analysis was performed using two-way analysis of variance (ANOVA) with Tukey's post-hoc test (*GraphPad Prism 6*). A p-value < 0.05 was considered statistically significant. All results are presented as mean ± standard deviation of at least three independent experiments (n = 3).

References

[1] G. Decher, J.D. Hong, J. Schmitt, Buildup of ultrathin multilayer films by a self-assembly process: III. Consecutively alternating adsorption of anionic and cationic polyelectrolytes on charged surfaces, Thin Solid Films, 210–211 (1992) 831-835.

[2] S. Facca, C. Cortez, C. Mendoza-Palomares, N. Messadeq, A. Dierich, A.P. Johnston, D. Mainard, J.C. Voegel, F. Caruso, N. Benkirane-Jessel, Active multilayered capsules for in vivo bone formation, Proc. Natl. Acad. Sci. U. S. A., 107 (2010) 3406-3411.

[3] A.C. Mendes, E.T. Baran, R.C. Pereira, H.S. Azevedo, R.L. Reis, Encapsulation and survival of a chondrocyte cell line within xanthan gum derivative, Macromol. Biosci., 12 (2012) 350-359.

[4] Y. Ma, Y. Zhang, Y. Liu, L. Chen, S. Li, W. Zhao, G. Sun, N. Li, Y. Wang, X. Guo, G. Lv, X. Ma, Investigation of alginate-epsilon-poly-L-lysine microcapsules for cell microencapsulation, J. Biomed. Mater. Res. Part A, 101 (2013) 1265-1273.

[5] W.H. Tan, S. Takeuchi, Monodisperse Alginate Hydrogel Microbeads for Cell Encapsulation, Adv. Mater., 19 (2007) 2696-2701.

[6] J. Kim, D.R. Arifin, N. Muja, T. Kim, A.A. Gilad, H. Kim, A. Arepally, T. Hyeon, J.W. Bulte, Multifunctional capsule-in-capsules for immunoprotection and trimodal imaging, Angew. Chem., 50 (2011) 2317-2321.
[7] A.L. Hillberg, K. Kathirgamanathan, J.B. Lam, L.Y. Law, O. Garkavenko, R.B. Elliott, Improving alginate-poly-L-ornithine-alginate capsule biocompatibility through genipin crosslinking, J. Biomed. Mater. Res. Part B, Applied Biomat., 101 (2013) 258-268.
[8] R.R. Costa, J.F. Mano, Polyelectrolyte multilayered assemblies in biomedical technologies, Chem. Soc. Rev., 43 (2014) 3453-3479.
[9] R.R. Costa, E. Castro, F.J. Arias, J.C. Rodriguez-Cabello, J.F. Mano, Multifunctional compartmentalized capsules with a hierarchical organization from the nano to the macro scales, Biomacromolecules, 14 (2013) 2403-2410.
[10] R.R. Costa, C.A. Custódio, F.J. Arias, J.C. Rodríguez-Cabello, J.F. Mano, Nanostructured and thermoresponsive recombinant biopolymer-based microcapsules for the delivery of active molecules, Nanomedicine, 9 (2013) 895–902.
[11] F. Caruso, R.A. Caruso, H. Möhwald, Nanoengineering of inorganic and hybrid hollow spheres by colloidal templating, Science, 282 (1998) 1111-1114.
[12] E. Donath, B.G. Sukhorukov, F. Caruso, S.A. Davis, H. Möhwald, Novel hollow polymer shells by colloid-templated assembly of polyelectrolytes, Angew. Chem., 37 (1998) 2201–2205.
[13] N.L. Costa, P. Sher, J.F. Mano, Liquefied capsules coated with multilayered polyelectrolyte films for cell immobilization, Adv. Eng. Mater., 13 (2011) B218-B224.
[14] D.G. Shchukin, G.B. Sukhorukov, H. Möhwald, Smart inorganic/organic nanocomposite hollow microcapsules, Angew. Chem., 42 (2003) 4472–4475.
[15] R.M. Hernandez, G. Orive, A. Murua, J.L. Pedraz, Microcapsules and microcarriers for in situ cell delivery, Adv. Drug Delivery Rev., 62 (2010) 711-730.

[16] A.K. Brun-Graeppi, C. Richard, M. Bessodes, D. Scherman, O.W. Merten, Cell microcarriers and microcapsules of stimuli-responsive polymers, J. Controlled Release, 149 (2011) 209-224.
[17] A.D. Augst, H.J. Kong, D.J. Mooney, Alginate hydrogels as biomaterials, Macromol. Biosci., 6 (2006) 623-633.
[18] O. Smidsrød, G. Skja˚k-Br1k, Alginate as immobilization matrix for cells, Trends Biotechnol., 8 (1990) 71-78.
[19] J.A. Rowley, G. Madlambayan, D.J. Mooney, Alginate hydrogels as synthetic extracellular matrix materials, Biomaterials, 20 (1999) 45-53.
[20] M. Rinaudo, Chitin and chitosan: Properties and applications, Prog. Polym. Sci., 31 (2006) 603-632.
[21] M. Rinaudo, Main properties and current applications of some polysaccharides as biomaterials, Polym. Int., 57 (2008) 397-430.
[22] Z. Liu, H. Wang, Y. Wang, Q. Lin, A. Yao, F. Cao, D. Li, J Zhou, C. Duan, Z. Du, Y. Wang, C. Wang, The influence of chitosan hydrogel on stem cell engraftment, survival and homing in the ischemic myocardial microenvironment, Biomaterials, 33 (2012) 3093-3106.
[23] H.Y. Zhang, E.A. Tehrany, C.J.F. Kahn, M. Ponçot, M. Linder, F. Cleymand, Effects of nanoliposomes based on soya, rapeseed and fish lecithins on chitosan thin films designed for tissue engineering, Carbohydr. Polym., 88 (2012) 618-627.
[24] M.E. Frohbergh, A. Katsman, G.P. Botta, P. Lazarovici, U.G.K. Wegst, P.I. Lelkes, Electrospun hydroxyapatite-containing chitosan nanofibers crosslinked with genipin for bone tissue engineering, Biomaterials, 33 (2012) 9167-9178.
[25] C. Isikli, V. Hasirci, N. Hasirci, Development of porous chitosan–gelatin/hydroxyapatite composite scaffolds for hard tissue-engineering applications, J. Tissue Eng. Regener. Med., 6 (2012) 135-143.
[26] M. Rinaudo, G. Pavlov, J. Desbrières, Solubilization of chitosan in strong acid medium, Int. J. Polym. Anal. Charact., 40 (1999) 7029-7032.
[27] A. Domard, pH and c.d. measurements on a fully deacetylated chitosan: Application to Cu II-polymer interactions, Int. J. Biol. Macromol., 9 (1998) 98-104.

[28] M. Rinaudo, J. Reguant, Polysaccharide derivatives, in: C.J. Brine, P.A. Sandford, J.P. Zikakis (Eds.), Advances in Chitin and Chitosan, Elsevier, London and New York, 1992, pp. 556-564.
[29] F. Lim, A.M. Sun, Microencapsulated islets as bioartificial endocrine pancreas, Science, 210 (1980) 908-910.
[30] D. Hunkeler, Polymers for bioartificial organs, Trends Polym. Sci., 5 (1999) 286-293.
[31] B.L. Strand, L. Ryan, P.I. Veld, B. Kulseng, A.M. Rokstad, G. Skjåk-Braek, T. Espevik, Poly-L-Lysine induces fibrosis on alginate microcapsules via the induction of cytokines, Cell Transplant., 10 (2001) 263-275.
[32] S. Darquy, M. Pueyo, F. Capron, G. Reach, Complement activation by alginate-polylysine microcapsules used for islet transplantation, Artif. Organs, 18 (1994) 898–903.
[33] M. Pueyo, S. Darquy, F. Capron, G. Reach, In vitro activation of human macrophages by alginate–polylysine microcapsules, J. Biomater. Sci. Polym. Ed., 5 (1993) 197–203.
[34] S. Juste, M. Lessard, N. Henley, M. Ménard, J. Hallé, Effect of poly-L-lysine coating on macrophage activation by alginate-based microcapsules, J. Biomed. Mater. Res., 72 (2005) 389–398.
[35] G. Orive, S.K. Tam, J.L. Pedraz, J.P. Halle, Biocompatibility of alginate–poly-L-lysine microcapsules for cell therapy, Biomaterials, 27 (2006) 3691–3700.
[36] W. Yuan, Z. Lu, C.M. Li, Controllably layer-by-layer self-assembled polyelectrolytes/nanoparticle blend hollow capsules and their unique properties, J. Mater. Chem., 21 (2011) 5148-5155.
[37] T. Haque, H. Chen, W. Ouyang, C. Martoni, B. Lawuyi, A.M. Urbanska, S. Prakash, Superior cell delivery features of poly(ethylene glycol) incorporated alginate, chitosan, and poly-L-lysine microcapsules, Mol. Pharm., 2 (2005) 29-36.
[38] S. Gil, C.R. Correia, J.F. Mano, Magnetically labeled cells with surface-modified Fe_3O_4 spherical and rod-shaped magnetic nanoparticles for tissue engineering applications, Adv. Healthcare Mater., 4 (2015) 883-891.

[39] P.A. Zuk, M. Zhu, P. Ashjian, D.A.D. Ugarte, J.I. Huang, H. Mizuno, Z.C. Alfonso, J.K. Fraser, P. Benhaim, M.H. Hedrick, Human adipose tissue is a source of multipotent stem cells, Mol. Biol. Cell, 13 (2002) 4279-4295.
[40] J. Wei, X.-J. Ju, X.-Y. Zou, R. Xie, W. Wang, Y.-M. Liu, L.-Y. Chu, Multi-stimuli-responsive microcapsules for adjustable controlled-release, Adv. Funct. Mater., 24 (2014) 3312-3323.
[41] Y.P. Jiao, F.Z. Cui, Surface modification of polyester biomaterials for tissue engineering, Biomed. Mater., 2 (2007) R24-37.
[42] M. Yaszemski, R. Payne, W. Hayes, R. Langer, A. Mikos, Evolution of bone transplantation: Molecular, cellular and tissue strategies to engineer human bone, Biomaterials, 17 (1996) 175-185.
[43] G. Khang, S. Lee, J. Jeon, J. Lee, H. Lee, Interaction of fibroblast cell onto physicochemically treated PLGA surfaces, Polymer, 24 (2000) 869–876.
[44] J. Tjia, B. Aneskievich, P. Moghe, Substrate-adsorbed collagen and cell secreted fibronectin concertedly induce cell migration on poly(lactide-glycolide) substrates, Biomaterials, 20 (1999) 2223-2233.
[45] S. Viguet-Carrin, P. Garnero, P.D. Delmas, The role of collagen in bone strength, Osteoporos. Int., 17 (2006) 319-336.
[46] D. Eyre, Collagen of articular cartilage, Arthritis. Res., 4 (2002) 30-35.
[47] A.M. Freyria, F. Mallein-Gerin, Chondrocytes or adult stem cells for cartilage repair: The indisputable role of growth factors, Injury, 43 (2012) 259-265.
[48] B.E. Bobick, F.H. Chen, A.M. Le, R.S. Tuan, Regulation of the chondrogenic phenotype in culture, Birth Defects Res. Part C, 87 (2009) 351–371.
[49] F. Barry, R.E. Boynton, B. Liu, J.M. Murphy, Chondrogenic differentiation of mesenchymal stem cells from bone marrow: Differentiation-dependent gene expression of matrix components, Exp. Cell Res., 268 (2001) 189-200.
[50] S. Shanmugasundaram, S. Logan-Mauney, K. Burgos, M. Nurminskaya, Tissue transglutaminase regulates chondrogenesis in mesenchymal stem cells on collagen type XI matrices, Amino acids, 42 (2012) 1045-1053.

[51] L. Lorand, R.M. Graham, Transglutaminases: Crosslinking enzymes with pleiotropic functions, Nat. Rev. Mol. Cell Biol., 4 (2003) 140-156.
[52] M. Jones, P. Messersmith, Facile coupling of synthetic peptides and peptide-polymer conjugates to cartilage via transglutaminase enzyme, Biomaterials, 28 (2007) 5215-5224.
[53] P. Zuk, M. Zhu, H. Mizuno, J. Huang, J. Futrell, A. Katz, P. Benhaim, H. Lorenz, M. Hendrick, Multilineage cells from human adipose tissue: Implications for cell-based therapies, Tissue Eng., 7 (2001) 211-228.
[54] J. Borges, J.F. Mano, Molecular interactions driving the layer-by-layer assembly of multilayers, Chem. Rev., 114 (2014) 8883-8942.
[55] S. De Koker, L.J. De Cock, P. Rivera-Gil, W.J. Parak, R. Auzely Velty, C. Vervaet, J.P. Remon, J. Grooten, B.G. De Geest, Polymeric multilayer capsules delivering biotherapeutics, Adv. Drug Delivery Rev., 63 (2011) 748-761.
[56] K. Ariga, Y.M. Lvov, K. Kawakami, Q. Ji, J.P. Hill, Layer-by-layer self-assembled shells for drug delivery, Adv. Drug Delivery Rev., 63 (2011) 762-771.
[57] M.T. Cerqueira, L.P.d. Silva, T.C. Santos, R.P. Pirraco, V.M. Correlo, R.L. Reis, A.P. Marques, Gellan gum-hyaluronic acid spongy-like hydrogels and cells from adipose tissue synergize promoting neoskin vascularization, Appl. Mater. Interfaces, 6 (2014) 19668-19679.
[58] J. Liu, H.K. Nam, C. Campbell, K.C. Gasque, J.L. Millan, N.E. Hatch, Tissue-nonspecific alkaline phosphatase deficiency causes abnormal craniofacial bone development in the Alpl(-/-) mouse model of infantile hypophosphatasia, Bone, 67 (2014) 81-94.
[59] L.M. Grover, A.J. Wright, U. Gbureck, A. Bolarinwa, J. Song, Y. Liu, D.F. Farrar, G. Howling, J. Rose, J.E. Barralet, The effect of amorphous pyrophosphate on calcium phosphate cement resorption and bone generation, Biomaterials, 34 (2013) 6631-6637.
[60] J.P.v. Straalen, E. Sanders, M.F. Prummel, G.T.B. Sanders, Bone-alkaline phosphatase as indicator of bone formation, Clin. Chim. Acta, 201 (1991) 27-33.

[61] B.T. Estes, B.O. Diekman, J.M. Gimble, F. Guilak, Isolation of adipose-derived stem cells and their induction to a chondrogenic phenotype, Nat. Protoc., 5 (2010) 1294-1311.

3

Experimental results

Chapter III

Liquified chitosan-alginate multilayer capsules incorporating poly(L-lactic acid) microparticles as cell carriers

Chapter IV

Multilayered hierarchical capsules providing cell adhesion sites

Chapter V

A closed chondromimetic environment within magnetic-responsive liquified capsules encapsulating stem cells and collagen II/TGF-β3 microparticles

Chapter VI

Semipermeable capsules wrapping a multifunctional and self-regulated co-culture microenvironment for osteogenic differentiation

Chapter VII

In vivo osteogenic differentiation of stem cells inside compartmentalized capsules loaded with co-cultured endothelial cells

Chapter III

Liquified chitosan-alginate multilayer capsules incorporating poly(L-lactic acid) microparticles as cell carriers [3]

Abstract

We report the development of liquified multilayer hierarchical capsules capable to provide cell adhesion sites to the encapsulated cells. The *proof of principle* is demonstrated on the example of a chitosan-alginate shell *via* layer-by-layer assembly, encapsulating cells adhered at the functionalized surface of poly(L-lactic acid) microparticles.

[3] Based on the publication: C.R. Correia, P. Sher, R.L. Reis, J.F. Mano, Liquified chitosan-alginate multilayer capsules incorporating poly(L-lactic acid) microparticles as cell carriers, Soft Matter, 9 (2013) 2125-2130.

1. Introduction

Since the pioneering study of Decher [1], the layer-by-layer (LbL) assembly technique has been widely used to produce polymeric multilayer capsules (PMCs). The fabrication is based on the set-wise assembly of oppositely charged polyelectrolytes onto a sacrificial template before the decomposition of its core [2, 3] PMCs have attracted immense attention due to their great applicability in various scientific fields, such as in medical imaging [4, 5], controlled drug delivery systems [6], biosensors [7, 8], synthetic vaccines [9], cell encapsulation [10], nanoreactors [11], catalysts [12], and many others. Due to the high versatility of the LbL technique, different properties of the capsules can be easily tailored, e.g. the permeability of the shell can be controlled by varying the number of layers deposited and the surface of the capsules can be customized by endowing nanoparticles, lipids, viruses, among others [13]. Moreover, LbL can be performed in mild conditions. Drawn by these appealing properties, PMCs have found great potential in bioencapsulation systems. The LbL shell allows the diffusion of nutrients, oxygen, metabolites and waste products, maximized by the liquified core, while avoiding the entrance of high molecular weight immune system components, such as immunoglobulins and immune cells [14]. However, most cells cannot grow in suspension and need to adhere to a solid structure. Encapsulated in the liquified environment of capsules and deprived of a physical support, anchorage-dependent cells are not able to adhere and proliferate. In fact, bioencapsulation is often performed using alginate hydrogel particles since the crosslinked core provides physical support for cell adhesion. However, alginate requires a covalently modification with peptides and proteins, such as arginine-glycine-aspartic [15], in order to promote cell attachment. Additionally, the diffusion of essential molecules for cell survival in hydrogels is less efficient compared to the liquified environments of capsules [16, 17]. Therefore, the existing capsules for cell immobilization are more focused in the delivery of cells rather than tissue formation [10, 14].

To achieve an efficient diffusion provided by liquified environments, which simultaneously are able to provide cell adhesion sites, we propose the development of liquified multilayer capsules containing microparticles as cell supports. A schematic representation is given in **Scheme III.1**.

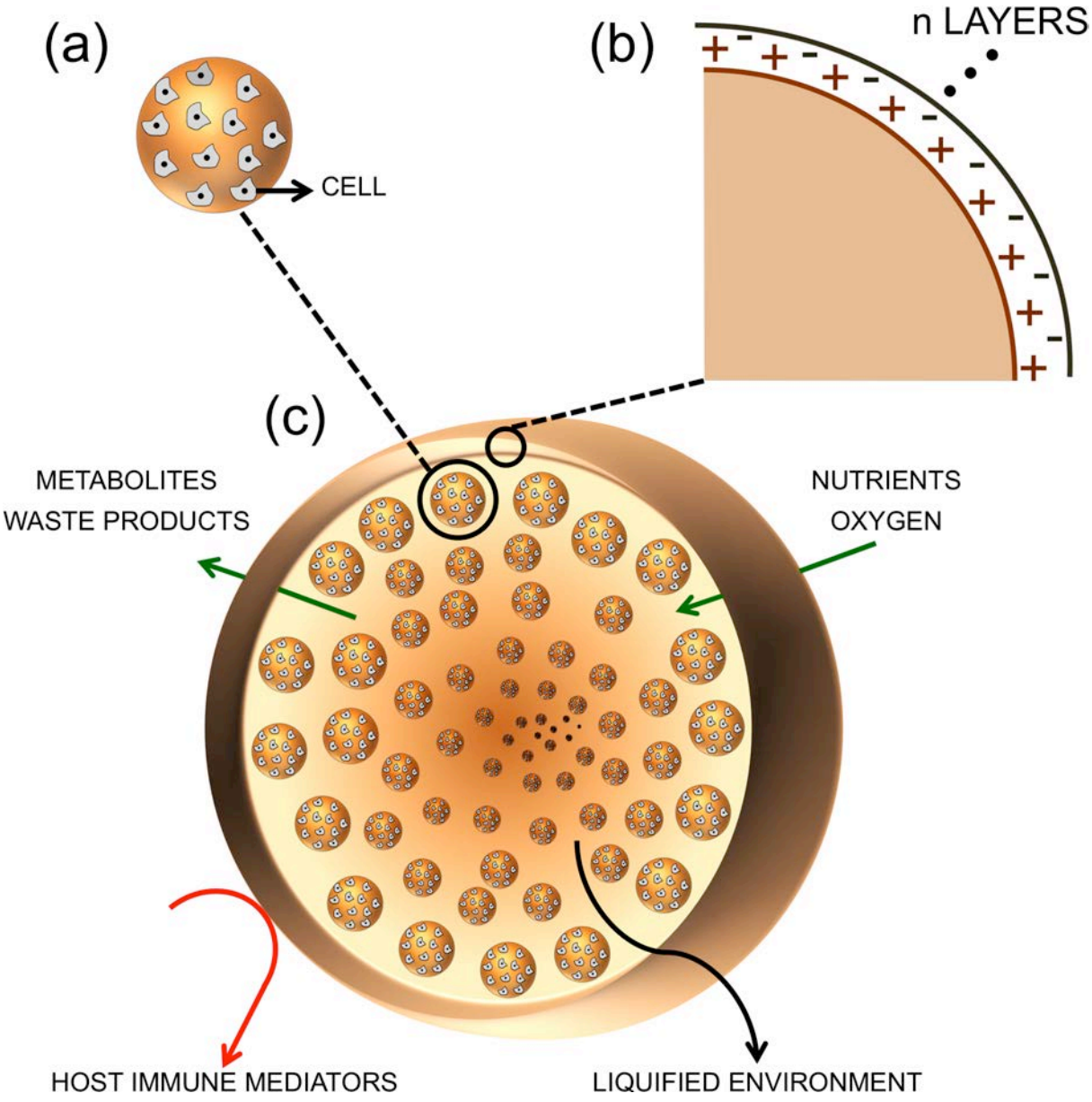

Scheme III.1 - A schematic representation of the organization of the proposed liquified multilayer capsules. (a) Cells are seeded at the surface of microparticles, originating the production of microcarriers. (b) After encapsulation of the obtained microcarriers in sacrificial hydrogel particles, oppositely charged polymers are deposited at their surface by layer-by-layer technique. (c) Upon core dissolution, liquified multilayer capsules are obtained. The permselective ability of the shell of the capsules allows the diffusion of nutrients, oxygen, metabolites and waste products, while avoiding the entrance of host immune mediators.

Here, we report the general idea in which capsules composed by a permselective multilayered membrane of chitosan and alginate incorporate poly(L-lactic acid) (PLLA) microparticles as cell microcarriers. Due to the excellent biocompatibility of chitosan and alginate, these two natural polymers are often applied as polycation and polyanion electrolytes, respectively, in biomedical applications of drug delivery systems and tissue engineering (TE) approaches [18-20]. The successful assembly of chitosan (CHT) and alginate (ALG) has already been reported to produce capsules for cell immobilization [21], drug delivery systems [22] or scaffolds for TE [23, 24].

2. Materials and Methods

2.1 Production of poly(L-lactic acid) microparticles

PLLA microparticles were produced by emulsion solvent evaporation technique as elsewhere described with minor modifications [25]. Briefly, 1 g of PLLA (M_w~1600-2400, 70% crystallinity, Polysciences, Germany) was dissolved in 20 mL of methylene chloride (CH_2Cl_2, Fisher Chemical, UK) to obtain a 5% w/v transparent solution of PLLA/CH_2Cl_2. This solution was added under agitation to 100 mL of polyvinyl alcohol 0.5% w/v (PVA, Sigma-Aldrich, USA). The resulting solution was left to stir for 2 days at room temperature (RT) in order to evaporate the organic solvent. The produced PLLA microparticles were collected by filtration and washed several times with distilled water. Ultimately, microparticles were subsequently frozen at -80ºC and lyophilized (Cryodos, Telstar) for 3 days. PLLA microparticles diameter (n = 185) was measured by using Image J software. Prior to usage, microparticles were stored at 4°C. PLLA microparticles were then surface modified by plasma treatment technique. Microparticles were placed inside the plasma reactor chamber (PlasmaPrep5, Gala Instrumente, Germany) fitted with a radio-frequency generator. Oxygen was used as the working atmosphere. After the pressure of the chamber had stabilized to ~0.2 mbar, a glow discharge plasma was created by controlling the electrical power at 30 V of electrical potential

difference. The plasma-treated microparticles were treated for 15 minutes. 450 mg of PLLA plasma treated microparticles were sterilized by UV radiation for 30min and then immersed in 30 mL of 0.02 M acetic acid (Carlo Erba, Italy) containing 1200 µg collagen I (Rat Tail, Invitrogen) for 4 h at RT. Microparticles were collected and washed with sterile phosphate buffer saline (PBS, Sigma-Aldrich, USA).

2.2 Production of liquified capsules

Sodium alginate from brown algae (ALG, Sigma-Aldrich, USA) was dissolved in 0.15 M sodium chloride (NaCl, Panreac, Spain) at a concentration of 1.5% w/v. The pH of alginate solution was adjusted to 7. To produce capsules containing microparticles, surface modified PLLA microparticles was added to the template solution at a concentration of 4.5% w/v. Under agitation rate by a mechanical stirrer, alginate solutions with or without PLLA microparticles were dropwise to a 0.1 M calcium chloride solution (Merck, Germany) using an 18 G needle. Droplets were immediately transformed into hydrogel particles by ionotropic gelation, due to the ionic crosslinking of the alginate matrix. Hydrogel particles formed were left to stir for 20 min. Then, hydrogels were collected and rinsed in 0.15 M NaCl. Once obtained the alginate particles with or without PLLA microparticles, the external membrane was processed by layer-by-layer deposition. Hydrogel particles were first immersed in water-soluble highly purified chitosan (CHT, Protasan UP CL 213, viscosity 107 mPa.s, molecular weight M_w = 2.7x105 $g.mol^{-1}$, degree of deacetylation DDA = 83%, NovaMatrix, Norway) and subsequently in ALG. Polymers were dissolved in 0.15 M NaCl at a concentration of 0.5 $mg.mL^{-1}$. The pH of ALG was set to 7 and, in the case of chitosan, to 6.4. At these pH values the polyelectrolytes maintain their positive or negative required charges and cell viability is not affected. Following a 10 min of each polymer adsorption, the excess of macromolecules was removed by immersion in 0.15 M NaCl for 5 min. The washing step removes the remaining unabsorbed polyelectrolyte and its non-reactive groups, in order to maximize the polymeric adsorption of the following

layer. This process was repeated in order to obtain an 8-bilayered membrane on the surface of the hydrogel particles. The core-shell alginate particles obtained were immersed in 0.02 M ethylenediaminetetraacetic acid (EDTA, Sigma-Aldrich, USA) at pH 7 for 5 min to liquefy the alginate core.

2.3 Quartz-crystal microbalance with dissipation monitoring

The build-up process of the membrane growth was monitored by quartz-crystal microbalance with dissipation monitoring (QCM-D, QSense E4, Sweden) in a liquid environment. An equivalent circuit model (IPC High Precision Multichannel Dispenser, ISMATEC) was fitted to the impedance curve, and the obtained parameters were used to calculate the thickness of the multilayers. Briefly, CHT and ALG multilayers were deposited on gold-coated quartz crystals. Before adsorption, the quartz crystals were cleaned with 0.15 M sodium chloride solution at 25°C until a baseline was obtained. All conditions, such as, polymer cycle, concentration, pH, and time of deposition, as previously described to obtain the LbL membrane, were also used in the QCM-D analysis. Polymeric and washing solutions were alternatively introduced into the measuring chamber at a flow rate of 100 $\mu L.min^{-1}$. Variations in frequency (ΔF) and in dissipation (ΔD) were monitored in real time up to a deposition of 8 cycles. The frequency of each overtone was normalized to the fundamental resonant frequency of the quartz-crystal ($\Delta F\nu/\nu$ in which ν stands for the overtone). Thickness assessment was estimated using the Voigt viscoelastic model implemented in the QTools software from QSense.

2.4 Mechanical resistance evaluation

The influence of depositing different number of layers on the mechanical stability of capsules was evaluated using a rotational stress test. Three types of membrane were tested, namely 4, 6 or 8-bilayered capsules (n = 15 in triplicates). Capsules were placed in centrifuge tubes containing 5mL of PBS. The tubes were rotated at a speed of 200 rpm for 60 min at RT. At every 15 min of rotation, the number of damage capsules was observed and counted

under a light microscope. The intact capsules were placed again inside the centrifuge tubes to continue the rotational test.

2.5 Scanning electron microscopy

The membrane morphology of 4, 6 or 8-bilayered capsules was characterized by scanning electron microscopy (SEM). Capsules composed by 4, 6 or 8-bilayers were dehydrated using sequential ethanol series, namely 45%, 50%, 60%, 70%, 80%, 90%, 96% and 100% v/v, 10min each. Prior to SEM visualization, cross-sections of capsules were gold-coated using a sputter coater. Cross-sectional morphologies were visualized using a FEI Nova™ NanoSEM 200 operating at 5.0 kV accelerating voltage.

2.6 Ion Coupled Plasma

Ion Coupled Plasma (ICP) was performed to quantify the release of calcium during and after the liquefying process. Capsules with 8-bilayers were placed in EDTA solution with different concentrations, namely 0.02 M, 0.05 M or 0.1 M. At each 5 min, 3 mL of EDTA solution were withdrawn and replaced by fresh solution. The concentration of calcium in solution was measured by ICP (SPS-1500VR, Seiko Instruments Inc., Japan). Additionally, capsules were placed in EDTA solutions for 5 min and then transferred to a 0.15 M sodium chloride solution. Similarly, at each 5 min, 3 mL of sodium chloride solution were withdrawn and replaced by fresh solution. For both experiments, after 30 min, capsules were destroyed ensuring the total release of the remaining calcium. Data analysis was performed as a cumulative release assay.

2.7 Live-dead and DAPI-phalloidin fluorescence assays

Alginate particles (control) and ALG and PLLA capsules were incubated for 1, 3, and 7 days at 37°C and in a humidified 5% CO_2 atmosphere. Live-dead and DAPI-phalloidin fluorescence assays were performed at each time culture period.

Calcein-AM and propidium iodide dyes (1 mg.mL^{-1}, Molecular Probes, Invitrogen, USA) were used to perform the live-dead assay (n = 5 particles or capsules per well, in triplicate). Briefly, at each timepoint, culture medium was removed and 1 mL of PBS containing 2 µL of calcein-AM (1 mg.mL^{-1}) and 1 µL of propidium iodide (1 mg.mL^{-1}) was added to each well. Samples were then incubated at 37°C for 10 min protected from light. Afterwards, samples were washed three times with PBS and immediately visualized in the dark by fluorescence microscopy (Axioimage RZ1M, Zeiss, Germany).

4,6-Diaminidino-*2*-phenylindole-dilactate (DAPI, 20 mg.mL^{-1}, Sigma-Aldrich, USA) and phalloidin tetramethylrhodamine B isothiocyanate dyes (phalloidin, 10 mg.mL^{-1}, Sigma-Aldrich, USA) were used to perform a DAPI-phalloidin assay. Prior to staining, at each timepoint, culture medium was removed and 10% of formalin was added to each well (n = 5 particles or capsules per well, in triplicate). After 1 h at RT, formalin was removed and replaced by 0.1% Triton X for 5 min to permeabilize cells. Upon PBS washing, 1 mL of PBS containing 1 µL of DAPI and 10 µL of phalloidin was added. After 1 h at RT and protected from light, samples were washed three times with PBS and immediately visualized in the dark by fluorescence microscopy. Cells nuclei appeared bright blue and F-actin filaments appeared bright red due to DAPI and phalloidin dyes, respectively.

In both assays, double staining was obtained in Z-stack mode with a resolution of 17 µm between slides by using the AxioVision software.

2.8 MTS viability assay

Capsules with 8-bilayeres were tested for cytotoxicity and suitability for live cell encapsulation using a MTS colorimetric assay (Cell Titer 96® AQueous One Solution Cell Proliferation Assay, Promega, USA). Briefly, alginate particles (control) and capsules with (PLLA capsules) or without (ALG capsules) microparticles encapsulating L929 cells were placed in cell culture plates (n = 5 per well, in triplicate) and incubated at 37°C and 5% CO_2. Similarly, particles and capsules without cells were used as background control. At 1, 3 and 7

days of culture, the MTS assay was performed protected from light. Culture medium was removed and 1 mL serum-free DMEM containing MTS solution with a dilution ratio of 1:5 was added to each well. Samples were then incubated in the dark at 37ºC and 5% CO_2. After 3 h, 100 µL of each well (in triplicate) were transferred to a 96-well plate. The amount of formazan product was measured by absorbance at a wavelength of 490 nm using a multiwall spectrophotometer (Synergy HT, Bio-TEK). The background was corrected by subtracting the absorbance obtained from particles and capsules without cells to those with cells encapsulated.

3. Results and discussion

Capsules were tested regarding their feasibility, membrane stability and ability to support cell survival. The assembly of the two natural polymers used to produce the layer-by-layer shell, chitosan and alginate, was monitored by quartz-microbalance with dissipation monitoring (QCM-D). **Figure III.1a** shows the normalized frequency ($\Delta F\nu/\nu$) and dissipation (ΔD) variations obtained at the third overtone during the construction of 8 layers. The decrease in the frequency variation after each successive layer of polyelectrolyte adsorption (**Figure III.1a** arrows) suggests a gradual growth of the polymeric film. Dissipation increases with time revealing that the film is not rigid and can dissipate energy, evidencing the viscoelastic behavior of macromolecules. The QCM results show that a stable multilayer nanostructure was obtained, thus membrane production is ensured. Over time, the assembly of chitosan and alginate, originating the construction of the polymeric film was verified. Alginate, as a polyanion, interacts with the positively charged chitosan amine groups. The pH of the chitosan solution used was adjusted to 6.4, bellow its pKa value of 6.5 [26], in order to ensure its polycation behavior. Alginate, with pKa values of 3.38 and 3.65, for mannuronic (M) and guluronic (G) acids [27], respectively, tends to be negatively charged across a wide range of pH values. Therefore, the pH of alginate was adjusted to 7 to ensure a more cell friendly environment in further biological studies. QCM analysis proved the effective

interaction between the two polyelectrolytes at the selected concentration and pH values. Additionally, the thickness of the multilayer film was also estimated using the Voigt viscoelastic model [20] (**Figure III.1b**). The assembly of chitosan and alginate followed a linear regime growth, resulting in a polymeric film with 56 nm of thickness after the construction of 8 layers. Once assessed the construction of the shell in a two-dimensional system, the liquefying process and the mechanical properties were evaluated in a three-dimensional (3D) system, i.e. capsules.

To produce the capsules, an alginate solution of 1.5% w/v was added dropwise to a 0.1 M calcium chloride solution and stirred for 20 min. The template particles were collected and sequentially immersed in 0.5 $mg.mL^{-1}$ solutions of chitosan and alginate for 10 min, until achieving the desire number of layers. Between each deposition step, particles were washed in a 0.15 M sodium chloride solution to remove the remaining unabsorbed polyelectrolyte and its non-reactive groups. Liquified capsules were obtained through ionic chelation by immersing the coated beads in a 0.02 M ethylenediaminetetraacetic acid (EDTA) solution for 5min. EDTA, a divalent ion chelator often used to produce capsules [6, 21, 22, 28-30] was used to free the calcium ions crosslinked within the core matrix of the alginate hydrogel.

The mechanical resistance of capsules with 4, 6 or 8-bilayers was tested (**Figure III.1c**) as elsewhere described [31] with minor modifications. Results show that as the number of deposition cycles increases, the mechanical resistance also increases. Therefore, capsules with 8-bilayers were the most resistant to impact. Moreover, the shell of the developed 8-bilayered capsules was able to maintain its integrity without releasing the liquified core, even when they were not immersed (**Video III.1**). The liquified core was only released upon damage with a needle.

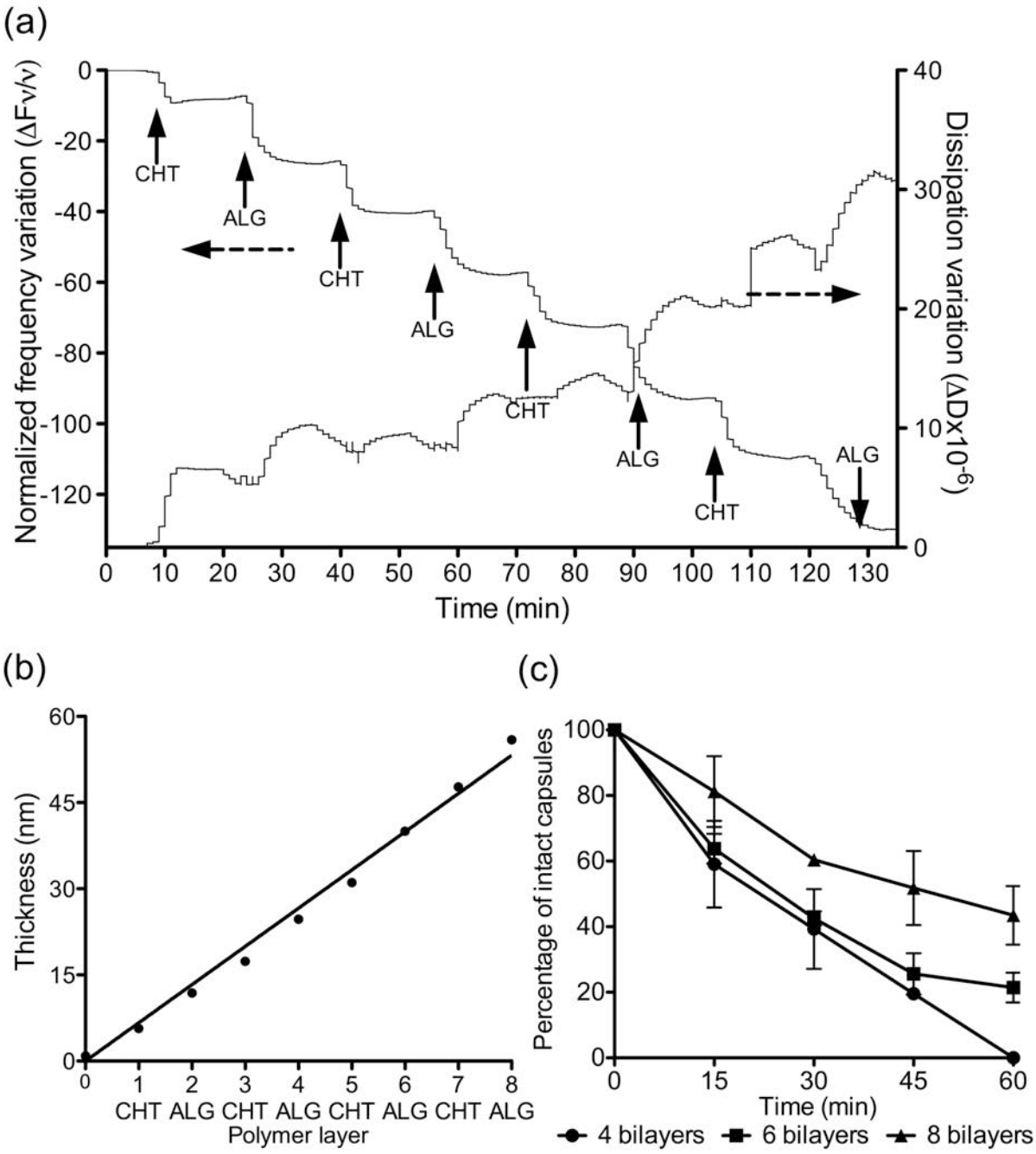

Figure III.1 · **(a)** Build-up assembly assessment of chitosan (CHT) and alginate (ALG) up to 8 deposition layers. Results correspond to the quartz-crystal microbalance with dissipation monitoring (QCM-D) of normalized frequency ($\Delta F_v/v$) and dissipation (ΔD) variations at the third overtone as a function of time. Arrows point to the end of polyelectrolytes adsorption. **(b)** Cumulative thickness evolution of the polymeric film as a function of the number of deposition layers. The thickness of the film was estimated using the Voigt viscoelastic model. The line represents a linear trend line with R^2=0.991. **(c)** Mechanical resistance of the liquefied capsules (n=15 in triplicate) after a rotational stress of 200 rpm for 60 min. Every 15 min, capsules where visualized and the number of intact capsules was assessed. Capsules with 4, 6 or 8-bilayers were tested.

Figure III.2 evidences the stratified structure of the shell composed by 4-, 6- or 8-bilayered by scanning electron microscopy (SEM). Results show that the thickness of the membrane of the capsules increases with the number of deposition cycles. The thickness differences found may be correlated to the superior mechanical resistance of capsules with higher number of layers. Using the Image J software, the thickness of each shell presented in **Figure III.2 (a)**, **(b)** and **(c)** was measured and divided by the number of layers, namely 8, 12 and 16 layers, respectively. Results show that each deposition layer measured 1.22 μm ± 0.01.

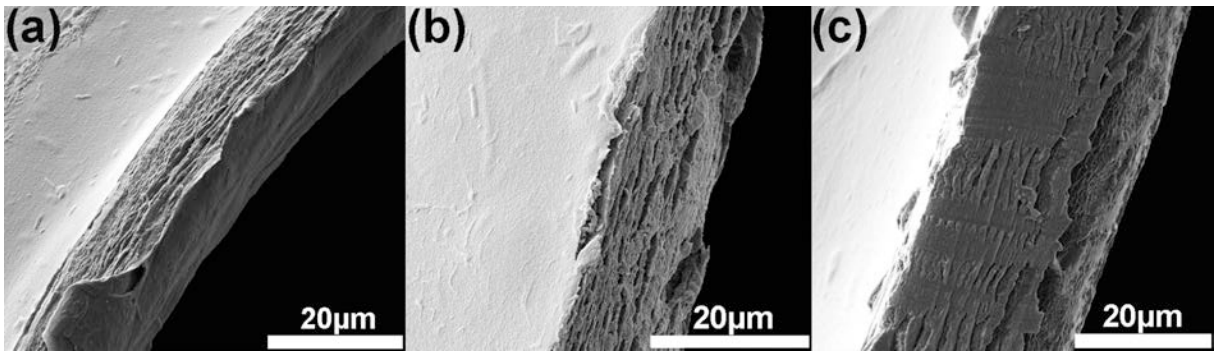

Figure III.2 - Scanning electron microscopy (SEM) of cross-sections of capsules composed by **(a)** 4-, **(b)** 6- or **(c)** 8-bilayers. Scale bar represents 20 μm.

Ion Coupled Plasma (ICP) was performed to evaluate the liquefying process of the 8-bilayered capsules. The assay was conducted regarding the cumulative release of calcium ions as a function of time of immersion in sodium chloride solution after 5 min of EDTA treatment (**Figure III.3**) or directly in EDTA solution (**Figure III.3** inset). As showed by the inset in **Figure III.3**, after capsules being immersed in EDTA solution with different concentrations, namely 0.0 2M, 0.05 M and 0.1 M, the cumulative release of calcium increases with time. Different concentrations of EDTA resulted in similar calcium release profiles. At 5 min of EDTA immersion, the amount of calcium release was around 20% of the total calcium incorporated. Since after 5 min of EDTA the core was liquified as shown in **Video III.1**, we intended to assess if after the stipulated time of EDTA treatment the calcium is continually being released in

sodium chloride solution. This behavior was confirmed, as showed in **Figure III.3**.

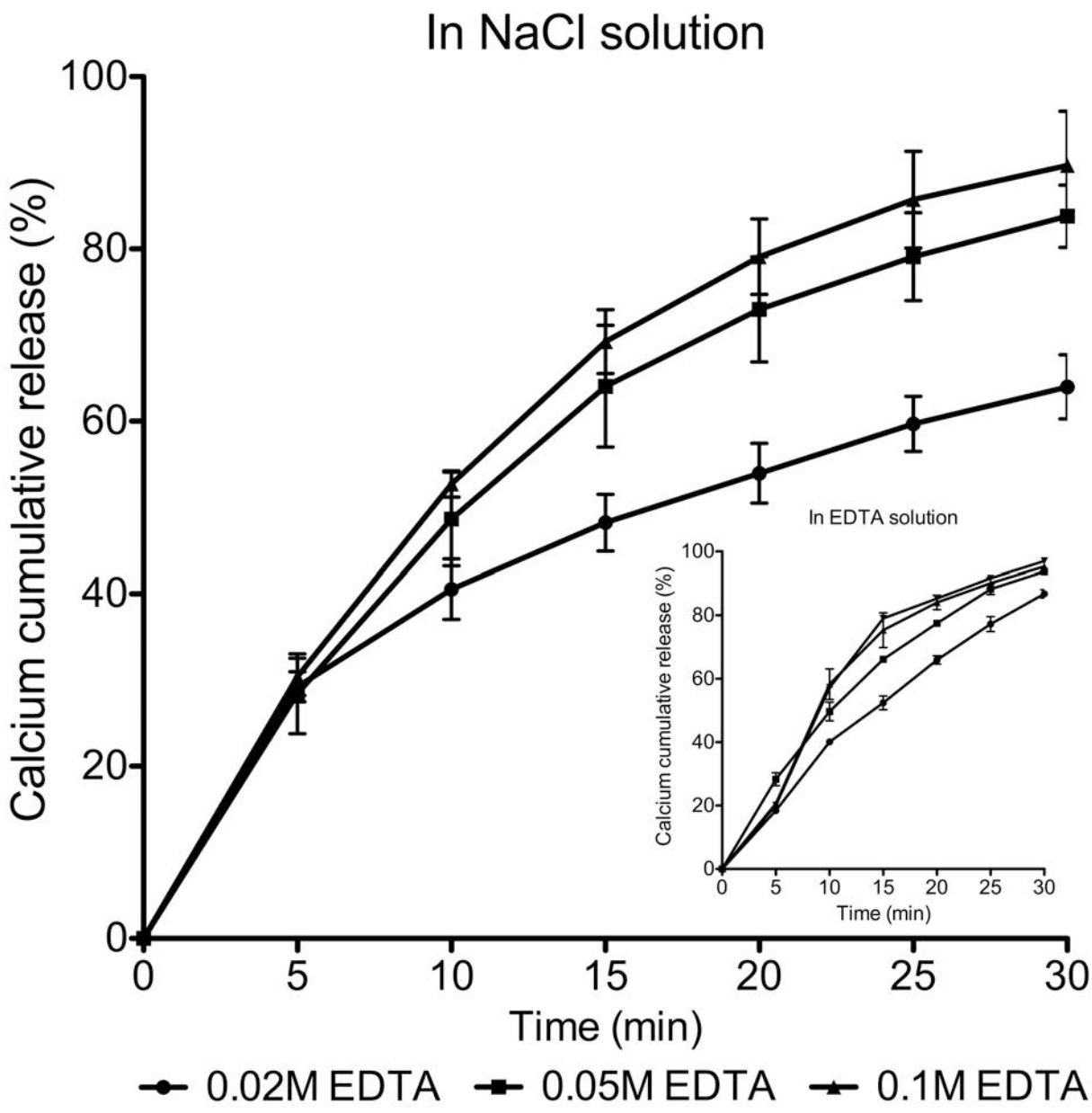

Figure III.3 - Calcium cumulative release as a function of time measured by Ion Coupled Plasma analysis. Capsules with 8-bilayers were placed in sodium chloride solution (NaCl) after being immersed in 5 min of EDTA treatment or directly in EDTA solution (inset). Different concentrations of EDTA were used, namely 0.02 M, 0.05 M and 0.1 M.

The lowest concentration of EDTA, namely 0.02 M, had the slowest release of calcium, however after 24 h all the calcium was released as occurred with the

other formulations. Therefore, 0.02 M of EDTA for 5 min was efficient in liquefying the alginate core.

The capability of capsules to adapt to different structures, such as syringes, was assessed (**Video III.2**). Capsules were collected, demonstrating a certain jamming resistance when passing through thinner regions of a syringe. The variable shape ability of capsules is also assured because the size of the solid PLLA microparticles is almost two orders of magnitude lower than the size of the flexible capsules. This ability is of huge interest for encapsulation systems since it offers capsules the ability of being implanted by minimal invasive methods in transplantation procedures. **Figure III.4** shows capsules and microparticles visualized by light microscopy. The average diameter of capsules was 1.8 ± 0.08 mm and the diameter of the PLLA microparticles covered the range 20-100 μm. Microparticles revealed a smooth surface, which could jeopardize cell adhesion. Moreover, PLLA lacks of natural cell recognition sites, and its hydrophobicity and low surface energy are known to affect cell attachment and proliferation [32]. Therefore, prior to biological assays, PLLA microparticles were surface modified to enhance cell adhesion affinity.

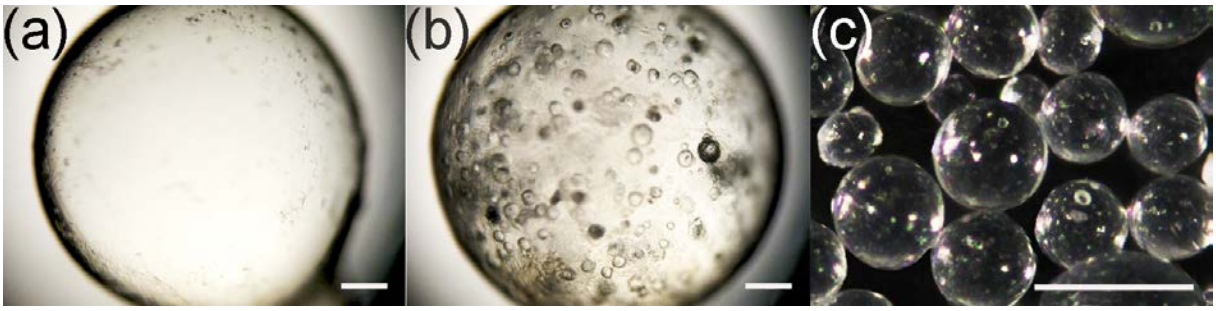

Figure III.4 – Liquified capsules **(a)** without (ALG capsules) and **(b)** with PLLA microparticles (PLLA capsules). Scale bar is 250 μm. **(c)** PLLA microparticles. Scale bar is 100 μm.

The ability of capsules to support cell survival was evaluated by encapsulating an immortalized mouse lung fibroblast cell line (L929, European Collection of Cell Cultures). PLLA microparticles were produced by solvent-emulsion technique and further modified by plasma-technique before collagen I coating.

After sterilization with UV-radiation, L929 cells were cultured at the surface of the microparticles at a density of $1x10^6$ cells per mL of alginate. Then, 4.5% w/v surface functionalized microparticles were added to a 1.5% w/v alginate solution. This template solution was used to produce capsules (PLLA capsules) as previously described. All solutions were sterilized by filtration using a 0.22 μm filter. Capsules without PLLA microparticles (ALG capsules) were also produced and used as negative controls. Before the production of the layer-by-layer shell, hydrogel particles were collected and used as a 3D culture system control (control). The biocompatibility of the capsules was assessed by live-dead (**Figure III.5a-c**) and MTS viability assays (**Figure III.5e**) up to 7 days of culture. Additionally, to evaluate if cells were adhered to the surface of PLLA microparticles, a DAPI-phalloidin fluorescence assay was also performed (**Figure III.5d**). In the live-dead assay, capsules had a good viability with any detectable dead cells. On the other hand, control particles revealed cell death at the inner areas of the structure with living cells concentrated to the peripheral regions. This may be due to the fact that control particles had a significant swelling increase at 37°C, and thus the culture medium may not reach those inner areas. Additionally, since the core is crosslinked, the diffusion efficiency of nutrients and oxygen might be also compromised. MTS results corroborate the observed good viability of capsules. Cells were metabolically active and at day 7 the viability of capsules compared to the control particles exceeded 100%. DAPI-Phalloidin assay showed that cells encapsulated in PLLA capsules adhered with the actin filaments being spread across the surface of PLLA microparticles, proving that the surface modification was efficient.

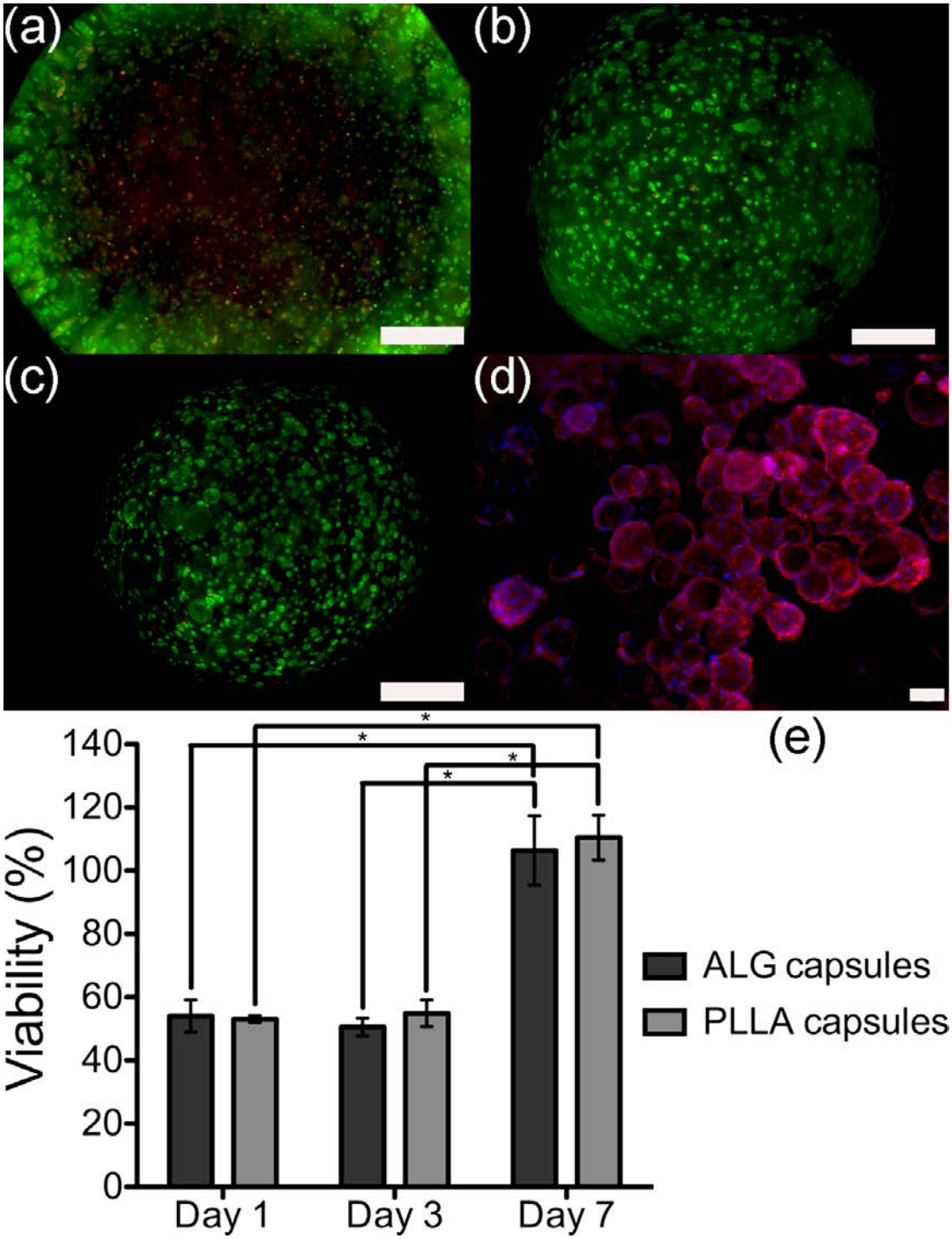

Figure III.5 - (a) Live-dead assay of control particles and **(b)** capsules without PLLA microparticles (ALG capsules) or **(c)** capsules with PLLA microparticles (PLLA capsules) at day 7 culture. Living cells were stained green by calcein and dead cells red by propidium iodide. Scale bar is 500 µm. **(d)** DAPI-phalloidin fluorescence assay of PLLA capsules at day 7 of culture. Cells adhered at the surface of the PLLA microparticles. Cells nuclei were stained blue and F-actin filaments red. Scale bar is 50 µm. **(e)** MTS viability assay at 1, 3 and 7 days of culture. Core-crosslinked alginate particles (control) and ALG and PLLA capsules were tested. Absorbance was read at a wavelength of 490 nm. Statistical differences are marked with (*), which stands for $p<0.001$.

4. Conclusion

Liquified capsules encapsulating cells and PLLA microparticles were successfully developed. The membrane of the capsules, which was produced by layer-by-layer, provided stability to capsules, even when they are not immersed in a liquid environment, and allowed the diffusion of essential molecules for cell survival. The encapsulation system proposed not only alleviates the current bioencapsulation issues but also allows tailoring membrane permselective ability, capsule mechanical integrity, as well as, optimizing and customizing a cell friendly environment inside the capsule. The developed approach can potentially be used to encapsulate anchorage dependent cells and control the phenotype of primary cells or stem cells fate. Moreover, different microparticles can be encapsulated which may be loaded with growth factors and other biomolecules of interest, customized to the type of cell encapsulated.

Acknowledgements

The authors acknowledge the financial support by the Portuguese Foundation for Science and Technology (FCT) through the Doctoral and Post-doctoral grants with the reference numbers SFRH/BD/69529/2010 and SFRH/BPD/48948/2008, respectively, co-financed by the Operational Human Potential Program (POPH) developed under the scope of the National Strategic Reference Framework (QREN) from the European Social Fund (FSE). The authors also acknowledge the financial support from the MP-2008-Small-2 project (Find&Bind) developed under the scope of the EU 7th Framework Programme.

Supplementary information

Videos of the release of the liquified alginate core after damage (**Video III.1**) and capsules ability to adapt to different structures, such as syringes and needles (**Video III.2**) are available at the Soft Matter website: *http://pubs.rsc.org* (**DOI:** 10.1039/C2SM26784E).

References

[1] G. Decher, J.-D. Hong, Buildup of ultrathin multilayer films by a self-assembly process, 1 consecutive adsorption of anionic and cationic bipolar amphiphiles on charged surfaces, Makromol. Chem. Macromol. Symp., 46 (1991) 321-327.

[2] F. Caruso, R.A. Caruso, H. Mohwald H, Nanoengineering of inorganic and hybrid hollow spheres by colloidal templating, Science, 282 (1998) 1111-1114.

[3] E. Donath, G.B. Sukhorukov, F. Caruso, S.A. Davis, H. Mohwald, Novel hollow polymer shells by colloid-templated assembly of polyelectrolytes, Angew. Chem., 37 (1998) 2201-2205.

[4] O. Shimoni, A. Postma, Y. Yan, A.M. Scott, J.K. Heath, E.C. Nice, A.N. Zelikin, F. Caruso, Macromolecule functionalization of disulfide-bonded polymer hydrogel capsules and cancer cell targeting, ACS Nano, 6 (2012) 1463-1472.

[5] J. Kim, D.R. Arifin, N. Muja, T. Kim, A.A. Gilad, H. Kim H, A. Arepally, T. Hyeon, J.W.M. Bulte, Multifunctional capsule-in-capsules for immunoprotection and trimodal imaging, Angew. Chem., 50 (2011) 2317-2321.

[6] C. Li, Z.-Y. Li, J. Zhang, K. Wang, Y.-H. Gong, G.-F. Luo, R.-X. Zhuo, X.-Z. Zhang, Porphyrin containing light-responsive capsules for controlled drug release, J. Mater. Chem., 22 (2012) 4623-4626.

[7] C. Lin, W. Zhu, H. Yang, Q. An, C.-an Tao, W. Li, J. Cui, Z. Li, G. Li, Facile fabrication of stimuli-responsive polymer capsules with gated pores and tunable shell thickness and composite, Angew. Chem., 123 (2011) 5049-5053.

[8] H.-Y. Lee, K.R. Tiwari, S.R. Raghavan, Biopolymer capsules bearing polydiacetylenic vesicles as colorimetric sensors of pH and temperature, Soft Matter, 7 (2011) 3273-3276.

[9] B.G. De Geest, M.A. Willart, B.N. Lambrecht, C. Pollard, C. Vervaet, J.P. Remon, J. Grooten, S. De Koker, Surface-engineered polyelectrolyte multilayer capsules: Synthetic vaccines mimicking microbial structure and function, Angew. Chem., 124 (2012) 3928-3932.

[10] G. Stoychev, N. Puretskiy, L. Ionov, Self-folding all-polymer thermoresponsive microcapsules, Soft Matter, 7 (2011) 3277-3279.
[11] M. Sanlés-Sobrido, M. Pérez-Lorenzo, B. Rodríguez-González, V. Salgueiriño, M.A. Correa-Duarte, Highly active nanoreactors: Nanomaterial encapsulation based on confined catalysis, Angew. Chem., 51 (2012) 3877-3882.
[12] Q. Jin, J. Bao, H. Sakiyama, N. Tsubaki, Preparation, structure and performance of TS-1 zeolite-coated Au–Pd/TiO_2–SiO_2 capsule catalyst for propylene epoxidation with oxygen and hydrogen, Res. Chem. Intermed., 37 (2011) 177-184.
[13] D. Shchukin, G. Sukhorukov, H. Mohwald, Smart inorganic/organic nanocomposite hollow microcapsules, Angew. Chem., 42 (2003) 4472-4475.
[14] R.M. Hernández, G. Orive, A. Murua, J.L. Pedraz, Microcapsules and microcarriers for in situ cell delivery, Adv. Drug Delivery Rev., 62 (2010) 711-730.
[15] O. Jeon, C. Powell, S.M. Ahmed, E. Alsberg, Biodegradable, photocrosslinked alginate hydrogels with independently tailorable physical properties and cell adhesivity, Tissue Eng. Part A, 16 (2010) 2915-2925.
[16] P.L. Chang, M. Shen, A.J. Westcott, Delivery of recombinant gene products with microencapsulated cells in vivo, Hum. Gene Ther., 4 (1993) 433-440.
[17] R.L. Broughton, M.V. Sefton MV, Effect of capsule permeability on growth of CHO cells in Eudragit EL microcapsules: Use of FITC-dextran as a marker of capsule quality, Biomaterials, 10 (1989) 462-465.
[18] B.C. Dash, G. Réthoré, M. Monaghan, K. Fitzgerald, W. Gallagher, A. Pandit, The influence of size and charge of chitosan/polyglutamic acid hollow spheres on cellular internalization, viability and blood compatibility, Biomaterials, 31 (2010) 8188-8197.
[19] W. Yuan, H. Dong, C.M. Li, X. Cui, L. Yu, Z. Lu, pH-controlled construction of chitosan/alginate multilayer film: Characterization and application for antibody immobilization, Langmuir, 23 (2007) 13046-13052.

[20] R.R Costa, C.A. Custódio, F.J. Arias, J.C. Rodríguez-Cabello, J.F. Mano, Layer-by-layer assembly of chitosan and recombinant biopolymers into biomimetic coatings with multiple stimuli-responsive properties, Small, 7 (2011) 2640-2649.
[21] N.L. Costa, P. Sher, J.F. Mano, Liquefied capsules coated with multilayered polyelectrolyte films for cell immobilization, Adv. Biomater., 13 (2011) B218-B224.
[22] Q. Zhao, B. Han, Z. Wang, C. Gao, C. Peng, J. Shen, Hollow chitosan-alginate multilayer microcapsules as drug delivery vehicle: Doxorubicin loading and in vitro and in vivo studies, Nanomedicine, 3 (2007) 3, 63-74.
[23] P. Sher, C.A. Custódio, J.F. Mano, Layer-by-layer technique for producing porous nanostructured 3D constructs using moldable freeform assembly of spherical templates, Small, 6 (2010) 2644-2648.
[24] S.M. Miranda, T.H. Silva, R.L. Reis, J.F. Mano, Nanostructured natural-based polyelectrolyte multilayers to agglomerate chitosan particles into scaffolds for tissue engineering, Tissue Eng. Part A, 17 (2011) 2663-2674.
[25] R. Bodmeier, J. McGinity, Solvent selection in the preparation of poly(D,L-lactide) microspheres prepared by the solvent evaporation method, Int. J. Pharm., 1988, 43, 179-186.
[26] M.A. Pujana, L. Pérez-Álvarez, L.C.C Iturbe, I. Katime, Water dispersible pH-responsive chitosan nanogels modified with biocompatible crosslinking-agents, Polymer, 53 (2012) 3107-3116.
[27] F. Kurayama, S. Suzuki, T. Oyamada, T. Furusawa, M. Sato, N. Suzuki, Facile method for preparing organic/inorganic hybrid capsules using amino-functional silane coupling agent in aqueous media, J. Colloid Interface Sci., 349 (2010) 70-76.
[28] A. Szarpak, D. Cui, F. Dubreuil, B. G. De Geest, L. J. De Cock, C. Picart, R. Auzély-Velty, Designing hyaluronic acid-based layer-by-layer capsules as a carrier for intracellular drug delivery, Biomacromolecules, 11 (2010) 713-720.

[29] H. Zhu, R. Srivastava, M. J. McShane, Spontaneous loading of positively charged macromolecules into alginate-templated polyelectrolyte multilayer microcapsules, Biomacromolecules, 6 (2005) 2221-2228.
[30] W. Yuan, Z. Lu, C. M. Li, Controllably layer-by-layer self-assembled polyelectrolytes/nanoparticle blend hollow capsules and their unique properties, J. Mater. Chem., 21 (2011) 5148-5155.
[31] T. Haque, H. Chen, W. Ouyang, C. Martoni, B. Lawuyi, A.M. Urbanska, S. Prakash, Superior cell delivery features of poly(ethylene glycol) incorporated alginate, chitosan, and poly-L-lysine microcapsules, Mol. Pharmaceutics, 2 (2004) 29-36.
[32] Y. Hong, C. Gao, Y. Xie, Y. Gong, J. Shen, Collagen-coated polylactide microspheres as chondrocyte microcarriers, Biomaterials, 26 (2005) 6305-6313.

Chapter IV

Multilayered hierarchical capsules providing cell adhesion sites [4]

Abstract

Liquified capsules featuring *(i)* an external shell by layer-by-layer assembly of poly(L-lysine), alginate and chitosan, and encapsulating *(ii)* surface functionalized poly(L-lactic acid) (PLLA) microparticles were developed. We hypothesize that, while the liquified environment enhances the diffusion of essential molecules for cell survival, microparticles dispersed in the liquified core of capsules provide the physical support required for cellular functions of anchorage-dependent cells. The influence of the incorporation of PLL on the regime growth, thickness and stability was analyzed. Results show a more resistant and thicker film with an exponential build-up growth regime. Moreover, capsules ability to support cell survival was assessed. Capsules containing microparticles revealed an enhanced biological outcome in cell metabolic activity and proliferation, suggesting their potential to boost the development of innovative biomaterials designs for bioencapsulation systems and tissue engineering products.

[4] Based on the publication: C.R. Correia, R.L. Reis, J.F. Mano, Multilayered hierarchical capsules providing cell adhesion sites, Biomacromolecules, 14 (2013) 743-751.

1. Introduction

Bioencapsulation represents an evolving branch of tissue engineering and regenerative medicine, providing a range of therapeutic treatments, such as for diabetes [1, 2], bone [3], and cartilage [4] defects and cancer [5]. The hydrophilic nature, which provides a highly hydrated microenvironment similar to the extracellular matrix (ECM), made hydrogel particles the most widely used system [6]. Particularly, alginate is the most frequently employed biomaterial due to its abundance, water solubility, mild gelling properties, high biocompatibility and resemblance to the natural ECM [6-8].

Based on the early pioneering study of Iler [9], the approach to coat charged surfaces was introduced by Decher [10]. This method is based on the layer-by-layer (LbL) adsorption of oppositely charged macromolecules on the surface of particles. The multilayers can be made from a variety of constituents such as synthetic and natural polyelectrolytes, nanoparticles, lipids and multivalent dyes [11]. The core of the LbL particles can be further dissolved or eliminated originating capsules. Capsules has been widely used particularly in cell encapsulation systems, but also have found great applicability in drug delivery or screening systems, biosensors, catalysis, reactors, immunoisolation and medical image due to their versatile wall functions, capability to load active substances and unique permeability [2, 12–18].

In bioencapsulation systems, the diffusion efficiency is a main issue since it influences the viability of the encapsulated cells by controlling the exchange of nutrients, oxygen, metabolites and waste products. Former studies compared the biological outcome of encapsulated cells in capsules with different core permeability. Results showed that as the dissolution of the core increased, encapsulated cells presented higher viability and proliferation [19, 20].

The main drawback of capsules in cell encapsulation approaches is related with the fact that most cells are anchorage-dependent and, thus, cannot grow in suspension and need to adhere to a solid substrate [8]. Therefore, maximizing the core dissolution or even perform its elimination to achieve an excellent diffusion of essential molecules will, on the other hand, compromise

cell survival. To overcome this main issue, we hypothesized that capsules encapsulating microparticles are a promising attempt. While the liquified environment of capsules ensures the required excellent diffusion, cell adhesion sites required for cellular functions are provided by the encapsulated microparticles. We propose an innovative concept termed here as Multifunctional Capsules (MCs). MCs are composed by *(i)* a permselective multilayered membrane and *(ii)* poly(L-lactic acid) (PLLA) microparticles. A schematic representation of MCs is given in **Scheme IV.1**. To obtain the membrane, poly(L-lysine) (PLL), chitosan (CHT) and alginate (ALG) polyelectrolytes were combined by LbL assembly. Besides being a versatile and low-cost technique, one of the main advantages of LbL for bioencapsulation systems is the possibility to be performed in mild conditions. Due to the excellent biocompatibility of chitosan and alginate, the two natural polymers are often applied as polycation and polyanion electrolytes, respectively, in biomedical applications of drug delivery systems and tissue engineering (TE) approaches [12, 21, 22]. The successful assembly of CHT and ALG has already been reported to produce capsules for cell immobilization [23], drug delivery systems [24], or scaffolds for TE [25, 26]. PLL is a synthetic biocompatible polycation [27, 28] often applied to improve the mechanical strength of alginate capsules, as first reported elsewhere [29]. Although PLL-ALG membranes have been shown to support tissue growth, studies demonstrated the formation of fibrotic tissue around the membrane surface when transplanted in rat models [30]. Therefore, to produce capsules for cell encapsulation we intend to take advantage of the high biocompatibility of CHT and ALG combined with the mechanical stability provided by PLL. This assembly of three-component polyelectrolytes via alternate deposition has fuelled much interest recently due to its demonstrated superior tunability and versatility to the traditional 2-component method [18, 31].

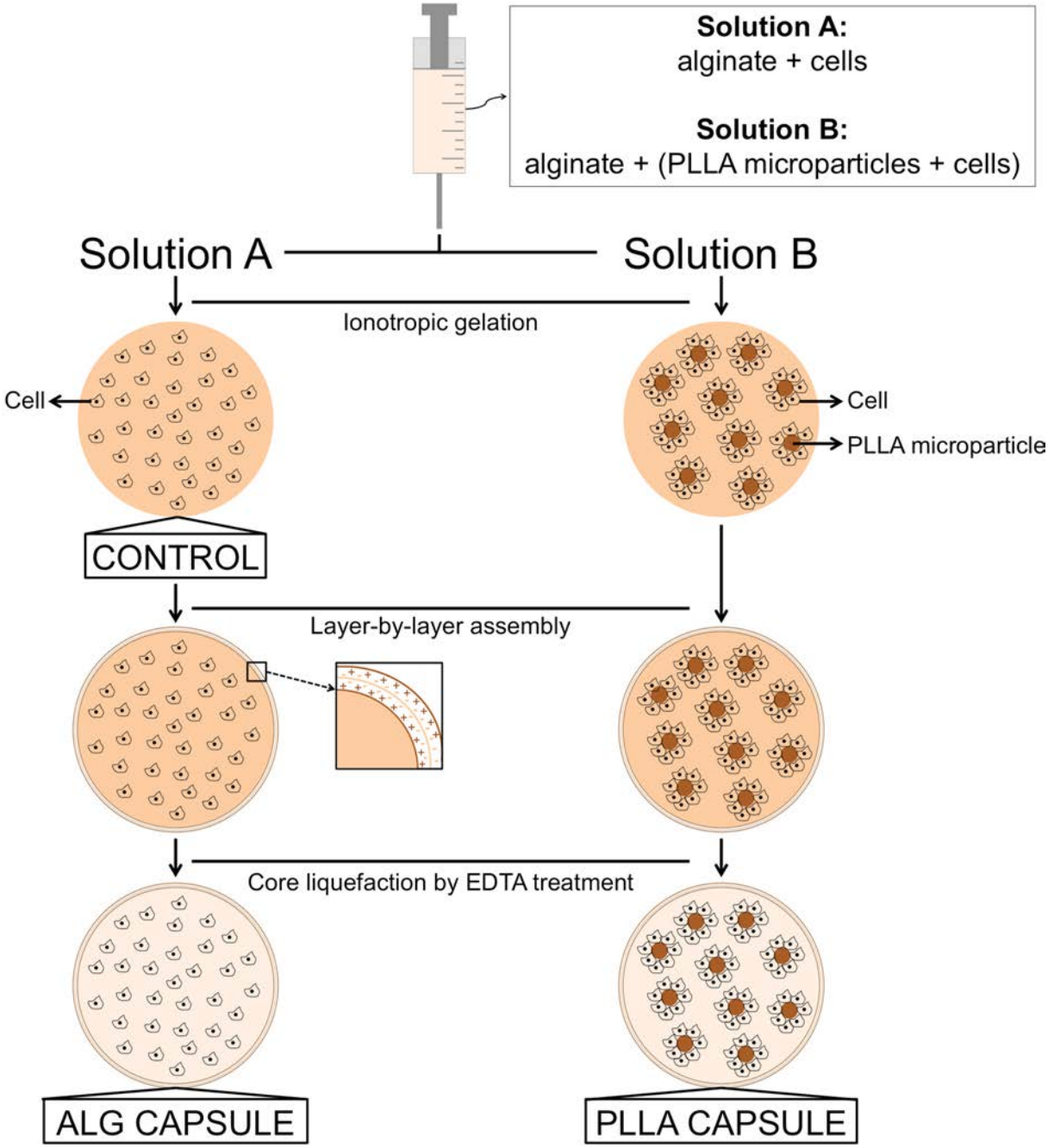

Scheme IV.1 - A schematic representation of the production of Multifunctional Capsules (MCs). Cells are mixed with an alginate solution (Solution A) or with an alginate solution containing poly(L-lactic acid) microparticles (PLLA) (Solution B). Both solutions are extruded separately, originating alginate particles by ionotropic gelation. Alginate particles obtained with solution A will be used as control. Afterwards, an external shell is developed at the surface of the obtained particles by layer-by-layer technique. The crosslinked alginate core is further liquified by ethylenediaminetetraacetic acid (EDTA) treatment, originating liquified capsules encapsulating cells (ALG capsules) or encapsulating cells and PLLA microparticles (PLLA capsules).

2. Materials and Methods

2.1 Materials

Poly(L-lactic acid) (PLLA) with a molar mass M_w~1,600-2,400 and 70% of crystallinity was purchased from Polysciences (Germany). Methylene chloride (CH_2Cl_2) was purchased from Fisher Chemical (UK). Polyvinyl alcohol (PVA), phosphate buffer saline (PBS), low viscosity sodium alginate from brown algae (ALG, ~250cP), poly(L-lysine) (PLL, M_w~30,000-70,000), ethylenediaminetetraacetic acid (EDTA), low glucose Dulbecco's Modified Eagle's Medium (DMEM), sodium bicarbonate, 4,6-Diaminidino-2-phenylindole-dilactate (DAPI, 20 $mg.mL^{-1}$) and phalloidin tetramethylrhodamine B isothiocyanate (10 $mg.mL^{-1}$) were purchased from Sigma-Aldrich (USA). Acetic acid was purchased from Carlo Erba (Italy). Collagen type I Rat Tail in liquid form (5 $mg.mL^{-1}$), fetal bovine serum (FBS), penicillin-streptomycin and trypsin-EDTA solution were purchased from Invitrogen. Sodium chloride (NaCl) was purchased from Panreac (Spain). Calcium chloride was purchased from Merck (Germany). Water-soluble highly purified chitosan (CHT, Protasan UP CL 213, viscosity 107 mPa.s, molecular weight Mw= $2.7x10^5$ $g.mol^{-1}$, 83% degree of deacetylation) was purchased from NovaMatrix (Norway). The immortalized mouse lung fibroblast cell line (L929) was purchased from the European Collection of Cell Cultures. The MTS colorimetric assay (Cell Titer 96® AQ_{ueous} One Solution Cell Proliferation Assay) was purchased from Promega (USA). Calcein-AM and propidium iodide (PI) dyes (1 $mg.mL^{-1}$) and the Quant-iT™ PicoGreen® dsDNA Assay Kit were purchased from Molecular Probes-Invitrogen (USA).

2.2 PLLA microparticles production

PLLA microparticles were produced by emulsion solvent evaporation technique as elsewhere described [32] with minor modifications. Briefly, 1 g of PLLA was dissolved in 20 mL of CH_2Cl_2 to obtain a 5% w/v transparent solution of PLLA/CH_2Cl_2. This solution was added under agitation to 100 mL of 0.5% w/v

PVA. The resulting solution was left to stir for 2 days at room temperature (RT) in order to evaporate the organic solvent. The produced PLLA microparticles were collected by filtration and washed several times with distilled water. Ultimately, microparticles were subsequently frozen at -80°C and lyophilized (Cryodos, Telstar) for 3 days. Prior to usage, microparticles were stored at 4°C.

2.3 PLLA microparticles surface functionalization

PLLA microparticles were surface modified by plasma treatment technique. PLLA microparticles were placed inside the plasma reactor chamber (PlasmaPrep5, Gala Instrumente, Germany) fitted with a radio-frequency generator. Air was used as the working atmosphere. After the pressure of the chamber had stabilized to ~0.2 mbar, a glow discharge plasma was created by controlling the electrical power at 30 V of electrical potential difference. The plasma-treated microparticles were treated for 5 min. The sample was removed from the chamber and a gentle mixing was employed in order to maximize the PLLA surface exposition to plasma treatment. This procedure was repeated three times in order to apply a total plasma reaction time of 15 min. 450 mg of PLLA plasma treated microparticles were sterilized by UV radiation for 30 min and then immersed in 30 mL of 0.02 M acetic acid containing 1200 µg of collagen I for 4 h at RT. A mild shaking was employed every hour. Ultimately, microparticles were collected and washed three times PBS.

2.4 Preparation of capsules

1.5% w/v of alginate (pH 7, ALG) was dissolved in 0.15 M NaCl. To produce capsules containing microparticles, 4.5% w/v surface modified PLLA microparticles was added to the template solution. Under agitation rate by a mechanical stirrer, alginate solutions with or without PLLA microparticles were dropwise to a 0.1 M calcium chloride solution using an 18 G needle. Droplets were immediately transformed into hydrogel particles by ionotropic gelation due to the ionic crosslinking of the alginate matrix. The hydrogel particles

formed were left to stir for 20 min and then washed with NaCl. Once obtained the alginate particles, the external membrane by LbL assembly was processed. Hydrogel particles were first immersed in PLL, and subsequently in ALG, CHT and in ALG again. Between each polyelectrolyte immersion of 10 min, the excess of macromolecules was removed by immersion in NaCl for 5min. This process was repeated three times in order to obtain a 12-layered membrane on the surface of the hydrogel particles. Core-shell hydrogel particles obtained were then immersed in 0.02 M EDTA at pH 7 for 5 min to liquefy the alginate core. The polyelectrolyte solutions with a concentration of 0.5 $mg.mL^{-1}$ were dissolved in 0.15 M NaCl. The pH of PLL and ALG was set to 7 and, in the case of chitosan, to 6.4.

2.5 Microparticles and capsules morphology

The surface of PLLA microparticles before and after plasma treatment was visualized by scanning electron microscopy (SEM). Microparticles were gold-coated using a sputter coater and visualized using a Leica Cambridge S-360 operating at 15 kV accelerating voltage. Additionally, microparticles and capsules encapsulating surface modified PLLA microparticles were visualized by optical microscopy. Microparticle (n = 185) and capsules (n = 20) diameters were measured by using Image J software.

2.6 Quartz-crystal microbalance with dissipation monitoring

The build-up process of the ability of PLL, CHT and ALG to adsorb in a sequential fashion was performed on planar gold surfaces. The process was monitored by quartz-crystal microbalance with dissipation monitoring (QCM-D, QSense E4, Sweden) in a liquid environment. The instrument measuring principle is based on the analysis of the quartz crystal impedance at multiple overtones. An equivalent circuit model (IPC High Precision Multichannel Dispenser, ISMATEC) was fitted to the impedance curve and the obtained parameters were used to calculate the regime growth of the multilayers. Briefly, PLL, ALG and CHT multilayers were deposited on gold-coated quartz

crystals. Before adsorption, the quartz crystals were cleaned with 0.15 M NaCl at 25ºC until a baseline was obtained. Since the quartz crystals surface is negatively charged, as well as the surface of the alginate hydrogel particles, it was possible to follow the same polymer cycle previously described to produce capsules. Moreover, all conditions such as concentration, pH, and time of deposition, and washing as previously described to obtain the LbL membrane, were also used in the QCM-D analysis. Polymeric and washing solutions were alternatively introduced into the measuring chamber at a flow rate of 100 $\mu L.min^{-1}$. Variations in frequency (ΔF) and in dissipation (ΔD) were monitored in real time up to a deposition of 12 polymer layers. The frequency of each overtone was normalized to the fundamental resonant frequency of the quartz-crystal ($\Delta F_{\nu}.\nu^{-1}$, in which ν stands for the overtone). Thickness measurements were estimated using the Voigt viscoelastic model implemented in the *QTools* software from *QSense*.

2.7 Capsules membrane stability test

The influence of the introduction of PLL on the mechanical stability of capsules was evaluated using a rotational mechanical test. Since the aim of this test is to assess membrane resistance, only capsules without PLLA microparticles were used (ALG capsules). Two types of membrane were tested, namely 12-layered capsules with PLL (PLL-ALG-CHT), and 12-layered capsules without PLL (CHT-ALG) (n = 10 in triplicates). The two types of ALG capsules were placed in centrifuge tubes containing 5 mL of PBS. The tubes were rotated at a speed of 200 rpm for 60 min. At every 15 min of rotation, the number of damage capsules was observed and counted under a light microscope. The intact capsules were placed again inside the centrifuge tubes to continue the rotational test. After the time of experiment an additional rotation at a speed of 2000 rpm for 15 min was performed.

2.8 *In vitro* cell culture

Cells were routinely cultured with low glucose DMEM supplemented with 3.7 $g.L^{-1}$ sodium bicarbonate, 10% FBS and 1% penicillin-streptomycin at pH 7.4. Cells were grown in 75 cm^2 tissue culture flasks and incubated at 37°C in a humidified air atmosphere of 5% CO_2. Every 3-4 days fresh medium was added.

2.9 Cell encapsulation

At 90% of confluence, L929 cells grown in tissue culture flasks were washed with PBS and subsequently detached by a chemical at 37°C in a humidified air atmosphere of 5% CO_2. To inactivate the trypsin effect, cell culture medium was added. Cells were then centrifuged at 300 g and 25°C for 5 min and the medium was decanted. Afterwards, cells were mixed with 1.5% w/v ALG. Cell density was set to $1x10^6$ cells per mL of alginate. This solution was then used to produce alginate particles (control) and capsules without PLLA microparticles (ALG capsules). To produce capsules with PLLA microparticles (PLLA capsules) a concentrated cell suspension with $1x10^6$ cells per mL of alginate was first seeded on the surface of PLLA microparticles. PLLA microparticles were then incubated at 37°C and 5% CO_2 for 3h. Afterwards, 1.5% w/v alginate solution was mixed with cells and microparticles. The same procedure used to produce capsules previously described was performed to produce ALG and PLLA capsules encapsulating cells. Layer-by-layer assembly and EDTA treatment were not performed in alginate hydrogel particles, which were used as a 3D cell culture control. The entire procedure was performed under sterile conditions. All the solutions used at this step were sterilized by filtration through a 0.22 µm filter.

2.10 Cell morphology

The morphology of the encapsulated cells adhered at the surface of the modified PLLA microparticles was analyzed by SEM. PLLA capsules encapsulating L929 cells were incubated at 37°C and 5% CO_2. At day 1 and 7,

culture medium was removed and 10% formalin was added to each well (n = 5 capsules per well). After 1h at RT, formalin was removed and capsules were dehydrated using sequential ethanol series, namely 60%, 70%, 80%, 90%, 96% and 100%, 10 min each. Prior to SEM visualization, capsules were destroyed to release the core contents. Subsequently, the released microparticles with cells were gold-coated using a sputter coater and visualized using a Leica Cambridge S-360 operating at 15 kV accelerating voltage.

2.11 MTS viability assay

Capsules were tested for cytotoxicity and suitability for live cell encapsulation using a MTS colorimetric assay. This assay is based on the bioreduction ability of mitochondrial dehydrogenase enzymes present in viable cells to convert the MTS compound into a cell culture soluble brown formazan product. Briefly, alginate particles and capsules encapsulating L929 cells were placed in a non-treated surface 12-well cell culture plate (n = 5 per well, in triplicate) and incubated at 37°C and 5% CO_2. Alginate particles and capsules without cells were used as a background control. At 1, 3 and 7 days of culture, the MTS assay was performed protected from light. Briefly, culture medium was removed and 1 mL of serum-free DMEM containing MTS solution with a dilution ratio of 1:5 was added to each well. Samples were then incubated in the dark at 37°C and 5% CO_2. After 3 h, 100 µL of each well (in triplicate) were transferred to a 96-well plate. The amount of formazan product was measured by absorbance at a wavelength of 490 nm using a multiwall spectrophotometer (Synergy HT, Bio-TEK). The background was corrected by subtracting the absorbance obtained from particles and capsules without cells to those with cells encapsulated.

2.12 Fluorescence assays

Alginate particles (control) and capsules (n = 5 samples per well, in triplicate, both assays) were incubated for 1, 3, 7, 14, 21 and 28 days at 37°C and in a

humidified 5% CO_2 atmosphere. Live-dead and DAPI-phalloidin fluorescence assays were performed at each time culture period.

Calcein-AM and propidium iodide dyes were used to perform a live-dead assay. Calcein-AM is a membrane-permeant dye, which is hydrolyzed by endogenous esterase into the highly negatively charged green fluorescent cell marker calcein retained in the cytoplasm. PI is a membrane impermeant and, thus, binds to DNA of dead cells. Briefly, at each timepoint, culture medium was removed and 1mL of PBS containing 2 µL of calcein-AM and 1 µL of PI was added to each well. Samples were then incubated at 37°C for 10 min protected from light. Afterwards, samples were washed three times with PBS and immediately visualized in the dark by fluorescence microscopy (Axioimage RZ1M, Zeiss, Germany). With calcein-AM, trough a fluorescent filter (fluorescence excitation of 494 and emission of 517 nm), living cells appeared bright green. With PI, trough a rhodamine filter (fluorescence excitation of 535 nm and emission of 617 nm), dead cells appeared bright red.

DAPI and phalloidin dyes were used to perform a DAPI-phalloidin assay. DAPI stains preferentially double-stranded DNA by delineating cells nuclei in blue. Phalloidin is a bicyclic peptide with selectivity to label F-actin, revealing the distribution of actin filaments in fixed cells. Prior to staining, at each timepoint, culture medium was removed and 10% formalin was added to each well (n = 5 particles or capsules per well, in triplicate). After 1 h at RT, formalin was removed and replaced by 0.1% Triton X for 5 min to permeabilize cells. Upon PBS washing, 1 mL of PBS containing 1 µL of DAPI and 10 µL of phalloidin was added to each well. After 1 h at RT protected from light, samples were washed three times with PBS and immediately visualized in the dark by fluorescence microscopy. Cells nuclei appeared bright blue and F-actin filaments appeared bright red due to DAPI and phalloidin dyes, respectively.

In both fluorescence assays, double staining was obtained in Z-stack mode with a resolution of 17 µm between slides by using the AxioVision software.

2.13 DNA quantification assay

Capsules ability to support encapsulated cells proliferation was tested by DNA quantification assay. Alginate particles (control) and capsules (n = 5 samples per well, in triplicate) were incubated in 12-well plates with non-treated surfaces for 1, 3, 7, 14, 21 and 28 days at 37ºC and humidified 5% CO_2 atmosphere. Similarly, particles and capsules without cells were used as background control. At each time culture period, each well was washed with PBS and 1 mL of ultra-pure sterile water was added. Upon mixing, contents were transferred to eppendorf tubes, which were then placed in a shaking water bath at 37ºC for 1 h. Ultimately, the tubes were immediately stored at -80ºC until use. Quantification of total DNA was determined after cell lysis, according to the manufacturer's description. After transferring each solution to a 96-well white opaque plate (in triplicates), the plate was incubated at RT protected from light for 10 min. The standard curve for DNA analysis was generated with provided DNA from the assay kit. Fluorescence was read at excitation of 485/20 nm and emission of 528/20 nm using a multiwall spectrophotometer (Synergy HT, BioTek, USA). The background was corrected by subtracting results obtained from particles and capsules without cells to those with cells encapsulated.

2.14 Statistical analysis

MTS and DNA data were grouped by timepoint, namely 1, 3 and 7 days or 1, 3, 7, 14, 21 and 28 days, respectively, in order to analyze significant differences between formulations. Additionally, both data were also grouped by formulation, namely, control, ALG capsules and PLLA capsules, in order to assess time-course significant differences of each formulation. Statistical analysis of both data cases was performed using two-way analysis of variance (ANOVA) with Bonferroni post-test using GraphPad Prism 5.0 software. A p-value<0.05 was considered statistically significant. Significant differences in grouped by timepoint were marked with an asterisk character (*). In grouped by formulation all results were significant different unless otherwise marked

with a cardinal character (#). All results are presented as mean ± standard deviation.

3. Results

3.1 Morphological analysis of PLLA microparticles and capsules

Capsules encapsulating microparticles with an average diameter of 1.8 ± 0.06 mm were visualized by optical microscopy (**Figure IV.1a**). Microparticles (**Figure IV.1b**) had a diameter range of 45.6 ± 13.5 µm, with 90.0 µm and 15.5 µm of maximum and minimum diameters, respectively. SEM analysis evidenced the smooth surface of the produced microparticles, as shown in **Figure IV.1c**. After plasma treatment, the roughness of the surface of PLLA microparticles significantly increased as shown in **Figure IV.1d**.

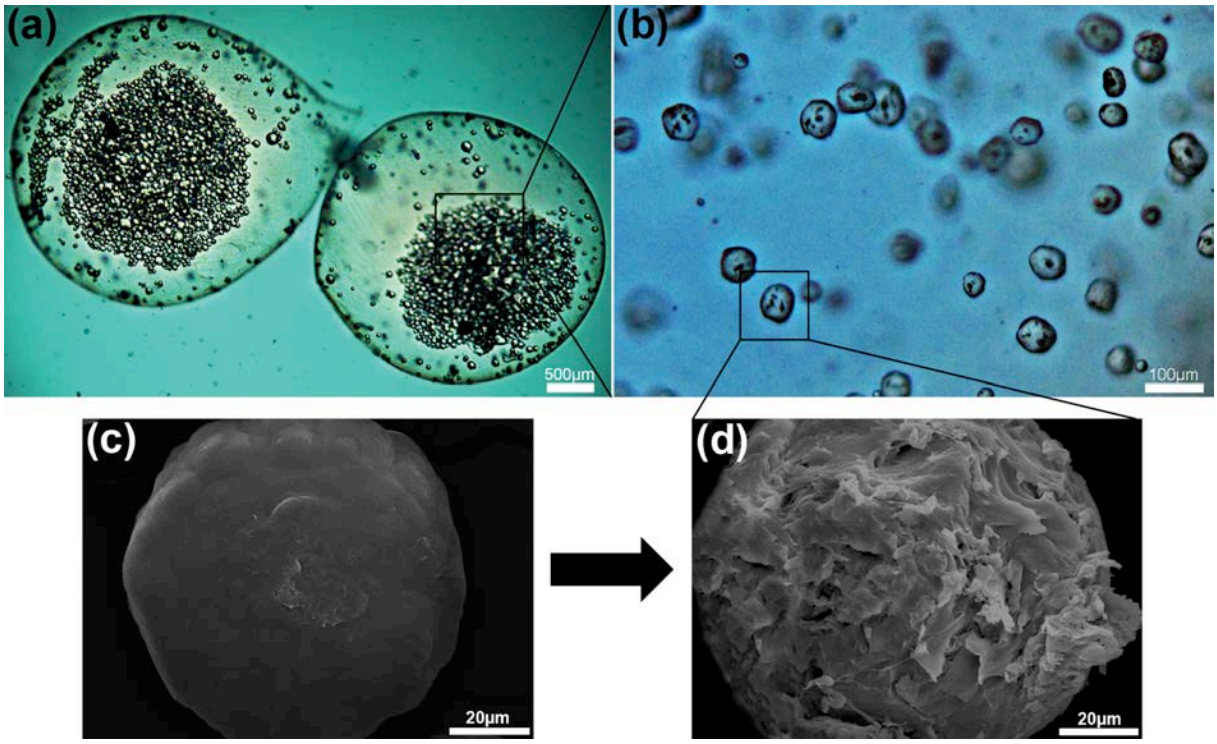

Figure IV.1 - Optical microscopy of **(a)** liquified capsules encapsulating **(b)** PLLA microparticles. Scale bar represents 500 µm and 100 µm for **(a)** capsules and **(b)** microparticles images, respectively. Scanning electron microscopy of a poly(L-lactic acid) (PLLA) microparticle **(c)** before and **(b)** after plasma treatment. Scale bar represents 20 µm with 1000x of magnification.

3.2 Polyelectrolytes interaction and thickness measurements

The assembly of PLL, ALG and CHT polyelectrolytes was characterized by QCM-D analysis. **Figure IV.2a** shows the normalized frequency ($\Delta F_v.v^{-1}$) and dissipation (ΔD) variations for the third overtone (15 MHz) after the deposition of 12 layers. Two different profiles were obtained, namely PLL-ALG-CHT (**Figure IV.2a**, continuous line) or ALG-CHT (**Figure IV.2a**, dotted line). The frequency shift (see vertical arrows in **Figure IV.2a**) evidences the deposition of each successive layer of polyelectrolyte on the surface of the quartz-crystals. For PLL-ALG-CHT profile, after the construction of 12 layers, the frequency decreased about 255 Hz. For CHT-ALG profile the frequency decreased about 210 Hz, after the same number of deposition layers. In both profiles the dissipation variation increased during the experiment. The QCM-D data was further used to estimate the thickness variations of the films with each adsorption cycle, as shown in **Figure IV.2b** and **Figure IV.2c**. In the PLL-ALG-CHT profile, the thickness of the film increased exponentially (dotted line in **Figure IV.2b** with $R^2 = 0.985$) with the number of deposition steps. At the end of the deposition cycle the estimated thickness of the PLL-ALG-CHT film was around 110 nm. On the other hand, the thickness of the CHT-ALG film (**Figure IV.2c**) increased linearly (dotted line in **Figure IV.2b** with $R^2 = 0.997$) up to a final estimated value around 80 nm.

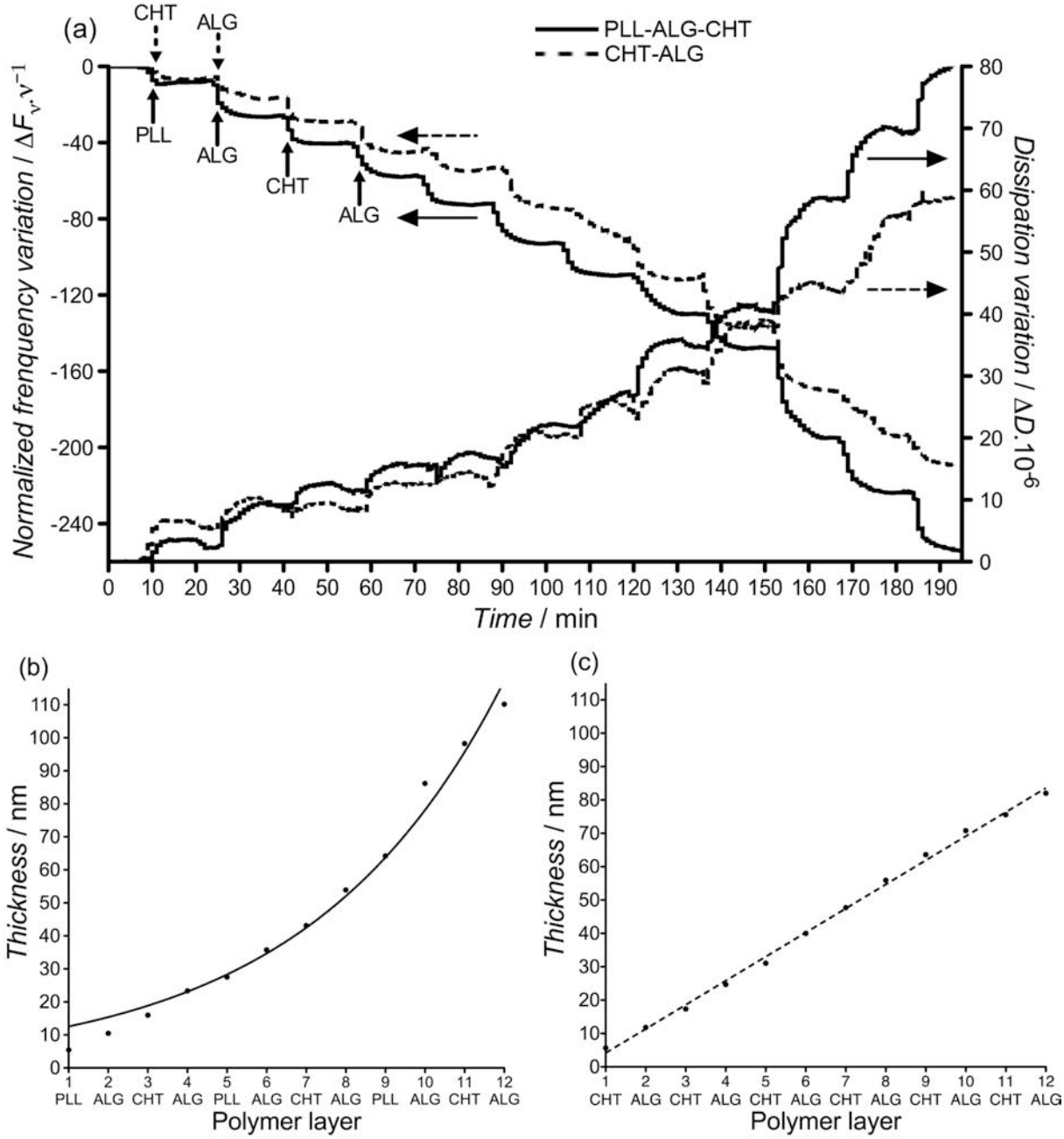

Figure IV.2 - Build-up assembly assessment of poly(L-lysine) (PLL), alginate (ALG) and chitosan (CHT) up to 12-deposition layers. **(a)** Quartz-crystal microbalance with dissipation monitoring (QCM-D) of normalized frequency ($\Delta F_v/v$) and dissipation (ΔD) variations at the third overtone as a function of time. PLL-ALG-CHT and CHT-ALG profiles are represented by the continuous and dotted line, respectively. **(b)** Cumulative thickness evolution for PLL-ALG-CHT polymeric film as a function of the number of deposition layers. The dotted line represents an exponential trend line with $R^2 = 0.985$. **(c)** Cumulative thickness evolution for CHT-ALG polymeric film as a function of the number of deposition layers. The dotted line represents a linear trend line with $R^2 = 0.997$. Thickness measurements were estimated using the Voigt viscoelastic model.

3.3 Membrane mechanical stability test

The assessment of the mechanical properties of capsules is important to determine the durability of capsules during production and handling. Additionally, mechanical properties of capsules are an indication of the membrane integrity. The ability of the membrane to maintain its integrity after being subjected to mechanical impact by rotational stress was assessed (**Figure IV.3**). The percentage of rupture capsules with a PLL-ALG-CHT membrane increased up to 27% ± 6 after 60 min of rotation at 200 rpm. Similarly, after applying a 2000 rpm rotational stress for 15 min, the percentage of ruptured capsules slightly increased to 33% ± 6. On the other hand, the percentage of rupture capsules with a CHT-ALG membrane rapidly increased to 43% ± 6 after the first 15 min of rotation and continued to increase with further mechanical stresses.

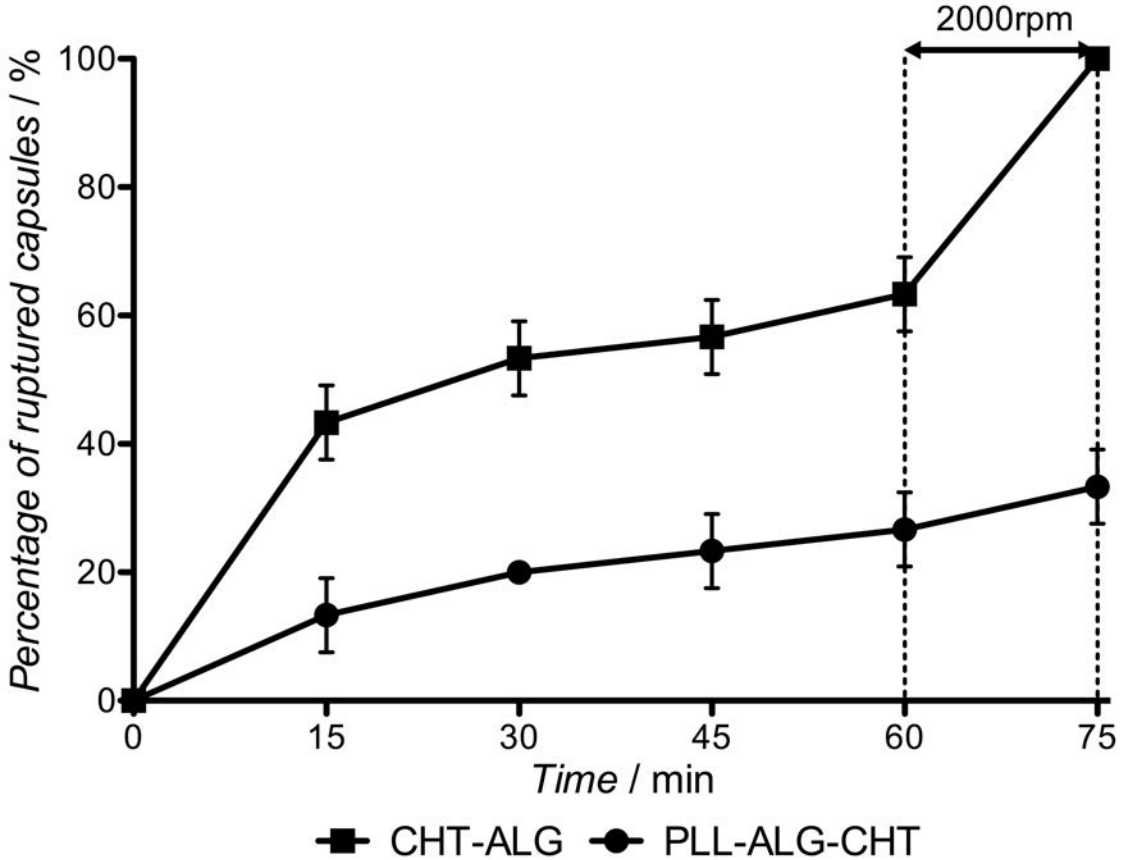

Figure IV.3 - The effect of rotational mechanical impact at 200 rpm up to 60 min and for an extra time of 15 min at 2000 rpm on capsules with 12-deposition layers was assessed. Two different capsules were tested, namely a two-component membrane capsule composed by chitosan and alginate (CHT-ALG, •) and a three-component membrane capsule composed by poly(L-lysine), alginate and chitosan (PLL-ALG-CHT, ■).

3.4 Morphology of encapsulated cells

Cell-material interactions of the encapsulated cells with microparticles were visualized by SEM (**Figure IV.4**). At day 1, cells were adhered and spread across the surface of microparticles (**Figure IV.4a**). At day 7, large aggregates of microparticles and cells could be detected as evidenced by **Figure IV.4c**. The encapsulated cells maintained their elongated fibroblast-like morphology as evidenced in higher magnification **Figure IV.4b** and **Figure IV.4d**.

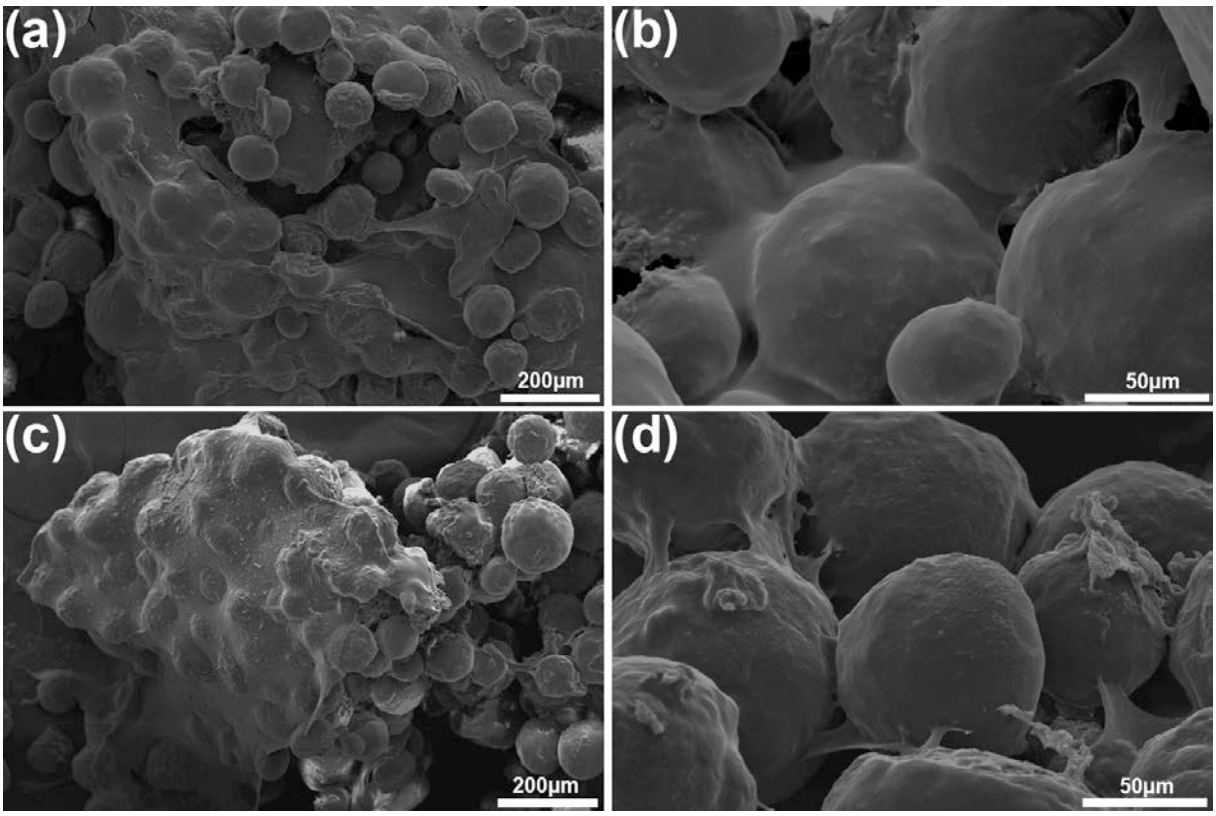

Figure IV.4 - Scanning electron microscopy of encapsulated PLLA microparticles and cells at **(a)** day 1 and **(c)** day 7 of culture. Scale bar represents 200 µm with 200x of magnification. Pictures **(b)** and **(d)** represent higher magnification images of days 1 and 7, respectively. Scale bar is 50 µm with 500x of magnification.

3.5 Metabolic activity and cell viability of encapsulated cells

Cell metabolic activity of encapsulated L929 cells was evaluated by MTS assay for 1, 3 and 7 days (**Figure IV.5**). The formazan absorbance of PLLA capsules was significantly higher than ALG capsules and control particles at day 1 and

day 3, respectively. At day 7, PLLA capsules absorbance was significantly higher compared to control and ALG capsules.

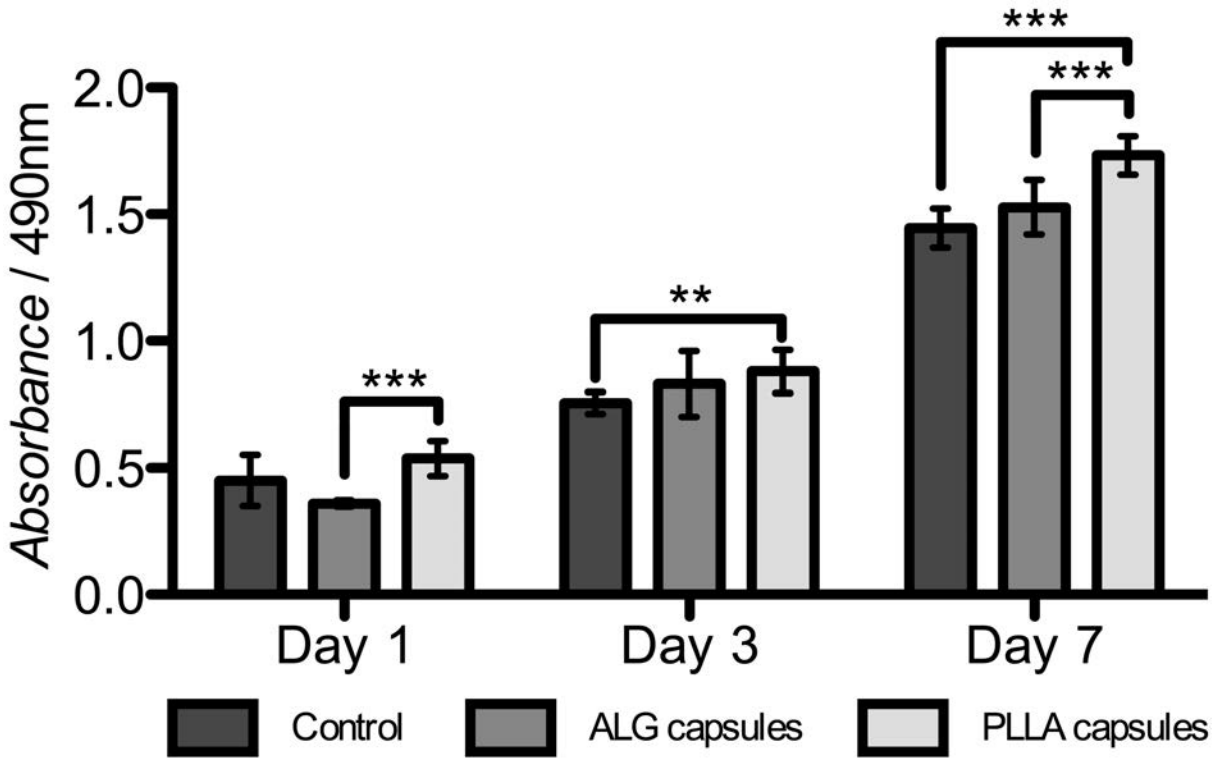

Figure IV.5 - MTS viability assay at 1, 3 or 7 days of culture. Alginate particles (control) and capsules with (PLLA capsules) or without (ALG capsules) PLLA microparticles were tested. Absorbance was read at a wavelength of 490 nm. Statistical differences in grouped by timepoint analysis are marked with (**) and (***), which stand for $p<0.01$ and $p<0.001$, respectively. Statistical differences in grouped by formulation analysis were found for all formulations unless otherwise marked with # character.

Moreover, all samples had a significant increase in the time-course absorbance. In addition, a fluorescence viability staining was performed to assess living and dead cells dispersed in the liquified capsule environment, using a live-dead assay (**Figure IV.6**). Control and ALG capsules exhibited a higher number of dead cells compared to PLLA capsules. This difference becomes more evident as the time of culture increases, particularly from day 14. Overall, MTS and live-dead data suggest a good viability for all formulations, particularly for PLLA capsules.

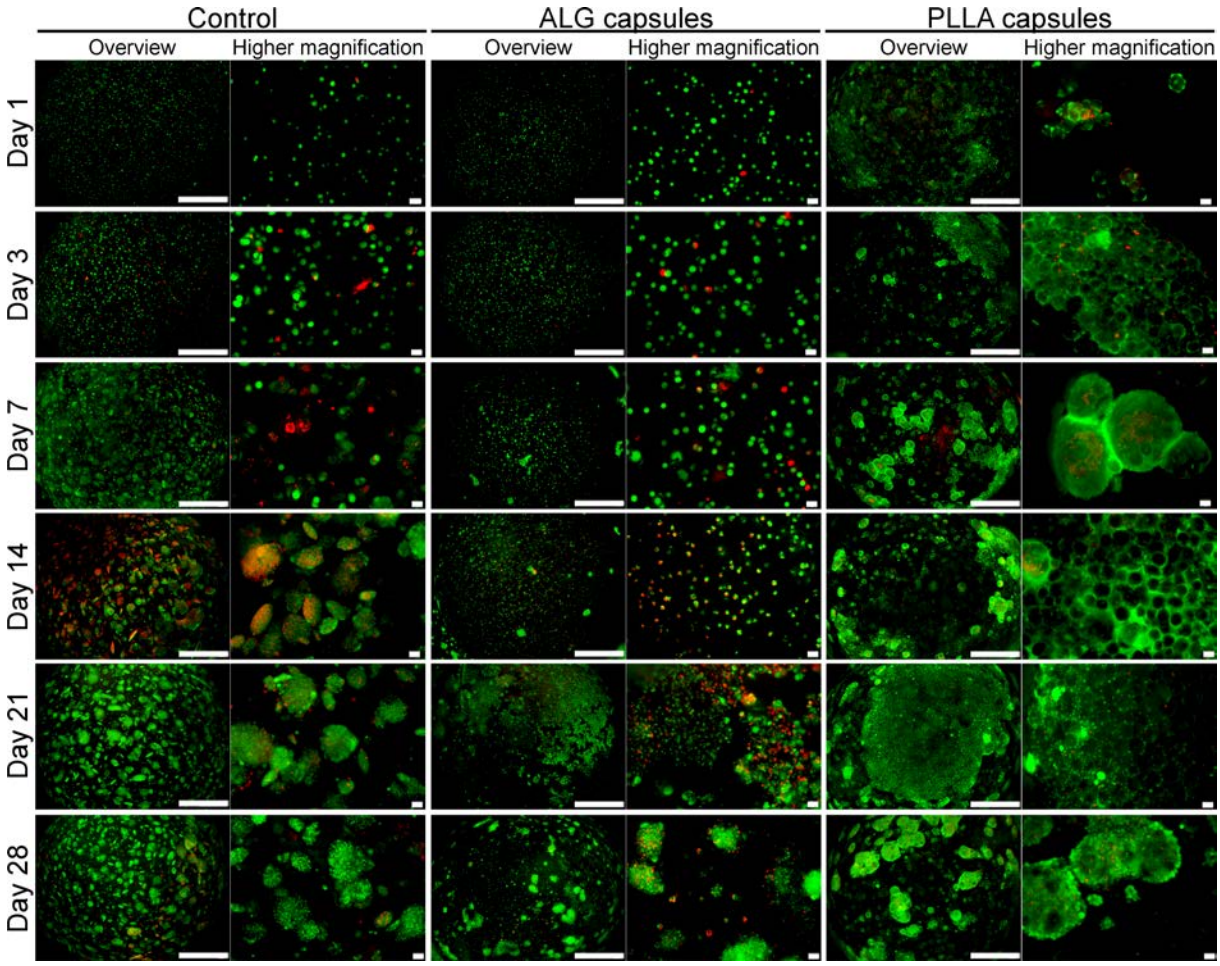

Figure IV.6 - Live-dead fluorescence assay at 1, 3, 7, 14, 21 or 28 days of culture. Alginate particles (control) and liquified capsules with (PLLA capsules) or without (ALG capsules) PLLA microparticles were tested. Living cells were stained green by calcein and dead cells red by propidium iodide. Scale bar represents 500 μm and 40 μm in overview and higher magnification images, respectively.

3.6 Cell organization and proliferation studies

The distribution and structural organization of encapsulated cells within the crosslinked core of control particles or the liquified environment of capsules was assessed by DAPI-phalloidin fluorescence assay (**Figure IV.7**).

Cell proliferation was assessed as a function of culture time up to 28 days by DNA quantification assay (**Figure IV.8**). Overall, during the time of the experiment, both ALG and PLLA capsules had a significant higher proliferation compared with control particles. Particularly, PLLA capsules had the highest cell proliferation. ALG capsules had an increase in time-course proliferation up to 21 days of culture, and then at day 28 the proliferation decreases to an

intermediate value not significant different from days 14 and 21. Cells encapsulated in PLLA capsules exhibited a rapid and significant increase of proliferation up to 7 days of culture. At day 14 the proliferation profile appears to stabilize to an intermediate value no statistical different from days 7 and 21. Due to the smooth and continuous increase, at day 21 the DNA content is statistical different compared to day 7, followed by a significant increase at day 28. In control particles, cell proliferation increased up to 14 days of culture, without significant differences compared to day 21. However, at day 28, a significant decrease was observed. DAPI-phalloidin and DNA data suggest an improved value provided by PLLA capsules regarding cell-material interactions and cell proliferation.

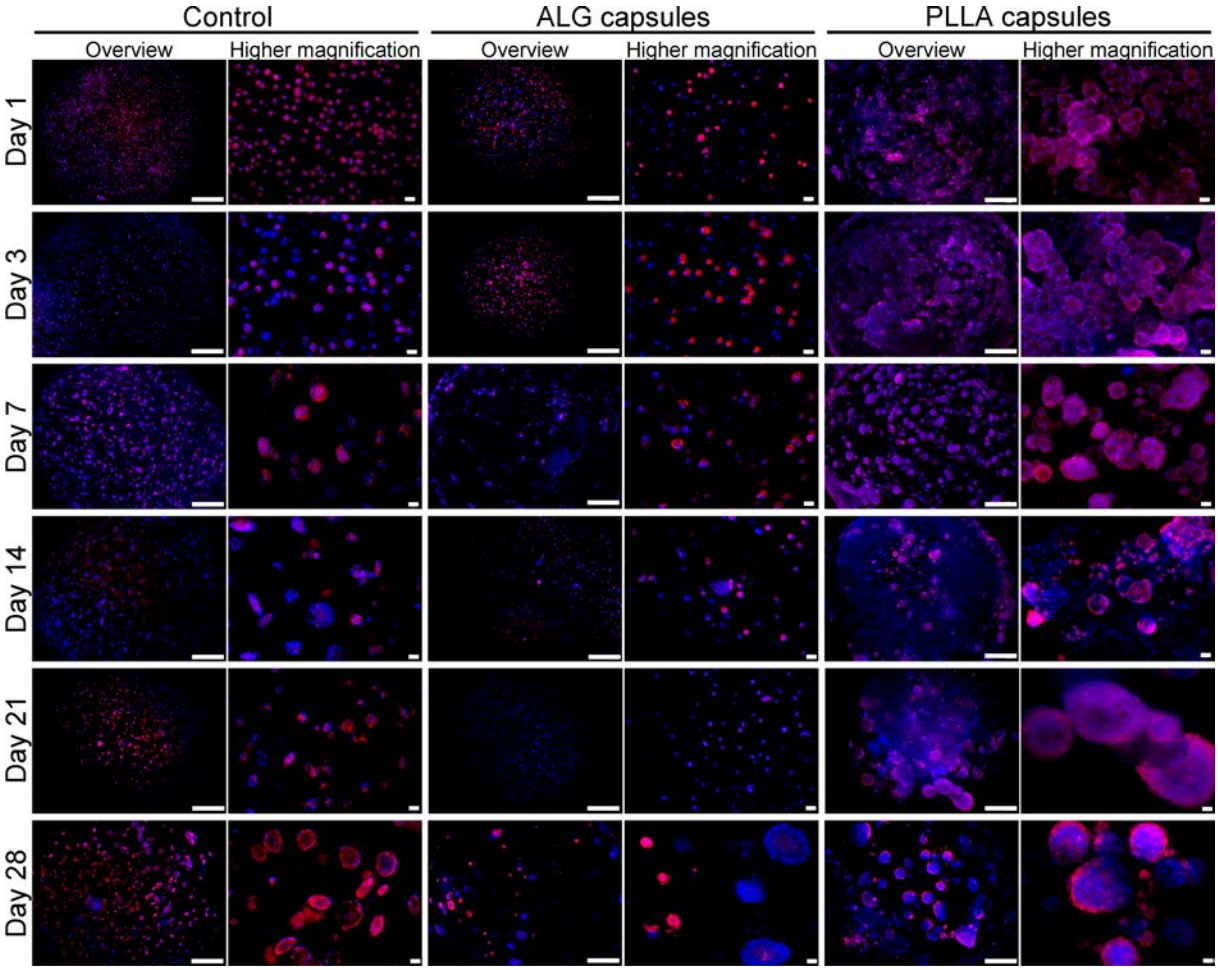

Figure IV.7 - DAPI-phalloidin fluorescence assay at 1, 3, 7, 14, 21 or 28 days of culture. Alginate particles (control) and liquified capsules with (PLLA capsules) or without (ALG capsules) PLLA microparticles were tested. Cells nuclei were stained blue by DAPI and F-actin filaments in red by phalloidin. Scale bar represents 500 µm and 40 µm in overview and higher magnification images, respectively.

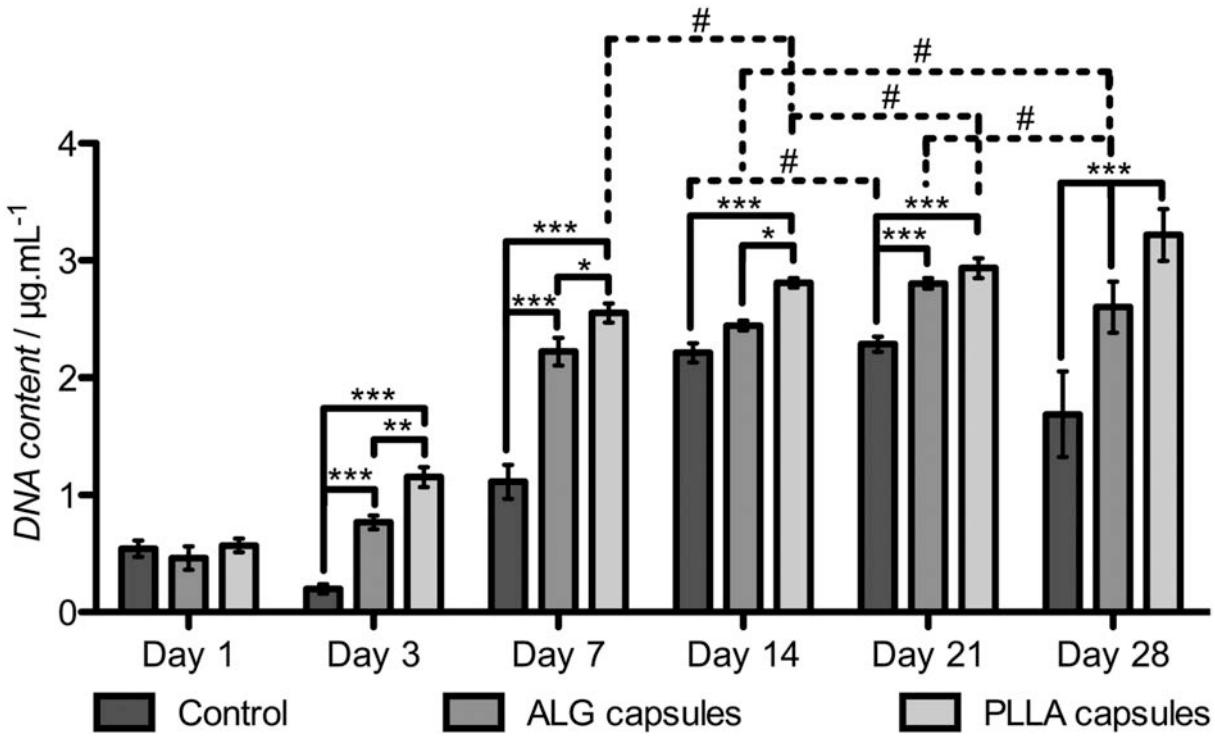

Figure IV.8 - DNA quantification assay at 1, 3, 7, 14, 21 or 28 days of culture. Alginate particles (control) and capsules with (PLLA capsules) or without (ALG capsules) PLLA microparticles were tested. Statistical differences in grouped by timepoint analysis are marked with (*), (**) and (***), which stands for $p<0.05$, $p<0.01$ and $p<0.001$, respectively. Statistical differences in grouped by formulation analysis were found for all formulations unless otherwise marked with # character.

4. Discussion

Results from the current study investigated the biological outcome when anchorage-dependent cells are encapsulated with PLLA microparticles. Microparticles and cells were both confined inside liquified capsules built by multilayers of PLL, ALG and CHT. The contribution of PLL in the mechanical strengthening of the capsules membrane was also evaluated.

PLLA microparticles featured an appropriate diameter in the micro-scale range to be used as cell microcarriers (**Figure IV.1b-d**). In order to improve cell adhesion, the smooth surface of PLLA microparticles (**Figure IV.1b**) was treated by plasma. Plasma technique is a very simple and well-known technique applied to modify biomaterials surface, including PLLA [33]. As showed in **Figure IV.1c**, the plasma treatment clearly enhanced the surface roughness of microparticles. Moreover, modified microparticles are able to

offer the great advantage of providing a large surface area for cellular adhesion and growth compared to traditional 2D cell culture systems or empty capsules. In order to create a system in which the developed microparticles together with cells would be entrapped, a multilayered membrane was developed by LbL assembly. The interaction of three different polymers was tested by QCM-D. The experimental pH range of 7 for PLL and ALG and 6.4 for CHT polyelectrolytes were set. At pH 7 both PLL and the carboxylate groups of alginate remain deprotonated due to the dissociation constants (pKa) of ~10 for PLL and 3.38 for mannuronic (M) and 3.65 for guluronic (G) acid alginate monomers [16, 34]. The protonation of amine groups on chitosan glucosamine monomers is kept at pH 6.4 since the pKa of chitosan is ~6.5 [35, 36] enabling chitosan to interact with the anionic components. Therefore, the working pH range allowed the interaction of oppositely charged polyelectrolytes, as showed by the continuous frequency decrease in QCM-D analysis (**Figure IV.2a**). Moreover, cell viability is not compromised (**Figures IV.5** and **IV.6**) because the working pH range is slightly bellow physiological conditions. The swelling is also more controlled at this pH range, not compromising the LbL membrane build-up, since capsules containing polymers with amino groups swell at alkaline pH [37]. Consequently, up to the later culture time of 28 days, the membrane of capsules remained stable in culture medium at 37ºC. The incorporation of PLL led to a higher frequency decrease compared to the CHT-ALG profile. Additionally, PLL incorporation also led to an exponential regime growth and to a thicker film (**Figure IV.2b**) compared to the typical linear regime growth of the two-component CHT-ALG LbL system (**Figure IV.2c**). Therefore, in this particular case, the presence or absence of PLL modulated the growth type of build-up process. Accordingly to the explanation of exponential growth regimes in literature [38, 39], PLL polyelectrolyte diffuses “in” and “out” of the film during build-up. Thus, in the presence of the ALG solution, PLL diffuses out of the film to form PLL/polyanion complexes at the outer layer. The thickness of the new forming layer on the surface of the film is then proportional to the amount of PLL

chains that diffuse out of the multilayer to interact with ALG. The film thickness obtained after 12 deposition layers is within the typical hundreds of nanometers reported for exponential multilayer films growth.[38] The exponential growth contribution of PLL was already been reported, for example when combined with hyaluronic acid [38–40] or poly(L-glutamic acid) [38, 41]. In the absence of PLL, a linear growth was observed (**Figure IV.2c**). CHT and ALG polyelectrolytes interaction was restricted to the outer layer of the film, which is a characteristic behavior of a linear growth. The increase in dissipation variation during both films build-up reveals that the films are viscoelastic and, thus, not rigid [22]. This represents a great advantage since viscoelasticity gives capsules a certain jamming resistance. Moreover, the liquified core of capsules (**Video IV.1**) also allows capsules to adapt to structures with variable shapes, such as syringes (**Video IV.2**). This ability is of huge interest for encapsulation systems since it offers capsules the ability of being implanted by minimal invasive methods in transplantation procedures. The injectability of the liquified capsules is also assured because the size of the stiff PLLA microparticles is almost two orders of magnitude lower than the size of the flexible capsules.

The capsules coated with the three macromolecular components showed an improved mechanical stability (**Figure IV.3**). This result can be correlated to the thickness increase in PLL-ALG-CHT film. The strength of the obtained capsules permits its manipulation and expected implantation without compromising their mechanical integrity.

The biological performance of the PLL-ALG-CHT membrane capsules was evaluated. Here, the contribution of adding surface modified PLLA microparticles to the liquified environment of capsules was assessed. Despite the advantages of PLLA, such as nontoxicity, easy processing and biodegradability, its surface is hydrophobic, has low surface energy and lacks of natural recognition sites for cells, thus compromising cell adhesion [42, 43]. Therefore, PLLA microparticles were surface modified by combining plasma treatment with collagen, which as a natural biomacromolecule possesses

domains that are recognized as ligands that can specifically bind to integrin. **Figure IV.4** evidences the interaction of surface modified microparticles with encapsulated cells. Cells adhered and spread across the modified surface of microparticles, evidencing their fibroblast-like elongated morphology.

Up to 7 days of culture, encapsulated cells had a continuous increase in the metabolic activity for all formulations (**Figure IV.5**). Specifically, PLLA capsules at day 7 had the highest cell viability, since cells were more metabolically active compared to control and ALG capsules. In concordance, despite of all formulations presented a good amount of well spread living cells (green spots in **Figure IV.6**), PLLA capsules had much less dead cells (red spots in figure 6) compared to control and ALG capsules. Especially from day 14, more dead cells were detected in control and ALG capsules. This may be due to the fact that L929 cells are anchorage dependent and, thus, the cell adhesion sites provided by PLLA microparticles increased the surface area for cell growth. Consequently, PLLA capsules presented an enhanced metabolic activity and cell viability. Moreover, the good viability of capsules suggested by MTS and live-dead data are a indicator factor that the membrane allowed the diffusion of nutrients and exchange of waste products for a prolonged time period.

DAPI-phalloidin assay showed that cells adhered to PLLA microparticles surface treated with collagen I. Interestingly, cells started to form large aggregates with PLLA microparticles constructing their own 3D cell culture assembly system. This cell behavior was already observed in spherical particles for injectable systems [44]. Ultimately, cell proliferation was improved with the presence of PLLA microparticles (**Figure IV.8**). PLLA capsules had the highest cell proliferation during culture time, which had a continuous increase up to 28 days of culture. On the other hand, at 28 days ALG capsules proliferation did not increase and a significant decrease in control particles was observed. Besides the lack of adhesion sites, these results may also corroborate the jeopardized diffusion rate offered by the crosslinked core of control particles.

5. Conclusion

Multilayered liquified capsules of poly(L-lysine), alginate and chitosan for cell encapsulation were successfully obtained using the layer-by-layer technique. The incorporation of PLL led to an exponential regime growth of the polymeric film and improved the mechanical stability of capsules. Capsules containing PLLA microparticles resulted in the highest cell metabolic activity and proliferation. We believe that the knowledge generated by this research will have a strong impact and open new prospects in many areas, including cell encapsulation. The most characteristic and promising feature of the proposed multilayered capsules is the ability to tailor different properties in one structure and to create novel multifunctional materials in accordance with the target application field.

Acknowledgements

The present work was financial supported by the Portuguese Foundation for Science and Technology (FCT) through the PhD grant with the reference number SFRH/BD/69529/2010, co-financed by the Operational Human Potential Program (POPH) developed under the scope of the National Strategic Reference Framework (QREN) from the European Social Fund (FSE). The authors also acknowledge the financial support from the MP-2008-Small-2 project (Find&Bind) developed under the scope of the EU 7th Framework Programme.

Supplementary information

Videos of the release of the liquified alginate core encapsulating PLLA microparticles (**Video IV.1**) and capsules being aspirated by a syringe (**Video IV.2**) are available at the ACS Publications website http://pubs.acs.org (DOI: 10.1021/bm301833z).

References

[1] S. Efrat, Beta-cell replacement for insulin-dependent diabetes mellitus, Adv. Drug Delivery Rev., 60 (2008) 114-123.

[2] J. Kim, D.R. Arifin, N. Muja, T. Kim, A.A. Gilad, H. Kim, A. Arepalley, T. Hyeon, J.W.M. Bulte, Multifunctional capsule-in-capsules for immunoprotection and trimodal imaging, Angew. Chem., 50 (2011) 2317-2321.

[3] M. Tang, W. Chen, M.D. Weir, W. Thein-Han, H.H.K Xu, Human embryonic stem cell encapsulation in alginate microbeads in macroporous calcium phosphate cement for bone tissue engineering, Acta Biomater., 8 (2012) 3436-3445.

[4] R. Jin, L.S. Moreira-Teixeira, P.J. Dijkstra, M. Karperien, C.A. van Blitterswijk, Z.Y. Zhong, J. Feijen, Injectable chitosan-based hydrogels for cartilage tissue engineering, Biomaterials, 30 (2009) 2544-2551.

[5] P. Cirone, J.M. Bourgeois, R.C. Austin, P.L. Chang, A novel approach to tumor suppression with microencapsulated recombinant cells, Hum. Gene Ther., 13 (2002) 1157-1166.

[6] R.M. Hernández, G. Orive, A. Murua, J.L. Pedraz, Microcapsules and microcarriers for in situ cell delivery, Adv. Drug Delivery Rev., 62 (2010) 711-730.

[7] W.H. Tan, S. Takeuchi, Monodisperse alginate hydrogel microbeads for cell encapsulation, Adv. Mater., 19 (2007) 2696-2701.

[8] A.K.A.S Brun-Graeppi, C. Richard, M. Bessodes, D. Scherman, O.-W.J. Merten, Cell microcarriers and microcapsules of stimuli-responsive polymers, J. Control. Release, 149 (2011) 209-224.

[9] R.K. Iler, Multilayers of colloidal particles, Colloid Interf. Sci., 21 (1966) 569-594.

[10] G. Decher, J.-D. Hong, Buildup of ultrathin multilayer films by a self-assembly process, 1 consecutive adsorption of anionic and cationic bipolar amphiphiles on charged surfaces, Makromol. Chem. Macromol. Symp., 46 (1991) 321-327.

[11] G.B. Sukhorukov, H. Möhwald, Multifunctional cargo systems for biotechnology, Trends Biotechnol., 25 (2007) 93-98.
[12] B.C. Dash, G. Réthoré, M. Monaghan, K. Fitzgerald, W. Gallagher, A. Pandit, The influence of size and charge of chitosan/polyglutamic acid hollow spheres on cellular internalization, viability and blood compatibility, Biomaterials, 31 (2010) 8188-8197.
[13] A. Szarpak, D. Cui, F. Dubreuil, B.G. de Geest, L.J. de Cock, C. Picart, R. Auzély-Velty, Designing hyaluronic acid-based layer-by-layer capsules as a carrier for intracellular drug delivery, Biomacromolecules, 11 (2010) 713-720.
[14] S. Ponce, G. Orive, R. Hernández, A.R. Gáscon, J.L. Pedraz, B.J. de Haan, M.M. Faas, H.J. Mathieu, P. de Vos, Chemistry and the biological response against immunoisolating alginate–polycation capsules of different composition, Biomaterials, 27 (2006) 4831-4839.
[15] C. Li, Z.-Y. Li, J. Zhang, K. Wang, Y.-H. Gong, G.F. Luo, R.-X. Zhuo, X.-Z. Zhang, Porphyrin containing light-responsive capsules for controlled drug release, J. Mater. Chem., 22 (2012) 4623-4626.
[16] A.J. Amali, N.H. Awwad, R.K. Rana, D. Patra, Nanoparticle assembled microcapsules for application as pH and ammonia sensor, Anal. Chim. Acta, 708 (2011) 75-83.
[17] C. Lin, W. Zhu, H. Yang, Q. An, C.-an Tao, W. Li, J. Cui, Z. Li, G. Li, Facile fabrication of stimuli-responsive polymer capsules with gated pores and tunable shell thickness and composite, Angew. Chem., 123 (2011) 5049-5053.
[18] W. Yuan, Z. Lu, C.M. Li, Controllably layer-by-layer self-assembled polyelectrolytes/nanoparticle blend hollow capsules and their unique properties, J. Mater. Chem., 21 (2011) 5148-5155.
[19] P.L. Chang, N. Shen, A.J. Westcott, Delivery of recombinant gene products with microencapsulated cells in vivo, Hum. Gene Ther., 4 (1993) 433-440.
[20] R.L. Broughton, M.V. Sefton, Effect of capsule permeability on growth of CHO cells in Eudragit EL microcapsules: Use of FITC-dextran as a marker of capsule quality, Biomaterials, 10 (1989) 462-465.

[21] W. Yuan, H. Dong, C.M. Li, X. Cui, L. Yu, Z. Lu, Q. Zhou, pH-controlled construction of chitosan/alginate multilayer film: Characterization and application for antibody immobilization, Langmuir, 23 (2007) 13046-13052.
[22] R.R. Costa, C.A. Custódio, F.J. Arias, J.C. Rodríguez-Cabello, J.F. Mano, Layer-by-layer assembly of chitosan and recombinant biopolymers into biomimetic coatings with multiple stimuli-responsive properties, Small, 7 (2011) 2640-2649.
[23] N.L. Costa, P. Sher, J.F. Mano, Liquefied capsules coated with multilayered polyelectrolyte films for cell immobilization, Adv. Biomater., 13 (2011) B218-B224.
[24] Q. Zhao, B. Han, Z. Wang, C. Gao, C. Peng, J. Shen, Hollow chitosan-alginate multilayer microcapsules as drug delivery vehicle: Doxorubicin loading and in vitro and in vivo studies, Nanomedicine, 3 (2007) 63-74.
[25] P. Sher, C.A. Custódio, J.F. Mano, Layer-by-layer technique for producing porous nanostructured 3d constructs using moldable freeform assembly of spherical templates, Small, 6 (2010) 2644-2648.
[26] E.S. Miranda, T.H. Silva, R.L. Reis, J.F. Mano, Nanostructured natural-based polyelectrolyte multilayers to agglomerate chitosan particles into scaffolds for tissue engineering, Tissue Eng. Part A, 17 (2011) 2663-2674.
[27] C. Porcel, P. Lavalle, V. Ball, G. Decher, B. Senger, J.-C. Voegel, P. Schaaf, From exponential to linear growth in polyelectrolyte multilayers, Langmuir, 22 (2006) 4376-4383.
[28] L. Jourdainne, Y. Arntz, B. Senger, C. Debry, J.-C. Voegel, P. Schaaf, P. Lavalle, Multiple strata of exponentially growing polyelectrolyte multilayer films, Macromolecules, 40 (2007) 316-321.
[29] F. Lim, A.M. Sun, Microencapsulated islets as bioartificial endocrine pancreas, Science, 210 (1980) 908-910.
[30] A.M. Rokstad, S. Holtan, B. Strand, B Steinkjer, L. Ryan, B. Kulseng, G. Skjåk-Bræk, T. Espevik, Microencapsulation of cells producing therapeutic proteins: Optimizing cell growth and secretion, Cell Transplant., 11 (2002) 313-324.

[31] T. Haque, H. Chen, W. Ouyang, C. Martoni, B. Lawuyi, A.M. Urbanska, S. Prakash, Superior cell delivery features of poly(ethylene glycol) incorporated alginate, chitosan, and poly-L-lysine microcapsules, Mol. Pharmaceutics, 2 (2004) 29-36.
[32] R. Bodmeier, J.W. McGinity, Solvent selection in the preparation of poly(DL-lactide) microspheres prepared by the solvent evaporation method, Int. J. Pharm., 43 (1988) 179-186.
[33] W. Song, D.D. Veiga, C.A. Custódio, J.F. Mano, Bioinspired degradable substrates with extreme wettability properties, Adv. Mater., 21 (2009) 1830-1834.
[34] F. Kurayama, S. Suzuki, T. Oyamada, T. Furusawa, M. Sato, N.J. Suzuki, Facile method for preparing organic/inorganic hybrid capsules using amino-functional silane coupling agent in aqueous media, Colloid Interface Sci., 349 (2010) 70-76.
[35] M. Jean, M. Alameh, D. De Jesus, M. Thibault, M. Lavertu, V. Darras, M. Nelea, M.D. Buschmann, A. Merzouki, Chitosan-based therapeutic nanoparticles for combination gene therapy and gene silencing of in vitro cell lines relevant to type 2 diabetes, Eur. J. Pharm. Sci., 45 (2012) 138-149.
[36] M.A. Pujana, L. Pérez-Álvarez, L.C.C. Iturbe, I. Katime, Water dispersible pH-responsive chitosan nanogels modified with biocompatible crosslinking-agents, Polymer, 53 (2012) 3107-3116.
[37] C. Déjugnat, G.B. Sukhorukov, pH-responsive properties of hollow polyelectrolyte microcapsules templated on various cores, Langmuir, 20 (2004) 7265-7269.
[38] P. Lavalle, C. Picart, J. Mutterer, C. Gergely, H. Reiss, J.-C. Voegel, B. Senger, P. Schaaf, Modeling the buildup of polyelectrolyte multilayer films having exponential growth, J. Phys. Chem. B, 108 (2004) 635-648.
[39] C. Picart, J. Mutterer, L. Richert, Y. Luo, G.D. Prestwich, P. Schaaf, J.-C. Voegel, P. Lavalle, Molecular basis for the explanation of the exponential growth of polyelectrolyte multilayers, Proc. Natl. Acad. Sci. U. S. A., 99 (2002) 12531-12535.

[40] C. Picart, Ph. Lavalle, P. Hubert, F.J.G. Cuisinier, G. Decher, P. Schaaf, J.-C. Voegel, Buildup mechanism for poly(L-lysine)/hyaluronic acid films onto a solid surface, Langmuir, 17 (2001) 7414-7424.

[41] Ph. Lavalle, C. Gergely, F.J.G. Cuisinier, G. Decher, P. Schaaf, J.-C. Voegel, C. Picart, Comparison of the structure of polyelectrolyte multilayer films exhibiting a linear and an exponential growth regime: An in situ atomic force microscopy study, Macromolecules, 35 (2002) 4458-4465.

[42] J. Yang, J. Bei, S. Wang, Enhanced cell affinity of poly (D,L-lactide) by combining plasma treatment with collagen anchorage, Biomaterials, 23 (2002) 2607-2614.

[43] Y. Hong, C. Gao, Y. Xie, Y. Gong, J Shen, Collagen-coated polylactide microspheres as chondrocyte microcarriers, Biomaterials, 26 (2005) 6305-6313.

[44] M.B. Oliveira, W. Song, L. Martín, S.M. Oliveira, S.G. Caridade, M. Alonso, J.C. Rodríguez-Cabello, J.F. Mano, Development of an injectable system based on elastin-like recombinamer particles for tissue engineering applications, Soft Matter, 7 (2011) 6426-6434.

Chapter V

A closed chondromimetic environment within magnetic-responsive liquified capsules encapsulating stem cells and collagen II/TGF-β3 microparticles[5]

Abstract

TGF-β3 is enzymatically immobilized by transglutaminase-2 action to poly(L-lactic acid) microparticles coated with collagen II. Microparticles are then encapsulated with stem cells inside liquified spherical compartments enfolded with a permselective shell through layer-by-layer adsorption. Magnetic-nanoparticles are electrostatically bounded to the multilayered shell, conferring magnetic-response ability. Our goal is to engineer a closed environment inside which encapsulated stem cells would undergo a self-regulated chondrogenesis. To test our hypothesis, capsules are cultured in chondrogenic differentiation medium without TGF-β3. Their biological outcome is compared with capsules encapsulating microparticles without TGF-β3 immobilization and cultured in normal chondrogenic differentiation medium containing soluble TGF-β3. Results show that similar chondrogenesis levels are achieved, as demonstrated by glycosaminoglycans quantification. Moreover, collagen fibrils resembling the native extracellular matrix of cartilage can be observed. Importantly, the genetic evaluation of characteristic cartilage markers confirms the successful chondrogenesis, while hypertrophic markers are downregulated. In summary, the engineered capsules are able to provide a suitable and stable chondrogenesis environment for stem cells without the need of TGF-β3 supplementation. This kind of self-regulated capsules with softness, robustness and magnetic responsive characteristics is expected to provide injectability and *in situ* fixation, which is of great advantage for minimal invasive strategies to regenerate cartilage.

[5] Based on the publication: C.R. Correia, S. Gil, R.L. Reis, J.F. Mano, A Closed chondromimetic environment within magnetic-responsive liquified capsules encapsulating stem cells and collagen II/TGF-β3 microparticles, Adv. Funct. Mater., DOI: 10.1002/adhm.201600034 (2016) (*in press)*

1. Introduction

A healthy adult cartilage tissue consists of a relatively sparse single population of non-proliferating chondrocytes embedded within an extracellular matrix (ECM). Because of its hypocellular structure and the lack of neural connections, vascularization, and a latent pool of stem cells [1, 2], cartilage has a very limited capacity of regeneration through endogenous healing. While in current clinical practice different techniques are being used with promising outcomes, they are generally not applicable for large cartilage defects or for degenerative joint diseases such as osteoarthritis. Meanwhile, numerous surgical cases have not yet proven to be successful for long-term applications [1]. In this regard, different cartilage tissue engineering (TE) strategies have emerged as alternative treatment methods of this uniquely challenging tissue. Integral to such approaches is the need for an abundant and easily accessible source of cells. The use of adult stem cells presents a viable alternative. Amongst the different multipotent sources, adipose stem cells (ASCs) has been shown to exhibit the potential for chondrogenesis [3] and they can be easily obtained from liposuction waste [4, 5]. Controlling the differentiation fate of stem cells represents a challenging task requiring a three-dimensional (3D) environment, which is commonly achieved by micromass culture [6, 7] or using scaffolds composed by natural and/or synthetic polymers [8-10], collagen sponges [11, 12], hydrogels [13-16], fiber meshes [17-20], and microparticles [21-23] combined with a finely tuned supply of growth factors (GFs). The most commonly used GF able to modulate the chondrocyte phenotype contains members of the TGF-β family, including TGF-β3 which has the highest and rapid chondrogenic potential among the different isoforms [24-26].

Herein, we propose an injectable cartilage TE strategy composed by different components orchestrated in a hierarchical manner to fulfill the different above-referred requirements. For that, ASCs were encapsulated with surface modified poly(L-lactic acid) (PLLA) microparticles within liquified capsules coated with magnetic nanoparticles (MNPs). The surface of PLLA microparticles was

coated with collagen II that was then enzymatically conjugated with TGF-β3 by the action of transglutaminase-2 (TG2). TG2 is a ubiquitously expressed member of an enzyme family catalyzing Ca^{2+} dependent transamidation of proteins via ε(γ-glutamyl)lysine bonds, being its ability to crosslink proteins, including collagen II, well described in the literature [11, 27, 28].

The engineered microparticles have two purposes, namely to provide a 3D culture environment to the stem cells, and also to provide immobilized TGF-β3. We envisage that the liquified environment of capsules would facilitate not only the diffusion of essential molecules for cell survival, but also allow the encapsulated cells to freely construct a hierarchical structure by the assembling of microparticles. As a *proof-of-concept*, we also conferred magnetic-response ability to the capsules by electrostatically bond to the multilayered membrane magnetic nanoparticles (MNPs).

The suitability for cell encapsulation of the liquified capsules containing solid microparticles was already successfully validated in our previous studies [29-31]. Here, it is the first time that we test its suitability for cartilage regeneration by including new features, such as the use of instructive microparticles and a magnetic-responsive shell through GFs and MNPs immobilization, respectively. **Scheme V.1** shows the schematic representation of the proposed liquified capsules.

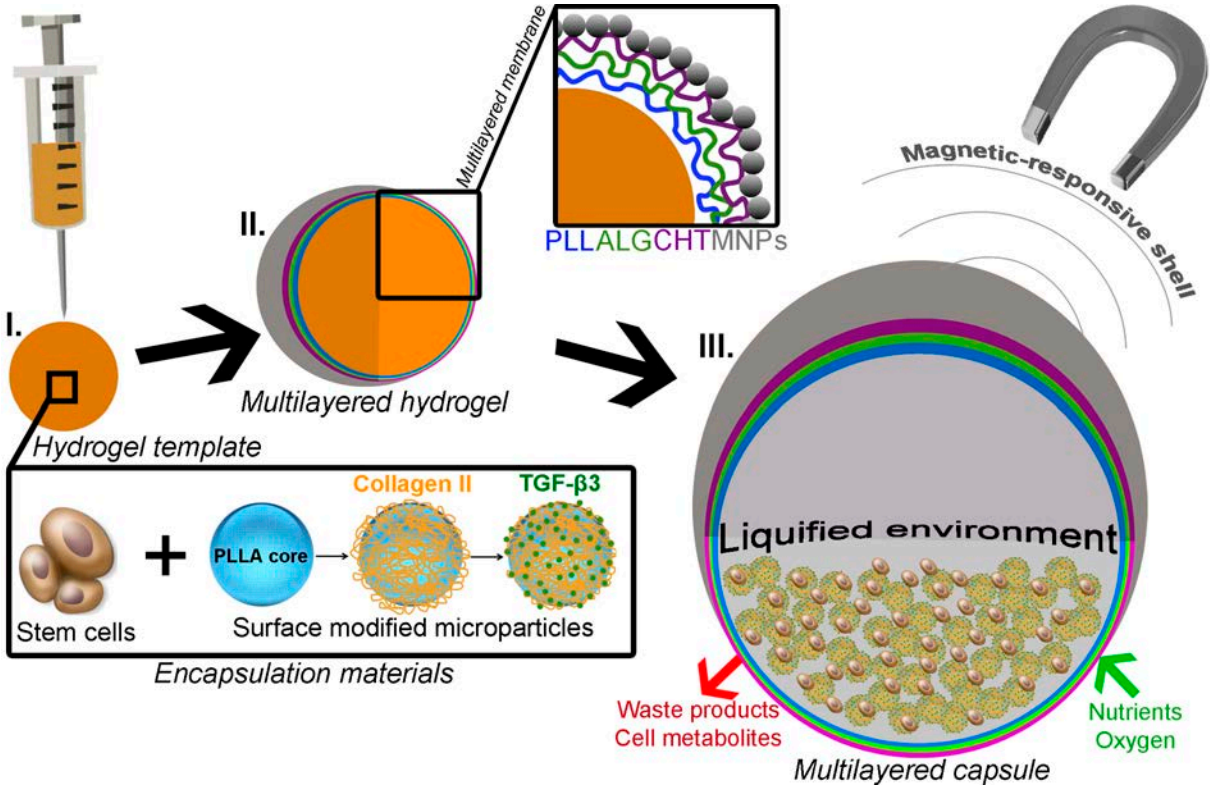

Scheme V.1. Representation of the proposed magnetic-responsive liquified capsules. **(I)** Alginate hydrogel particles encapsulating stem cells and surface modified poly(L-lactic acid) (PLLA) microparticles are obtained by dropwise into a calcium chloride bath. The surface of the PLLA microparticles is modified with collagen II and enzymatically crosslinked by the action of transglutaminase 2 to TGF-β3. **(II)** Alginate hydrogels are used as templates to produce a multilayered shell by sequential adsorption of poly(L-lysine) (PLL), alginate (ALG), and chitosan (CHT) (n = 11 layers). In the last layer, surface modified magnetic-nanoparticles (MNPs) are incorporated in the CHT solution to confer to the capsules magnetic-response ability. **(III)** The multilayered hydrogels are immersed in EDTA solution to liquefy the core, originating liquified capsules.

Our hypothesis is that an engineered chondromimetic environment would be developed in order to led encapsulated stem cells to differentiate into a stable chondrogenic lineage, i.e. avoiding de-differentiation, without requiring endogenous TGF-β3 supplementation. To test our hypothesis, two different capsules were produced, *(i)* capsules encapsulating PLLA microparticles coated with collagen II and TGF-β3 enzymatically crosslinked by TG2 (Coll-II/TGF-β3 capsules), and *(ii)* capsules encapsulating PLLA microparticles coated only with collagen II (Coll-II capsules). Coll-II/TGF-β3 capsules were cultured in chondrogenic differentiation medium without TGF-β3 supplementation ($CD^{-TGF-\beta3}$), while Coll-II capsules were cultured in normal

chondrogenic differentiation medium ($CD^{+TGF\text{-}\beta3}$). As control, both capsules were cultured in growth medium (GM).

2. Materials and methods

2.1 Synthesis and characterization of magnetic-nanoparticles

The production of the magnetite nanoparticles was based from our previously described protocol [32]. Briefly, Fe_3O_4 MNPs were synthesized by the co-precipitation reaction of ferrous ($FeCl_2.4H_2O$, Sigma-Aldrich) and ferric ($FeCl_3.6H_2O$, Sigma-Aldrich) salts in the presence of ammonium hydroxide (NH_4OH, Sigma-Aldrich) under a nitrogen atmosphere at 60°C. MNPs were washed with deionized water and ethanol for several times, and ultimately dried in a VD23 (Binder, Germany) vacuum oven. MNPs had a hydrodynamic size of 20.2 nm ± 0.8 and -37.9 mV ± 0.3 measured by zeta potential as described in our previous report [33].

2.2 Microparticles production and diameter measurements

PLLA microparticles were produced by oil/water (o/w) emulsion technique [29-31] and surface modified by combining plasma treatment with the coating and immobilization materials. Briefly, PLLA (5% w/v, 1.25 g/cm^3, 70% crystallinity, Polysciences) was dissolved in methylene chloride (CH_2Cl_2, Fisher Chemical) and added under agitation to polyvinyl alcohol (0.5% w/v, PVA, Sigma-Aldrich). The microparticles were subsequently collected, washed with distilled water, and lyophilized (Cryodos, Telstar). The microparticles obtained have a medium diameter of 45.5 µm ± 0.50 (n = 400 microparticles per batch, n = 3 batches) ranging from a maximum diameter of 85.3 µm ± 8.2 to a minimum of 15.1 µm ± 1.5. Diameter measurements were obtained using ImageJ software (version 1.44o, Wayne Rasband, USA).

2.3 Microparticles surface functionalization

Lyophilized microparticles were placed in a plasma reactor chamber (PlasmaPrep5, Gala Instrumente) fitted with a radio frequency generator. Air was used as the working atmosphere. A glow discharge plasma (0.2 mbar, 30 V) was created for 15 min. Microparticles were then sterilized for 2 h in ethanol (70% v/v) and immediately immersed in collagen II (170 µg per 50 mg of microparticles, rat protein tail, Gibco) overnight at 37°C under agitation. After washing with phosphate-buffered saline (PBS, Sigma-Aldrich), microparticles were immersed in a solution containing TGF-β3 (10 ng per 50 mg of microparticles, Peprotech) and TG2 (0.01 U per 50 mg of microparticles, guinea pig liver, Sigma-Aldrich) overnight at 4°C.

2.4 Collagen II quantification

The amount of collagen II coating the PLLA microparticles was quantified by Sircol Collagen assay (Biocolor) using manufacturer's specifications. Briefly, 50 mg of microparticles coated with collagen II (n = 5) were used. Before adding the Alkali reagent, the stained microparticles were visualized by optical microscopy. Then, absorbance was read at 555 nm.

2.5 Human TGF-β3 ELISA quantification

The amount of TGF-β3 in the supernatant coating solution was quantified by a commercially available human TGF-β3 ELISA kit (Omnikine, Tebu-Bio). Absorbance was read at 450 nm with correction wavelength set to 570 nm in a microplate reader (Gen 5 2.01, Synergy HT, Biotek). The amount of TGF-β3 coating the microparticles was calculated by subtracting the ELISA quantification results to the initial amount of the TGF-β3 solution (10 ng). Then, the microparticles immobilized with TGF-β3 were immersed in PBS for 7 days. This solution was also quantified by ELISA to assess the release of TGF-β3.

2.6 Immunofluorescence of TGF-β3

After surface functionalization, collagen II-TGF-β3 microparticles were immersed in PBS at 37ºC for 7 days. Samples were collected by centrifugation and subsequently immersed in bovine serum albumin (BSA, 3% w/v, Sigma-Aldrich) for 30 min at RT, and then incubated overnight at 4ºC with the primary antibody rabbit anti-human TGF-β3 (5 $\mu g.mL^{-1,}$ Abcam). After PBS washing, samples were incubated for 1 h at RT with the secondary antibody anti-rabbit AlexaFluor 488 (1:500, BD Biosciences). Samples were visualized by fluorescence microscopy (Axio Imager Z1m, Zeiss).

2.7 Isolation of adipose stem cells

Subcutaneous adipose tissue from liposuction procedures was used to isolate human ASCs as previously described [34]. The collected tissues were obtained under a cooperation agreement between the 3B's Research Group and Hospital da Prelada (Porto, Portugal), after approval of the respective ethical committees. The patient's informed consent and anonymity was assured. Samples were transported in PBS supplemented with penicillin-streptomycin (10%, pen-strep, Gibco) and kept at 4ºC. The lipoaspirates were washed with PBS and incubated with collagenase type II A (0.05% w/v, Sigma-Aldrich) for 45 min at 37ºC in a shaking water bath. The digested samples were filtered and centrifuged at 800 g for 10 min at 4ºC. The obtained stromal vascular fraction (SVF) was resuspended in erythrocyte lysis buffer at pH 7.4 containing ammonium chloride (155 mM, Merk), potassium bicarbonate (5.7 mM, Riedel-de-Häen), and ethylenediaminetetraacetic acid (0.1 M, EDTA, Sigma-Aldrich) in distilled water. After 10 min of incubation at room temperature (RT), the mixture was centrifuged at 300 g for 5 min. To isolate the ASCs the red blood cell-free SFV was resuspended in α-MEM medium (Invitrogen) supplemented with fetal bovine serum (10%, FBS, Invitrogen) and pen-strep (1:100, Gibco). Culture medium was changed 48 h after initial plating and then every 3-4 days until confluence.

2.8 Bioencapsulation set-up within magnetic-responsive multilayered capsules

At 90% confluence, ASCs (passage 2) grown in T150 tissue culture flasks were washed with PBS and subsequently detached using TrypLE™ Express solution (Life Technologies) at 37ºC for 5 min. PBS was added and the cell suspensions were centrifuged for 5 min at 300 g. Low viscosity sodium alginate from brown algae (1.5% w/v, ALG, ~250cP, Sigma-Aldrich) was dissolved in sodium chloride (0.15 M, NaCl, Enzymatic) containing MES hydrate (25 mM, Sigma-Aldrich) at pH 7. The solution was sterilized by 0.22 µm filtration. $5x10^6$ ASCs ($5x10^6$ cells per mL of alginate solution) were added to the surface functionalized PLLA microparticles with collagen II or with collagen II- TGF-β3 (50 mg microparticles per mL of alginate solution). Under agitation, the alginate solutions loaded with the microparticles and the stem cells, were added drop wise using a 21 G needle to a calcium chloride solution (0.1 M, $CaCl_2$, Merck) buffered with MES hydrate (25 mM, Sigma-Aldrich) at pH 7. After 20 min at RT, alginate hydrogel particles were collected and rinsed in a washing solution of NaCl (0.15 M, Sigma-Aldrich). The external membrane was processed by subsequent adsorption of oppositely charged polyelectrolytes by layer-by-layer deposition. Alginate hydrogel particles were first immersed in a poly(L-lysine) solution (PLL, Mw~30,000-70,000, pH 7, Sigma-Aldrich), and subsequently in ALG solution (pH 7), water-soluble highly purified chitosan solution (CHT, pH 6, Protasan UP CL 213, viscosity 107 mPa.s, $M_w = 2.7x10^5$ $g.mol^{-1}$, 83% degree of deacetylation, NovaMatrix) and, ultimately, in ALG solution again. The polyelectrolyte solutions (0.5 $mg.mL^{-1}$) were dissolved in NaCl (0.15 M, Sigma-Aldrich) containing MES hydrate (25 mM, Sigma-Aldrich). Following an adsorption of 10 min for each polyelectrolyte, the excess of macromolecules was removed by immersion in NaCl (0.15 M, Sigma-Aldrich) for 5 min. This process was repeated until an 11-layered membrane was built. In the last adsorption of chitosan, the solution was loaded with the MNPs (1 $mg.mL^{-1}$). The coated hydrogels were immersed in EDTA (20 mM, Sigma-Aldrich) at pH 7 for 5 min to liquefy the alginate core. Capsules with a

diameter of 1.5 mm ± 0.3 were obtained (measured by ImageJ software). The two formulations of liquified capsules obtained, namely CoII-II/TGF-β3 and CoII-II capsules were cultured in chondrogenic differentiation medium without ($CD^{-TGF-\beta3}$) or with ($CD^{+TGF-\beta3}$) TGF-β3 supplementation, respectively. The chondrogenic differentiation medium was prepared according to previously established culture conditions for ASCs chondrogenesis [3], namely DMEM-High glucose (Life Technologies), FBS (10% v/v, Invitrogen), pen/step (1:100, Gibco), ITS+premix (1:100, Life Sciences), MEM sodium pyruvate (1:100, Life Technologies), proline (0.4 mM, Sigma-Aldrich), dexamethasone (100 nM, Sigma-Aldrich), and TGF-β3 (10 $ng.mL^{-1}$, Peprotech). Additionally, capsules were also cultured in growth factor medium containing only DMEM-High glucose (Life Technologies), FBS (10% v/v, Invitrogen), and pen/step (1:100, Gibco). Capsules were transferred to non-adhesive 24-well plates and incubated at 37°C in a humidified 5% CO_2 air atmosphere.

2.9 MTS quantification

The viability of the encapsulated cells was assessed by mitochondrial metabolic activity quantification using a MTS colorimetric assay (CellTiter96® AQueous one solution cell proliferation assay, Promega) according to manufacture's specifications. Capsules (n = 4 per well in triplicate) were incubated with the reagent kit (1 mL per well) at 37°C protected from light. After 3 h, absorbance was read at 490 nm using a microplate reader (Gen 5 2.01, Synergy HT, Biotek).

2.10 DNA quantification

Total DNA quantification was performed after cell lysis (Quant-iT™ PicoGreen® dsDNA assay kit, Life Technologies). Samples (n = 4 per well in triplicate) were suspended in ultra-pure sterile water (1 mL per well). After 1 h in a 37°C shaking water bath, samples were frozen at -80°C overnight. Samples were defrosted and used according to the specifications of the kit. A standard curve for DNA analysis was generated with the provided dsDNA solution. After 10

min of incubation at RT, fluorescence was read at an excitation wavelength of 485/20 nm and 528/20 nm of emission using a microplate reader (Gen 5 2.01, Synergy HT, Biotek).

2.11 Glycosaminoglycans quantification

The quantification of sulfated glycosaminoglycans (GAGs) was performed by the dimethylmethylene blue (DMB) assay [3]. Briefly, a digestion buffer at pH 6.8 composed by phosphate buffer (200 nM, Na_2PO_4 and NaH_2PO_4, Sigma-Aldrich) and EDTA (1 mM, Sigma-Aldrich) was prepared. To the digestion buffer (50 mL), papain (25 mg, papaya latex solution, Sigma-Aldrich) and L-cysteine hydrochloride anhydrous (48 mg, Sigma-Aldrich) were added. The prepared papain solution was added to each well containing the capsules (1 mL, n = 4 capsules, in triplicate). Samples were incubated at 65°C for 18 h. To perform the DMB assay, a standard curve with chondroitin *4*-sulfate (chondroitin sulfate A sodium salt from bovine trachea, Sigma-Aldrich) was prepared. Additionally, the DMB dye (16 mg, Sigma-Aldrich) was dissolved in absolute ethanol (5 mL), and then NaCl (2.37 g, Sigma-Aldrich) and glycine (3.04 g, Sigma-Aldrich) dissolved in distilled water (900 mL) were added. The pH was set to 3 and distilled water was added to make up 1 L. Samples or chondroitin sulfate standards (20 µL) were mixed with the prepared DMB dye (250 µL, Sigma-Aldrich) in a transparent 96-well plate. Absorbance was read at 595 nm using a microplate reader (Gen 5 2.01, Synergy HT, Biotek). Total DNA quantification was used to normalize the DMB content.

2.12 Histological analysis

Capsules were collected and processed in an automatic ethanol-xylene spin tissue processor (STP120-2, Microm) for histological analysis. Afterwards, samples were embedded in paraffin and cut into sections of 5 µm thickness using a microtome (HM355S, Microm). Sections were subsequently deparaffinized, rehydrated, and automatically stained (HMS740, Microm) for safranin-O (0.1%, Sigma-Aldrich) and alcian blue (1%, Sigma-Aldrich)

stainings. Samples were then dehydrated and immersed in xylene, before being mounted (Entellan, Millipore). The stained sections were analyzed by inverted microscopy (Axio Imager Z1m, Zeiss). The presence of collagen II I the histological analysis was also assessed by an immunofluorescence assay. The antigen retrieval was performed in a heat-mediated sodium citrate buffer (10 mM, Sigma-Aldrich). Non-specific binding was blocked by immersion in hydrogen peroxide (3% v/v) followed by BSA (3% w/v), each for 30 min at RT. Samples were then incubated overnight at 4°C with the primary antibody rabbit anti-human collagen II (1:200 in 1% BSA, abcam). After PBS washing, samples were incubated for 1 h at RT with the secondary antibody anti-rabbit AlexaFluor 488 (1:500 in 1% BSA, Molecular Probes). Ultimately, samples were subsequently counterstained with DAPI (1 $mg.mL^{-1}$ diluted 1:1000 in PBS, Sigma-Aldrich) for 5 min at RT, immediately mounted (Permafluor, ThermoFisher Scientific), and analyzed in the dark by fluorescence microscopy (Axio Imager Z1m, Zeiss).

2.13 Scanning electron microscopy (SEM) with energy dispersive X-ray spectroscopy (EDS)

Capsules were washed with PBS and fixed at RT in formalin (10% v/v). After 1 h, samples were dehydrated in an increasing gradient series of ethanol for 10 min each. EDPS mapping (15kV, JSM-6010LV, Jeol) of iron was performed at the surface of the capsules to visualize the surface adhesion of the MNPs. Afterwards, the membrane of the capsules was destroyed to expose the core contents. Samples were gold sputtering and subsequently visualized by SEM (15 kV, JSM-6010LV, Jeol).

2.14 RNA extraction and cDNA production

Capsules (n = 5 per well, in triplicate) stored in TRIzol (800 µL, Sigma-Aldrich) at -80°C were slowly defrosted on ice and chloroform (160 µL, Fisher Chemical) was added. After 15 min at 4°C, samples were centrifuged at 13000 rpm (Bioline, MCF-2360) for 15 min. The aqueous part of each sample was

collected and isopropanol (400 µL, BDH Prolabo) was added. Following an overnight incubation at -20°C, samples were centrifuged at 13000 rpm for 10 min at 4°C. The resulting pellets were washed with ethanol (70% v/v) in RNase/DNase free distilled water (Lonza) and let to partially dry on air. Subsequently, the pellets were dissolved in RNase/DNase free distilled water (10 µL). RNA quantity and purity was determined in nanodrop spectrophotometer (NanoDrop ND-1000, ThermoScientific). Samples with a 260/280 purity ratio higher than ~1.8 were used for cDNA synthesis. The cDNA synthesis was performed using a qScript cDNA SuperMix kit (Quanta Biosciences) and the MiniOpticon Real-time PCR Detection System (MJ Mini, BioRad). All samples were normalized (1 µg of RNA in 20 µL of RNase/DNase free distilled water).

2.15 Quantitative real-time polymerase chain reaction

The expression of the target genes were quantified in the cDNA samples using a real-time polymerase chain reaction (PCR) reaction. The target genes were normalized with *18S rRNA* as the housekeeping. Th e primers (200nM) were designed to span exon-exon junctions using the primer-BLAST tool. The real-time PCR reaction was performed using the PerfeCTa SYBR Green FastMix Reaction Mixes (Quanta Biosciences), according to manufacturer's specifications. The reactions were monitored in a Mastercycler (Realplex4, Eppendorf) using the software realplex version 2.2 (Eppendorf). The $2^{-\Delta\Delta CT}$ method (Perkin-Elmer) was used to convert the normalized gene expression levels to fold differences. Results are expressed relatively to gene expression levels of ColI-II-PLLA capsules in chondrogenic medium at day 1. The primer sequences used in this analysis were: *18S*: 5'-GAAACCTTCCGACCCCTCTC-3', 5'-TACGAGGTCGATTTGGCGAG-3'; *COLLAGEN II*: 5'-CGGTGAGAAGGGAGAAGTTG-3', 5'-GACCGGTCACTCCAGTAGGA-3'; *AGGRECAN:* 5'-TGAGTCCTCAAGCCTCCTGT-3', 5'-TGGTCTGCAGCAGTTGATTC-3'; *SOX9:* 5'-TTCATGAAGATGACCGACGC-3', 5'-GTCCAGTCGTAGCCCTTGAG-3'; *COLLAGEN I:* 5'-AAGAACCCCAAGGACAAGAG-3', 5'-GTAGGTGATGTTCTGGGAGG-3';

COLLAGEN X: 5'-CAGGCATAAAAGGCCCACTA-3', 5'-AGGACTTCCGTAGCCTGGTT-3'.

2.16 Statistical analysis

Statistical analysis was performed using two-way analysis of variance (ANOVA) with Tukey's post-hoc test (GraphPad Prism 6.0) and multiple comparisons. A p-value <0.05 was considered statistically significant. All results are presented as mean ± standard deviation.

3. Results and discussion

3.1. Functionalization features of the liquified magnetic-responsive capsules

An overview of the proposed magnetic-responsive capsules is shown in **Figure V.1A** by light microscopy. The immobilization of the MNPs at the surface of the multilayered shell is evidenced in the histological cut of **Figure V.1B**. This allowed conferring magnetic-response properties to the capsules. By applying an external magnetic field, the movement of the capsules could be easily manipulated (**Figure V.1B.1**). Additionally, the movement of the capsules could be controlled to achieve aggregation or fixation at specific sites, as evidenced in **Video V.S1**. The membrane of the capsules was also analyzed by SEM (**Figure V.1B.2**), which revealed the morphology of MNPs. Due to the magnetite composition of the MNPs, their spatial dispersion could be also assessed by iron detection through EDS analysis (red dots in **Figure V.1B.3**). The presence of MNPs at the surface of the multilayered membrane indicates that they did not diffuse out, even after core liquefaction. This behavior is due to the electrostatic attraction between the negatively charged nanoparticles, and the positively charged chitosan polyelectrolyte solution used to construct the multilayered shell. The electrostatic attraction between chitosan and MNPs was studied by Wei *et al.* [35] by the production of microcapsules composed by crosslinked chitosan with embedded MNPs. Due to electrostatic attraction, it was observed that the MNPs could be kept stably inside the membrane even

after swelling in acidic conditions. By employing magnetic manipulation we envisage that capsules can aggregate and form moldable and complex macrostructures, in which each liquified capsules could work as compartmentalized building blocks. Capsules can be fixated *in situ*, and their motion can be controlled and guided into a specific spot. These features might be useful for the handling of the capsules during *in vitro* studies but also to guide and fixate the injectable capsules into a lesion site during implantation procedures. Additionally, due to the spherical shape of the capsules, and the flexibility of the shell combined with the liquified environment, we envisage that they can be implanted by injection. Importantly, besides movement control, the high surface area to volume ratio of MNPs provides abundant chemically active sites for functionalization and biomolecule conjugation, which may allow the implementation of other features. For example, it might allow incorporating anti-inflammatory drugs that might be useful during the healing process. In particular, Fe_3O_4 nanoparticles have received enormous interests and attracted the most attention due to its unique magnetic properties and biocompatibility. Therefore, capsules and MNPs have been combined in several biomedical applications, including targeted drug delivery, tissue engineering, magnetic thermotherapy (hyperthermia), magnetic resonance imaging, among others [36-38]. Previously, we immobilized rhodamine after a modification with a silane (APTES) at the surface of the proposed MNPs to monitor the cellular uptake and then further assemble cells in a sheet-like 3D structure [33]. Moreover, due to the multilayered shell, the encapsulated material is physically isolated from the surrounding environment. This can represent a great advantage for cartilage regeneration strategies since it can prevent not only the invasion of cells from the immune system, but also to customize the ability of the membrane to avoid the ingrowth of the vascular system, thus recapitulating the avascular environment of natural cartilage.

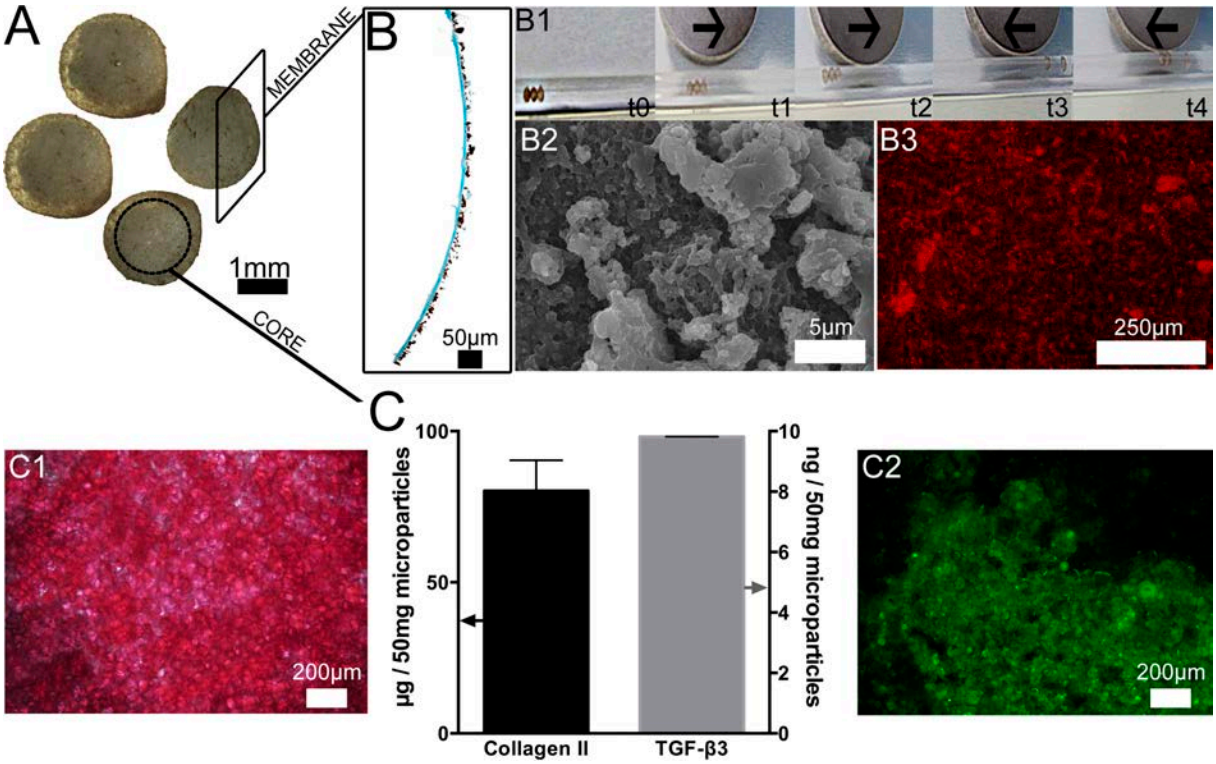

Figure V.1 - (A) Macroscopic visualization of magnetic-responsive liquified capsules encapsulating PLLA microparticles coated with collagen II and immobilized TGF-β3. **(B)** Membrane visualization with surface modified MNPs at the surface after histological cut of a liquified capsule. **(B1)** The magnetic-response ability of capsules is showed by manipulation of its movement in different directions (arrows) with the aid of an external magnet from t0-t3 (t stands for time). The presented images are print screens from **Video V.S1**. **(B2)** SEM visualization of MNPs and **(B3)** its dispersion by EDS iron mapping (red) at the surface of the multilayered membrane of capsules. **(C)** Quantification of collagen II (µg) by Sircol Collagen assay and TGF-β3 (ng) by ELISA assay of 50 mg of microparticles (n = 5). **(C1)** Collagen staining (red) at the surface of microparticles before Sircol quantification. **(C2)** Immunofluorescence of TGF-β3 (green) at the surface of microparticles after 7 days of immersion in PBS.

The functionalization of the encapsulated PLLA microparticles was performed by collagen II coating, a main component of cartilage, and TGF-β3 immobilization, a well-known chondrogenic differentiation factor. Combing plasma treatment with collagen coating allow to improve cell adhesion properties of the surface of PLLA microparticles, either by improving its roughness and by creating cell-material binding domains, as previously showed in our report with collagen I and L929 cells [30]. The amount of collagen II and TGF-β3 on the surface of 50 mg of microparticles was quantified by Sircol Collagen and ELISA assays, respectively (**Figure V.1C)**. For a quantification of

79.63 μg ± 9.71 of collagen II, the amount calculated per area is 1.5 μg/cm^2 ± 0.2, using the PLLA density (1.25 g/cm^3) and the area and volume equations of spheres with the medium diameter of 45.5 μm. As showed in **Figure V.1C.1** the collagen II coating stained in red was uniformly distributed at the surface of microparticles. The amount of TGF-β3 in the surface of microparticles was calculated after ELISA quantification of the supernatant solution. Similarly, for a quantification of 9.81 ng ± 0.01 the amount calculated per area is 0.2 ng/cm^2. Only a small amount remained in the supernatant solution, indicating that a large amount of the TGF-β3 present in the coating solution was used to coat the surface of the PLLA microparticles. Additionally, after 7 days of PBS immersion, the presence of TGF-β3 at the surface of the microparticles could be detected by green fluorescence (**Figure V.1C.2**), while no traces of TGF-β3 release in the PBS solution could be detected by ELISA assay (data not shown). This can be explained by the sustained release of TGF-β3, and thus the amount of protein released could be bellow the detection level of ELISA assay, or by an irreversibly crosslinking to the surface of the PLLA microparticles that avoids the protein release. Nevertheless, either sustained or avoided, it revealed a strong binding of TGF-β3 to the surface of microparticles that might be explained by the efficient enzymatic crosslinking reaction with TG2. *In vitro* studies demonstrated that a wide range of natural and synthetic biomaterials crosslinked by TG2 have improved stability by increasing strength and resistance to proteolytic digestion [39, 40]. Overall, TG2 contributes significantly to the organization of ECM by mediating cell-matrix interactions that affect cell spreading and migration [41, 42], and also has an interesting role in the activation of the latent form TGF-β in the ECM [43]. Some of the tasks of TG2 are accomplished through its unique ability to bind fibronectin, as firstly reported by Lorand *et al.* [44] and further generate ternary complexes with collagen [45], and integrins (β1 and β3) [46]. In articular cartilage, TG2 contributes to the control of cell differentiation and it is involved in the crosslinking of a number of cartilage components, such as fibronectin, collagen II, and osteopontin [27]. *In vitro* studies already showed that the TG2

crosslinking of collagen matrices with TGF-β3 promoted the chondrogenic differentiation of human bone marrow-derived mesenchymal stem cells [47]. Although providing soluble TGF-β3 in the culture medium has been widely used for stem cells chondrogenesis *in vitro* [3], this strategy is difficult to apply *in vivo* because of complexities involved in spatially controlling dosing locale, maintaining constant concentration over time and mitigating cost. Therefore, those systems require previous *in vitro* differentiation of stem cells before implantation. However, readily to use devices are much more attractive in TE applications. Therefore, we envisage that the immobilization of TGF-β3 in the microparticles surface will provide an appropriate 3D platform for chondrogenic differentiation, which could be proposed as a readily implantation device for cartilage regeneration.

3.2. Cell viability, proliferation and morphology, and glycosaminoglycans production

The viability of the encapsulated cells and their ability to proliferate and produce glycosaminoglycans within the liquified compartments were assessed up to 28 days post-encapsulation (**Figure V.2A**). Overall, MTS and DNA results increased with time, demonstrating that the process of generating capsules did not jeopardize the viability and proliferation of the encapsulated cells. Cells encapsulated in capsules cultured in chondrogenic differentiation medium have a significantly increase viability against growth medium. Of note, Coll-II/TGF-β3 capsules cultured in $CD^{-TGF-\beta3}$ reached a maximum value at 21 days, while Coll-II capsules cultured in $CD^{+TGF-\beta3}$ at 14 days. This difference can be explained by the different proliferation profiles as showed after DNA quantification. DNA quantification results demonstrate that the encapsulated cells were able to proliferate in both capsules. Analyzing the two proliferation profiles, it seemed that the proliferation ability of the Coll-II capsules cultured in $CD^{+TGF-\beta3}$ evolved in a more restrained fashion since the beginning of the experiment, with no significant differences between 14 and 21 days. On the other hand, this occurred later for the Coll-II/TGF-β3 capsules cultured in CD^{-}

$^{TGF\text{-}\beta3}$ in which no significant differences were found between 21 and 28 days. The two different proliferation profiles might be indicative of two different cell differentiation profiles, in which an earlier differentiation might be occurring in the CoII-II capsules. On the other hand, as observed in the viability results, capsules cultured in growth medium have a significant lower proliferation against chondrogenic medium.

To test the hypothesis of having two different cell differentiation profiles when providing TGF-β3 by two different pathways, glycosaminoglycans (GAGs) production, a key component of cartilage-specific matrix, was quantified. The results found for GAGs production corroborate the hypothesis formulated when analyzing the proliferation ability, namely the existence of two different cell differentiation profiles. While CoII-II/TGF-β3 capsules cultured in $CD^{-TGF\text{-}\beta3}$ show a more discreet increase in the GAGs production, in CoII-II capsules cultured in $CD^{+TGF\text{-}\beta3}$ a rapid increase in the beginning of the experiment was observed. Nevertheless, after 28 days of culture both formulations of capsules produced similar amounts of GAGs. Therefore, an important finding to highlight is that not only the immobilization of TGF-β3 was sufficient to stimulate the encapsulated stem cells to differentiate into the chondrogenic lineage in chondrogenic medium without TGF-β3 supplementation, but also that it lead to similar levels of GAGs production compared to the CoII-II capsules with exogenous TGF-β3 supplementation. Importantly, CoII-II/TGF-β3 capsules cultured in GM revealed production levels of GAGs significantly higher at day 28 compared to CoII-II capsules in the same medium. Therefore, although significantly lower compared to capsules in chondrogenic medium, the immobilization of TGF-β3 when using GM contributed to a higher GAGs production compared to CoII-II capsules cultured in the same medium. Importantly, this demonstrates that the immobilized TGF-β3 on the surface of microparticles is influencing the production of GAGs, thus demonstrating its bioactivity. The significantly lower GAGs production in CoII-II/TGF-β3 cultured in GM compared to the same capsules cultured in $CD^{+TGF\text{-}\beta3}$ or to CoII-II capsules in $CD^{-TGF\text{-}\beta3}$ might be increased with increasing the immobilization of

TGF-β3. As quantified by ELISA (**Figure V.1C**), since almost all of TGF-β3 was used to coat the microparticles, with increasing concentrations of TGF solution a higher amount of protein might be immobilized. In future developments, we intend to test different concentrations of TGF-β3 to immobilize at the surface of microparticles and study its influence on chondrogenesis of stem cells.

The ECM deposited by the encapsulated cells inside ColI-II/TGF-β3 capsules cultured in $CD^{-TGF-\beta3}$ or ColI-II capsules in $CD^{+TGF-\beta3}$ was analyzed by SEM (**Figure V.2B**). At day 7 of post-encapsulation, collagen fibrils characteristic from a cartilage-like ECM could be seen in the core of both capsules. In natural cartilage, the collagen fibrils are located throughout the matrix and are intertwined with highly concentrated negatively charged proteoglycan matrix [3]. Moreover, several aggregates could be found inside liquified capsules, as showed in the 150x magnification images at day 28. Besides the influence of growth factors, the three-dimensional (3D) environment is also an essential component in the chondrogenesis ability [48]. The use of a pellet culture mimics the development of cartilage during limb formation and is therefore often used as a method for understanding how the interaction of cells, growth factors and environmental factors promotes a chondrogenic phenotype [49]. The co-encapsulation of stem cells with microparticles within a liquified environment allowed cells to differentiate and freely construct their own 3D physical support, giving rise to micro aggregates. In capsules cultured in GM, the formation of collagen fibrils could not be visualized (**Figure V.SI**) neither the formation of large aggregates. However, in ColI-II capsules a dense ECM deposition covering the microparticles could be visualized, with encapsulated cells presenting a highly stretched morphology. If chondrogenesis might be occurring on those capsules, this could be indicative of a more hypertrophic chondrogenic differentiation pathway.

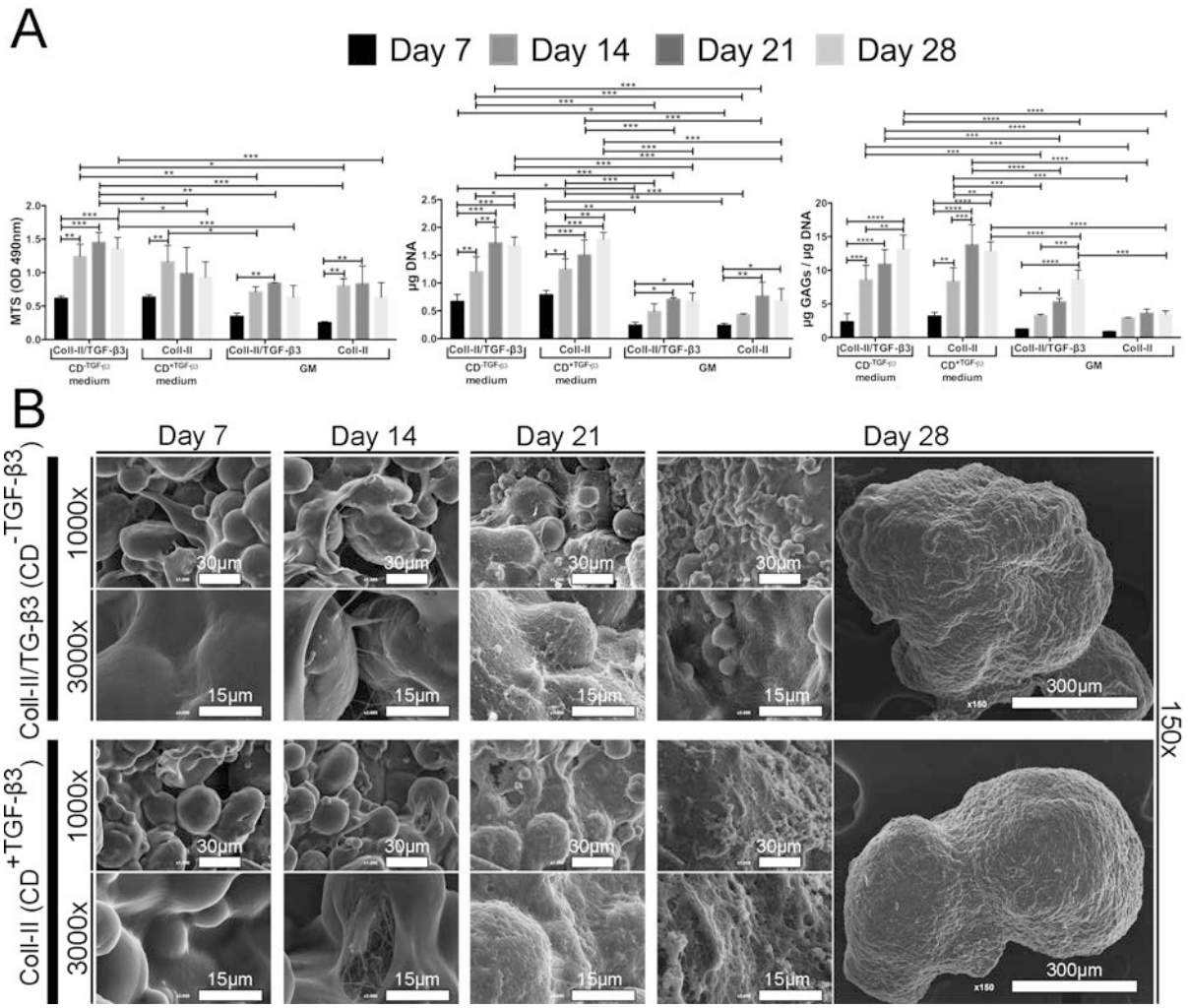

Figure V.2 – (A) MTS, DNA and GAGs quantification of ColI-II/TGF-β3 capsules cultured in chondrogenic differentiation medium without TGF-β3 supplementation ($CD^{-TGF-\beta3}$) and ColI-II capsules cultured in chondrogenic differentiation medium with TGF-β3 supplementation ($CD^{+TGF-\beta3}$) up to 28 days. ColI-II/TGF-β3 and ColI-II capsules cultured in growth medium (GM) were also analyzed. GAGs results were normalized by total DNA. Significant differences were marked with *($p < 0.05$), **($p < 0.01$), ***($p < 0.001$) and ****($p < 0.0001$) ($n = 3$ with 4 capsules per well). **(B)** SEM images of the core of ColI-II/TGF-β3 and ColI-II capsules cultured in $CD^{-TGF-\beta3}$ or CD $CD^{+TGF-\beta3}$, respectively, revealing the presence of collagen fibrils in the extracellular matrix. Magnifications of 3000x and 1000x are showed. Magnifications of 150x show an overview of the aggregates formed inside liquified capsules.

3.3 Histological analysis of the cartilage-like extracellular matrix

The histological evaluation, presented in **Figure V.3**, corroborated the findings of a cartilage-like ECM found inside ColI-II/TGF-β3 cultured in $CD^{-TGF-\beta3}$ and ColI-II capsules in $CD^{+TGF-\beta3}$. With increasing cell culture time, the staining of glycosaminoglycans (in red by safranin-O staining) and proteoglycans (in blue

by alcian blue staining) become more intense. At day 28, an ECM fully rich in glycosaminoglycans and proteoglycans was found. As already observed by SEM (**Figure V.2B**), in which micro aggregates composed by cells and microparticles were visualized, in the rich ECM of the aggregates the blank dots correspond to the space previously occupied by the microparticles. Moreover, the ECM of the capsules was positive for the chondrogenic marker collagen II (in green by immunofluorescence staining). On the other hand, as expected by the above-discussed results, capsules in GM had a lower staining intensity of GAGs (**Figure V.SI**). However, in ColI-II/TGF-β3 in GM higher GAGs content could be visualized compared to ColI-II capsules in the same medium.

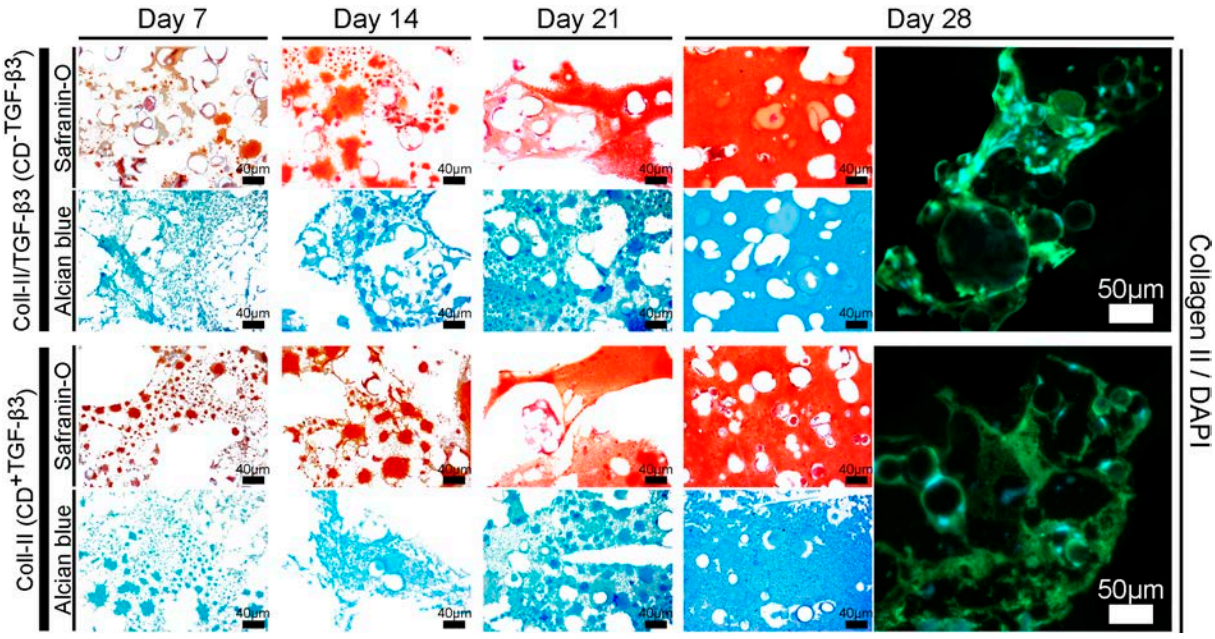

Figure V.3 - Histology analysis of ColI-II/TGF-β3 and ColI-II capsules cultured in chondrogenic differentiation medium without ($CD^{-TGF-\beta3}$) or with ($CD^{+TGF-\beta3}$) TGF-β3 supplementation, respectively. The presence of sulfated glycosaminoglycans is evidenced in red and blue by safranin-O and alcian blue stainings, respectively. At day 28, the presence of collagen II (green) in extracellular matrix is visualized counterstained with DAPI (blue) by immunocytochemistry.

3.4 Genetic quantification of chondrogenic markers

Gene expression levels of selected chondrogenic and hypertrophic markers after 28 days of culture are shown in **Figure V.4**. Results show that the expressions of *COLLAGEN II*, *AGGRECAN*, and *SOX9* in the ColI-II/TGF-β3

capsules were similar to ColI-II capsules when comparing both formulations within each medium, namely chondrogenic differentiation (-TGF-β3 or +TGF-β3) or growth media. Therefore, the immobilization of TGF-β3 in the microparticles was efficient in upregulating the chondrogenic markers to similar levels compared to the standard condition, i.e. the supplementation of TGF-β3 in the culture medium. Knowing that in the native ECM of cartilage, collagen II is the primary protein and aggrecan the main proteoglycan found, and that *SOX9* encodes a potent chondrogenic transcription factor closely correlated with collagen II transcription [50], it can be stated that a successful chondrogenic differentiation within ColI-II/TGF-β3 capsules in the absent of exogenous TGF-β3 was achieved. TGF-β3 has been proposed as the initial differentiation stimulus of stem cells towards the chondrogenic lineage [51]. After achieving the chondrogenic differentiation inside the ColI-II/TGF-β3 capsules, our main concern was the maintenance of the phenotype to avoid the characteristic drawback of dedifferentiation. In fact, the most challenging achievement when aiming chondrogenesis is not the differentiation pathway but rather the maintenance of the phenotype. Commonly, these cells shift the synthesis of collagen II to I, a characteristic marker of a fibroblastic cartilage [4]. In an attempt to avoid hypertrophic differentiation along the chondrogenesis of stem cells different strategies have been successfully proposed. Kim *et al.* [52] showed that a brief exposure of only 1 week of MSC cultures to high levels (100 $ng.mL^{-1}$) of TGF-β3 was capable of inducing and maintaining stem cells chondrogenesis. Dahlin *et al.* [17] co-cultured stem cells and chondrocytes in chondrogenic differentiation medium for two weeks, and showed their phenotype stability after the removal of TGF-β3 for an additional culture time of two weeks. Others suggested that hypoxia, like growth factors or hormones, may be a potential tool to control the hypertrophic differentiation of stem cells [53].

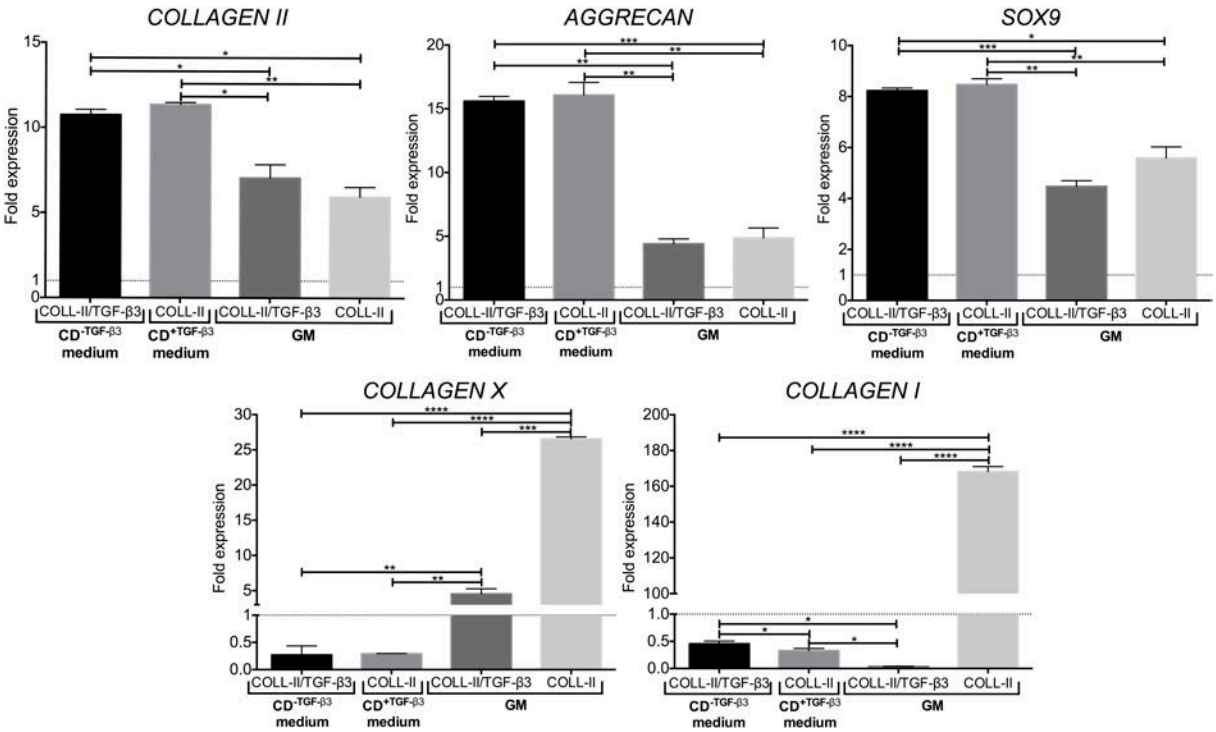

Figure V.4 – Gene expression in fold changes, first internally normalized to *18S* and then normalized to the expression of Coll-II capsules in normal chondrogenic medium at day 1, which was normalized to 1 (dotted line at y = 1). Chondrogenic (*COLLAGEN II*, *AGGRECAN,* and *SOX9)* and hypertrophic (*COLLAGEN X* and *COLLAGEN I*) markers are tested after 28 days post-encapsulation. Coll-II/TGF-β3 capsules cultured in chondrogenic differentiation medium without TGF-β3 supplementation ($CD^{-TGF-\beta3}$) or in growth medium (GM), and Coll-II capsules cultured in chondrogenic differentiation medium with TGF-β3 supplementation ($CD^{+TGF-\beta3}$) or in growth medium (GM) are analyzed. Significant differences were marked with *($p < 0.05$), **($p < 0.01$), ***($p < 0.001$) and ****($p < 0.0001$) (n = 3 with 4 capsules per well).

In our work, although at lower levels, the chondrogenic genes were also upregulated in the capsules cultured in growth medium. Knowing that ASCs highly express collagen I [3], it is relevant to monitor its expression. The collagen I transcripts reveal the degree to which fibrous tissue may develop. Additionally, collagen X, the hallmark of hypertrophic cartilage [54], is found in the transition from articular cartilage to bone. Analyzing the expression of *COLLAGEN I* and *X* in the capsules cultured in growth medium, they were upregulated in Coll-II capsules, while in Coll-II/TGF-β3 capsules only *COLLAGEN X* was upregulated. Considering the high expression level of *COLLAGEN X* in Coll-II/TGF-β3 capsules cultured in GM, we consider that the tissue formed within those capsules was toward an ossification pathway,

corroborating the SEM observations. Despite the upregulation of *COLLAGEN X*, the positive effect on ASCs chondrogenesis after the immobilization of TGF-β3 is again demonstrated when comparing the genetic profiles of both capsules in growth medium. Therefore, this particular result highlights not only the positive influence resulted from the immobilization of TGF-β3 in the surface of microparticles, by limiting to a certain extend the hypertrophic differentiation of chondrogenically-induced stem cells; but it also highlights the bioactivity of the immobilized TGF-β3. On the other hand, in Coll-II/TGF-β3 capsules cultured in chondrogenic medium without TGF-β3, both hypertrophic genes were downregulated. The same behavior was found for Coll-II capsules cultured in normal chondrogenic medium. Notably, the genetic profile analysis shows that the immobilization of TGF-β3 was not only able to differentiate the encapsulated stem cells but to maintain their chondrogenic phenotype of a hyaline cartilage. The *in vivo* delivery of effective concentrations of growth factors can be challenging as the *in vivo* environment can lead to rapid removal of the proteins from the lesion site, loss of bioactivity, or low availability as a result of the slow tissue diffusion of large proteins [55]. Hence, we believe that the results obtained in this work are of great importance for cartilage regeneration strategies. We trust that the proposed capsules with immobilized TGF-β3 might potentially allow for better success in regenerating the cartilage tissue.

4. Conclusion

The suitability for chondrogenic differentiation within magnetic-responsive liquified capsules co-encapsulating stem cells and surface modified PLLA microparticles was assessed. The results showed that, in the absence of TGF-β3 supplementation, the immobilization of TGF-β3 crosslinked by TG2 to collagen II was able to induce the chondrogenic differentiation and, importantly, the phenotype maintenance of the encapsulated stem cells. Notably, the chondrogenesis observed occurred in similar levels of those found for capsules cultured in normal chondrogenic differentiation medium, which

used higher amounts of TGF-β3. We demonstrated the feasibility of an engineered self-regulated chondromimetic device that represents an efficient easy-to-handle and injectable tool aiming cartilage regeneration. The use of such capsules can be further envisaged as a one-step clinically translatable protocol for cartilage repair, presenting many advantages over current treatments. In future works, we envisage to test different amounts of protein immobilization and assess its influence on achieving different chondrogenesis levels. We also propose to add more features to the chondromimetic device to fulfill all the required and challenging conditions for a successful total cartilage repair, as well as to assess the outcome of this promising encapsulation strategy *in vivo*.

Acknowledgements

The present work was financially supported by the Portuguese Foundation for Science and Technology (FCT) through the Ph.D. grant of Clara Correia (SFRH/BD/69529/2010), and by the project SUPRARELAX with reference number PTDC/FIS/115048/2009/FCOMP-01–0124- FEDER/015340.

Supplementary information

The video record of the magnetic-response capability of the multilayered and liquified capsules (**Video V.S1**) is available at the Wiley Online Library website http://pubs.acs.org (DOI: 10.1002/adhm.201600034).

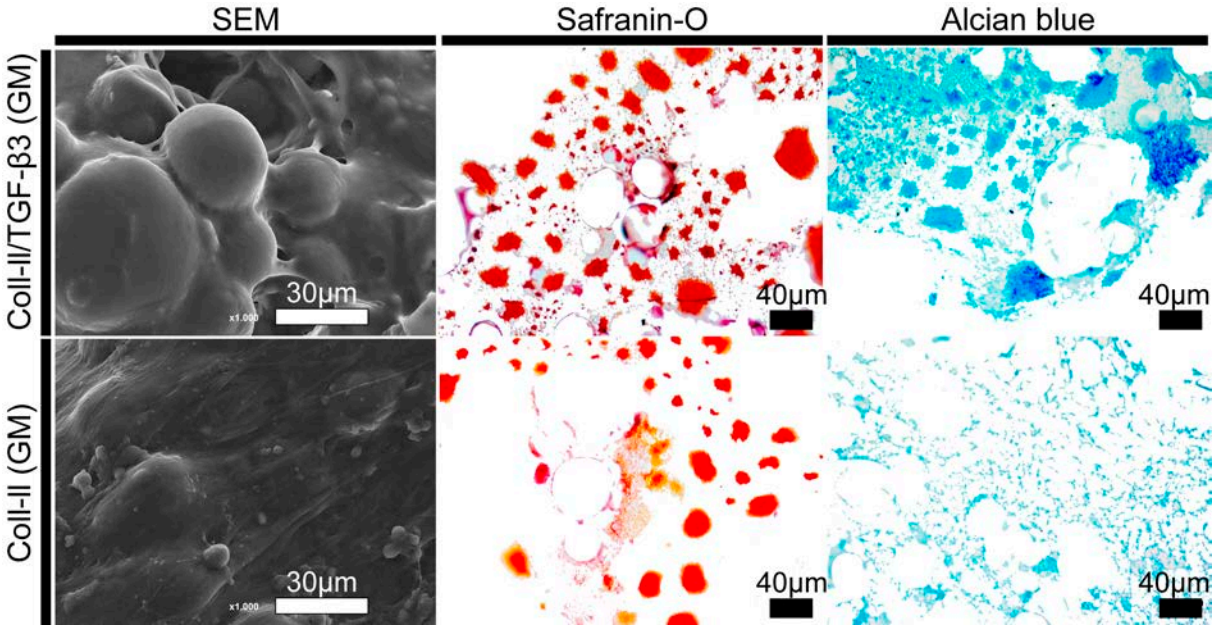

Figure V.SI - SEM images and histology analysis by safranin-O and alcian blue stainings of the core of ColI-II/TGF-β3 and ColI-II capsules cultured in growth medium (GM) for 28 days.

References

[1] H. Chiang, C.-C. Jiang, J. Formosan., Repair of articular cartilage defects: Review and perspectives, Med. Assoc., 108 (2009) 87-101.

[2] Z. Ge, C. Li, B. C. Heng, G. Cao, Z. Yang, Functional biomaterials for cartilage regeneration, J. Biomed. Mater. Res. Part A., 100 (2012) 2526-2536.

[3] B. T. Estes, B.O. Diekman, J. M. Gimble, F. Guilak, Isolation of adipose-derived stem cells and their induction to a chondrogenic phenotype, Nat. Protoc., 5 (2010) 1294-1311.

[4] L. Aust, B. Devlin, S. J. Foster, Y. D. C. Halvorsen, K. Hicok, T. du Laney, A. Sen, G. D. Willingmyre, J. M. Gimble, Yield of human adipose-derived adult stem cells from liposuction aspirates, Cytotherapy, 6 (2004) 7-14.

[5] J. M. Gimble, F. Guilak, Differentiation potential of adipose derived adult stem (ADAS), Cells Curr. Top. Dev. Biol., 58 (2003) 137-160.

[6] D. Fayol, G. Frasca, C. Le Visage, F. Gazeau, N. Luciani, C. Wilhelm, Use of magnetic forces to promote stem cell aggregation during differentiation, and cartilage tissue modeling, Adv. Mater., 25 (2013) 2611-2616.

[7] N. Georgi, C. A. van Blitterswijk, M. Karperien, Mesenchymal stromal/stem cell-or chondrocyte-seeded microcarriers as building blocks for cartilage tissue engineering, Tissue Eng. Part A, 20 (2014) 2513-2523.
[8] C. R. Correia, L. S. Moreira-Teixeira, L. Moroni, R. L. Reis, C. A. van Blitterswijk, M. Karperien, J. F. Mano, Chitosan scaffolds containing hyaluronic acid for cartilage tissue engineering, Tissue Eng. Part C, 17 (2011) 717-730.
[9] J. M. Silva, N. Georgi, R. Costa, P. Sher, R. L. Reis, C. A. van Blitterswijk, M. Karperien, J. F. Mano, Nanostructured 3D constructs based on chitosan and chondroitin sulphate multilayers for cartilage tissue engineering, PloS One, 8 (2013) e55451.
[10] S. Camarero-Espinosa, B. Rothen-Rutishauser, C. Weder, E. J. Foster, Directed cell growth in multi-zonal scaffolds for cartilage tissue engineering, Biomaterials, 74 (2016) 42-52.
[11] S. Shanmugasundaram, S. Logan-Mauney, K. Burgos, M. Nurminskaya, Tissue transglutaminase regulates chondrogenesis in mesenchymal stem cells on collagen type XI matrices, Amino Acids, 42 (2012) 1045-1053.
[12] Y. Zhua, Y. Wanb, J. Zhangc, D. Yinb, W. Cheng, Manufacture of layered collagen/chitosan-polycaprolactone scaffolds with biomimetic microarchitecture, Colloids Surf. B, 113 (2014) 352-360.
[13] K. Kim, J. Lam, S. Lu, P. P. Spicer, A. Lueckgen, Y. Tabata, M. E. Wong, J. A. Jansen, A. G. Mikos, F. K. Kasper, Osteochondral tissue regeneration using a bilayered composite hydrogel with modulating dual growth factor release kinetics in a rabbit model, J. Controlled Release, 168 (2013) 166-178.
[14] M. Endres, N. Wenda, H. Woehlecke, K. Neumann, J. Ringe, C. Erggelet, D. Lerche, C. Kaps, Microencapsulation and chondrogenic differentiation of human mesenchymal progenitor cells from subchondral bone marrow in Ca-alginate for cell injection, Acta Biomater., 6 (2010) 436-444.
[15] L. Bian, D. Y. Zhai, E. Tous, R. Rai, R. L. Mauck, J. A. Burdick, Enhanced MSC chondrogenesis following delivery of TGF-β3 from alginate microspheres within hyaluronic acid hydrogels in vitro and in vivo, Biomaterials, 32 (2011) 6425-6434.

[16] P. A. Parmar, L. W. Chow, J. P. St-Pierre, C. M. Horejs, Y. Y. Peng, J. A. Werkmeister, J. A. Ramshaw, M. M. Stevens, Collagen-mimetic peptide-modifiable hydrogels for articular cartilage regeneration Biomaterials, 54 (2015) 213-225.
[17] R. L. Dahlin, M. Ni, V. V. Meretoja, F. K. Kasper, A. G. Mikos, TGF-β3-induced chondrogenesis in co-cultures of chondrocytes and mesenchymal stem cells on biodegradable scaffolds, Biomaterials, 35 (2014) 123-132.
[18] R. Cai, T. Nakamoto, N. Kawazoe, G. Chen, Influence of stepwise chondrogenesis-mimicking 3D extracellular matrix on chondrogenic differentiation of mesenchymal stem cells, Biomaterials, 52 (2015) 199-207.
[19] X. Liu, X. Jin, P. X. Ma, Nanofibrous hollow microspheres self-assembled from star-shaped polymers as injectable cell carriers for knee repair, Nat. Mater., 10 (2011) 398-406.
[20] S. D. McCullen, H. Autefage, A. Callanan, E. Gentleman, M. M. Stevens, Anisotropic fibrous scaffolds for articular cartilage regeneration, Tissue Eng. Part A, 18 (2012) 2073-2083.
[21] J. Fang, Y. Zhang, S. Yan, Z. Liu, S. He, L. Cui, J. Yin, Poly(L-glutamic acid)/chitosan polyelectrolyte complex porous microspheres as cell microcarriers for cartilage regeneration, Acta Biomater., 10 (2014) 276-288.
[22] M. Morille, T. Van-Thanh, X. Garric, J. Cayon, J. Coudane, D. Noel, M. C. Venier-Julienne, C. N. Montero-Menei, New PLGA-P188-PLGA matrix enhances TGF-β3 release from pharmacologically active microcarriers and promotes chondrogenesis of mesenchymal stem cells, J. Controlled Release, 170 (2013) 99-110.
[23] S. Ansboro, J. S. Hayes, V. Barron, S. Browne, L. Howard, U. Greiser, P. Lalor, F. Shannon, F. P. Barry, A. Pandit, J. M. Murphy, A chondromimetic microsphere for in situ spatially controlled chondrogenic differentiation of human mesenchymal stem cells, J. Controlled Release., 179 (2014) 42-51.
[24] A. M. Freyria, F. Mallein-Gerin, Chondrocytes or adult stem cells for cartilage repair: The indisputable role of growth factors, Injury, 43 (2012) 259-265.

[25] B. E. Bobick, F. H. Chen, A. M. Le, R. S. Tuan, Regulation of the chondrogenic phenotype in culture, Birth Defects Res. Part C, 87 (2009) 351-371.
[26] F. Barry, R. E. Boynton, B. Liu, J. M. Murphy, Chondrogenic differentiation of mesenchymal stem cells from bone marrow: Differentiation-dependent gene expression of matrix components, Exp. Cell Res., 268 (2001) 189-200.
[27] L. Lorand, R. M. Graham, Transglutaminases: Crosslinking enzymes with pleiotropic functions, Nat. Rev. Mol. Cell Biol., 4 (2003) 140-156.
[28] M. E. Jones, P. B. Messersmith, Facile coupling of synthetic peptides and peptide-polymer conjugates to cartilage via transglutaminase enzyme, Biomaterials, 28 (2007) 5215-5224.
[29] C. R. Correia, P. Sher, R. L. Reis, J. F. Mano, Liquified chitosan–alginate multilayer capsules incorporating poly(L-lactic acid) microparticles as cell carriers, Soft Matter, 9 (2013) 2125-2130.
[30] C. R. Correia, R. L. Reis, J. F. Mano, Multilayered hierarchical capsules providing cell adhesion sites, Biomacromolecules, 14 (2013) 743-751.
[31] C. R. Correia, R. P. Pirraco, M. T. Cerqueira, A. P. Marques, R. L. Reis, J. F. Mano, Semipermeable capsules wrapping a multifunctional and self-regulated co-culture microenvironment for osteogenic differentiation, Sci. Rep., 6 (2016) 21883.
[32] S. Gil, E. Castro, J. F. Mano, Synthesis and characterization of stable dicarboxylic pegylated magnetite nanoparticles, Mater. Lett., 100 (2013) 266-270.
[33] S. Gil, C. R. Correia, J. F. Mano, Magnetically labeled cells with surface-modified Fe_3O_4 spherical and rod-shaped magnetic nanoparticles for tissue engineering applications, Adv. Healthcare Mater., 4 (2015) 883-891.
[34] P. A. Zuk, M. Zhu, P. Ashjian, D. A. D. Ugarte, J. I. Huang, H. Mizuno, Z. C. Alfonso, J. K. Fraser, P. Benhaim, M. H. Hedrick, Human adipose tissue is a source of multipotent stem cells, Mol. Biol. Cell., 13 (2002) 4279-95.

[35] J. Wei, X.-J. Ju, X.-Y. Zou, R. Xie, W. Wang, Y.-M. Liu, L.-Y. Chu, Multi-stimuli-responsive microcapsules for adjustable controlled-release, Adv. Funct. Mater., 24 (2014) 3312-3323.
[36] B. G. De Geest, N. N. Sanders, G. B. Sukhorukov, J. Demeester, S. C. De Smedt, Release mechanisms for polyelectrolyte capsules, Chem. Soc. Rev., 36 (2007) 636-649.
[37] R. Cheng, F. Meng, C. Deng, H. A. Klok, Z. Zhong, Dual and multi-stimuli responsive polymeric nanoparticles for programmed site-specific drug delivery, Biomaterials, 34 (2013) 3647-3657.
[38] S. Gil, J. M. Silva, J. F. Mano, Magnetically multilayer polysaccharide membranes for biomedical applications, ACS Biomater. Sci. Eng., 1 (2015) 1016-1025.
[39] D. Y. S. Chau, R. J. Collighan, E. A. M. Verderio, V. L. Addy, M. Griffin, The cellular response to transglutaminase-cross-linked collagen, Biomaterials, 26 (2005) 6518-6529.
[40] R. J. Collighan, M. Griffin, Transglutaminase 2 cross-linking of matrix proteins: Biological significance and medical applications, Amino Acids, 36 (2009) 659-670.
[41] C. A. Gaudry, E. Verderio, D. Aeschlimann, A. Cox, C. Smith, M. Griffin, Cell surface localization of tissue transglutaminase is dependent on a fibronectin-binding site in its N-terminal β-sandwich domain, J. Biol. Chem., 274 (1999) 30707-30714.
[42] S. S. Akimov, A. M. Belkin, Cell surface tissue transglutaminase is involved in adhesion and migration of monocytic cells on fibronectin, Blood, 98 (2001), 1567-1576.
[43] I. Nunes, P.-E. Gleizes, C. N. Metz, D. B. Rifkin, Latent transforming growth factor-β binding protein domains involved in activation and transglutaminase-dependent cross-linking of latent transforming growth factor-β, J. Cell Biol., 136 (1997) 1151-1163.

[44] L. Lorand, J. Dailey, P. Turner, Fibronectin as a carrier for the transglutaminase from human erythrocytes, Proc. Natl. Acad. Sci. U. S. A., 85 (1988) 1057-1059.
[45] P. Turner, L. Lorand, Complexation of fibronectin with tissue transglutaminase, Biochemistry, 28 (1989) 628-635.
[46] S. S. Akimova, D. Krylova, L. F. Fleischmana, A. M. Belkin, Tissue transglutaminase is an integrin-binding adhesion coreceptor for fibronectin, J. Cell Biol., 148 (2000) 825-838.
[47] C. Niger, K. E. Beazley, M. Nurminskaya, Induction of chondrogenic differentiation in mesenchymal stem cells by TGF-β cross-linked to collagen-PLLA [poly(L-lactic acid)] scaffold by transglutaminase 2, Biotechnol. Lett., 35 (2013) 2193-2199.
[48] L. Galois, S. Hutasse, D. Cortial, C. F. Rousseau, L. Grossin, M.-C. Ronziere, D. Herbage, A.-M. Freyria, Bovine chondrocyte behaviour in three-dimensional type I collagen gel in terms of gel contraction, proliferation and gene expression, Biomaterials, 27 (2006) 79-90.
[49] B. Diekman, C. Rowland, A. Caplan, D. Lennon, F. Guilak, Chondrogenesis of adult stem cells from adipose tissue and bone marrow: Induction by growth factors and cartilage derived matrix, Tissue Eng. Part A, 16 (2010) 523-533.
[50] V. Lefebvre, W. Huang, V. Harley, P. Goodfellow, B. De Crombrugghe, SOX9 is a potent activator of the chondrocyte-specific enhancer of the pro alpha1(II) collagen gene, Mol. Cell. Biol., 17 (1997) 2336-2346.
[51] A.T. Mehlhorn, P. Niemeyer, S. Kaiser, G. Finkenzeller, G.B. Stark, N.P. Südkamp, H. Schmal, Differential expression pattern of extracellular matrix molecules during chondrogenesis of mesenchymal stem cells from bone marrow and adipose tissue, Tissue Eng., 12 (2006) 2853.-2862
[52] M. Kim, I. E. Erickson, M. Choudhury, N. Pleshko, R. L. Mauck, Transient exposure to TGF-β3 improves the functional chondrogenesis of MSC-laden hyaluronic acid hydrogels, J. Mech. Behav. Biomed. Mater., 11 (2012) 92-101.
[53] C. Merceron, S. Portron, M. Masson, B. H. Fellah, O. Gauthier, J. Lesoeur, Y. Chérel, P. Weiss, J. Guicheux, C. Vinatier, Cartilage tissue engineering: From

hydrogel to mesenchymal stem cells, Bio-Med. Mater. Eng., 20 (2010) 159-166.
[54] Y. He, A. S. Siebuhr, N. U. Brandt-Hansen, J. Wang, D. Su, Q. Zheng, O. Simonsen, K. K. Petersen, L. Arendt-Nielsen, T. Eskehave, H. C. Hoeck, M. A. Karsdal, A. C. Bay-Jensen, Type X collagen levels are elevated in serum from human osteoarthritis patients and associated with biomarkers of cartilage degradation and inflammation, BMC Musculoskeletal Disord., 15 (2014) 309-319.
[55] F. M. Chen, M. Zhang, Z. F. Wu, Toward delivery of multiple growth factors in tissue engineering, Biomaterials, 31 (2010) 6279-6308.

Chapter VI

Semipermeable capsules wrapping a multifunctional and self-regulated co-culture microenvironment for osteogenic differentiation [6]

Abstract

A new concept of semipermeable reservoirs containing co-cultures of cells and supporting microparticles is presented, inspired by the multi-phenotypic cellular environment of bone. Based on the deconstruction of the "stem cell niche", the developed capsules are designed to drive a self-regulated osteogenesis. PLLA microparticles functionalized with collagen I, and a co-culture of adipose stem (ASCs) and endothelial (ECs) cells are immobilized in spherical liquified capsules. The capsules are coated with multilayers of poly(L-lysine), alginate, and chitosan nano-assembled through layer-by-layer. Capsules encapsulating ASCs alone or in a co-culture with ECs are cultured in endothelial medium with or without osteogenic differentiation factors. Results show that osteogenesis is enhanced by the co-encapsulation, which occurs even in the absence of differentiation factors. These findings are supported by an increased ALP activity and matrix mineralization, osteopontin detection, and the up regulation of *BMP-2, RUNX2* and *BSP*. The liquified co-capsules also act as a VEGF and BMP-2 cytokines release system. The proposed liquified capsules might be a valuable injectable self-regulated system for bone regeneration employing highly translational cell sources.

[6] Based on the publication: C.R. Correia, R.P. Pirraco, M.T. Cerqueira, A.P. Marques, R.L. Reis, J.F. Mano, Semipermeable capsules wrapping a multifunctional and self-regulated co-culture microenvironment for osteogenic differentiation, Sci. Rep., 6 (2016) 21883.

1. Introduction

The successful regeneration of bone remains a significant challenge in orthopedic research. Strong affords have been made as a potential alternative to the conventional use of bone grafts due to their limitless supply and no disease transmission. In particular, vascularization remains an obstacle to engineer large volume bone tissues. In order to face such challenges, new generations of devices for tissue engineering (TE) should improve the physical and biochemical cues operating in tandem during native regeneration, in particular at the scale/organizational-level of the stem cell niche. The understanding and the deconstruction of these factors (e.g. multiple cell types exchanging both paracrine and direct signals, structural and chemical arrangement of the extracellular matrix, mechanical signals) should be then incorporated into the design of advanced and clinically relevant biomimetic biomaterials [1]. Moreover, biomimetic biomaterials have been increasingly combined with multi-phenotypic cells to produce new advanced systems that better model the complex cellular environment of natural tissues. Particularly, considering the highly vascularized network of bone, osteoprogenitor cells inevitably interact with endothelial cells (ECs) in a synergetic fashion [2, 3]. The cellular interactions facilitate viability and proliferation as well as generation of growth factors and proteins that promote osteogenic and angiogenic differentiation, while enabling other key biological tasks during bone development [4, 5]. Different fundamental studies have established that a reciprocal interaction, both physical and biochemical, between osteoblasts, stem cells and endothelial cells occurs during osteogenesis, as well as the 2D interaction between endothelial and stem cells towards osteogenic differentiation was already demonstrated *in vitro* and *in vivo* [6-13]. While endothelial cells secrete numerous regulatory molecules that influence the differentiation and activity of bone forming cells [14-17], osteoblasts/osteoprogenitor cells release diverse pro-angiogenic growth factors [7, 18-20]. However, the commonly used co-culture systems involve the

challenge of generating stable *in vitro* pre-vasculature in the constructs with typically a slow rate of anastomosis efficacy. Moreover, conventional porous hybrid scaffolds have typically a fixed geometry and need to be implanted under open surgery. Alternatives to transport biomaterials and cells are injectable systems that could carry all the necessary cargo able to stimulate upon implantation the formation of new bone vascularized tissue using minimally invasive procedures [21]. To achieve such concept, one could envisage the development of an injectable device, pre-cultured with cells that could have all the necessary instructive signals to upon implantation generate new bone tissues and an initial support for angiogenesis that is expected to integrate with time with the surrounding vasculature. Considering the referred requirements, we propose a rather unique combination of functional biomaterials and cells for the groundbreaking advances of engineering self-regulated 3D compartmentalized devices. We aim to transfigure the concept of conventional 3D scaffolds for TE, typically associated on the use of porous structures or hydrogels to support cells, by using an alternative hierarchical methodology in which solid microparticles and cells are wrapped by semipermeable capsules. Our previous studies demonstrated already the suitability of the liquified capsules as successful bioencapsulation devices [22, 23]. In this work, inspired by the native co-existence of multiple cell types and from the concept of deconstructing the "stem cell niche" [1], we propose for the first time to use liquified capsules as self-regulated co-encapsulation reservoirs of stem and endothelial cells. Owing to a number of appealing features, such as being available in large quantities with diminutive donor site morbidity or patient discomfort, adipose tissue was the source used to isolate both cell types. **Scheme VI.1** represents the methodology of the production of the capsules. Capsules are composed by three essential components: *(i)* a permselective membrane barrier that wraps the liquefied core of the capsule, ensuring permeability to essential molecules for cell survival, flexibility to the capsule, and enhancing direct contact between the encapsulated materials; *(ii)*

surface functionalized collagen I poly(L-lactic acid) (PLLA) microparticles as cell adhesion sites; and *(iii)* a co-culture of adipose stem (ASCs) and endothelial (ECs) cells.

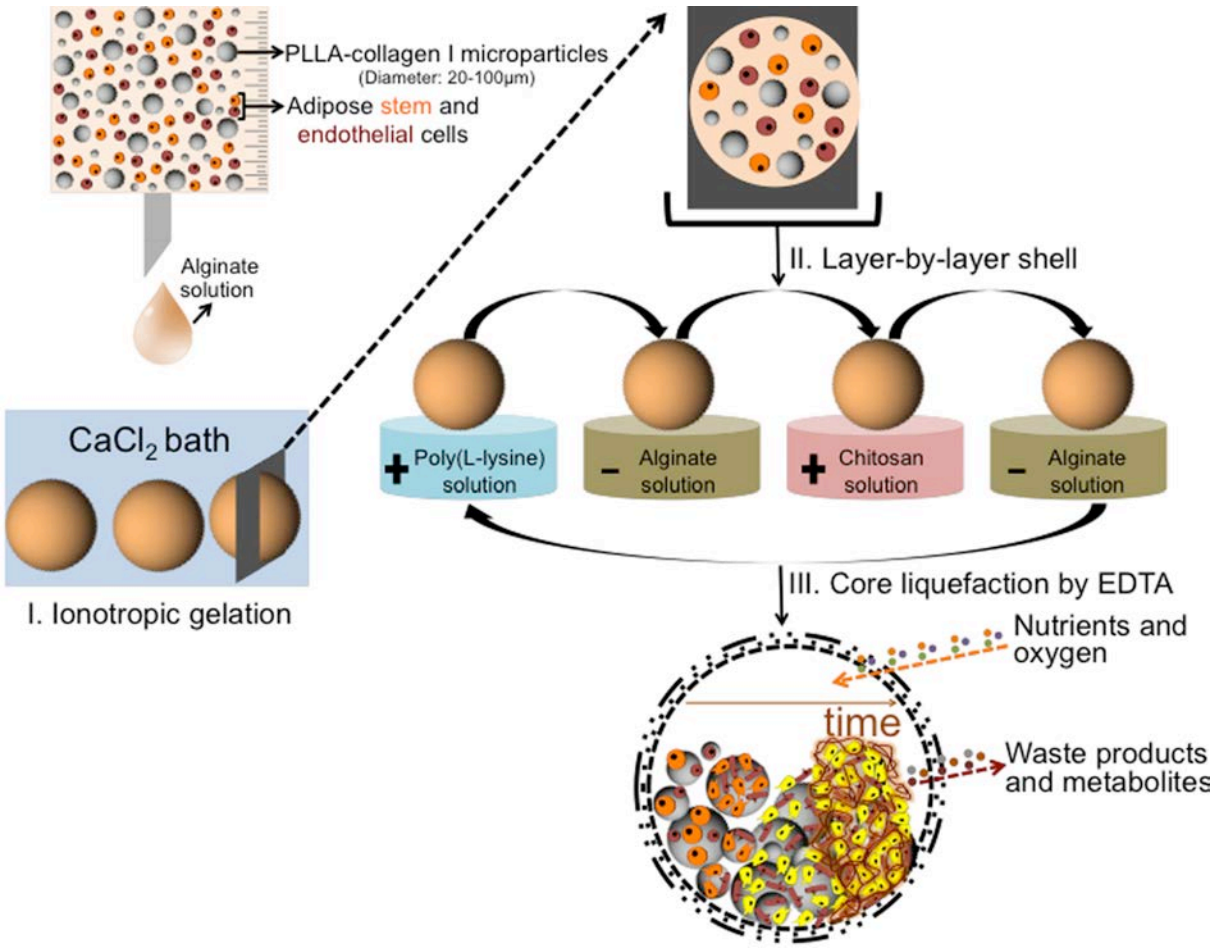

Scheme VI.1 - Production of the proposed liquified multilayered capsules encapsulating poly(L-lactic acid) microparticles coated with collagen I, and adipose stem (orange, ASCs) and endothelial cells (red). The loaded hydrogel particles are obtained after the ionotropic gelation of alginate in a calcium chloride ($CaCl_2$) bath. Then, layer-by-layer is performed with the polyelectrolytes, namely poly(L-lysine), alginate, and chitosan, in order to produce the multilayered membrane. Ultimately, the liquified core is obtained by chelation with EDTA. As the time of culture increases, the encapsulated cells subsequently adhere to the surface of microparticles, proliferate, and create cell aggregates. The ASCs start to differentiate into the osteogenic lineage (color change from orange to yellow) and ultimately a mineralized osteogenic matrix is obtained inside the liquified environment of capsules. The multilayered membrane allows the exchange of essential molecules for cell survival.

The membrane of the capsules is produced using the layer-by-layer assembly. Although many interactions may be employed for the build-up of the multilayers [24], we employed simple electrostatic forces for assembling oppositely charged polyelectrolytes. Our main hypothesis is that ECs would provide a more physiologically relevant microenvironment, while regulating the structure and function of ASCs towards the osteogenic lineage (ASCs have been shown in numerous studies to exhibit the potential to contribute to chondrogenesis, osteogenesis, adipogenesis, myogenesis as well as some aspects of neurogenesis [25-28]). Therefore, we expect that ECs would led ASCs to differentiate without requiring the supplementation of two main osteogenic differentiation factors, namely dexamethasone and ascorbic acid. Moreover, we expect that the liquefied environment of the capsules will assure the excellent diffusion of nutrients to the encapsulated cells, even those at the inner region of the capsule, and spatial freedom for cell communication and self-organization. The biodegradable nature of the capsules, combined with their intrinsic osteo- and angiogenic natures, could engender a novel generation of injectable biomimetic systems with clinically viability to be used in orthopedic applications. To test our hypothesis, the multifunctional liquified capsules encapsulating only ASCs (MONO capsules) or a co-culture with ECs (CO capsules) were cultured in endothelial medium with (EDAG medium) or without (EG medium) osteogenic differentiation factors.

2. Materials and methods

2.1 Cells isolation from adipose tissue

Subcutaneous adipose tissue from liposuction procedures was used to isolate both human adipose stem cells (ASCs) [29] and human adipose microvascular endothelial cells (ECs) [30]. The collected tissues were obtained under a cooperation agreement between the 3B's Research Group and Hospital da Prelada (Porto, Portugal), after approval of the Competent Ethics Committee

(CEC). The human tissues received were handled in accordance with the guidelines approved by the CEC. Informed consent was obtained from all subjects. Briefly, samples were transported in phosphate-buffered saline (PBS, Sigma-Aldrich) supplemented with penicillin-streptomycin (10%, pen-strep, Gibco) and kept at 4ºC. The lipoaspirates were washed with PBS and incubated with collagenase type II A (0.05% w/v, Sigma-Aldrich) for 45 min at 37ºC in a shaking water bath. The digested samples were filtered (200 μm) and centrifuged at 800 g for 10 min at 4ºC. The obtained stromal vascular fraction (SVF) was resuspended in erythrocyte lysis buffer at pH 7.4 containing ammonium chloride (155 mM, Merk), potassium bicarbonate (5.7 mM, Riedel-de-Häen), and ethylenediaminetetraacetic acid (0.1 M, EDTA, Sigma-Aldrich) in distilled water. After 10 min of incubation at room temperature (RT), the mixture was centrifuged at 300 g for 5 min. To isolate the ASCs the red blood cell-free SFV was resuspended in α-MEM medium (Invitrogen) supplemented with fetal bovine serum (10%, FBS, Invitrogen) and pen-strep (1% v/v). To isolate the ECs the red blood cell-free SFV was resuspended in EndoGro^{TM}-MV-VEGF complete media kit (Millipore Iberica). The ECs were plated in cell culture flasks, previously coated with gelatin (0.7% w/v, porcine skin type A, Sigma-Aldrich) for 30 min at 37ºC. Culture medium was changed 48 h after initial plating and then every 3-4 days for both cell phenotypes.

2.2 Microparticles production and surface functionalization

PLLA microparticles were produced by oil/water (o/w) emulsion technique and surface modified by combining plasma treatment with collagen I as similarly described in our previous reports [22, 23]. PLLA (5% w/v, M_w~1,600-2,400, 70% crystallinity, Polysciences) was dissolved in methylene chloride (CH_2Cl_2, Fisher Chemical). Under agitation, this solution was added to polyvinyl alcohol (0.5%, PVA, Sigma-Aldrich). After 2 days at RT, the produced microparticles were subsequently collected, washed with distilled water, and lyophilized (Cryodos, Telstar). Microparticles were then placed in a plasma reactor

chamber (PlasmaPrep5, Gala Instrumente) fitted with a radio frequency generator. Air was used as the working atmosphere. A glow discharge plasma (0.2 mbar, 30 V) was created for 15 min. Subsequently, microparticles (500 mg) were immersed in collagen I (1200 µg, rat protein tail, Gibco) diluted in acetic acid (0.02 M) for 4 h at RT.

2.3 Mono- and co-cultures set up

At 90% confluence, ASCs (passage 2) and ECs (passage 4-6) grown in T150 tissue culture flasks were washed with PBS and subsequently detached using TrypLE™ Express solution (Life Technologies) at 37°C for 5 min. PBS was added and the cell suspensions were centrifuged for 5 min at 300 g. Low viscosity sodium alginate from brown algae (1.5% w/v, ALG, ~250 cP, Sigma-Aldrich) was dissolved in sodium chloride (0.15 M, NaCl, Enzymatic) containing MES hydrate (25 mM, Sigma-Aldrich) at pH 7. The solution was sterilized by 0.22 µm filtration. $5x10^6$ ASCs ($5x10^6$ cells per mL^{-1} of alginate) alone or mixed with ECs ($5x10^6.mL^{-1}$ of alginate, co-culture ratio 1:1) were added to the microparticles ($50mg.mL^{-1}$ of alginate). The alginate solutions were then used to produce liquified capsules encapsulating ASCs alone (MONO capsules) or in co-culture with ECs (CO capsules).

2.4 Liquified multilayered capsules production

All the conditions used to produce the liquified capsules (the combination of the polyelectrolytes, concentration, pH, number of layers, and time of adsorption and liquefaction) were optimized in our previous studies [22, 23]. The alginate solutions containing cells and microparticles were added drop wise using a 21 G needle to calcium chloride (0.1 M, $CaCl_2$, VWR) buffered with MES hydrate (25 mM, Sigma-Aldrich) at pH 7. After 20 min at RT, alginate hydrogels were collected and rinsed in a washing solution of NaCl (0.15 M). The external membrane was processed by subsequent adsorption of oppositely charged polyelectrolytes by layer-by-layer deposition. Alginate hydrogel

particles were first immersed in a poly(L-lysine) (PLL, M_w~30,000-70,000, pH 7, Sigma-Aldrich), and subsequently in ALG solution (pH 7), water-soluble highly purified chitosan (CHT, pH 6, Protasan UP CL 213, viscosity 107 mPa.s, M_w=2.7x10^5 g.mol^{-1}, 83% degree of deacetylation, NovaMatrix), and, ultimately, in ALG solution again. The polyelectrolyte solutions (0.5 mg.mL^{-1}) were dissolved in NaCl (0.15 M) containing MES hydrate (25 mM). Following a 10 min period for each polymer adsorption, the excess of macromolecules was removed by immersion in NaCl (0.15 M) for 5 min. This process was repeated three times in order to obtain a 12-layered membrane. The coated hydrogels were immersed in EDTA (20 mM) at pH 7 for 5 min to liquefy the alginate core. The two formulations of liquified capsules obtained were cultured in EndoGro™-MV-VEGF complete kit media without ascorbic acid (E). To the E medium, β-glycerophosphate (10 mM, G, Sigma-Aldrich) were added, here termed as EG medium. Additionally, capsules were also cultured in E medium containing all the osteogenic differentiation factors, namely, dexamethasone (10 nM, D, Sigma-Aldrich), ascorbic acid (50 µg.mL^{-1}, A), and β-glycerophosphate (10 mM, G, Sigma-Aldrich), here termed as EDAG medium. Capsules were transferred to non-adhesive 24-well plates and incubated at 37°C in a humidified 5% CO_2 air atmosphere. The entire procedure was performed under sterile conditions. All the solutions used at this step were sterilized by filtration through a 0.22 µm filter.

2.5 Flow cytometry analysis

The phenotypic profile of ASCs and ECs was assessed regarding mesenchymal (CD105-FITC, Arium; CD90-APC, and CD73-PE, BD Biosciences) and endothelial (CD31-APC, Citomed) markers before and after encapsulation within MONO and CO capsules. Isolated and encapsulated cells were harvested by TrypLE™ Express solution (Life Technologies) at 37°C for 5 min, and centrifuged. Samples were resuspended in PBS solution containing bovine serum albumin (3% w/v, BSA, Sigma-Aldrich) and the specified antibodies at

the dilutions defined by the manufacture's specifications. After 20 min at RT, samples were subsequently washed with PBS, centrifuged, fixed in PBS with formaldehyde (1% v/v, Sigma-Aldrich), and analyzed in a flow cytometer (BD FACSCalibur, CellQuest v3.3 software, BD Biosciences).

2.6 Lipophilic fluorescent labeling

Prior to encapsulation, ASCs and ECs were incubated with the lipophilic dyes *3,3'*-dioctadecyloxacarbocyanine perchlorate (DIO, green) and *1,1'*-dioctadecyl-*3,3,3',3'*-tetramethylindocarbocyanine perchlorate (DIL, orange), respectively. Cells were incubated with each dye (1 mL, 2 µM per $1x10^6$ cells) at 37°C for 10 min. Labeled cells in the MONO and CO capsules were visualized by confocal microscopy (TCS SP8, Leica).

2.7 Mitochondrial metabolic activity quantification

Mitochondrial metabolic activity quantification was performed using a MTS colorimetric assay (CellTiter96® AQueous one solution cell proliferation assay, Promega) according to manufacture's specifications. Capsules (n = 4 per well in triplicate) were incubated with the reagent kit (1 mL per well) at 37°C protected from light. After 3 h, absorbance was read at 490 nm using a microplate reader (Gen 5 2.01, Synergy HT, Biotek).

2.8 Cell proliferation quantification

Total DNA quantification was performed after cell lysis (Quant-iT™ PicoGreen® dsDNA assay kit, Life Technologies). Samples (n = 4 per well in triplicate) were suspended in ultra-pure sterile water (1 mL per well). After 1 h in a 37°C shaking water bath, samples were frozen at -80°C overnight. Samples were defrosted and used according to the specifications of the kit. A standard curve for DNA analysis was generated with the provided dsDNA solution. After 10 min of incubation at RT, fluorescence was read at an excitation wavelength of

485/20 nm and 528/20 nm of emission using a microplate reader (Gen 5 2.01, Synergy HT, Biotek).

2.9 Imaging cell morphology by scanning electron microscopy (SEM)

Samples (n = 4 per well in triplicate) were washed with PBS and fixed at RT in formalin (10% v/v). After 1 h, samples were dehydrated in an increasing gradient series of ethanol for 10 min each. The membrane of capsules was destroyed to expose the core contents. After gold sputtering, samples were visualized by SEM (15kV, JSM-6010LV, Jeol).

2.10 Alkaline phosphatase activity quantification

The activity of alkaline phosphatase was determined by the amount of *p*-nitrophenol. A substrate solution (pH 9.8) was prepared by dissolving *4*-nitrophenylphosphate disodium salt hexahydrate (0.2% w/v, Sigma-Aldrich) in diethanolamine (1 M, Sigma-Aldrich). Each sample (20 µL, in triplicate) was mixed with the prepared substrate solution (60 µL). After 45 min at 37ºC protected from light, the reaction was stopped (80 µL) with NaOH (2 M) and EDTA (0.2 mM). A standard curve with a range of concentrations was prepared by diluting *4*-nitrophenol solution (10 mM, Sigma-Aldrich) in the stop solution. Absorbance was read at 405 nm in a microplate reader (Gen 5 2.01, Synergy HT, Biotek). Results were normalized with dsDNA quantification data.

2.11 Calcium quantification

Samples were washed with PBS and resuspended in 100 µL of HCl (6 M). A standard curve was prepared with a $CaCl_2$ solution (5 mM). 10 µL of each sample and standard (in triplicate) were transferred to a 96-well plate. Upon mixing the calcium kit components according to manufacture's specifications (Roche), absorbance was read at 570 nm in a microplate reader (Gen 5 2.01, Synergy HT, Biotek).

2.12 Histological mineralization analysis

MONO and CO capsules cultured in EG or EDAG media were collected after 21 days, washed in PBS, and processed in an automatic spin tissue processor (STP120-2, Microm) for histological analysis. Afterwards, samples were embedded in paraffin and cut into sections of 5 μm thickness using a microtome (HM355S, Microm). To visualize calcium-rich deposits, sections were deparaffinized and subsequently immersed in alizarin red staining solution for 5 min at RT. Samples were then mounted and analyzed (Axio Imager Z1m, Zeiss).

2.13 Immunofluorescence staining on 3D structures and histological sections

Samples were fixed in formalin (10% v/v, BD Biosciences) for 30 min at RT. After fixation, capsules were destroyed and cells were permeabilized for 5 min at RT with Triton-X (0.1% v/v, Sigma-Aldrich). Samples were immersed in BSA (3% w/v) for 30 min at RT to block non-specific binding and then incubated overnight at 4°C with the primary antibody rabbit anti-human osteopontin (Promega, 1:100 in 1% BSA). After PBS washing, samples were incubated for 1 h at RT with the secondary antibody anti-rabbit AlexaFluor 488 (BD Biosciences, 1:500 in 1% BSA). The immunofluorescence staining in the histological sections was performed in CO capsules cultured in EG or EDAG media for 21 days. Samples were washed in PBS and processed in an automatic spin tissue processor (STP120-2, Microm) for histological analysis. Afterwards, samples were embedded in paraffin and cut into sections of 5 μm thickness using a microtome (HM355S, Microm). After the deparaffinization process, the antigen retrieval was performed in a microwave-heated sodium citrate buffer (10 mM, Sigma-Aldrich). Samples were immersed in hydrogen peroxide (3% v/v, VWR) at RT for 30 min. The same immunofluorescence staining protocol used for the 3D structures was repeated with the adding of the primary antibody mouse anti-human CD31 (Sigma-Aldrich, 1:100 in 1% BSA) conjugated with the osteopontin and the secondary antibody anti-mouse

AlexaFluor 594 (BD Biosciences, 1:500 in 1% BSA). Ultimately, 3D and 2D structures were counterstained with DAPI (Sigma-Aldrich, 1 $mg.mL^{-1}$ diluted 1:1000 in PBS) for 5 min at RT and analyzed by confocal microscopy (TCS SP8, Leica).

2.14 Quantification of cytokines

The supernatants (500 µL) were stored at -80°C with a diluted protease inhibitor cocktail (1:100, Sigma-Aldrich) until analysis. Commercially available human BMP-2 and VEGF ELISA development kits (Peprotech) were used according to manufacture's specifications. Absorbance was read at 405-650 nm in a microplate reader (Gen 5 2.01, Synergy HT, Biotek).

2.15 RNA extraction and cDNA production

The extraction of mRNA was performed using TRIzol reagent (Sigma-Aldrich). Capsules (n = 5 per well in triplicate) were stored in TRIzol (800 µL) at -80°C until analysis. Samples were slowly defrosted on ice and chloroform (160 µL, Sigma-Aldrich) was added. After 15 min at 4°C, samples were centrifuged at 13,000 rpm (Bioline, MCF-2360) for 15 min. The aqueous part of each sample was collected and isopropanol (400 µL, Sigma-Aldrich) was added. Following an overnight incubation at -20°C, samples were centrifuged at 13,000 rpm for 10 min at 4°C. The supernatant was discarded and the resulting pellets were washed with ethanol (70% v/v) in RNase/DNase free distilled water (VWR). The pellets were let to partially dry on air, and dissolved in RNase/DNase free distilled water (10 µL). RNA quantity and purity was determined in nanodrop spectrophotometer (NanoDrop ND-1000, ThermoScientific). Samples with a 260/280 purity ratio higher than ~1.8 were used for cDNA synthesis. The cDNA synthesis was performed using a qScript cDNA SuperMix kit (VWR) and the MiniOpticon Real-time PCR Detection System (MJ Mini, BioRad). All samples were normalized (1 µg of RNA in 20 µL of RNase/DNase free distilled water).

2.16 Quantitative real-time polymerase chain reaction

The expression of the osteogenic genes bone morphogenic protein-2 (*BMP-2*), transcription factor *RUNX2*, and bone sialoprotein (*BSP*), and of the angiogenic genes von Willebrand factor (*vWF*), *CD31*, and vascular endothelial growth factor A (*VEGF*) were quantified in the cDNA samples using a real-time PCR reaction. The target genes were normalized with *18S rRNA* as the housekeeping. The primers (200 nM) were designed to span exon-exon junctions using the primer-BLAST tool (sequences in **Table VI.SI**). The real-time PCR reaction was done using the PerfeCTa SYBR Green FastMix Reaction Mixes (Quanta Biosciences), according to manufacturer's specifications. The reactions were monitored in a Mastercycler (Realplex4, Eppendorf) using the software realplex version 2.2 (Eppendorf). The relative quantification of the osteogenic and angiogenic markers expression was performed using the $2^{-\Delta\Delta CT}$ method (Perkin-Elmer). Results are expressed relatively to gene expression levels of day 3.

2.17 Statistical analysis

Statistical analysis was performed using two-way analysis of variance (ANOVA) with Tukey's post-hoc test (GraphPad Prism 6.0). A p-value < 0.05 was considered statistically significant. Only non-significant differences (ns) were marked to facilitate the interpretation of the data. All results are presented as mean ± standard deviation.

3. Results and discussion

3.1 Encapsulation of cells within multilayered liquified capsules

The successful isolation of ASCs and ECs from adipose tissue was determined by flow cytometry (**Figure VI.1A**). More than 90% of the ASCs were found to be positive for the mesenchymal stem cell markers CD105, CD90, and CD73, whilst all cells lacked the expression of the endothelial marker CD31. On the

other hand, the endothelial phenotype of ECs was confirmed by the CD31 expression. The maintenance of the mesenchymal and endothelial phenotypes after cell encapsulation in MONO and CO capsules also confirmed that the encapsulation process did not affect the cells. Moreover, the expression of CD31 by 47.14% ± 3.31 of the cells in the CO capsules confirmed the 1:1 ratio of the co-cultures as well as the inertness of the method. The random distribution of both cell types within the capsules was confirmed upon microscopic analysis. In the MONO capsules only green fluorescence corresponding to ASCs could be detected, while in the CO capsules both green and orange fluorescence identifying respectively ASCs and ECs could be visualized (**Figure VI.1B**).

3.2 Metabolic activity, proliferation, and morphology of the encapsulated cells

MONO capsules in EDAG medium showed an increasing metabolic activity (**Figure VI.2A**) and DNA content (**Figure VI.2B**) up to 14 days of culture. However, at day 21, no significant differences were found in comparison to day 14 for both parameters. On the other hand, cells in MONO capsules cultured in EG medium kept proliferating up to the end timepoint, which was also traduced in significantly higher metabolic activity. The same trend found in MONO capsules cultured in EDAG medium was observed for the CO capsules cultured in both media. The stagnation in the metabolic activity and in the DNA content between 14 and 21 days of culture in MONO capsules cultured in EDAG medium, and in CO capsules cultured in both media might be an indication that cell differentiation is occurring. The cells interacting with the microparticles in the core of both MONO and CO capsules was visualized by SEM after 21 days of culture (**Figure VI.2C**). In order to visualize the core contents by SEM, the layer-by-layer membrane of the capsules, which remained stable up to the 21 days of *in vitro* culture, was disrupted. In all conditions cells adhered to the surface of the microparticles, proliferated, and

deposited matrix in such a way that the particles were assembled in large 3D constructs.

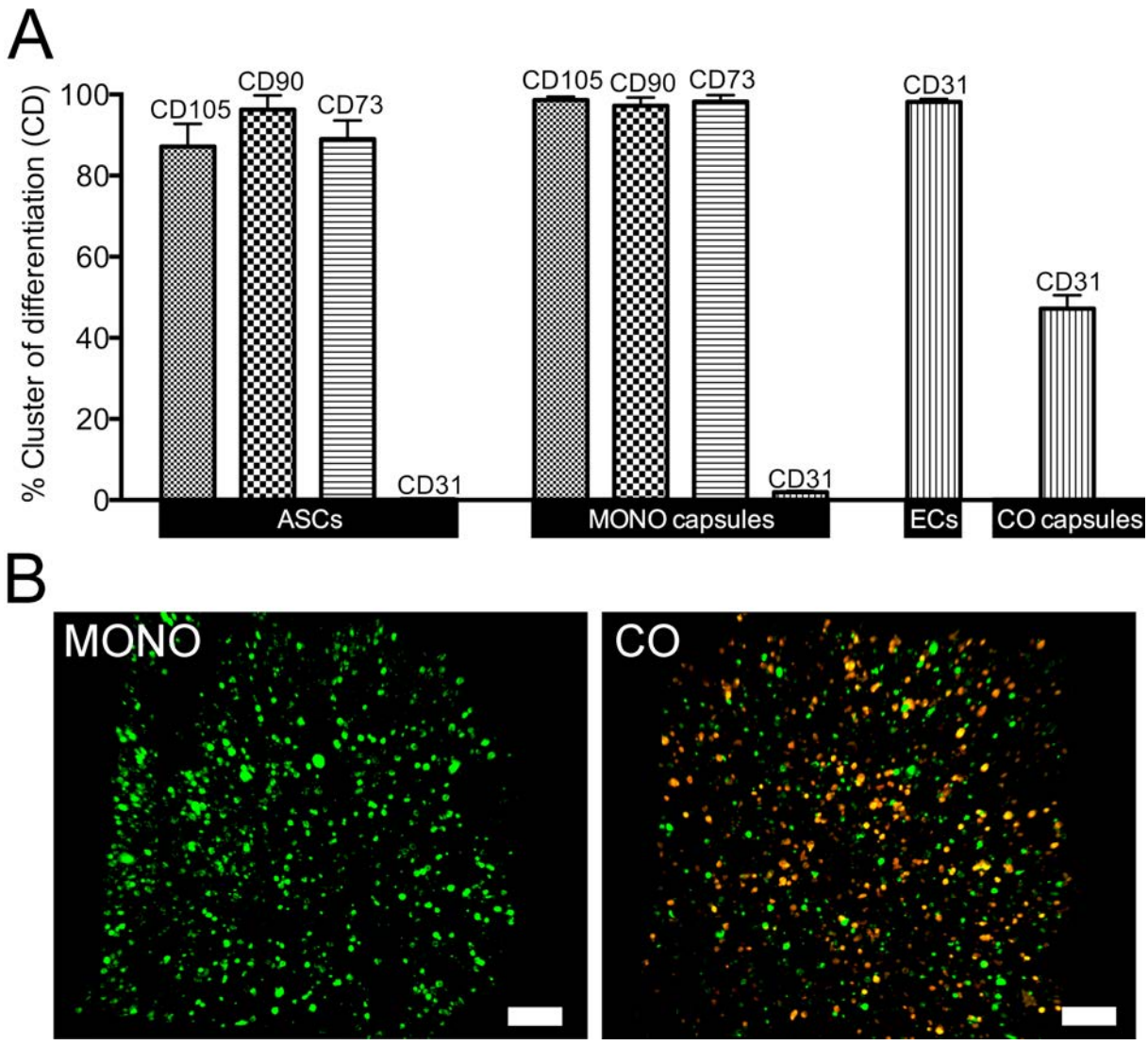

Figure VI.1 - (**A)** Flow cytometry analysis of human adipose stem cells (ASCs) and human microvascular endothelial cells (ECs) after isolation and encapsulation at day 0 within MONO and CO capsules. **(B)** Confocal images of MONO and CO capsules encapsulating cells at day 0 previously labeled with DIO (green, ASCs) and DIL (orange, ECs) lipophilic fluorescent dyes. Scale bar is 200 µm.

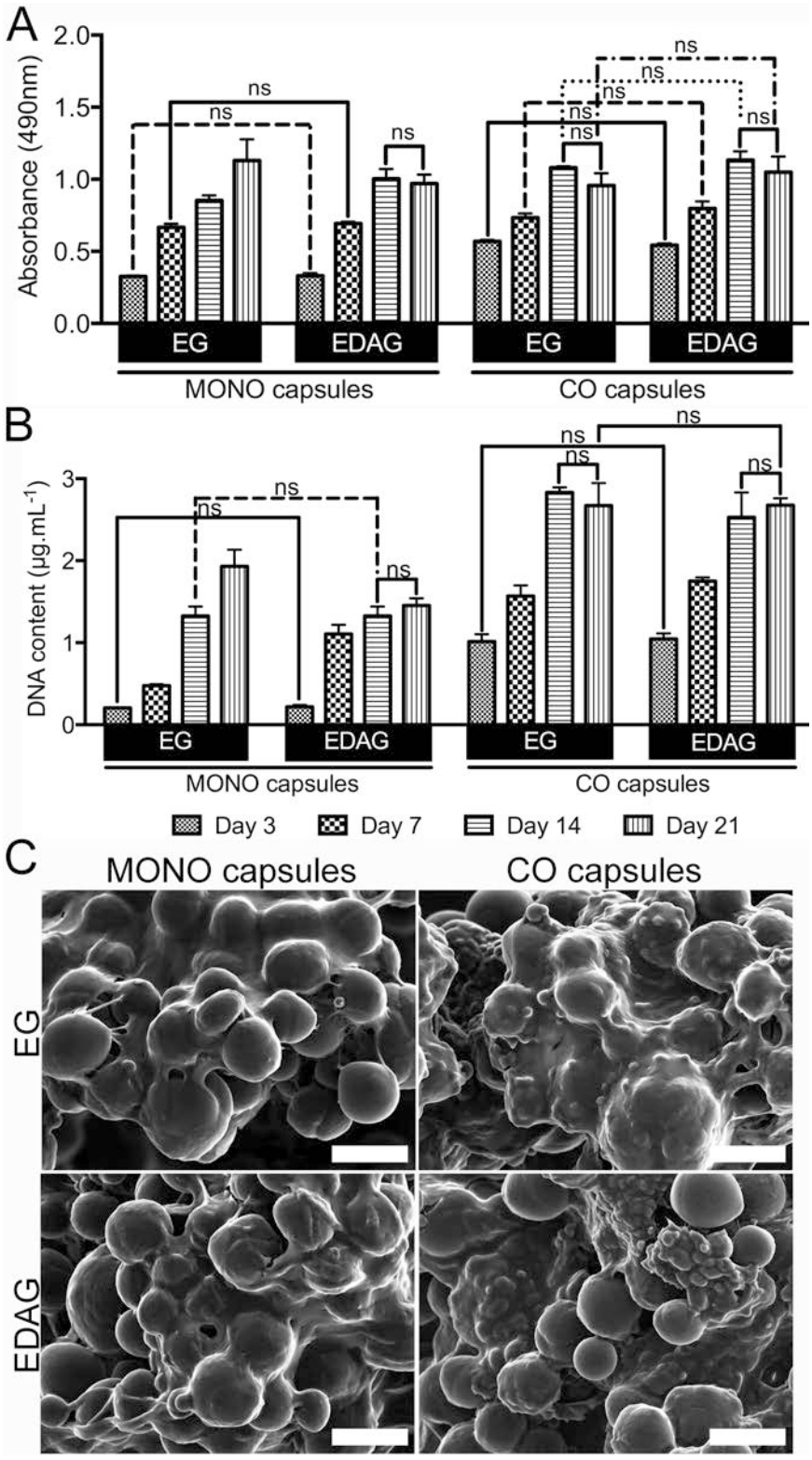

Figure VI.2 - (A) Cell metabolic activity determined by MTS colorimetric assay and **(B)** cell proliferation by DNA quantification. All results were significantly different unless marked with ns ($p>0.05$). **(C)** SEM images of the encapsulated microparticles and cells inside MONO and CO capsules after 21 days (magnification: 500x, scale bar: 50µm). The symbols * and # mark the microparticles and the extracellular matrix deposition of the encapsulated cells, respectively.

3.3 *In vitro* assessment of the osteogenic potential of liquified multilayered capsules

3.3.1 Quantification of ALP activity and mineralization evaluation

Knowing that increased levels of ALP activity are correlated with enhanced osteogenic differentiation [31], it can be stated that cell differentiation occurred earlier in MONO and CO capsules cultured in EDAG medium (**Figure VI.3A**). However, as the time of culture increased, ALP activity in CO capsules cultured in EG also increased. At day 14 both CO capsules showed the highest levels of ALP activity. Therefore, co-cultures in the liquefied capsules led to an enhanced cell differentiation, although delayed when co-cultured in EG medium. MONO capsules cultured in EG medium presented the lowest ALP activity levels during the entire experiment. ALP is secreted by active osteoblasts and is responsible for the cleavage of pyrophosphate ions, which are inhibitors of the formation of hydroxyapatite crystals. The hydrolysis reaction results in the saturation of the extracellular fluid with orthophosphates that induce mineralization [32, 33]. Hence, ALP activity results were corroborated with calcium quantification (**Figure VI.3B**). Similarly, calcium deposits were hardly detected in MONO capsules cultured in EG medium whilst earlier detected in the capsules cultured in EDAG compared to CO capsules cultured in EG medium. In the end, co-cultures resulted in an enhanced newly deposited mineralized ECM, even in EG medium. Mineralization was qualitatively assessed by alizarin red staining at day 21 (**Figure VI.3C**), confirming the deposition of calcium.

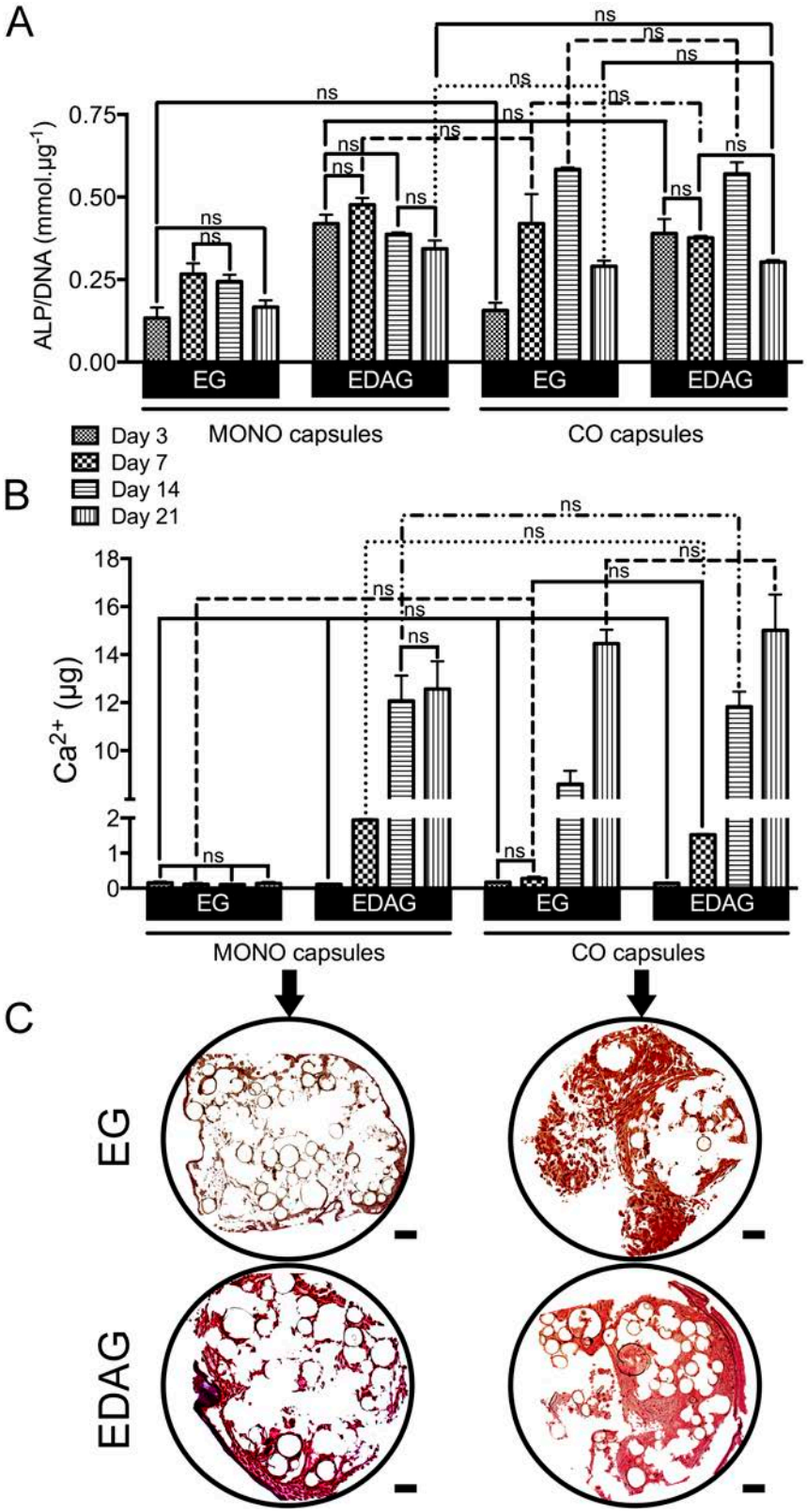

Figure VI.3 - (A) Alkaline phosphatase (ALP) activity normalized by DNA content and **(B)** quantification of calcium. All results were significantly different unless marked with ns ($p > 0.05$). **(C)** Alizarin red staining on histological sections of MONO and CO capsules cultured in EG or EDAG media after 21 days. Calcium deposits were stained in red. Scale bar is 50 µm.

3.3.2 Osteopontin and CD31 immunofluorescence detection

The secretion of the late osteogenic marker osteopontin in MONO and CO capsules after 21 days of culture in EG and EDAG media was confirmed (**Figure VI.4A**). On the other hand, cells in the MONO capsules cultured in EG medium did not secrete osteopontin. The presence of the ECs in the CO capsules cultured in both media was assessed by the expression of CD31. The immunofluorescence could only be detected after histological cuts. This indicates that ECs were located in the inner regions of cell aggregates enfolded by ASCs, probably due to the higher proliferative rate of the latter. Altogether, these results indicate not only that cells were able to spread throughout the inner areas of capsules, but also that the diffusion of essential and signaling molecules for cell survival, proliferation, and differentiation was allowed. The diffusion of molecules in 3D systems is a major concern in tissue engineering strategies, since it dictates the success or failure of the regeneration process [34]. Its inefficiency can lead to tissue repair only at the circular periphery of 3D constructs, while cell death occurs in the inner areas. The liquified environment of capsules led to an excellent diffusion of molecules as already demonstrated in our previous studies [22, 23]. The layer-by-layer methodology, that has been proposed in a variety of biomedical applications [35], was effectively useful to produce a flexible permselective shell that sustained the viability of compartmentalized cells, while maintaining the mechanical integrity of the liquified capsules. The properties of the multilayers can be tuned to control the transfer properties of essential molecules [36]. However, the conception of a liquified environment required the introduction of solid microparticles to provide cell adhesion sites, since the encapsulated cells were anchorage dependent.

3.3.3 BMP-2 and VEGF cytokines release

The profile of BMP-2 and VEGF release into the supernatants of MONO and CO capsules cultured in EG or EDAG media is shown in **Figure VI.4B**. The release

of BMP-2 was similar for both MONO and CO capsules cultured in EDAG, which remained constant up to 14 days, and increase after 21 days. The highest amounts were detected for the CO capsules. On the other hand, for the CO capsules cultured in EG, BMP-2 was increasingly secreted along the entire experiment, reaching at day 14 the value detected for the CO capsules cultured in EDAG. Residual amounts of BMP-2 were detected for the MONO capsules cultured in EG during the entire experiment. The profile release of VEGF was similar for all conditions. The highest levels of VEGF were observed for MONO capsules cultured in EG, and then for CO capsules cultured in the same medium. However, as the culture time increased, the VEGF detected for CO capsules cultured in EG decreased to values similar to those observed for MONO and CO capsules cultured EDAG medium. Different studies [37-39] have already been show that ASCs stimulate blood vessel growth due to the secretion of many angiogenic and anti-apoptotic growth factors, such as VEGF, which is widely known to enhance the biological performance of endothelial cells [7, 19, 20]. Furthermore, a positive effect on the differentiation of osteoprogenitor cells when co-cultured with endothelial cells was already documented in different studies [6-8, 10-17, 19, 40-44]. As observed by ALP activity and calcium content results, a delayed osteogenic differentiation was observed in the CO capsules cultured in EG medium in comparison to capsules cultured in EDAG. Correlating the delay of the osteogenic differentiation in CO capsules cultured in EG medium with their initial release of higher levels of VEGF, and the absence of osteogenic differentiation in MONO capsules cultured in EG medium with their highest release of VEGF, it seems that the release of VEGF and the osteogenic stage of differentiation of the ASCs are intrinsically correlated. As time increased, while osteogenesis occurred in CO capsules cultured in EDAG the amount of VEGF decreased to similar values observed for capsules cultured in EDAG medium. These interesting findings might indicate that osteogenic differentiated ASCs have a decreased ability to enhance angiogenesis by diminishing VEGF release. A similar behavior was

already reported [45] for mesenchymal stem cells (MSCs). It was observed that MSCs cultured in a 2D cell culture system secreted the highest concentration of VEGF compared to MSCs cultured in osteogenic media, which down regulated the gene expression of pro-angiogenic factors. Therefore, although the ultimate goal of the proposed bioencapsulation system is to promote the osteogenic differentiation, the delayed osteogenesis observed in CO capsules in EG medium could represent an advantage - the higher amounts of VEGF released by those capsules in the initial times of culture can lead to an enhanced angiogenesis and, consequently, to a vascularized osteogenic tissue. Importantly, besides inducing angiogenesis, VEGF is also known to increase the osteogenic healing capacity of ASCs [46]. Likewise, Boletreau *et al.* [47] showed that microvascular endothelial cells were able to release BMP-2 by the action of VEGF treatment. Although MONO capsules cultured in EDAG medium also released BMP-2 during the entire experiment, this was enhanced by co-encapsulation. Interestingly, when the release of VEGF started to decrease in both CO capsules, the release of BMP-2 increased exponentially. In this case, the synergistic effect of the co-cultures and the presence of osteogenic differentiation factors in the culture medium resulted in the highest BMP-2 release by CO capsules cultured in EDAG medium. However, in later timepoints the co-culture was sufficient to stimulate BMP-2 release since the amount released by CO capsules cultured in EG was similar to the one observed for the EDAG. Since VEGF and BMP-2 were detected and measured in the culture medium surrounding the capsules, this indicates that the membrane is permeable to small molecules while remaining stable up to 21 days of *in vitro* culture. We envisage that after implantation, the developed capsules can positively influence the neighboring cells by paracrine signaling in the highly vascularized environment of bone.

3.3.4 Genetic profile quantification of osteogenic and angiogenic markers

The quantification of the transcripts for the osteogenic and angiogenic genes of interest was performed at the different timepoints (**Figure VI.4C**). The expression of the osteogenic genes *BMP-2, BSP, and RUNX2*, was up regulated in all capsules and at all the timepoints, excepting for MONO capsules cultured in EG media. While for *BMP-2* and *BSP* markers, the expression level increased with culture time, for *RUNX2* no significant differences were found over time, although a slight peak could be observed at day 14. Again, no significant and distinct results were found between CO capsules cultured in EG and EDAG media, indicating that the crosstalk between the two cell types was sufficient to induce the osteogenic differentiation. In all CO capsules the endothelial markers *vWF*, *CD31*, and *VEGF* were up regulated up to 21 days although its expression decreased with culture time, as similarly observed in co-culture systems [8]. This decrease might be explained by the fact that total RNA was used to normalize the genetic profile results, thus including RNA also from ASCs and not only from ECs. Significant differences were found for the expression of *VEGF* marker at days 7 and 14, and for *vWF* and *CD31* markers at day 7, at which CO capsules cultured in EG medium presented the highest expression.

Altogether these results showed that the crosstalk between ASCs and ECs played a significant role in osteogenic differentiation. More importantly, the co-encapsulation of ASCs and ECs suppressed the need of dexamethasone and ascorbic acid to osteoblastic differentiation occurs. Considering the reported findings, we believe that the proposed CO capsules will find great applicability in bone regeneration, while bringing new insights to bioencapsulation strategies. Additionally, in the present study a new 3D biomimetic platform to assess the interaction of stem and endothelial cells was developed. Importantly, the biological outcome demonstrated was achieved by using cells isolated from a waste and abundant tissue, which is highly desirable for tissue engineering applications considering the high number of cells required in 3D

systems. Since it was demonstrated that the capsules also release important cytokines for bone healing, namely VEGF and BMP-2, we thus believe to be close to a completely self-regulated confined system that could stimulate autonomous production mineralized bone tissue, with clear therapeutic advantages. The liquified environment of capsules is a key point in the novelty and success of the proposed system, since it allows the encapsulated cells to freely move and proliferate – as they can easily occupy the liquid space of the capsules environment – and self-organize a 3D culture composed by microparticles. Consequently, we envisage that in a dynamic culture the results obtained in the present study could be boosted by enhancing the diffusion of molecules across the liquified environment, such as essential molecules for cells survival or even signaling biomolecules either circulating outside the capsules environment or released by the encapsulated cells. Additionally, we trust that minimal invasive procedures could be adopted due to their injectability provided by the liquified environment. Moreover, having a single structure encapsulating all the different components might facilitate the implantation process, while avoiding their dispersion to other regions of the body. This study focused its applicability in the bone regeneration field, but we believe that such kind of complex hierarchical systems able to encapsulate multi-phenotypic cells could find important applications in other TE strategies, such as closed devices to be used in drug screening or disease models.

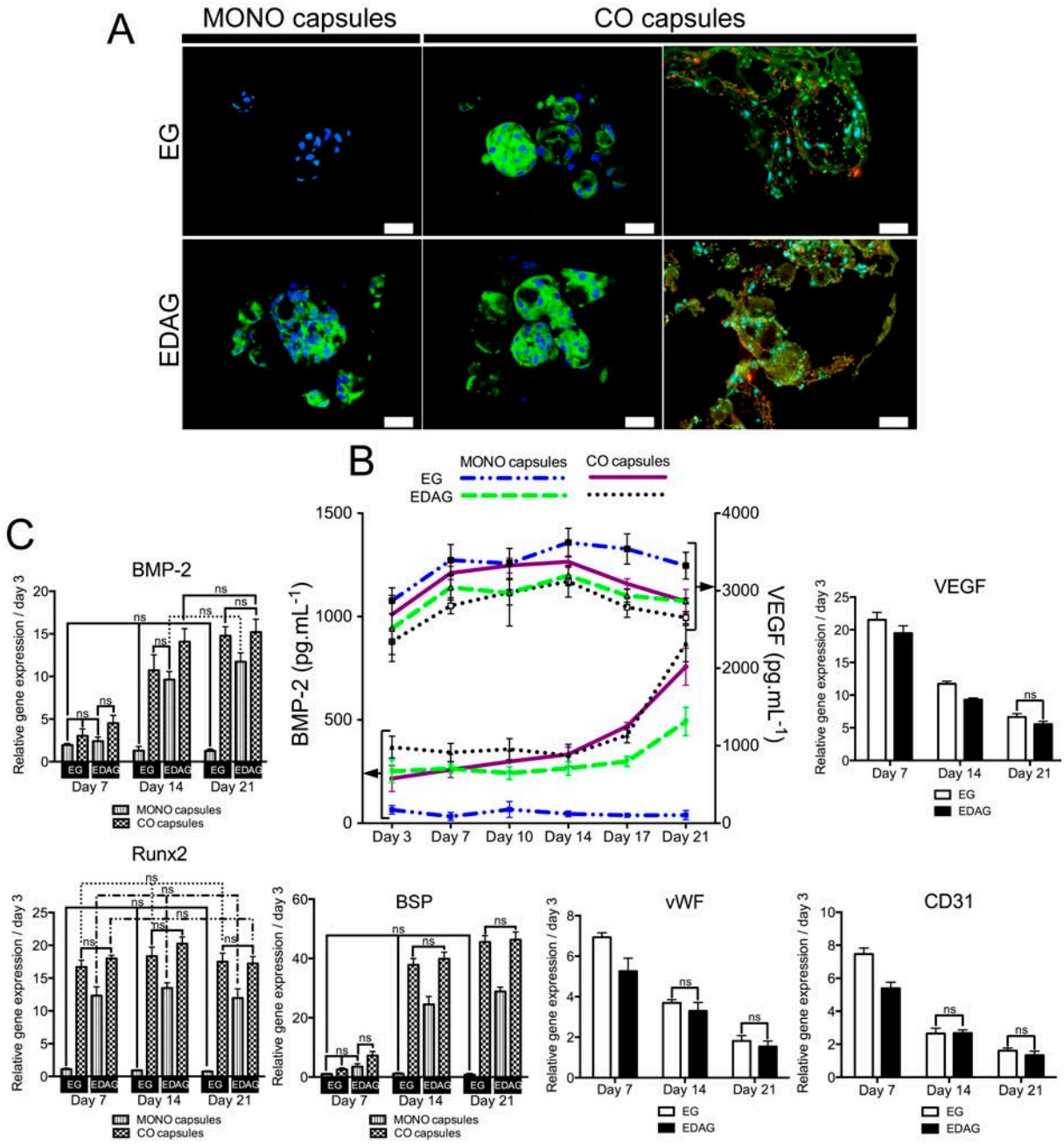

Figure VI.4 - (A) Immunofluorescence of osteopontin (green) in MONO and CO capsules cultured in EG and EDAG media after 21 days of culture. Cells nuclei were counterstained with DAPI (blue). To visualize the encapsulated ECs, CD31 (red) was identified by immunofluorescence staining in histological sections of CO capsules cultured for 21 days. Scale bar is 50 µm. **(B)** Quantification of BMP-2 and VEGF release by ELISA. **(C)** Relative expression of osteogenic (*BMP-2, RUNX2, and BSP*) and angiogenic (*VEGF, CD31*, and *vWF*) markers up to 21 days. All results were significantly different unless marked with ns ($p > 0.05$).

4. Conclusion

Inspired by the local interactions at the molecular level from the co-existence of stem and vascular cells in the native environment of bone, we developed a stem-cell based bioencapsulation strategy. The co-encapsulation of stem and endothelial cells, both derived from adipose tissue, within a single hierarchical structure proved to be an effective strategy for the *in vitro* osteogenic differentiation. Overall, the co-encapsulation of ECs lead ASCs to differentiate into the osteogenic lineage inside the liquified and multilayered capsules with microparticles, even in the absence of two major osteogenic differentiation factors, namely dexamethasone and ascorbic acid. Additionally, CO capsules released BMP-2 and VEGF, which evidences the potential of the capsules as a cytokine delivery system. We believe that the developed co-encapsulation strategy represents a ground-breaking advance in the engineering of 3D compartmentalized devices that aim to control the cascade of biological processes and lead to faster high-quality new tissue formation with minimum cell manipulation.

Acknowledgements

The authors acknowledge the financial support by the Portuguese Foundation for Science and Technology (FCT) through the Ph.D. (SFRH/BD/69529/2010-Clara R. Correia). This work was also supported by European Research Council grant agreement ERC-2014-ADG-669858 for project ATLAS.

Supplementary information

Table VI.SI – Primer sequences used for real-time polymerase chain reaction.

Type	Name	Forward/reverse sequence
Housekeeping	18S	5'-GAAACCTTCCGACCCCTCTC-3' 5'-TACGAGGTCGATTTGGCGAG-3'
Osteogenic markers	BMP-2	5'-TGAATCAGAATGCAAGCAGG-3' 5'-TCTTTTGTGGAGAGGATGCC-3'
	RUNX2	5'-TTCCAGACCAGCAGCACTC-3' 5'-CAGCGTCAACACCATCATTC-3'
	BSP	5'- ACTGAGCCTGTGTCTTGAAA-3' 5'-CTTCCAACAGCCAATCACTG-3'
Angiogenic markers	vWF	5'-CCCTGGGTACAAGGAAGAAAAT-3' 5'-AGTGTCATGATCTGTCTCCTCTTAG-3'
	CD31	5'-AAGGCCAGATGCACATCC-3' 5'-TTCTACCCAACATTAACTTAGCAGG-3'
	VEGF-A	5'- GATCCGCAGACGTGTAAATG-3' 5'-TACGAGGTCGATTTGGCGAG-3'

References

[1] J.F. Mano, Designing biomaterials for tissue engineering based on the deconstruction of the native cellular environment, Mater. Lett., 141 (2015) 198-202.

[2] S. Mendez-Ferrer, T.V. Michurina, F. Ferraro, A.R. Mazloom, B. D. MacArthur, S.A. Lira, D.T. Scadden, A. Ma'ayan, G.N. Enikolopov, P.S. Frenette, Mesenchymal and haematopoietic stem cells form a unique bone marrow niche, Nature, 466 (2010) 829-834.

[3] P. Bianco, Bone and the hematopoietic niche: A tale of two stem cells, Blood, 117 (2011) 5281-5288.

[4] E. Dohle, I. Bischoff, T. Böse, A. Marsano, A. Banfi, R.E. Unger, C.J. Kirkpatrick, Macrophage-mediated angiogenic activation of outgrowth endothelial cells in co-culture with primary osteoblasts, Eur. Cells Mater., 27 (2014) 149-165 (2014).

[5] K.G. Battiston, J.W. Cheung, D. Jain, J.P. Santerre, Biomaterials in co-culture systems: Towards optimizing tissue integration and cell signaling within scaffolds, Biomaterials, 35 (2014) 4465-4476.

[6] J. Kim, H.N. Kim, K.-T. Lim, Y. Kim, S. Pandev, P. Garg, Y.-H. Choung, P.-H. Choung, K.-Y. Suh, J.H. Chung, Synergistic effects of nanotopography and co-culture with endothelial cells on osteogenesis of mesenchymal stem cells, Biomaterials, 34 (2013) 7257-7268.
[7] R.P. Pirraco, T. Iwata, T. Yoshida, A.P. Marques, M. Yamato, R.L. Reis, T. Okano, Endothelial cells enhance the in vivo bone-forming ability of osteogenic cell sheets, Lab. Invest., 94 (2014) 663-673.
[8] M. Grellier, P.L. Granja, J.-C. Fricain, S.J. Bidarra, M. Renard, R. Bareille, C. Bourget, J. Amédée, M.A. Barbosa, The effect of the co-immobilization of human osteoprogenitors and endothelial cells within alginate microspheres on mineralization in a bone defect, Biomaterials, 30 (2009) 3271-3278.
[9] M.I.Santos, R.E. Unger, R.A. Sousa, R.L. Reis, C.J. Kirkpatrick, Crosstalk between osteoblasts and endothelial cells co-cultured on a polycapro-lactone-starch scaffold and the in vitro development of vascularization, Biomaterials, 30 (2009) 4407-4415.
[10] S.M. Mihaila, M.F. Resende, R.L. Reis, M.E. Gomes, A.P. Marques, Interactive endothelial phenotype maintenance and osteogenic differentiation of adipose tissue stromal vascular fraction SSEA-4^{+}-derived cells, J. Tissue Eng. Regener. Med., DOI:10.1002/term.2096 (2015).
[11] K. Joensuu, L. Uusitalo, J.J. Alm, H.T. Aro, T.A. Hentunen, T.J. Heino Enhanced osteoblastic differentiation and bone formation in co-culture of human bone marrow mesenchymal stromal cells and peripheral blood mononuclear cells with exogenous VEGF, Orthop. Traumatol. Surg. Res., 101 (2015) 381–386.
[12] T.O Pedersen, A.L Blois, Z. Xing, Y. Xue, Y. Sun, A. Finne-Wistrand, L.A. Akslen, J.B. Lorens, K.N. Leknes, I. Fristad, K. Mustafa, Endothelial microvascular networks affect gene-expression profiles and osteogenic potential of tissue-engineered constructs, Stem Cell Res. Ther., 4 (2013) 1-10.
[13] B. Guillotin, C. Bourget, M. Remy-Zolgari, R. Bareille, P. Fernandez, V. Conrad, J. Amédée-Vilamitjana, Human primary endothelial cells stimulate

human osteoprogenitor cell differentiation, Cell Physiol. Biochem., 14 (2004) 325-332.
[14] S.A. Saleh, M. Whyte, P.G. Genever, Effects of endothelial cells on human mesenchymal stem cell activity in a three-dimensional in vitro model, Eur. Cells Mater., 22 (2011) 242-257.
[15] N. B. Thébaud, R. Siadous, R. Bareille, M. Remy, R. Daculsi, J. Amédée, L. Bordenave, Whatever their differentiation status, human progenitor derived – or mature – endothelial cells induce osteoblastic differentiation of bone marrow stromal cells, J. Tissue Eng. Regener. Med., 6 (2012) e51-e60.
[16] S.B. Traphagen, I. Titushkin, S. Sun, K.K. Wary, M. Cho, Endothelial invasive response in a co-culture model with physically-induced osteodifferentiation, J. Tissue Eng. Regener. Med., 7 (2013) 621-630.
[17] J. Leszczynska, B. Zyzynska-Granica, K. Koziak, S. Ruminski, M. Lewandowska-Szumiel, Contribution of endothelial cells to human bone-derived cells expansion in coculture, Tissue Eng. Part A, 19 (2013) 393-402.
[18] E.A. Neofytou, E. Chang, B. Patlola, L.-M. Joubert, J. Rajadas, S.S. Gambhir, Z. Cheng, R.C. Robbins, R.E. Beygui, Adipose tissue-derived stem cells display a proangiogenic phenotype on 3D scaffolds, J. Biomed. Mater. Res. Part A, 98 (2011) 383-393.
[19] R.P. Pirraco, B. Melo-Ferreira, T.C. Santos, A.M. Frias, A.P. Marques, R.L. Reis, Adipose stem cell-derived osteoblasts sustain the functionality of endothelial progenitors from the mononuclear fraction of umbilical cord blood, Acta Biomater., 9 (2013) 5234-5242.
[20] E. Tumarkin, L. Tzadu, E. Csaszar, M. Seo, H. Zhang, A. Lee, R. Peerani, K. Purpura, P.w. Zandstra, E. Kumacheva, High-throughput combinatorial cell co-culture using microfluidics, Integr. Biol., 3 (2011) 653-662.
[21] D.Y. Ko, U.P. Shinde, B. Yeon, B. Jeong, Recent progress of in situ formed gels for biomedical applications, Prog. Polym Sci., 38 (2013) 672-701.

[22] C.R. Correia, P. Sher, R.L. Reis, J.F. Mano, Liquified chitosan–alginate multilayer capsules incorporating poly(L-lactic acid) microparticles as cell carriers, Soft Matter, 9 (2013) 2125-2130.
[23] C.R. Correia, R.L. Reis, J.F. Mano, Multilayered hierarchical capsules providing cell adhesion sites, Biomacromolecules, 14 (2013) 743-751.
[24] J. Borges, J.F. Mano, Molecular interactions driving the layer-by-layer assembly of multilayers, Chem. Rev., 11 (2014) 8883-8942.
[25] L.V. Rodriguez, Z. Alfonso, R. Zhang, J. Leung, B. Wu, L.J. Ignarro, Clonogenic multipotent stem cells in human adipose tissue differentiate into functional smooth muscle cells, Proc. Natl. Acad. Sci. U. S. A., 103 (2006) 12167-12172.
[26] W.L. Grayson, B.A. Bunnell, E. Martin, T. Frazier, B.P. Hung, J.M. Gimble, Stromal cells and stem cells in clinical bone regeneration, Nat. Rev. Endocrinol., 11 (2015) 140-150.
[27] B.T Estes, B.O. Diekman, J.M. Gimble, F. Guilak, Isolation of adipose-derived stem cells and their induction to a chondrogenic phenotype, Nat. Protoc., 5 (2010) 1294-1311.
[28] J.M. Gimble, A.J., Katz, B.A. Bunnell, Adipose-derived stem cells for regenerative medicine, Circ. Res., 100 (2007) 1249-1260.
[29] P.A. Zuk, M. Zhu, P. Ashjian, D.A. De Ugarte, J.I. Huang, H. Mizuno, Z.C. Alfonso, J.K. Fraser, P. Benhaim. M.H. Hedrick, Human adipose tissue is a source of multipotent stem cells, Mol. Biol. Cell, 13 (2002) 4279-4295.
[30] M.T. Cerqueira, L.P. da Silva, T.C. Santos, R.P. Pirraco, V.M. Correlo, R.L. Reis, A.P. Marques, Gellan gum-hyaluronic acid spongy-like hydrogels and cells from adipose tissue synergize promoting neoskin vascularization, ACS Appl. Mater. Interfaces, 6 (2014) 19668-19679.
[31] J.P. van Straalen, E. Sanders, M.F. Prummel, G.T.B. Sanders, Bone-alkaline phosphatase as indicator of bone formation, Clin. Chim. Acta, 20 (1991) 27-33.

[32] J. Liu, H.K. Nam, C. Campbell, K.C. da Silva Gasque, J.L. Millán, N.E. Hatch, Tissue-nonspecific alkaline phosphatase deficiency causes abnormal craniofacial bone development in the Alpl$^{-/-}$ mouse model of infantile hypophosphatasia, Bone, 67 (2014) 81-94.
[33] L.M. Grover, A.J. Wright, U. Gbureck, A. Bolarinwa, J. Song, Y. Liu, D.F. Farrar, G. Howling, J. Rose, J.E. Barralet, The effect of amorphous pyrophosphate on calcium phosphate cement resorption and bone generation, Biomaterials, 34 (2013) 6631-6637.
[34] K.A.Simon, K.M. Park, B. Mosadegh, A.B. Subramaniam, A.D. Mazzeo, P.M. Ngo, G.M. Whitsides, Polymer-based mesh as supports for multi-layered 3D cell culture and assays, Biomaterials, 35 (2014) 259-268.
[35] R.R. Costa, J.F. Mano, Polyelectrolyte multilayered assemblies in biomedical technologies, Chem. Soc. Rev., 43 (2014) 3453-3479.
[36] J.M. Silva, A.R.C. Duarte, S.G. Caridade, C. Picart, R.L. Reis, J.F. Mano, Tailored freestanding multilayered membranes based on chitosan and alginate, Biomacromolecules, 15 (2014) 3817-3826.
[37] J.H. Kang, J.M. Gimble, D.L. Kaplan, In vitro 3D model for human vascularized adipose tissue, Tissue Eng. Part A, 15 (2009) 2227-2236.
[38] F. Verseijden, H. Jahr, S.J. Posthumus-van Sluijs, T.L.T. Hagen, S.E.R. Hovius, A.L.B. Seynhaeve, J.W. van Neck, G.J.V.M. van Osch, S.O.P. Hofer, Angiogenic capacity of human adipose-derived stromal cells during adipogenic differentiation: An in vitro study, Tissue Eng. Part A, 15 (2009) 445-452.
[39] J. Rehman, D. Traktuev, J. Li, S. Merfeld-Clauss, C.J. Temm-Grove, J.E. Bovenkerk, C.L. Pell, B.H. Johnstone, R.V. Considine, K.L. March, Secretion of angiogenic and antiapoptotic factors by human adipose stromal cells, Circulation, 109 (2004) 1292-1298.
[40] J. Wang, Y. Ye, H. Tian, S. Yang, X. Jin, W. Tong, Y. Zhang, In vitro osteogenesis of human adipose-derived stem cells by coculture with human umbilical vein endothelial cells, Biochem. Biophys. Res. Commun., 412 (2011) 143-149.

[41] J. Rouwkema, J. de Boer, C.A. van Blitterswijk, Endothelial cells assemble into a 3-dimensional prevascular network in a bone tissue engineering construct, Tissue Eng., 12 (2006) 2685-2693.
[42] D.P.E. Herzog, E. Dohle, I. Bischoff, C.J. Kirkpatrick, Cell communication in a coculture system consisting of outgrowth endothelial cells and primary osteoblasts, BioMed Res. Int., 320123 (2014) 1-15.
[43] S. Fuchs, S. Ghanaati, C. Orth, M. Barbeck, M. Kolbe, A. Hofmann, M. Eblenkamp, M. Gomes, R.L. Reis, C.J. Kirkpatrick, Contribution of outgrowth endothelial cells from human peripheral blood on in vivo vascularization of bone tissue engineered constructs based on starch polycaprolactone scaffolds, Biomaterials, 30 (2009) 526-534.
[44] Y. Kang, S. Kim, M. Fahrenholtz, A. Khademhosseini, Y. Yang, Osteogenic and angiogenic potentials of monocultured and co-cultured human-bone-marrow-derived mesenchymal stem cells and human-umbilical-vein endothelial cells on three-dimensional porous beta-tricalcium phosphate scaffold, Acta Biomater., 9 (2013) 4906-4915.
[45] A.I. Hoch, B.Y. Binder, D.C. Genetos, J.K. Leach, Differentiation-dependent secretion of proangiogenic factors by mesenchymal stem cells, PloS One, 7 (2012) e35579.
[46] B. Behr, C. Tang, G. Germann, M.T. Longaker, N. Quarto, Locally applied vascular endothelial growth factor a increases the osteogenic healing capacity of human adipose-derived stem cells by promoting osteogenic and endothelial differentiation, Stem Cells, 29 (2011) 286-296.
[47] P.J. Bouletreau, S.M. Warren, J.A. Spector, Z.M. Peled, R.P. Gerrets, J.A. Greenwald, M.T. Longaker, Hypoxia and VEGF up-regulate BMP-2 mRNA and protein expression in microvascular endothelial cells: Implications for fracture healing, Plast. Reconstr. Surg., 109 (2002) 2384-2397.

Chapter VII

In vivo osteogenic differentiation of stem cells inside compartmentalized capsules loaded with co-cultured endothelial cells and microparticles [7]

Abstract

The regeneration of tissues through ready-to-use tissue engineering strategies requiring minimum *in vitro* manipulation is highly desirable. Here we show that by using a hierarchically engineered bioencapsulation system, self-regulated mineralized tissue could be generated *in vivo*. Capsules coated with nanostratified multilayered polyelectrolytes compose the proposed system, encapsulating adipose stem (ASCs) and endothelial cells (ECs) and surface modified microparticles. Microparticles and cells are freely dispersed in a liquified core, responsible to maximize the diffusion of essential molecules and allowing the geometrical freedom for the autonomous three-dimensional (3D) organization of cells. While the membrane wraps all the instructive cargo elements within a single structure, the microparticles provide a solid 3D substrate for the encapsulated cells. Our hypothesis is that inside this isolated biomimetic 3D environment, ECs would lead ASCs to differentiate into the osteogenic lineage to ultimately generate a mineralized tissue *in vivo*. To test our system, capsules encapsulating only ASCs (MONO capsules) or ASCs and ECs (CO capsules) were subcutaneously implanted in nude mice up to 6 weeks. Two implantation strategies were tested, namely capsules implanted immediately after production or after 21 days of *in vitro* osteogenic stimulation. Results show that all the implanted capsules were biotolerable, and no signs of necrosis or a severe infiltration of inflammatory cells were detectable. Of note, the most valuable outcome of the present study is the mineralized tissue in CO capsules without *in vitro* pre-differentiation, which occurred at similar levels compared to the pre-differentiated capsules *in vitro*. We believe that the proposed bioencapsulation strategy is a potent self-regulated system, which might find great applicability in bone tissue engineering.

[7] Based on the publication: C.R. Correia, T.C. Santos, R.P. Pirraco, M.T. Cerqueira, A.P. Marques, R.L. Reis, J.F. Mano, *In vivo* osteogenic differentiation of stem cells inside compartmentalized capsules loaded with co-cultured endothelial cells and microparticles (*submitted*).

1. Introduction

The regeneration of large bone defects remains a major concern in the orthopedic field. To avoid the potential disadvantages of autografts and allografts, namely their limited supply and disease transmission potential [1], engineered bone constructs have been proposed as promising alternatives in clinical applications. Donor-site morbidity associated to cell isolation (both osteoblasts or bone marrow-derived mesenchymal stem cells) and limited proliferative capacity of primary osteoblasts are major challenges in providing adequate numbers for transplantation [2, 3]. In addition to bone marrow, adipose tissue has been identified as a source of multipotent cells that due to the capacity to differentiate into adipogenic, chondrogenic, myogenic, and osteogenic lineages are seen as promising for tissue regeneration [4, 5]. Moreover, adipose tissue is often available in an abundant quantity after a relatively easy harvesting. However, controlling mesenchymal differentiation and engineering bone *in vivo* are challenging accomplishments, as it often leads to heterotypic and inferior osseous tissues. Additionally, when osteogenesis is aimed at, angiogenesis must be considered since it plays an important role during the development and maturation of bone [6, 7]. The induction of orchestrated osteo- and angiogenesis by biochemical stimulation [8, 9] or by co-culturing osteoprogenitor and endothelial cells [10-13] has been shown to better induce bone tissue formation, as well as to improve survival of the engineered tissues. Particularly, considering native bone vascular network, osteoprogenitor cells inevitably interact with endothelial cells (ECs) in a synergetic fashion [14, 15]. While endothelial cells secrete numerous regulatory molecules that influence the differentiation and activity of bone forming cells [16-19], osteoprogenitor cells release diverse pro-angiogenic growth factors [11, 13, 20, 21]. To mimic such concept, one could envisage the *in vitro* development of a single reservoir that contain instructive signals to, upon implantation, generate bone-like tissues. In this context, we propose a novel bioencapsulation strategy whose *in vivo* performance is assessed for the first time. With this work we expect to highlight the potential of liquified and

multilayered capsules as an alternative methodology to the commonly used 3D porous structures/hydrogels for TE. For that, mesenchymal stem and endothelial cells were both isolated from the adipose tissue and co-cultured within liquified and multilayered capsules. Following multi-scale assembling strategies [22], the capsules are composed by three essential components: *(i)* a permselective nanostructured membrane that wraps the liquefied core of the capsule ensuring permeability to essential molecules for cell survival, and the creation of a single reservoir to facilitate the implantation procedure of multiple components; *(ii)* poly(L-lactic acid) (PLLA) microparticles surface functionalized with plasma treatment and collagen I that create a 3D microenvironment for the encapsulated cell and act as cell adhesion sites; and *(iii)* adipose stem (ASCs) and endothelial (ECs) cells. The membrane was produced by layer-by-layer (LbL) technique, which is a versatile, low-cost technique, and more importantly for bioencapsulation systems, can be performed under mild conditions [23, 24]. We hypothesized that within the controlled environment of capsules, endothelial cells would promote the osteogenic differentiation of ASCs due to their specific crosstalk, leading to the formation of a mineralized tissue *in vivo.* The design of the experiment is represented in **Scheme VII.1**. Capsules containing only ASCs (MONO capsules) or ASCs and ECs (CO capsules) were produced 21 days before the implantation (day -21), and subsequently cultured in osteogenic differentiation medium to stimulate *in vitro* the differentiation of the ASCs. At the day of implantation (day 0), the production of MONO and CO capsules was repeated. Additionally, capsules without encapsulated cells (MATERIAL) were also produced. All the produced capsules, i.e. after 21 days of *in vitro* osteogenic stimulation or freshly prepared, were subcutaneously implanted in nude mice up to 6 weeks. Three capsules of the same formulation were implanted at each pocket (**Scheme VII.1A**). At predetermined intervals, the implants, which could be macroscopically identified (**Scheme VII.1B**), were retrieved for histological analysis.

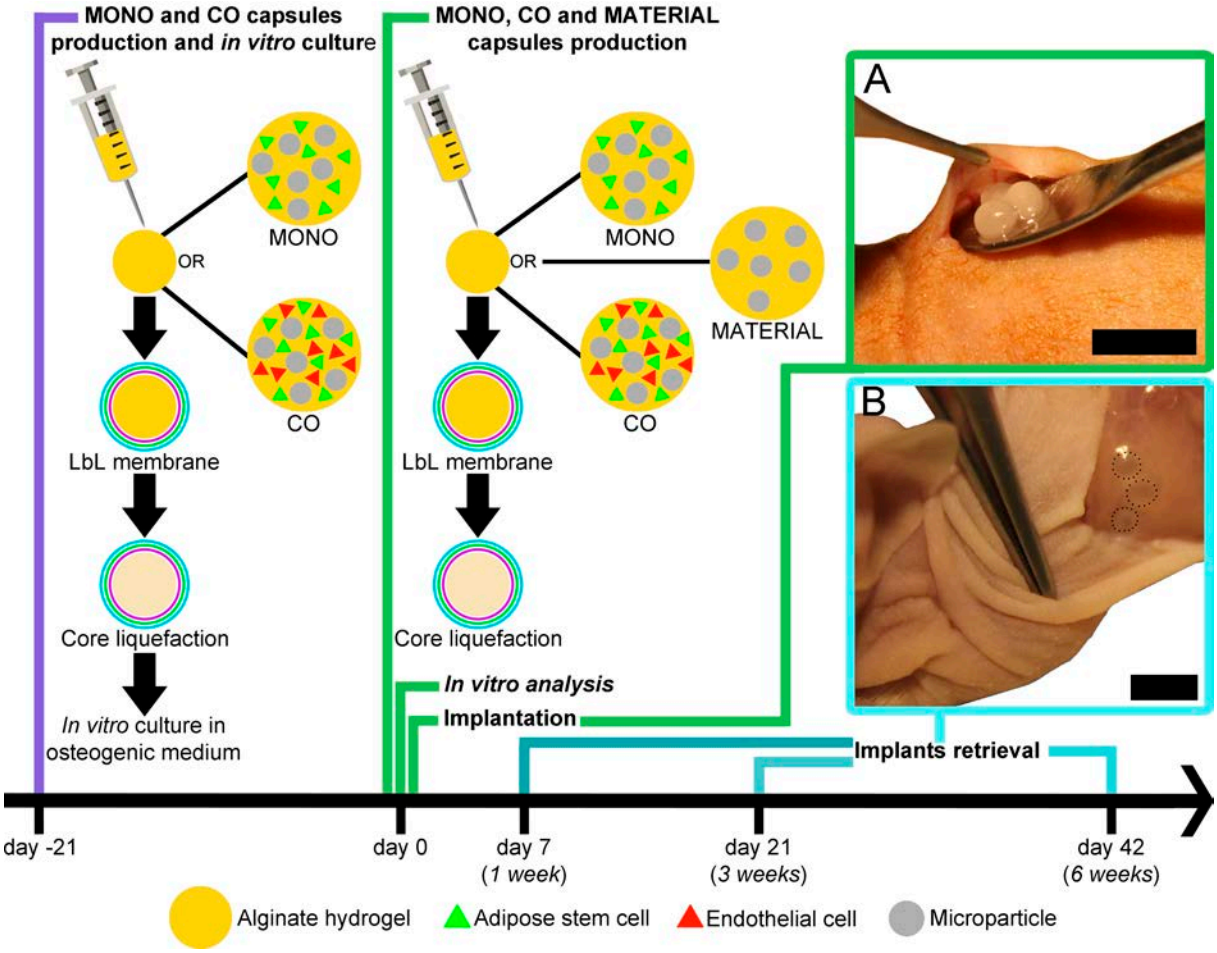

Scheme VII.1. Schematic representation of the experimental design. Capsules encapsulating only adipose stem cells (MONO capsules) or adipose stem cells and endothelial cells (CO capsules) were produced (day -21) and cultured *in vitro* in osteogenic differentiation medium for 21 days. At the day of implantation (day 0), MONO, CO and capsules without cells (MATERIAL) were freshly prepared. Capsules were implanted in nude mice up to 6 weeks. **(A)** Three capsules of the same formulation were implanted at each pocket. Scale bar is 1 cm. **(B)** After 1, 3, and 6 weeks, implants were retrieved. The localization of the implanted capsules could be macroscopically visualized. Scale bar is 1 cm.

2. Materials and methods

2.1 Cells isolation

Subcutaneous adipose tissue from liposuction procedures was used to isolate both human ASCs [25] and human ECs [26]. The collected tissues were obtained under a cooperation agreement between the 3B's Research Group and Hospital da Prelada (Porto, Portugal), after approval of the respective

ethical committees. Patient's informed consent and anonymity were assured. Samples were transported in phosphate-buffered saline (PBS, Sigma-Aldrich) supplemented with penicillin-streptomycin (10%, pen-strep, Gibco) and kept at 4°C for a maximum of 24 h. Lipoaspirates were washed with PBS and incubated with collagenase type II A (0.05% w/v, Sigma-Aldrich) for 45 minutes at 37°C in a shaking water bath. The digested samples were filtered (200 µm) and centrifuged at 800 g for 10 min at 4°C. The obtained stromal vascular fraction (SVF) was resuspended in erythrocyte lysis buffer at pH 7.4 containing ammonium chloride (155 mM, Merk), potassium bicarbonate (5.7 mM, Riedel-de-Häen), and ethylenediaminetetraacetic acid (0.1 M, EDTA, Sigma-Aldrich) in distilled water. After 10 min of incubation at room temperature (RT), the mixture was centrifuged at 300 g for 5 minutes. To obtain the ASCs cultures, the red blood cell-free SVF was resuspended in α-MEM medium (Invitrogen) supplemented with fetal bovine serum (10%, FBS, Invitrogen) and pen-strep (1% v/v). The ECs cultures were obtained from the red blood cell-free SVF that was resuspended in EndoGro^{TM}-MV-VEGF complete media kit (Millipore Iberica). ECs were plated in cell culture flasks, previously coated with gelatin (0.7% w/v, porcine skin type A, Sigma-Aldrich) for 30 min at 37°C. Culture medium was changed 48 h after initial plating and then every 3-4 days for both cell phenotypes.

2.2 Microparticles production and surface functionalization

Poly(L-lactic acid) microparticles (µPLLAs) were produced by an oil/water (o/w) emulsion technique and surface modified with collagen I after plasma treatment as similarly in our previous reports [27, 28]. Briefly, PLLA (5% w/v, M_w~1,600-2,400, 70% crystallinity, Polysciences) was dissolved in methylene chloride (CH_2Cl_2, Fisher Chemical). Under agitation, this solution was added to polyvinyl alcohol (0.5%, PVA, Sigma-Aldrich). After 2 days at RT, the produced µPLLAs were subsequently collected, washed with distilled water, and lyophilized (Cryodos, Telstar) for 3 days. Microparticles were then placed in a

plasma reactor chamber (PlasmaPrep5, Gala Instrumente) fitted with a radio frequency generator. Air was used as the working atmosphere. A glow discharge plasma (0.2 mbar, 30 V) was created for 15 min. Subsequently, microparticles (500 mg) were immersed for 4 h at RT in collagen I solution (1200 µg, rat protein tail, Gibco).

2.3 Mono- and co-cultures set up

Sodium alginate (1.5% w/v, ALG, ~250 cP, low viscosity from brown algae, Sigma-Aldrich) was dissolved in sodium chloride (0.15 M, NaCl, Enzymatic) buffered at pH 7 with MES hydrate (25 mM, Sigma-Aldrich). The solution was sterilized by 0.22 µm filtration prior mixing with the cells. At 90% confluence, ASCs (passage 2) and ECs (passage 4-6) were detached using TrypLE™ Express solution (Life Technologies) at 37°C for 5 min. PBS was added and the cell suspensions were centrifuged for 5 min at 300 g. Cells (ASCs alone or mixed with ECs, 1:1 ratio) resuspended in the alginate solution ($5x10^6$ cells per mL of alginate) were added to the microparticles (50 $mg.mL^{-1}$ of alginate) and then used to produce liquified capsules containing ASCs alone (MONO capsules) or in co-culture with ECs (CO capsules).

2.4 Liquified multilayered capsules production

All the conditions used to produce liquified capsules (the combination of the polyelectrolytes, concentration, pH, number of layers, and time of adsorption and liquefaction) were optimized in our previous studies [27, 28]. Briefly, alginate solutions containing cells were added drop wise using a 21 G needle to a calcium chloride solution (0.1 M, $CaCl_2$, VWR) buffered at pH 7 with MES hydrate (25 mM, Sigma-Aldrich). After 20 min at RT, alginate hydrogel particles were collected and rinsed in a washing solution of NaCl (0.15 M). The external membrane was processed by layer-by-layer adsorption. Hydrogel particles were subsequently immersed in poly-L-lysine (PLL, M_w ~ 30,000-70,000, pH 7, Sigma-Aldrich), ALG solution (pH 7), chitosan (CHT, pH 6, water-soluble highly purified, viscosity 107 mPa.s, M_w = $2.7x10^5$ $g.mol^{-1}$, 83%

degree of deacetylation, Protasan UP CL 213, NovaMatrix), and, ultimately, in ALG solution again. All the polyelectrolyte solutions (0.5 $mg.mL^{-1}$) were prepared in NaCl (0.15 M) containing MES hydrate (25 mM). Following a 10 min adsorption period for each polymer, the excess of macromolecules was removed by immersion in NaCl (0.15 M) for 5 min. This process was repeated three times in order to obtain a 12-layered membrane. Coated hydrogel particles were immersed in EDTA (20 mM) at pH 7 for 5 min to liquefy the alginate core. To induce osteogenic differentiation *in vitro*, MONO and CO capsules were cultured for 21 days in supplemented medium composed by complete EndoGro™-MV-VEGF medium supplemented with β-glycerophosphate (10 mM, Sigma-Aldrich), ascorbic acid (50 $\mu g.mL^{-1}$), and dexamethasone (10 nM, Sigma-Aldrich).

2.5 *In vitro* analysis

2.5.1 Lipophilic fluorescent labeling

Prior encapsulation, ASCs and ECs were incubated with lipophilic dyes, namely *3,3′*-dioctadecyloxacarbocyanine perchlorate (DIO, green) and *1,1′*-dioctadecyl-*3,3,3′,3′*-tetramethylindocarbocyanine perchlorate (DIL, red), respectively. Cells were incubated with each dye (1 mL, 2 μM per $1x10^6$ cells) at 37 °C for 10 min. Then, MONO and CO capsules were produced as previously described encapsulating fluorescently labeled cells. Capsules were visualized by fluorescence microscopy (Axio Imager Z1m, Zeiss).

2.5.2 DNA and alkaline phosphatase (ALP) activity quantification

MONO and CO capsules cultured in osteogenic differentiation medium for 21 days were analyzed after cell lysis for DNA amount and ALP activity. Four capsules per well were suspended in 1 mL of ultra-pure water. After 1 h in a 37°C shaking water bath, the solutions were frozen at -80°C overnight. Samples were defrosted and used according to the specifications of the kit

(Quant-iT™ PicoGreen® dsDNA assay kit, Life Technologies). A standard curve was generated with the provided dsDNA solution. After 10 min of incubation at RT, fluorescence was read at an excitation wavelength of 485/20 nm and 528/20 nm of emission using a microplate reader (Gen 5 2.01, Synergy HT, Biotek). Then, the activity of ALP in the remaining solutions was quantified. Briefly, a substrate solution (pH 9.8) was prepared by dissolving *4*-nitrophenylphosphate disodium salt hexahydrate (0.2% w/v, Sigma-Aldrich) in diethanolamine (1 M, Sigma-Aldrich). Each sample (20 µL) was mixed with the prepared substrate solution (60 µL). After 45 min at 37°C protected from light, the reaction was stopped with 80 µL of a NaOH (2 M) and EDTA (0.2 mM) solution. A standard curve was prepared with diluted series of *4*-nitrophenol solution (10 mM, Sigma-Aldrich). Absorbance was read at 405 nm in a microplate reader (Gen 5 2.01, Synergy HT, Biotek). ALP activity results were normalized with dsDNA quantification data of MONO capsules.

2.5.3 Mineralization analysis

MONO and CO capsules cultured in osteogenic differentiation medium for 21 days were washed in PBS, and processed in an automatic spin tissue processor (STP120-2, Microm) for histological analysis. Samples were embedded in paraffin and cut into sections of 5 µm thickness using a microtome (HM355S, Microm). To visualize calcium-rich deposits, sections were deparaffinized and subsequently immersed in alizarin red staining solution for 5 min at RT. Samples were then mounted and analyzed by microscopy (Axio Imager Z1m, Zeiss).

2.6 Animals surgery, euthanasia, and implants retrieval

The animal experimentation project was approved by the institutional Animal Welfare Body (SECVS 032/2015) and the National Authority Direção Geral de Alimentação e Veterinária. Five week-old male nude mice (average weight of 25 g) were used to subcutaneously implant MONO and CO capsules, either freshly prepared or after 21 days *in vitro* in osteogenic differentiation medium, and

capsules without encapsulated cells (MATERIAL). Four mice were used for each formulation and at each timepoint (1, 3, and 6 weeks). Under surgical sterile conditions, animals were anaesthetized with an intraperitoneal injection of a mixture of ketamine (75 $mg.kg^{-1}$, Imalgene®, Merial) and metedomidine (1 $mg.kg^{-1}$, Domitor®, Orion). One medial incision of approximately 0.7 cm was performed in the dorsum of the mice and two craniolateral-oriented pockets were subcutaneously created by blunt dissection. Three capsules were inserted into each pocket. Pockets without capsules were also used as control (EMPTY). Subsequently, the *panniculus carnosus* and the skin were carefully sutured with non-resorbable 4/0 sutures. After the surgical procedure, the animals were induced to recover from anaesthesia with an intraperitoneal injection of Atipazemol (1 $mg.kg^{-1}$, Antisedan, Orion). The animals were kept housed together (different conditions in each cage) with standard diet and water *ad libitum* during all the time of the experiment. After 1, 3, and 6 weeks of implantation, the animals were sacrificed by carbon dioxide inhalation. The implanted capsules and the respective surrounding tissue were explanted from each animal. The collected explants were subjected to macroscopic observation and fixed in 10% formalin for 24 h at RT. Samples were then processed for standard histological evaluation.

2.7 *In vivo* histological analysis

The explants were processed in an automatic ethanol-xylene spin tissue processor (STP120-2, Microm) and then embedded in paraffin. Histological sections (5 µm) were obtained using a microtome (HM355S, Microm, ThermoFisher Scientific). Before each histological staining, the sections were automatically deparaffinized and rehydrated (HMS740, Microm, ThermoFisher Scientific). After each staining protocol, unless otherwise specified, the sections were immediately dehydrated and immersed in xylene, before being mounted (Entellan, Millipore). Ultimately, the stained sections were visualized with Axio Imager Z1m (Zeiss).

2.7.1 Hematoxylin and eosin (H&E) staining

The samples for H&E staining protocol were automatically processed (HMS740, Microm, ThermoFisher Scientific). Briefly, histological sections were subsequently immersed in hematoxylin (BioOptica) and after bluing in an ammonia solution (1% v/v), in eosin y (BioOptica).

2.7.2 CD31 immunohistochemistry

Antigen retrieval was performed in heat-mediated (95-100ºC) sodium citrate buffer (10 mM, Sigma-Aldrich) for 20 min. After cool down for 20 min, endogenous peroxidases were inactivated with hydrogen peroxide (3% v/v, AnalaR Normapur) and non-specific binding blocked with horse serum incubation (2.5% NHS, Vectastain Universal Quick Kit, Vector Laboratories) for 30 min at RT. The sections were incubated with the primary antibody rabbit polyclonal anti-human to CD31 (1:50 diluted in PBS with NHS, abcam) in a humidified chamber at 4ºC overnight. The second antibody (Vectastain Universal Quick Kit, Vector Laboratories) was added for 1 h at RT, and the stained revealed with a DAB solution prepared according to manufacturer's specifications (Vectastain Universal Quick Kit, Vector Laboratories). Sections were counterstained with hematoxylin (BioOptica) before microscopic analysis.

2.7.3 Masson's trichrome staining

Sections were stained for 5 min in a solution containing azure B (0.5 g, Sigma-Aldrich), ammonium iron (5 g, ammonium iron sulfate (III) dodecahydrate, Millipore) and distilled water (100 mL). Sections were then subsequently stained with hematoxylin (BioOptica) and picric ethanol (1% w/v, Sigma-Aldrich) for 5 min each. After 10 min washing in running tap water, sections were stained with the solutions from the Trichrome Stain Masson kit (Sigma-Aldrich) according to the manufacturer's specifications.

2.7.4 Osteopontin immunofluorescence

The antigen retrieval was performed in a heat-mediated sodium citrate buffer (10 mM, Sigma-Aldrich). Non-specific binding was blocked by immersion in BSA (3% w/v) for 30 min at RT. Samples were then incubated overnight at 4°C with the primary antibody rabbit anti-human osteopontin (1:100 in 1% BSA, abcam). After a PBS washing, samples were incubated for 1 h at RT with the secondary antibody anti-rabbit AlexaFluor 488 (1:500 in 1% BSA, Molecular Probes). Samples incubated only with the secondary antibody were used as controls. Ultimately, samples were subsequently counterstained with DAPI (1 $mg.mL^{-1}$ diluted 1:1000 in PBS, Sigma-Aldrich) for 5 min at RT, immediately mounted (Permafluor, ThermoFisher Scientific), and analyzed by fluorescence microscopy (Axio Imager Z1m, Zeiss).

2.7.5 Alizarin red staining

To assess the presence of calcium-rich deposits (red), the sections were immersed in alizarin red solution (2% w/v, Sigma-Aldrich) for 5 min at RT.

2.8 Statistical analysis

All the results were expressed as mean ± standard deviation. Significant differences between the different groups were identified by one-way ANOVA using the *post-hoc* Tukey's with multiple comparison tests.

3. Results

3.1 I*n vitro* evaluation of the capsules

Prior implantation, ASCs and ECs were fluorescently marked with lipophilic dyes. Cells were then encapsulated in MONO (**Figure VII.1A**) and CO (**Figure VII.1B**) capsules and visualized by microscopy. In the MONO capsules only green fluorescence corresponding to ASCs could be detected, while in the CO capsules both green and red fluorescence were detected, identifying

respectively ASCs and ECs. After 21 days of culture in osteogenic differentiation medium, the secretion of the late osteogenic marker osteopontin was confirmed in MONO (**Figure VII.1C**) and CO capsules (**Figure VII.1D**). Additionally, mineralization was qualitatively assessed by alizarin red staining (**Figure VII.1E and VII.F**), confirming the deposition of calcium. Ultimately, capsules were tested for DNA quantification (**Figure VII.1G**) and ALP activity (**Figure VII.1H**). As expected, day 0 capsules have the lowest DNA amount compared to day 21 capsules. This indicates that the encapsulated cells in day 21 capsules have proliferated during the *in vitro* culture. Moreover, the efficient encapsulation of the cells was proven by the double amount of DNA detected in the CO capsules that corresponds to the additional and equal amount of endothelial cells used. CO capsules after 21 days of culture continued to present the highest DNA amount, which seems to indicate the absence of deleterious effects of the system. **Figure VII.1H** illustrates the ALP activity normalized per µg DNA of the MONO capsules at day 0 and after 21 days of *in vitro* culture. Again, day 0 capsules have a significant lower ALP activity compared to day 21 capsules since the latter were cultured *in vitro* in supplemented medium to stimulate the osteogenic differentiation of the ASCs. Importantly, CO capsules cultured for 21 days presented the highest ALP activity compared to MONO capsules.

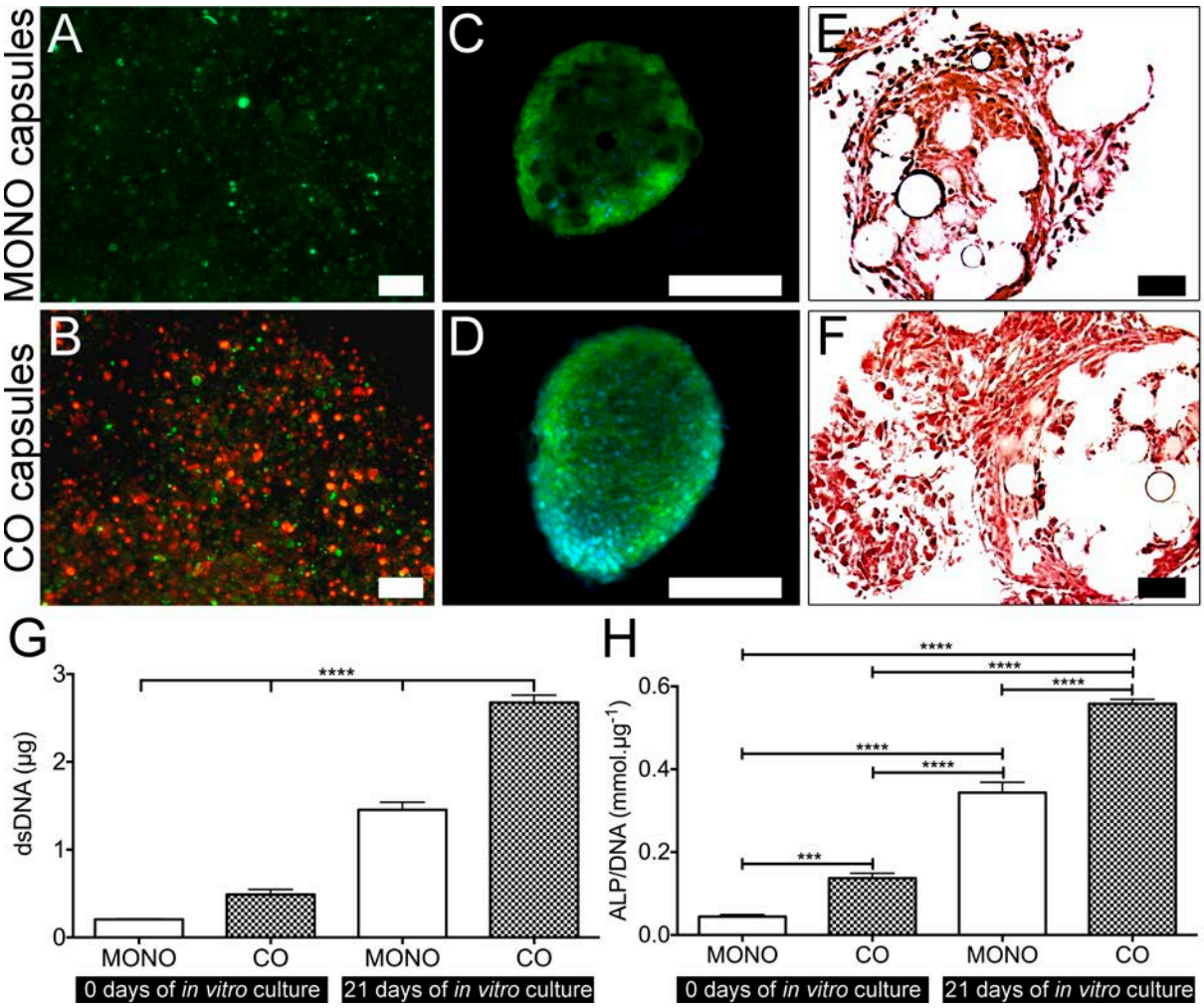

Figure VII.1. **(A)** MONO and **(B)** CO capsules encapsulating cells at day 0 previously labeled with DIO (green, ASCs) and DIL (red, ECs) lipophilic dyes. Scale bar is 200µm. **(C)** Osteopontin immunofluorescence (green) in MONO and **(D)** CO capsules cultured in osteogenic medium for 21 days. Cells nuclei were counterstained with DAPI (blue). Scale bar is 200µm. **(E)** Alizarin red staining on histological sections of MONO and **(F)** CO capsules cultured in osteogenic differentiation medium for 21 days. Calcium deposits were stained in red. Scale bar is 40µm. **(G)** DNA quantification and (H) ALP activity of MONO and CO capsules freshly prepared at the day of implantation (0 days of *in vitro* culture) or after 21 days in osteogenic differentiation medium (21 days of *in vitro* culture).

3.2 *In vivo* histological assessment

3.2.1 Morphological analysis

Histological analysis of explanted samples stained with H&E (**Figure VII.2**) showed good integration of all types of capsules within the surrounding host

tissue. At the first week of implantation, the fragmentation of the layer-by-layer membrane of the capsules and the dispersion of the μPLLAs within the tissue was visible. It seems that the disruption of the membrane occurred gradually since the encapsulation contents, composed by encapsulated cells and microparticles, remained grouped at the site of the implantation. Few inflammatory cells were found in the condition without cells (MATERIAL) up to 6 weeks of implantation, which also showed that the capsules did not elicit a severe infiltration of inflammatory cells. In addition, the histological evaluation with H&E staining also revealed the presence of various blood vessels in MONO and CO capsules against the few vessels that could be observed in MATERIAL capsules. In the empty control (**Figure VII.SI**), the presence of blood vessels could not be detected. After 6 weeks of implantation, immunostaining of CD31 (**Figure VII.3**) was performed in MONO and CO capsule. As evidenced, the capsules were permeated to blood vessels with intraluminal red blood cells. However, the CD31 was not specific for the endothelium, and particularly in the CO capsules, the expression was detected along the sections. This could be attributed to the fact that the co-encapsulated endothelial cells are also expressing CD31. The presence of collagen was then assessed by Masson's Trichrome staining. As evidenced in **Figure VII.4**, the presence of collagen (blue staining) could be visualized mostly in MONO and CO capsules with 21 days of previous *in vitro* culture. Notably, although in less quantify, the presence of collagen in the newly deposited ECM could also be detected in CO capsules without *in vitro* stimulation. Additionally, the Masson's Trichrome staining also allowed to visualize the presence of blood vessels inside the capsules environment. Importantly, the presence of a dense layer of fibrotic connective tissue surrounding the capsules could not be visualized, which highlights the biotolerability of the capsules.

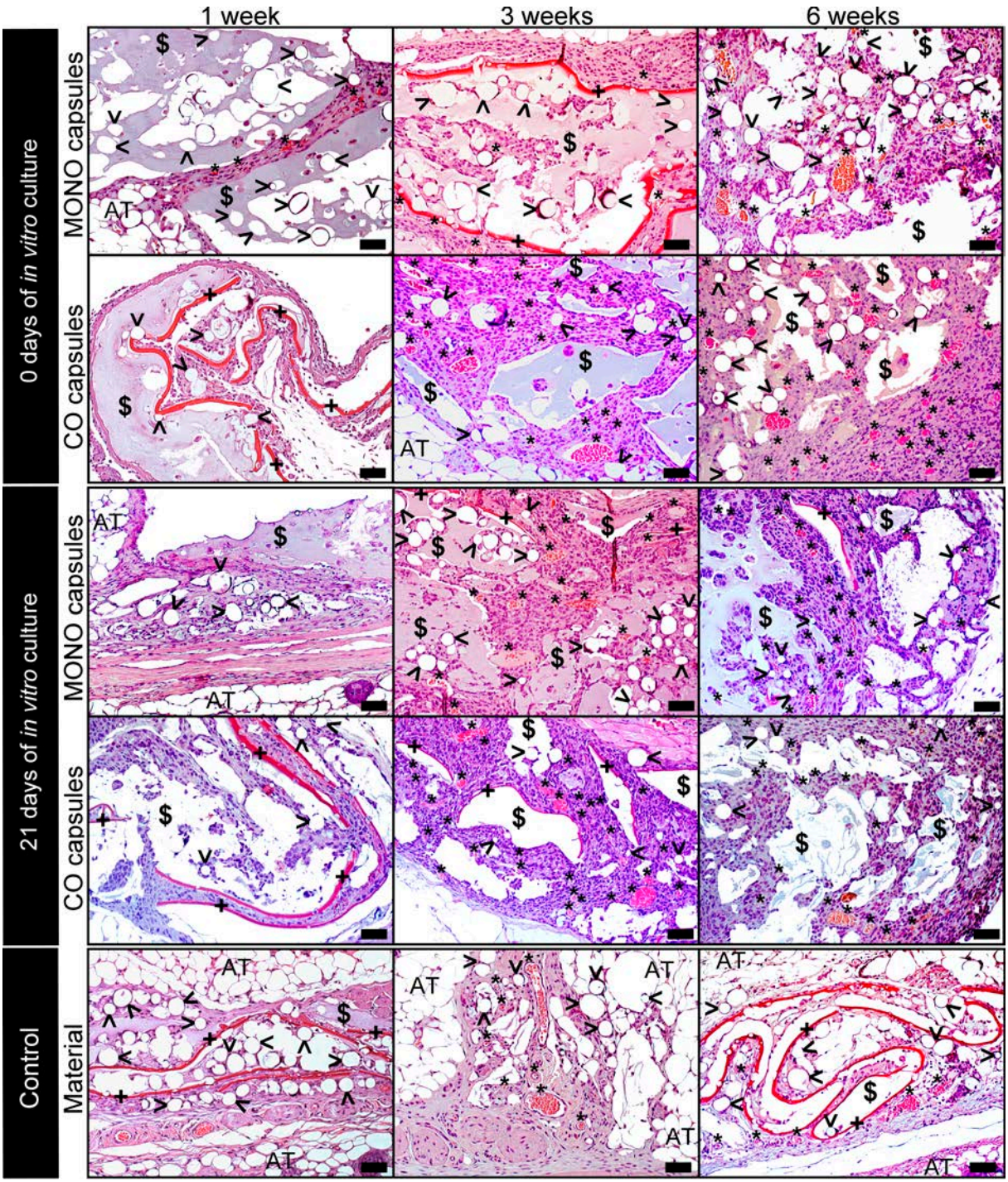

Figure VII.2 – H&E staining of representative sections from MONO and CO capsules (implantation at day 0 and day 21) and from capsules without cells (Material). Explants were retrieved after 1, 3, and 6 weeks of implantation (scale bar: 50μm). Abbreviations and signs used: microparticles (>), residual material of the liquified environment of capsules ($), layer-by-layer membrane (+), blood vessels (*) and regions of adipose tissue (AT) are marked.

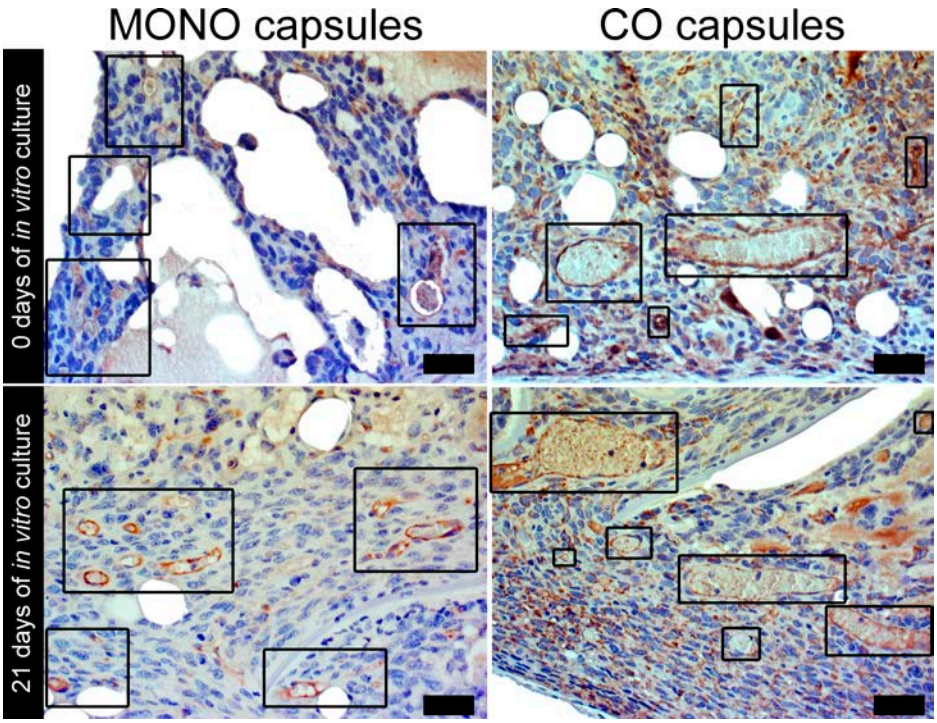

Figure VII.3 – CD31 immunohistochemistry of representative sections from MONO and CO capsules (implantation at day 0 and after 21 days of *in vitro* culture). The presence of blood vessels is evidenced with squares. Explants were analyzed after 6 weeks of implantation. Scale bar is 40 μm.

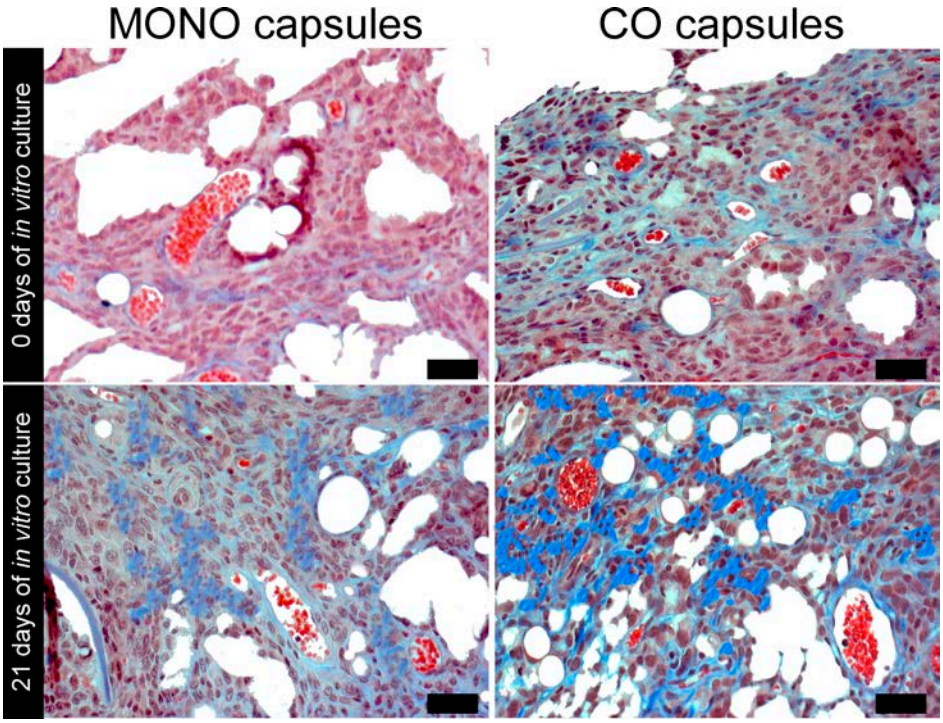

Figure VII.4 – Masson's trichrome staining of representative sections from MONO and CO capsules (implantation at day 0 and after 21 days of *in vitro* culture). Explants were analyzed after 6 weeks of implantation. Collagen is stained in blue. Scale bar is 40 μm.

3.2.2 Osteogenesis evaluation

The osteogenic marker OP was qualitatively detected by fluorescence microscopy (**Figure VII.5**). As expected, OP was expressed within *in vitro* pre-differentiated MONO and CO capsules (day 21 capsules). At the first week of implantation, OP could be earlier detected in pre-differentiated CO capsules. Latter, with increasing implantation time, the expression of OP could also be detectable in CO capsules without *in vitro* osteogenesis stimulation (day 0 capsules). The detection of OP with increased implantation time indicates the commitment of the encapsulated stem cells towards the osteogenic lineage. Only scarce fluorescence could be found in the material capsules as well as in day 0 MONO capsules formulations, indicating that osteogenic differentiation did not occur. Corroborating the OP results, mineralization (**Figure VII.6**) occurred in the pre-differentiated MONO and CO capsules, as well as in CO capsules without *in vitro* osteogenesis (day 0 capsules). Mineralization increased with the implantation time, and after 6 weeks of implantation calcium-rich deposits (stained in red) covered the entire region of the capsules. In the MONO capsules without pre-differentiation only a few mineralization spots were detected, while it was absence in the material capsules.

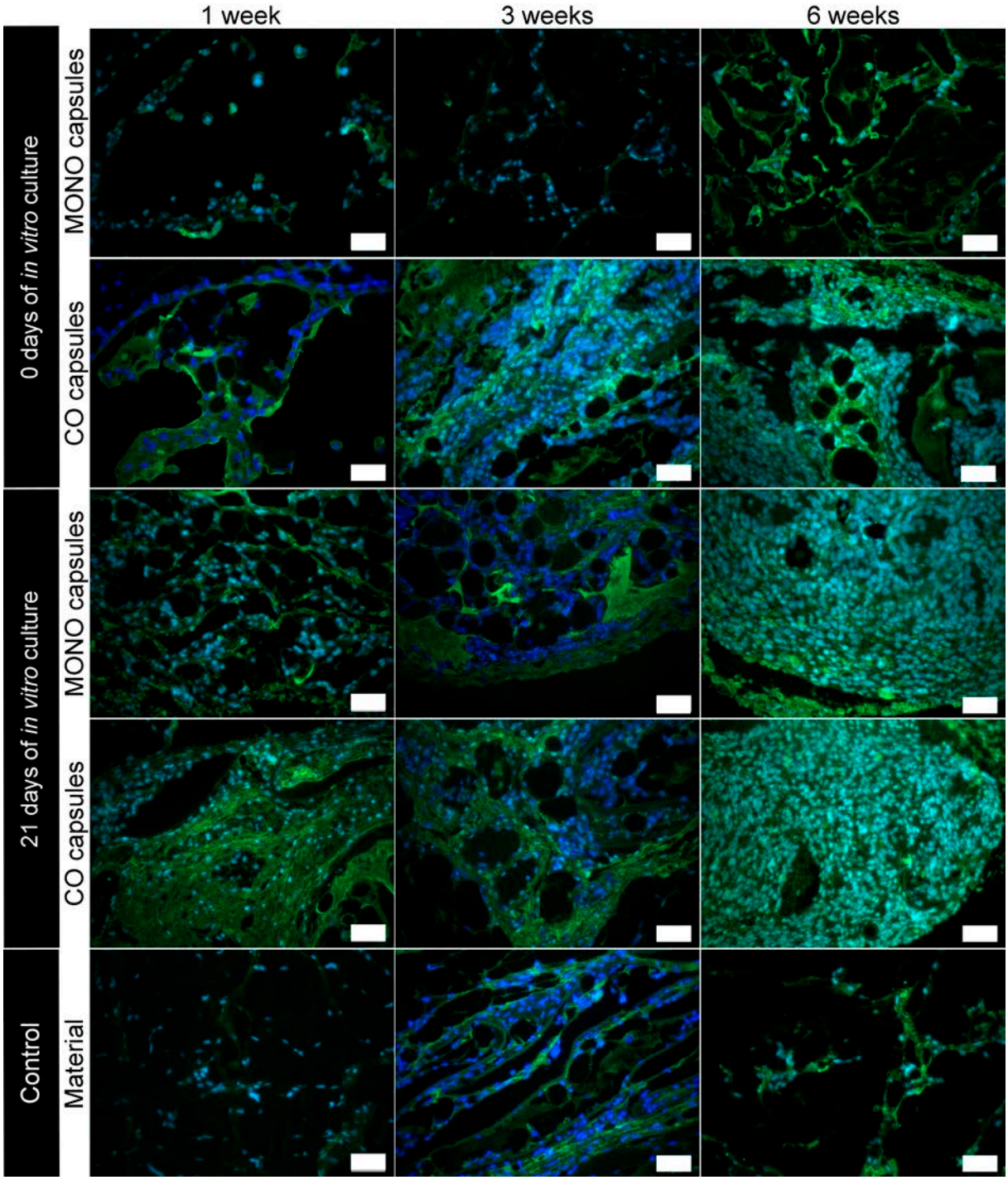

Figure VII.5 – Osteopontin (green) immunohistochemistry counterstained with DAPI (blue) of representative sections from MONO can CO capsules (implantation at day 0 and day 21) and, as control, from capsules without encapsulated cells (Material). Explants were analyzed after 1, 3, and 6 weeks of implantation. Scale bar is 50 µm.

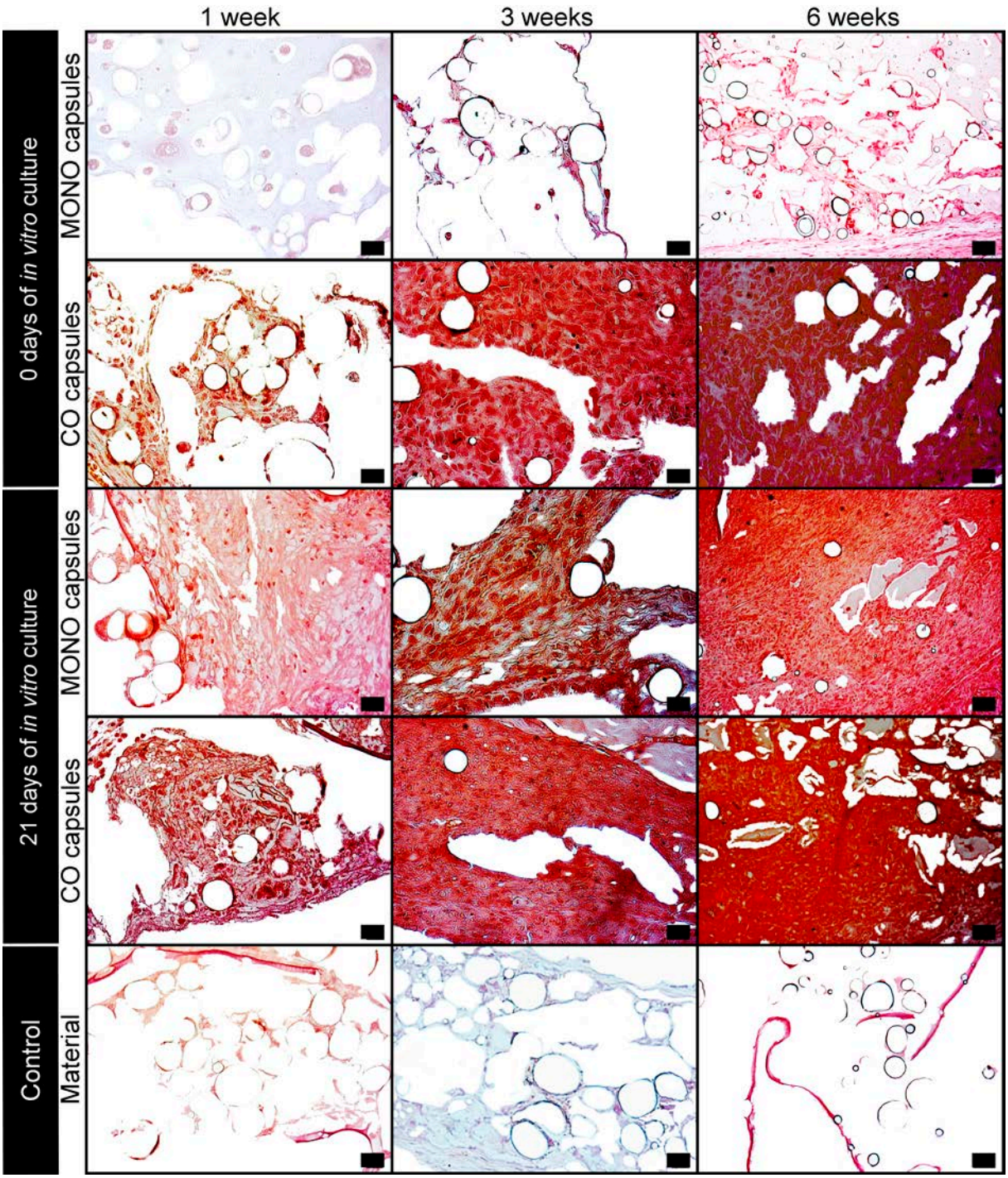

Figure VII.6 – Alizarin red staining of representative sections from MONO and CO capsules of representative sections from MONO can CO capsules (implantation at day 0 and day 21) and, as control, from capsules without encapsulated cells (Material). Explants were analyzed after 1, 3, and 6 weeks of implantation. Mineralization spots are stained in red. Scale bar is 20 μm.

4. Discussion

In the current study, we demonstrate for the first time the *in vivo* osteogenic differentiation of stem cells driven by co-culture with endothelial cells within liquified and multilayered capsules containing solid microparticles.

Among the different bioencapsulation systems proposed [29-33], the central issue is related with the diffusion of nutrients to prevent necrosis at the bulk of implanted materials. In fact, the consensus in all tissue engineering fields is that improved vascularization is the crux of all future scaffold designs [6, 7, 34]. Particularly in bone tissue engineering, engineered scaffolds transplanted to patients to restore or improve the functions of damaged tissue have often failed to produce the desired results due to a deficient oxygen and nutrient diffusion. In order to address this issue, we developed a bioencapsulation system, in which the core is in a liquid state, hence maximizing mass transportation within all the regions of the construct. However, the majority of cells used in tissue engineering are anchorage dependent, and consequently a physical support to process different cellular metabolisms is required. Therefore, along with the encapsulated cells, solid microparticles were incorporated inside the liquified environment of the capsules, which act as cell adhesion sites. Additionally, microparticles also allowed creating a biomimetic 3D environment inside the capsules. Surrounding the liquified core loaded with the encapsulated cells and microparticles is the layer-by-layer membrane. As shown, the thin multilayer remained stable during 21 days of *in vitro* culture, and allowed the required diffusion of essential molecules for cell survival. The membrane also allowed the diffusion of osteogenic differentiation factors added to the culture medium that led to *in vitro* pre-osteogenic stimulation of MONO and CO capsules. The presence of the membrane was also essential to assemble all the encapsulated components into a single reservoir. Having a single structure encapsulating all the different components facilitated the implantation process, while avoiding their dispersion to other regions of the body. However, notwithstanding the stability shown *in vitro*, after the first week of implantation the histological analysis of the capsules revealed that the

membrane was disrupted. Nevertheless, since the disruption of the membrane occurred only at some areas, the core contents of the capsules remained mobilized and aggregated at the site of implantation. The partial disruption could be explained by the fact that the capsules were implanted subcutaneously into created pockets, so they were under a squeeze effect between the host tissues. Additionally, as time increases, the presence of blood vessels could have also contributed to the disruption of the flexible membrane that together with the liquified core of capsules could not offer a rigid surface. However, the disruption of the membrane proved to be a great outcome since the blood vessels transport oxygen and nutrients necessary to the transplanted cells and to the tissue surrounding the implanted capsules. Our main hypothesis was that the co-encapsulation of endothelial cells with stem cells within the capsules environment would lead stem cells to differentiate into the osteogenic lineage and, ultimately, led to the formation of a mineralized tissue. Different fundamental studies [35-37] have been show that ASCs stimulate blood vessel growth due to the secretion of many pro-angiogenic factors, such as VEGF [11, 13, 21]. This explains the abundant presence of blood vessels in all capsules. Furthermore, endothelial cells also secrete numerous regulatory molecules for the differentiation and activity of bone forming cells [16-19]. However, *in vivo* this interaction is poorly characterized mainly because to the absence of appropriate engineered systems. Facca *et al.* [38] reported that although *in vitro* no substrate was required, the osteogenic differentiation of embryonic stem cells after *in vivo* implantation with microparticles incorporating BMP-2 and VEGF only occurred after incorporation of the contents in an alginate gel as a substrate. This was mainly attributed to the fact that the alginate matrix improved contact between the cells and the microparticles releasing system. In our strategy, the encapsulated stem and endothelial cells remained grouped due to the capsules structure. We believe that this has directly influenced the reported *in vivo* outcome by promoting a higher exposure to proangiogenic and osteogenic

factors released by stem and endothelial cells, respectively. This interaction explains the significant advance of this work, namely the *in vivo* osteogenesis with a mineralized and vascularized matrix observed in the CO capsules implanted immediately after production. This is a great achievement, indicating that CO capsules might be readily implanted into a bone defect, and osteogenesis can occur *in vivo*. The co-culture contribution is supported by the absence of mineralized tissue for the MONO capsules also implanted immediately after production. The pre-differentiation strategy of MONO and CO capsules during 21 days *in vitro* in culture medium containing osteogenic differentiation factors also demonstrated that the osteogenic differentiation pattern was maintained *in vivo*. However, the pre-differentiation of CO capsules, since endothelial cells are co-encapsulated, might result in a prevascularization *in vitro*. In bone TE, however, the *in vivo* success of *in vitro* prevascularization has so far been limited. Rouwkema *et al*. [39] have shown that vascular structures obtained from co-cultures of human umbilical vein endothelial cells (HUVECs) and human mesenchymal stem cells (hMSCs) were stable and organized into a more mature vascularization network after implantation. However, anastomosis of the invading vessels to the *in vitro* created vasculature was limited. Therefore, a vascularized osteogenic system that does not require *in vitro* culture before implantation is of great importance in TE strategies. Considering the reported findings, we believe that the proposed CO capsules might find great applicability in bone regeneration.

5. Conclusion

In this study, MONO and CO capsules with or without *in vitro* osteogenic pre-differentiation were subcutaneously implanted in nude mice up to 6 weeks. The *in vivo* implantation of capsules did not elicit a severe infiltration of inflammatory cells, demonstrating the biotolerability of the liquified capsules. Sign of necrosis, either in the host tissue surrounding the implanted capsules or in the newly formed tissue inside the capsules, could not be detected, which is a major concern when implanting 3D systems. The significant advance of

this work is that the co-encapsulation of endothelial cells with stem cells led to the formation of a mineralized tissue *in vivo*. This work is also a unique demonstration of the in vivo performance of a liquified and multilayered capsule containing microparticles and a co-culture of endothelial and stem cells. Considering the reported findings, we suggest the use of CO capsules as self-regulated reservoirs that after production can be readily implanted. By using this formulation we can incorporate different kinds of active molecules aimed at different applications, such as gene therapy, drug delivery, or tissue engineering. We believe that the developed capsules will find great applicability in bone regeneration, but also in other tissue engineering domains of complex tissue restoration.

Acknowledgements

The authors acknowledge the financial support by the Portuguese Foundation for Science and Technology (FCT) through the Ph.D. (SFRH/BD/69529/2010 for Clara R. Correia) and the Post-doc (SFRH/BPD/96611/2013 for Mariana T. Cerqueira) grants, and the funding of RL3-TECT-NORTE-01-0124-FEDER-000020 for Rogério P. Pirraco. The authors are also grateful to Teresa Oliveira for her valuable help with the tissue processing and histological procedures.

Supplementary information

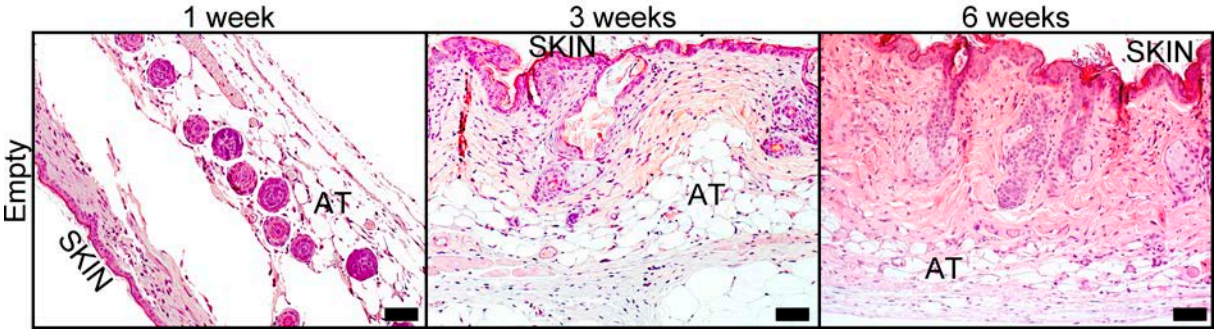

Figure VII.SI - H&E staining of representative sections from empty pockets. Explants were analyzed after 1, 3, and 6 weeks of implantation. Scale bar is 50 μm. Regions of skin and adipose tissue (AT) are marked.

References

[1] K.S. Griffin, K.M. Davis, T.O. McKinley, J.O. Anglen, T.-M.G. Chu, J.D. Boerckel, M.A. Kacena, Evolution of Bone Grafting: Bone Grafts and Tissue Engineering Strategies for Vascularized Bone Regeneration, Clinical Reviews in Bone and Mineral Metabolism, 1 (2015) 1-13.

[2] E.U. Alt, C. Senst, S.N. Murthy, D.P. Slakey, C.L. Dupin, A.E. Chaffin, P.J. Kadowitz, R. Izadpanah, Aging alters tissue resident mesenchymal stem cell properties, Stem Cell Research, 8 (2012) 215–225.

[3] C. Szpalski, M. Barbaro, F. Sagebin, S.M. Warren, Bone Tissue Engineering: Current Strategies and Techniques—Part II: Cell Types, Tissue engineering. Part B, Reviews, 18 (2012) 258-269.

[4] C.T. Gomillion, K.J. Burg, Stem cells and adipose tissue engineering, Biomaterials, 27 (2006) 6052-6063.

[5] F.H. Shen, B.C. Werner, H. Liang, H. Shang, N. Yang, X. Li, A.L. Shimer, G. Balian, A.J. Katz, Implications of adipose-derived stromal cells in a 3D culture system for osteogenic differentiation: an in vitro and in vivo investigation, Spine J, 13 (2013) 32-43.

[6] J. Rouwkema, N.C. Rivron, C.A. van Blitterswijk, Vascularization in tissue engineering, Trends Biotechnol, 26 (2008) 434-441.

[7] A.E. Mercado-Pagan, A.M. Stahl, Y. Shanjani, Y. Yang, Vascularization in bone tissue engineering constructs, Ann Biomed Eng, 43 (2015) 718-729.

[8] Z.S. Patel, S. Young, Y. Tabata, J.A. Jansen, M.E. Wong, A.G. Mikos, Dual delivery of an angiogenic and an osteogenic growth factor for bone regeneration in a critical size defect model, Bone, 43 (2008) 931-940.

[9] Y. Wang, Y. Wei, X. Zhang, M. Xu, F. Liu, Q. Ma, Q. Cai, X. Deng, PLGA/PDLLA core-shell submicron spheres sequential release system: Preparation, characterization and promotion of bone regeneration in vitro and in vivo, Chemical Engineering Journal, 273 (2015) 490-501.

[10] L.F. Mendes, R.P. Pirraco, W. Szymczyk, A.M. Frias, T.C. Santos, R.L. Reis, A.P. Marques, Perivascular-like cells contribute to the stability of the

vascular network of osteogenic tissue formed from cell sheet-based constructs, PloS one, 7 (2012) e41051.
[11] R.P. Pirraco, B. Melo-Ferreira, T.C. Santos, A.M. Frias, A.P. Marques, R.L. Reis, Adipose stem cell-derived osteoblasts sustain the functionality of endothelial progenitors from the mononuclear fraction of umbilical cord blood, Acta biomaterialia, 9 (2013) 5234-5242.
[12] J. Kim, H.N. Kim, K.T. Lim, Y. Kim, S. Pandey, P. Garg, Y.H. Choung, P.H. Choung, K.Y. Suh, J.H. Chung, Synergistic effects of nanotopography and co-culture with endothelial cells on osteogenesis of mesenchymal stem cells, Biomaterials, 34 (2013) 7257-7268.
[13] R.P. Pirraco, T. Iwata, T. Yoshida, A.P. Marques, M. Yamato, R.L. Reis, T. Okano, Endothelial cells enhance the in vivo bone-forming ability of osteogenic cell sheets, Laboratory investigation; a journal of technical methods and pathology, 94 (2014) 663-673.
[14] S. Mendez-Ferrer, T.V. Michurina, F. Ferraro, A.R. Mazloom, B.D. Macarthur, S.A. Lira, D.T. Scadden, A. Ma'ayan, G.N. Enikolopov, P.S. Frenette, Mesenchymal and haematopoietic stem cells form a unique bone marrow niche, Nature, 466 (2010) 829-834.
[15] P. Bianco, Bone and the hematopoietic niche: a tale of two stem cells, Blood, 117 (2011) 5281-5288.
[16] F.A. Saleh, M. Whyte, P.G. Genever, Effects of endothelial cells on human mesenchymal stem cell activity in a three-dimensional in vitro model, European Cells and Materials, 22 (2011) 242-257.
[17] N.B. Thebaud, R. Siadous, R. Bareille, M. Remy, R. Daculsi, J. Amedee, L. Bordenave, Whatever their differentiation status, human progenitor derived - or mature - endothelial cells induce osteoblastic differentiation of bone marrow stromal cells, Journal of tissue engineering and regenerative medicine, 6 (2012) e51-60.
[18] S.B. Traphagen, I. Titushkin, S. Sun, K.K. Wary, M. Cho, Endothelial invasive response in a co-culture model with physically-induced

osteodifferentiation, Journal of tissue engineering and regenerative medicine, 7 (2013) 621-630.
[19] J. Leszczynska, B. Zyzynska-Granica, K. Koziak, S. Ruminski, M. Lewandowska-Szumiel, Contribution of endothelial cells to human bone-derived cells expansion in coculture, Tissue engineering. Part A, 19 (2013) 393-402.
[20] E.A. Neofytou, E. Chang, B. Patlola, L.M. Joubert, J. Rajadas, S.S. Gambhir, Z. Cheng, R.C. Robbins, R.E. Beygui, Adipose tissue-derived stem cells display a proangiogenic phenotype on 3D scaffolds, Journal of biomedical materials research. Part A, 98 (2011) 383-393.
[21] E. Tumarkin, L. Tzadu, E. Csaszar, M. Seo, H. Zhang, A. Lee, R. Peerani, K. Purpura, P.W. Zandstra, E. Kumacheva, High-throughput combinatorial cell co-culture using microfluidics, Integrative biology : quantitative biosciences from nano to macro, 3 (2011) 653-662.
[22] S.M. Oliveira, R.L. Reis, J.F. Mano, Towards the design of 3D multiscale instructive tissue engineering constructs: Current approaches and trends, Biotechnol Adv, 33 (2015) 842-855.
[23] J. Borges, J.F. Mano, Molecular interactions driving the layer-by-layer assembly of multilayers, Chemical reviews, 114 (2014) 8883-8942.
[24] R.R. Costa, J.F. Mano, Polyelectrolyte multilayered assemblies in biomedical technologies, Chemical Society reviews, 43 (2014) 3453-3479.
[25] P.A. Zuk, M. Zhu, P. Ashjian, D.A.D. Ugarte, J.I. Huang, H. Mizuno, Z.C. Alfonso, J.K. Fraser, P. Benhaim, M.H. Hedrick, Human Adipose Tissue Is a Source of Multipotent Stem Cells, Molecular Biology of the Cell, 13 (2002) 4279-4295.
[26] M.T. Cerqueira, L.P.d. Silva, T.C. Santos, R.P. Pirraco, V.M. Correlo, R.L. Reis, A.P. Marques, Gellan Gum-Hyaluronic Acid Spongy-like Hydrogels and Cells from Adipose Tissue Synergize Promoting Neoskin Vascularization, Appl. Mater. Interfaces, 6 (2014) 19668-19679.
[27] C.R. Correia, P. Sher, R.L. Reis, J.F. Mano, Liquified chitosan–alginate multilayer capsules incorporating poly(L-lactic acid) microparticles as cell carriers, Soft Matter, 9 (2013) 2125-2130.

[28] C.R. Correia, R.L. Reis, J.F. Mano, Multilayered hierarchical capsules providing cell adhesion sites, Biomacromolecules, 14 (2013) 743-751.
[29] S. De Koker, L.J. De Cock, P. Rivera-Gil, W.J. Parak, R. Auzely Velty, C. Vervaet, J.P. Remon, J. Grooten, B.G. De Geest, Polymeric multilayer capsules delivering biotherapeutics, Adv Drug Delivery Rev, 63 (2011) 748-761.
[30] A.K. Brun-Graeppi, C. Richard, M. Bessodes, D. Scherman, O.W. Merten, Cell microcarriers and microcapsules of stimuli-responsive polymers, J Controlled Release, 149 (2011) 209-224.
[31] R.M. Hernandez, G. Orive, A. Murua, J.L. Pedraz, Microcapsules and microcarriers for in situ cell delivery, Advanced drug delivery reviews, 62 (2010) 711-730.
[32] L.J. De Cock, S. De Koker, B.G. De Geest, J. Grooten, C. Vervaet, J.P. Remon, G.B. Sukhorukov, M.N. Antipina, Polymeric multilayer capsules in drug delivery, Angewandte Chemie, 49 (2010) 6954-6973.
[33] M. Marguet, C. Bonduelle, S. Lecommandoux, Multicompartmentalized polymeric systems: towards biomimetic cellular structure and function, Chemical Society reviews, 42 (2013) 512-529.
[34] R.K. Jain, P. Au, J. Tam, D.G. Duda, D. Fukumura, Engineering vascularized tissue, Nature Biotechnology, 23 (2005) 821-823.
[35] J. Kang, J. Gimble, D. Kaplan, In vitro 3D model for human vascularized adipose tissue, Tissue engineering. Part A, 15 (2009) 2227-2236.
[36] F. Verseijden, H. Jahr, S.P.-v. Sluijs, T.T. Hagen, S. Hovius, A. Seynhaeve, J.v. Neck, G.v. Osch, S. Hofer, Angiogenic capacity of human adipose-derived stromal cells during adipogenic differentiation: An in vitro study, Tissue engineering. Part A, 15 (2009) 445-452.
[37] J. Rehman, D. Traktuev, J. Li, S. Merfeld-Clauss, C.J. Temm-Grove, J.E. Bovenkerk, C.L. Pell, B.H. Johnstone, R.V. Considine, K.L. March, Secretion of angiogenic and antiapoptotic factors by human adipose stromal cells, Circulation, 109 (2004) 1292-1298.

[38] S. Facca, C. Cortez, C. Mendoza-Palomares, N. Messadeq, A. Dierich, A.P. Johnston, D. Mainard, J.C. Voegel, F. Caruso, N. Benkirane-Jessel, Active multilayered capsules for in vivo bone formation, Proceedings of the National Academy of Sciences of the United States of America, 107 (2010) 3406-3411.
[39] J. Rouwkema, J.d. Boer, C.A. van Blitterswijk, Endothelial Cells Assemble into a 3-Dimensional Prevascular Network in a Bone Tissue Engineering Construction, Tissue Engineering, 12 (2006) 2685-2693.

4

Conclusion

Chapter VIII

Conclusions and future perspectives in cell encapsulation

Chapter VIII

Conclusions and future perspectives in cell encapsulation

Abstract

In the present chapter are discussed the main conclusions of the work developed in this thesis. Additionally, recent progress on cell encapsulation field for tissue regeneration and future research directions are also deliberated.

1. General conclusion

A wide range of polymers have been studied for cell encapsulation, in order to overcome numerous drawbacks, such as a lack of sufficient biotolerability in the host, undesired loss of the enveloped cells, an inability to achieve appropriate mechanical stability *in vivo*, and too low permeability that interferes with cell survival. Many of them never made it to the application phase since they did not meet one or more basic requirements for their use.

In parallel with the discovery of new polymers and biomaterials, cell encapsulation strategies became more complex, and its use was extrapolated to respond to requirements of complex fields, such as Tissue Engineering and Regenerative Medicine (TERM). In TERM field, the concept of encapsulating cells is different from the immunoprotection required to treat endocrine diseases. In TERM applications, it is often desirable that the encapsulation matrix degrades while the encapsulated cells proliferate and create their own extracellular matrix. Additionally, different pro-healing components, such as growth factors and cytokines can be co-encapsulated with cells, while being released in a sustained fashion through the encapsulation matrix.

In an attempt to create such challenging bioencapsulation system, liquified and multilayered capsules were developed, as discussed in the present thesis. The main goal was to create a sophisticated system with multiple functionalities to successfully stimulate the regeneration of damaged tissues.

In **Chapter III**, the application of liquified and multilayered capsules encapsulating cells and microparticles as a bioencapsulation system for tissue engineering was first successfully achieved. The different parameters to develop such system were optimized, and results showed that the multilayered chitosan-alginate membrane produced by layer-by-layer was able to provided stability to capsules up to 7 days of *in vitro* culture, while allowing the diffusion of essential molecules for cell survival. In **Chapter IV**, the optimized parameters to produce multilayered and liquified capsules were applied, however, in order to increase the mechanical stability of capsules to allow longer periods of cell encapsulation, poly(L-lysine) (PLL) was introduced into the multilayered membrane. The incorporation of PLL led to an exponential

regime growth of the polymeric film, against the linear growth with only chitosan and alginate polyelectrolytes. Therefore, the mechanical stability of capsules was improved and capsules were able to support living cell encapsulation up to 28 days. Additionally, the metabolic activity and proliferation of the encapsulated cells within the liquified capsules were superior compared to non-liquified systems or liquified capsules without poly(L-lactic acid) (PLLA) microparticles. With the successful of the developed bioencapsulation system, capsules were then applied in specific tissue engineering fields. In **Chapter V**, the suitability for chondrogenic differentiation within magnetic-responsive liquified capsules co-encapsulating stem cells and surface modified PLLA microparticles was assessed. The results showed that in the absence of supplementation with TGF-β3, the immobilization of TGF-β3 to microparticles coated with collagen II was able to induce the chondrogenic differentiation. Notably, the chondrogenesis observed occurred in similar levels of those found for capsules cultured in normal chondrogenic differentiation medium, which used higher amounts of TGF-β3. Therefore, it was demonstrated the feasibility of capsules as an engineered self-regulated chondromimetic device. In **Chapter VI**, inspired by the local interactions at the molecular level from the co-existence of stem and vascular cells in the native environment of bone, stem (ASCs) and endothelial (ECs) cells both derived from adipose tissue were co-encapsulated. Results showed that the co-encapsulation of ECs lead ASCs to differentiate into the osteogenic lineage inside the liquified and multilayered capsules with microparticles, even in the absence of two major osteogenic differentiation factors, namely dexamethasone and ascorbic acid. Additionally, capsules encapsulating both cells released BMP-2 and VEGF, which evidences the potential of the bioencapsulation system as a cytokine delivery system. Ultimately, in **Chapter VII**, capsules were tested *in vivo* after subcutaneous implantation in nude mice. This work was a unique demonstration of the *in vivo* performance of the liquified and multilayered capsules. Results confirmed *in vivo* the biotolerability of the bioencapsulation system, since signs of necrosis, either in the host tissue surrounding the implanted capsules or in the newly formed tissue inside

the capsules, could not be detected. This represents a great outcome in three-dimensional systems. Additionally, the co-encapsulation of endothelial cells with stem cells led to the formation of a mineralized tissue *in vivo*, thus validating the results obtained *in vitro* in **Chapter VI**.

2. Scientific progress and future research directions

In recent years there have been some interesting research developments in cell encapsulation. To face the demanding requirement of cell encapsulation systems for TERM, new methodologies are being recently applied to develop the next generation of cell encapsulation systems. By applying principles of layer-by-layer technology new sophisticated membranes are being proposed, composed by a wide variety of constituents. The only requirement is that multipoint interactions exist between each of them, such as electrostatic contacts, van der Walls forces, and hydrogen bonding. Additionally, ultimate microfluidics systems and three-dimensional bioprinting devices are being projected, which are the main responsible for the high level of complexity and hierarchical organization of the new generation of cell encapsulation systems.

Cell encapsulation is a technology with enormous clinical potential. Yet many difficulties remain, some of which will certainly challenge our scientific ingenuity. The stepwise analysis of the essential obstacles, coupled with increased international collaboration, should move the technology forward in a careful and controlled way and bring it much closer to clinical reality. This ambitious goal requires the interdisciplinary and integrated effort of scientists with different areas of expertise such as genetics, materials science, physicochemistry and chemical engineering, pharmaceutical technology, biology and medicine. Issues on long term viability, risk of immune response, together with the development of high biocompatible materials, with sufficient durability and appropriate permeability, should be addressed to further explore their possible clinical applications. Particularly, regarding the bioencapsulation system here proposed, although the developed capsules were tested for cartilage and bone regeneration, their application range is diverse due to the different components of the capsules that can be easily changed or combined

with new features, in accordance with the target tissue aimed to restore. Therefore, the developed capsules and can found application in other fields, such as biochemical and biological reactors, platforms for model diseases, drug analysis screening, and so on. With the knowledge generated by this work, it is expected that the proposed capsules will have a strong impact and open new prospects in the tissue regeneration field. The most characteristic and promising feature of the proposed multilayered and liquified system is the ability to tailor different properties in one single device. It is thus expected that the multilayered and liquified capsules encapsulating solid microparticles will find great applicability in tissue engineering domains of complex tissue restoration.